July bottom trawl survey biomasses of fishery species in Falkland Islands waters, 2017–2026

SA-2026-07

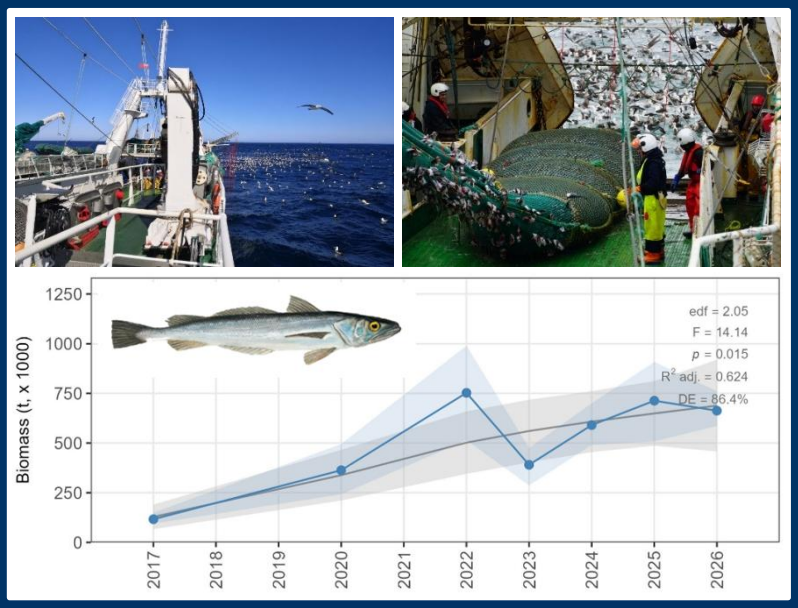

Jorge E. Ramos

Fisheries Department
Directorate of Natural Resources
Falkland Islands Government
Stanley, Falkland Islands

November 2026

For citation purposes this publication should be referenced as follows:

Ramos JE (2026) July bottom trawl survey biomasses of fishery species in Falkland Islands waters, 2017–2026. SA-2026-07. Fisheries Department, Directorate of Natural Resources, Falkland Islands Government, Stanley, Falkland Islands. 150 p.

© Crown Copyright 2026

No part of this publication may be reproduced without prior permission from the Falkland Islands Government-Fisheries Department.

Acknowledgements

We thank the captains and crews of the commercial fishing vessels, and the scientific observers of the Falkland Islands Fisheries Department (FIFD), that facilitated and assisted in catch, oceanographic, and biological data collection. Toni Trevizan and scientific observers assisted with data checks. Comments provided by Frane Skeljo and Andreas Winter. Cover photo credits: J.E. Ramos, FIFD (top left), Toni Trevizan, FIFD (top right).

Distribution: Public Domain

Reviewed and approved on 15 November 2026 by:



James Wilson
Director of Natural Resources
Falkland Islands Government

Table of Contents

1. Summary 1
2. Introduction 3
3. Methods 4
3.1. Bottom trawl stations 4
3.2. Catch recording 5
3.3. Abundance calculations 6
3.4. Temporal changes in biomass 8
3.4.1. Current year to baseline biomass comparisons 8
3.4.2. Temporal biomass trends 9
3.5. Spatial changes in biomass 11
3.6. Biological sampling 12
3.7. Length composition 12
3.7.1. Length-weight relationship. 12
3.7.2. Overall length composition 13
3.7.3. Comparative length composition at the survey and sex levels 13
3.7.4. Yearly length composition 14
3.8. Sex and maturity composition 14
4. Results and Discussion 15
4.1. Bottom trawl stations 15
4.2. Biomass estimates 15
4.3. Species summaries 21
4.3.1. Argentine shortfin squid (*Illex argentinus*) 21
4.3.2. Banded whiptail grenadier (*Coelorinchus fasciatus*) 31
4.3.3. Common hake (*Merluccius hubbsi*) 41
4.3.4. Hoki (*Macruronus magellanicus*) 51
4.3.5. Kingclip (*Genypterus blacodes*) 61
4.3.6. Patagonian squid (*Doryteuthis gahi*) 71
4.3.7. Patagonian toothfish (*Dissostichus eleginoides*) 81
4.3.8. Red cod (*Salilota australis*) 91
4.3.9. Rock cod (*Patagonotothen ramsayi*) 101
4.3.10. Southern blue whiting (*Micromesistius australis*) 111
4.3.11. Southern hake (*Merluccius australis*) 121
5. Conclusions 130

6. Recommendations 132
7. References 133
Appendix I. Length-weight relationship 141
Appendix II. July surveys catches 142
Appendix III. Year-to-baseline biomass differences 143
Appendix IV. Year-to-baseline biomass differences histograms 144
Appendix V. Generalised Additive Models for biomass trends 147
Appendix VI. Spatial distribution of Patagonian squid (*Doryteuthis gahi)* length 150

July bottom trawl survey biomasses of fishery species in Falkland Islands waters, 2017–2026

1. Summary

Biomass assessments were conducted for 11 commercially important fish stocks—Argentine shortfin squid, banded whiptail grenadier, common hake, hoki, kingclip, Patagonian squid, Patagonian toothfish, red cod, rock cod, southern blue whiting, and southern hake—across the northern and western areas of the Falkland Islands Interim Conservation and Management Zone (FICZ) and the Falkland Islands Outer Conservation Zone (FOCZ), including the 'Loligo Box'. These assessments were based on catch data from 882 bottom trawls conducted during the July parallel groundfish and calamari pre-season surveys in 2017, 2020, and 2022–2026. Changes in biomass were assessed by comparison of the biomass in 2026 to baseline years (2017, 2025, and 2023–2025 mean) and using Generalised Additive Models (GAMs) to model the temporal trends of the full time series (2017–2026). Changes in length were assessed using GAMs to model the temporal trend of the full time series. Sex and maturity composition were examined. The July 2020 groundfish survey was included in the analyses, although it is important to note that this survey was modified for a common hake demographic study, which may affect comparability.

The July surveys revealed divergent biomass trajectories for Falkland Islands marine resources from 2017 to 2026, with the short time-series limiting biomass trend interpretation. Species that exhibited signs of increasing biomass were:

Argentine shortfin squid biomass increased significantly from 2017 (140.98 t) to 2026 (1,323.96 t), while length showed no significant change throughout the time series, as revealed by GAMs. Females comprised the higher proportion of biomass, mainly at young or immature stages.

Common hake biomass showed a significant increasing trend from 2017 (116,485.35 t) to 2026 (662,873.79 t), with densities increasing predominantly in the west of the FICZ and to the south, including within the 'Loligo Box'. Females contributed most of the biomass, mainly at post-spawning maturity stages, while length declined throughout the time series.

Patagonian toothfish biomass peaked in 2026 (10,363.00 t), representing a significant increase from 2017 (1,323.17 t), in part driven by growth in body size of the 2022–2023 recruit cohorts. Biomass was dominated by females, all at immature stage. It must be noted that bottom trawl demersal surveys are not representative of the adult component of the stock, which is caught by longlines

Southern hake biomass increased significantly from 2017 (511.89 t) to 2026 (3,730.83 t), with females predominating, mostly at recovering spent or resting maturity, and no temporal trend in length. These results should be interpreted with caution, as estimates carry additional uncertainty arising from the difficulty of distinguishing this species from common hake (*M. hubbsi*) in bulk catches. Falkland Islands fisheries account for ≤ 12% of total southern hake catch across the Southwest Atlantic, and the limited local data further constrain comprehensive assessment of the status of this stock.

Species that exhibited signs of decreasing biomass were:

Hoki biomass showed a significant declining trend from 2017 (85,477.47 t) to 2026 (970.16 t). Females contributed a higher proportion of biomass than males, mainly at resting maturity stage. Length showed a non-significant increasing trend.

Patagonian squid biomass declined significantly from 2017 (344,472.91 t) to 2026 (97,819.97 t), together with a declining trend in length, a lower proportion of females in July 2026, and a shift from preparatory to immature individuals since 2020, suggesting a shift towards smaller, less mature individuals in the spring-spawning cohort.

Red cod biomass increased from 2017 (12,079.24 t) to 2022 (39,343.25 t) but decreased towards 2026 (14,080.62 t). Most biomass was comprised of females at resting maturity, together with an increase in size. Persistent low biomass and historical declines beyond the FICZ may indicate region-wide vulnerability.

Species with no significant biomass trends were:

Banded whiptail grenadier showed no significant change in biomass nor length throughout the time series. Females comprised most of the biomass, mainly at post-spawning maturity stages. Information on this species in Falkland Islands waters is limited.

Kingclip biomass remains at low levels with no clear trend (i.e., 2023–2025 mean = 41,393.40 t). Females, mainly at resting maturity stage, contributed most of the biomass. Length increased significantly over the time series; the presence of large individuals in recent years suggests potential for recovery if size-selective management measures are implemented in the commercial bottom trawl fishery.

Rock cod biomass remains at low levels, although with signs of stabilisation and minor increase in recent years (i.e., 2023–2025 mean = 57,152.07 t). Females contributed a slightly higher proportion of biomass than males, with no significant change in length, and in a variety of maturity stages.

Southern blue whiting showed no temporal biomass trend, and biomass remains at low levels (i.e., 2023–2025 mean = 654.42 t). Biomass consisted of a higher proportion of males than females, both mostly at immature and early developing stages. Length increased throughout the time series.

Some of these species are not at their peak of abundance in Falkland Islands waters during July (e.g., Argentine shortfin squid, hoki, southern blue whiting) or they may be under-represented due to the fishing gear used for the surveys (i.e., bottom trawl, whereas the Argentine shortfin squid is mainly caught by jiggers, and the adult portion of the Patagonian toothfish stock is caught by longlines).

Many of the stocks assessed are targeted across multiple nations' Exclusive Economic Zones (EEZs), with the Falkland Islands contributing a relatively small proportion to the total shared catch for some species in the Southwest Atlantic and Southeast Pacific. Declines in biomass for some of these stocks may be partially attributed to fishing pressure outside Falklands waters. However, the Falkland Islands fisheries contribute a significant proportion to the total catch for certain stocks, such as rock cod and red cod, and several species' spawning grounds lie within the Falkland Islands shelf, including hoki, red cod, rock cod, and southern blue whiting. As such, management decisions made by the Falkland Islands Fisheries Department (FIFD) are critical for the sustainability of these stocks.

2. Introduction

The Falkland Islands shelf is located within the Patagonian Large Marine Ecosystem, one of the world's most productive fishing areas (Arkhipkin et al. 2012). The Patagonian Large Marine Ecosystem comprises two distinct sub-regions: a southern temperate ecosystem in the north and a sub-Antarctic ecosystem in the south (Boltovskoy 1999). The temperate ecosystem lies within waters of subtropical origin, transported onto the shelf by the Brazil Current and mixed with temperate shelf waters. The region's productivity is largely driven by tidal mixing oceanographic fronts and seasonal fronts formed by cold freshwater inflows from the Strait of Magellan. The sub-Antarctic ecosystem is influenced by waters of sub-Antarctic origin carried by the Falkland Current (Peterson & Whitworth 1989). The Falkland Current, which diverges from the Antarctic Circumpolar Current in the Drake Passage, splits into two branches at the continental slope south of the Falkland Islands—one weaker and one stronger—flowing around the west and east of the islands, respectively (Bianchi et al. 1982). These oceanographic features play a crucial role in the distribution and abundance of marine species, such as Argentine shortfin squid (*Illex argentinus*) and hoki (*Macruronus magellanicus*), which migrate to frontal zones for feeding and return to non-frontal zones for spawning (Agnew 2002). In contrast, deep-water species like Patagonian toothfish (*Dissostichus eleginoides*) are influenced by sub-Antarctic water intrusions into the shelf (Laptikhovsky et al. 2008; Arkhipkin & Laptikhovsky 2010).

Commercial squid and fish stocks around the Falkland Islands have been targeted by international fishing fleets for decades, with systematic catch data starting in 1987 (Falkland Islands Government 1989). Total catches reached a peak of 462,487 tonnes in 2015, largely due to an unusually large influx of *I. argentinus* into Falkland waters from April to May 2015, resulting in record catches of 332,862 t for the species (Winter 2015; Falkland Islands Government 1989, 2025). Finfish licence allocations in the Falkland Islands were determined using Total Allowable Effort (TAE), based on the catchability of an index species representing the main target of the fishery. This approach works under the assumption of consistent relationships among catch, effort, and biomass. The first index species for finfish TAE was southern blue whiting (*Micromesistius australis*). However, catches of southern blue whiting declined in the 1990s and the stock collapsed by 2009. Rock cod (*Patagonotothen ramsayi*) was first targeted in 2007 due to the lack of marketability in previous years (Winter et al. 2010), and its catches peaked in 2010 (Laptikhovsky et al. 2013; Ramos & Winter 2023a). The index species was re-examined (Payá et al. 2010) and switched in 2011 from southern blue whiting to rock cod to set effort allocation. However, catches of rock cod decreased considerably after 2010 (Ramos & Winter 2023a; Falkland Islands Government 2026). In parallel, catches of common hake (*Merluccius hubbsi*) increased, with a peak of 63,365 t in 2025 (Falkland Islands Government 2026). The use of an index species to manage all Falkland Islands commercial finfish species was thus considered unreliable, and the Falkland Islands Government, on advice from MacAlister Elliott & Partners Ltd, UK (MEP 2020), switched to assessing each individual commercial stock to better inform fisheries management.

Scientific surveys are a key source of fisheries-independent data, offering standardised sampling plan and constant catchability that are not influenced by commercial fishing activities (Hilborn & Walters 1992; Alglave et al. 2022; Gallo et al. 2022). The Falkland Islands Fisheries Department (FIFD) has conducted parallel groundfish and calamari (*Doryteuthis gahi*) pre-season surveys every February since 2010, except for 2012, 2013, and 2014. The groundfish surveys are conducted along the north, west and south-west in Falkland Islands

waters. The calamari pre-season surveys are conducted along the 'Loligo Box' to the east of the Falkland Islands.

Initially, these surveys aimed to provide biomass estimates for rock cod on the entire Falklands fishing grounds during the austral summer (Winter et al. 2010), which has since been expanded to provide information on other commercial stocks. It is noted, however, that Falkland Islands waters represent only part of the range for most stocks examined. For certain migratory species, such as common hake (Arkhipkin et al. 2015) and kingclip (*Genypterus blacodes*) (Arkhipkin et al. 2012), the February surveys may not coincide with peak abundance periods. Therefore, July surveys that follow the same methodology as the February surveys have also been conducted since 2017 to estimate biomass during the austral winter. Increasing abundance of common hake in the Falkland Shelf in recent years (Ramos & Winter 2022a) triggered a demography survey conducted exclusively for this species during July 2020 (Randhawa et al. 2020).

This report summarises biomass estimates for key commercial species in Falkland Islands waters based on catch data from both the groundfish and calamari pre-season surveys conducted in July 2017, 2020, and 2022–2026.

3. Methods

3.1. Bottom trawl stations

Concurrent groundfish and calamari pre-season research surveys were carried out during July 2017, 2020, and 2022–2026 onboard chartered fishing trawlers to cover the Falkland Islands fishing zone (Fig. 1). All trawls were bottom trawls; GPS latitude and longitude, net vertical opening, net horizontal opening, trawl door spread, and trawl speed were recorded on the ship's bridge when the net achieved the required configuration at the seafloor (based on net sensor readings, confirmed by the bridge officer), every 15 minutes during the progress of each trawl (in calamari pre-season surveys), and at the end of the trawl at the seafloor.

The duration of each trawl was approximately 60 min on the bottom during groundfish surveys, and 120 min on the bottom during calamari pre-season surveys. Characteristics of the trawl nets, trawl performance, and biological sampling during groundfish (Gras et al. 2017; Lee et al. 2022; Ramos et al. 2023b, 2024a; Soeth et al. 2025) and calamari pre-season (Winter et al. 2017, 2020, 2022, 2025; Chemshirova et al. 2023, 2024) surveys can be consulted in detail in their respective survey reports. These surveys were designed to be consistent in the number and position of stations across years. However, there were variations in the number of stations due to mechanical issues, unfavourable weather conditions, logistic setbacks (e.g., pandemic COVID-19), or objectives of each survey. Increasing abundance of common hake in the Falkland Shelf in recent years (Ramos & Winter 2022a) triggered a groundfish survey in July 2020, with emphasis on the abundance and biology of common hake (Randhawa et al. 2020). Data from the July 2020 groundfish survey are also included in this report.

3.2. Catch recording

All species from the catch of each trawl station were sorted by FIFD scientific staff and the vessel's factory crew. FIFD scientific staff recorded the total catch of each species assessed by a combination of weighing on an electronic balance to the nearest 0.01 kg and factory production records when complete weighing of large catches was not logistically feasible.

Eleven commercial species were assessed; these species have been typically assessed in February and July parallel demersal surveys conducted in Falkland Islands waters and represent important commercial targets in the Falkland Islands and other neighbour nations' fishing zones (Table I).

Table I. Main commercial species assessed in groundfish and calamari pre-season surveys in Falkland Islands waters during July 2017, 2020, and 2022–2026. Geographic distributions taken from http://www.fao.org/fishery/species/search/en

Common name	Scientific name	Distribution
Argentine shortfin squid	*Illex argentinus*	Southwest Atlantic: Brazil, Uruguay, Argentina, Falkland Islands.
Banded whiptail grenadier	*Coelorinchus fasciatus*	Southwest Atlantic: Brazil, Uruguay, Argentina, Falkland Islands. Southern Pacific: Chile, Australia, New Zealand. Southern Indian: Africa, Australia.
Common hake	*Merluccius hubbsi*	Southwest Atlantic: Brazil, Uruguay, Argentina, Falkland Islands.
Hoki	*Macruronus magellanicus*	Southwest Atlantic: Argentina, Falkland Islands. Southeast Pacific: Chile.
Kingclip	*Genypterus blacodes*	Southwest Atlantic: Brazil, Uruguay, Argentina, Falkland Islands. Southern Pacific: Chile, Australia, New Zealand.
Patagonian squid	*Doryteuthis gahi*	Southwest Atlantic: Argentina, Falkland Islands. Southern Pacific: Peru, Chile.
Patagonian toothfish	*Dissostichus eleginoides*	Southwest Atlantic: Argentina, Falkland Islands. Southeast Pacific: Chile. Southwest Pacific: Macquarie Island. Southern Ocean: South Georgia.
Red cod	*Salilota australis*	Southwest Atlantic: Argentina, Falkland Islands. Southeast Pacific: Chile.
Rock cod	*Patagonotothen ramsayi*	Southwest Atlantic: Argentina, Falkland Islands.
Southern blue whiting	*Micromesistius australis*	Southwest Atlantic: Argentina, Falkland Islands. Southeast Pacific: Chile. Southern Ocean: South Georgia, South Shetland, South Orkney Islands.
Southern hake	*Merluccius australis*	Southwest Atlantic: Argentina, Falkland Islands. Southern Pacific: Chile, New Zealand.

Station and catch data recorded during the surveys were checked and corrected following each survey's standard data management procedures, with groundfish survey data verified record by record. Analyses were conducted once both surveys' data were available in the FIFD database.

3.3. Abundance calculations

Trawls were excluded from abundance calculations if not quantifiable for the following reasons: 1) the trawl doors did not open properly, 2) the net broke during the trawl, or 3) if the net was quickly filled with medusae, which resulted in the trawl being stopped prematurely.

Density (kg/km^2) was calculated as the species catch weight divided by the trawl area (Winter 2019). Trawl area was calculated as the trawl distance covered × net horizontal opening. Trawl distance covered was calculated using the *geodist* package (Padgham & Sumner 2025) in R (version 4.5.1; R Core Team 2025). For calamari pre-season surveys, net horizontal opening was derived from the distance between trawl doors (Seafish 2010), except for July 2026 when Marport sensors were fitted to the extremities of the survey vessel's trawl net wings (Chemshirova *in prep.*). For groundfish surveys, the triangulation method that derives net horizontal opening from the distance between trawl doors is unsuitable because the geometry of the net is different (Ramos et al. 2024b). Since 2016, groundfish survey net horizontal opening has instead been measured directly from Marport sensors fitted to the extremities of the survey vessel's trawl net wings. Generalised Additive Models (GAMs; Wood 2017) were fitted using the *mgcv* package (Wood 2011) in R (version 4.5.1; R Core Team 2025) to calculate net horizontal opening when this was not recorded due to failure of the Marport sensors. Smooths were estimated by restricted maximum likelihood (REML; Wood 2011). The model assumed Gaussian distribution of the residuals and used an identity link. Smooth terms were used for door spread, net vertical opening, trawl speed, and depth, which were treated as random effects.

Yearly trawl biomass densities were extrapolated to the survey area combining the finfish zone (122,493.7 km^2) and 'Loligo Box' (31,296.9 km^2), partitioned into grids of 5×5 km^2. Position coordinates of trawls were converted to WGS 84 projection in UTM sector 21, and extrapolation was calculated using an inverse distance weighting algorithm (Winter 2019). The basic inverse distance weighting algorithm assigns a value *u* to any grid location *x* that is the weighted mean of a known scattered set of points x_i according to the inverse of the *i* points' distances from the grid location *x*:

$$u(\mathrm{x}) = \begin{cases} \dfrac{\sum_{i=1}^{N} w_i(\mathrm{x}) u_i}{\sum_{i=1}^{N} w_i(\mathrm{x})}, & \text{if } d(\mathrm{x}, \mathrm{x_i}) \neq 0 \\ u_i, & \text{if } d(\mathrm{x}, \mathrm{x_i}) = 0 \end{cases}$$

where

$$w_i(\mathrm{x}) = \frac{1}{d(\mathrm{x}, \mathrm{x_i})^p}$$

The power parameter *p* (a positive real number) adjusts the weight of points x_i as a function of distance (x, x_i); higher values of *p* put higher influence on the points x_i closest to a given interpolated point *x*. For this survey analysis, an empirical approach to selecting *p* was

used running the inverse distance weighting algorithm with *p* values from 1 to 25 by 0.25, and for each *p* calculating the aggregate of log proportional differences between the empirical values of density at every trawl and the interpolation at every trawl from all other trawls. The lowest aggregate of log proportional differences corresponded to the best *p* value. Because some points may be more clustered than others, an isolation parameter was assigned attributing more weight to points x_i in proportion to being further away from any other point x_i. Isolation parameters (*s*) per yearly survey were calculated as the standardised mean of distances between each point x_i and all other points x_j:

$$s(\mathrm{x_i}) = \overline{d(\mathrm{x_i}, \mathrm{x_j})}$$

An additional weighting factor was included to adjust for trawl differences in area coverage. Survey trawls are generally standardised (60 min duration in groundfish surveys and 120 min in calamari pre-season surveys) but may be shortened on immediate notice for reasons that include unmanageably large concentrations of fish accumulating in the net. Such instances will result in the trawl being stopped just when its biomass density is maximised, rather than being stopped independently of the biomass density, and thereby create a potential bias of the density estimate at that location. For shoaling fish in sparse, highly aggregated distributions, the effect can be substantial (i.e., hoki; Ramos & Winter 2022b). However, the trawl itself is not an error record that should be invalidated and removed from the data set. To mitigate the potential bias effect, the swept area of each trawl was taken as a proportional weighting parameter so that a shortened trawl covering, for example, only half as much ground would have only half as much weight. Like the isolation parameters $s(\mathrm{x_i})$, the area parameters $a(\mathrm{x_i})$ were standardised (divided by their mean among all trawls), then $s(\mathrm{x_i})$ and $a(\mathrm{x_i})$ were added together and divided again by their sum to give a factor centred on 1. The revised inverse distance weighting factor is:

$$w_i(\mathrm{x}) = \left(\frac{\left(\frac{s(\mathrm{x_i}) + a(\mathrm{x_i})}{\overline{(s(\mathrm{x_i}) + a(\mathrm{x_i}))}} \right)}{d(\mathrm{x}, \mathrm{x_i})} \right)^p$$

Distance $d(x, x_i)$ is inherently calculated as Euclidean (straight-line) distance. However, the survey area surrounds the Falkland Islands and between two remote points a fish or ship would have to travel a real distance longer than straight-line; circumnavigating the landmass. Therefore, an axial loop was drawn through the survey area (Fig. 1), and $d(x, x_i)$ was defined as the longer of either the Euclidean distance between *x* and x_i, or the distance on the axial loop between its two points respectively closest to *x* and x_i (Winter 2019).

As an extrapolation algorithm, calculated biomass over a given area will depend on the spatial distribution of surveyed densities, not just their total or mean value. Accordingly, the total biomass (deterministic biomass) is considered an estimate. Densities were interpolated over the same area for all species.

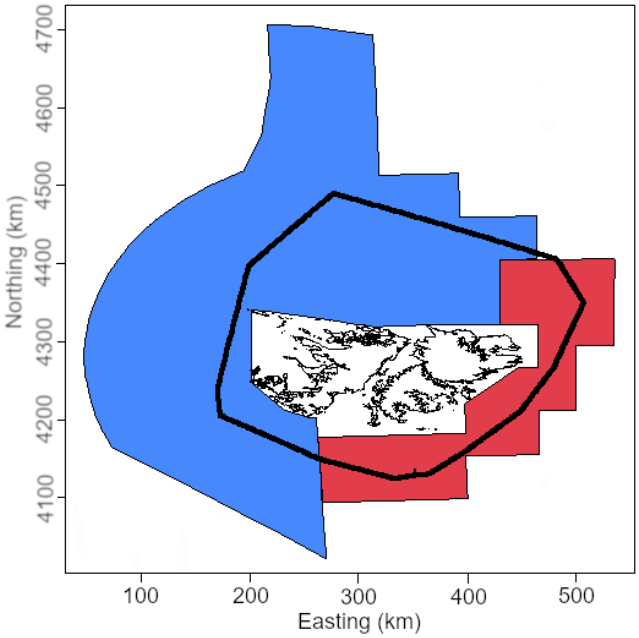

Fig. 1. Groundfish (blue) and calamari pre-season (red) survey areas, with axial loop (black line) used to define relative distances for the inverse distance weighting algorithm.

Uncertainty of the biomass estimate was calculated by a hierarchical bootstrap algorithm. First, survey trawls and their catches were randomly re-sampled with replacement for 10,000 iterations; each year's groundfish survey and parallel calamari pre-season survey were re-sampled separately so that both 'halves' of the survey area retained about the same relative coverage. Second, each re-sampled trawl was given a random uniform re-assignment of its coordinate position between start latitude and longitude and end latitude and longitude. Third, the isolation parameters were re-calculated for the randomised set of trawl data, and the inverse distance weighted algorithm re-applied. One iteration might thus re-sample any trawl twice or more, but each would have a slightly different position. The 95% confidence intervals (CI) of the 10,000 bootstrap iterations were used to infer uncertainty.

3.4. Temporal changes in biomass

3.4.1. Current year to baseline biomass comparisons

The difference in biomass across the 10,000 bootstrap samples was computed to assess the change in biomass of each species in the most recent year (2026) relative to a baseline year:

1) the most recent year (2026) relative to the first year (2017) in the time series. For July, the groundfish and calamari pre-season surveys were conducted in parallel for the first time in 2017. Therefore, 2017 was taken as the year one for comparative purposes. However, it must be noted that commercial fisheries have been conducted in the Southwest Atlantic for several decades already (Falkland Islands Government 1989), and that the state of the stocks in 2017 does not represent virgin stocks.

2) the most recent year (2026) relative to the previous year (2025) in the time series, and

3) the most recent year (2026) relative to the 2023–2025 mean. The three-year mean (2023–2025) minimises the influence of interannual variability in recent years, providing a more stable reference against which to assess the 2026 estimate. A total of 10,000 mean values were calculated from the respective 10,000 biomass samples from 2023, 2024, and 2025. These 10,000 mean values were then compared with the 10,000 biomass samples derived from 2026.

The change in biomass was calculated using the equation:

$$\Delta biomass = \frac{b.current}{b.baseline}$$

where *Δbiomass* is the ratio between *b.current* and *b.baseline*; *b.current* is the biomass calculated for the most recent year, i.e., 2026; *b.baseline* is the biomass calculated for the baseline year, i.e., 2017, 2025, 2023–2025 mean. *Δbiomass* > 1.0 indicates that *b.current* is higher than *b.baseline*, and therefore there was an increase in biomass in the current year compared to the baseline year, i.e., *Δbiomass* = 2.0 indicates a two-fold increase in biomass in the current year compared to the baseline year. *Δbiomass* = 1.0 indicates that *b.current* and *b.baseline* are equal, and therefore there was no change in biomass in the current year compared to the baseline year. *Δbiomass* < 1.0 indicates that *b.current* is lower than *b.baseline*, and therefore there was a decrease in biomass in the current year compared to the baseline year, i.e., *Δbiomass* = 0.5 indicates that the biomass in the current year corresponds to 50% of the biomass of the baseline year.

This method circumvented assumptions of normality and homogeneity of variance, which were violated by the distribution of biomass for certain species in some years. A difference was considered statistically significant if the 95% CI of the bootstrap distribution of differences excluded zero, indicating a deviation from equality. The Holm's method was used to control for the family-wise error rate across the three year-to-baseline comparisons, reducing the risk of Type I errors (false positives) by adjusting the p-value threshold (Holm 1979):

$$p_{adjusted} = \frac{\alpha}{m} = \frac{0.05}{3} = 0.017$$

where *α* is the significance level, and *m* is the number of tests (three comparisons: 2026 vs 2017, 2026 vs 2025, and 2026 vs 2023–2025 mean). The three comparisons are not independent, as they share the 2026 bootstrap samples and 2025 contributes to the 2023–2025 mean. Holm's method does not assume independence and controls the family-wise error rate under any dependence structure (Holm 1979), although it is conservative when tests are positively correlated.

3.4.2. Temporal biomass trends

Temporal trends in annual biomass were modelled using Generalised Additive Models (GAMs; Wood 2017) fitted with the *mgcv* package (Wood 2011) in R (version 4.5.1; R Core Team 2025).

The error distribution for each species-specific GAM was chosen using the skewness of its full bootstrap biomass distribution (n = 70,000 replicates: 10,000 replicates × 7 years) as

an initial guide, with the final family confirmed by comparing model fit (AIC) and residual diagnostics. Skewness quantifies the asymmetry of a distribution around its mean, with positive values indicating a longer right tail, negative values a longer left tail, and a value of zero denoting a perfectly symmetric distribution. Skewness was calculated for each species using the skewness function from the *moments* package (Komsta & Novomestky 2022) in R (version 4.5.1; R Core Team 2025). Most species exhibited right-skewed biomass distributions: i.e., Argentine shortfin squid (1.34), southern blue whiting (2.24), kingclip (2.08), rock cod (0.498), southern hake (2.07), red cod (1.32), Patagonian squid (0.736), Patagonian toothfish (0.541), banded whiptail grenadier (1.38), and hoki (2.12), with the exception of common hake (-0.307). As a starting point, a Gamma error distribution with a log link was considered for right-skewed (skewness > 1) and moderately right-skewed (0.5–1.0) species, and a Gaussian error distribution with an identity link for approximately symmetric species (skewness < 0.5); the final distribution for each species was confirmed by selecting the model with the lowest AIC and the best overall fit.

For each species, annual biomass was modelled as a smooth function of year using a penalised cubic regression spline (bs = "cr"), fitted by REML (Wood 2011). The basis dimension was set to k = 5 to prevent over-fitting given the relatively short time series (7 years: 2017, 2020, and 2022–2026).

To account for inter-annual differences in estimation uncertainty, observation weights were applied during model fitting, as initial unweighted fits indicated that some years dominated the smoother for some species. Weights were normalised within each species so that the maximum weight equalled one, ensuring numerical stability (Wood 2017). The weighting scheme was matched to the error family to maintain consistency between the assumed variance structure and the down-weighting of high-uncertainty years. For Gamma-family models, the normalised inverse coefficient of variation (CV) was used as the observation weight, as CV measures relative variability and is therefore consistent with the Gamma variance structure, in which variance is proportional to the square of the mean (Ver Hoef & Boveng 2007). For Gaussian-family models, the inverse variance and the square root of the inverse variance were examined as candidate weights; as no individual years disproportionately dominated the unweighted fits, the unweighted model was retained.

Four candidate model configurations were evaluated for each species, combining each error family (Gamma, Gaussian) with each weighting scheme (weighted, unweighted; Table II). Models were compared using the Akaike Information Criterion (AIC; Akaike 1974) and ΔAIC relative to the best model for each species. The preferred model was the one with the lowest AIC among the family–weight combinations appropriate for the species' skewness. R^2_{adj}, DE% and the F-test for the year smooth were used to interpret model fit and to support model selection. The model with the higher R^2_{adj} and DE% was preferred where candidate models had similar AIC values. R^2adj and DE% indicate the proportion of variation in biomass explained by the year smooth, and the F-test p-value indicates whether biomass showed a significant temporal trend ($p < 0.05$). The adequacy of the basis dimension *k* was verified using the *k*-index diagnostic (Wood 2017); a *k*-index substantially below 1.0 with a significant p-value (< 0.05) would indicate that the smoother was overly constrained and that *k* should be increased. The selected model for each species was used to generate fitted biomass trends and 95% CI calculated as the linear predictor ± 1.96 × SE on the link scale and back-transformed with the inverse link function, yielding year-specific trend estimates on the original biomass scale.

Table II. Candidate generalised additive model configurations evaluated to assess the biomass trend for each species. All models included a penalised cubic regression spline smoother of year (bs = "cr", *k* = 5) fitted by restricted maximum likelihood (REML).

Model	Family	Link	Smoother	Weighing
M1	Gamma	Log	s(Year)	Unweighted
M2	Gamma	Log	s(Year)	Normalised inverse coefficient of variation
M3	Gaussian	Identity	s(Year)	Unweighted
M4	Gaussian	Identity	s(Year)	Square-root normalised inverse variance

3.5. Spatial changes in biomass

The difference in density was computed for each grid (5×5 km^2) of the survey area to assess the change in biomass density of each species in the most recent year (2026) relative to a baseline year:

1) the most recent year (2026) relative to the first year (2017) in the time series. For July, the groundfish and calamari pre-season surveys were conducted in parallel for the first time in 2017. Therefore, 2017 was taken as the year one for comparative purposes. However, it must be noted that commercial fisheries have been conducted in the Southwest Atlantic for several decades already (Falkland Islands Government 1989), and that the state of the stocks in 2017 does not represent virgin stocks.

2) the most recent year (2026) relative to the previous year (2025) in the time series, and

3) the most recent year (2026) relative to the 2023–2025 mean. The three-year mean (2023–2025) minimises the influence of interannual variability in recent years, providing a more stable reference against which to assess the 2026 estimate. A mean density value was calculated for each grid from the 2023, 2024, and 2025 grid density values. The mean grid density values were then compared with the grid density from 2026.

The change in biomass density was calculated using the equation:

$$\Delta density = \frac{b.current}{b.baseline}$$

where *Δdensity* is the ratio between *b.current* and *b.baseline* at a grid square*; b.current* is the biomass calculated at grid square for the most recent year, i.e., 2026; *b.baseline* is the biomass calculated at grid square for the baseline year, i.e., 2017, 2025, 2023–2025 mean. The 2023–2025 mean at grid square was calculated as the mean of the density at grid square in 2023, 2024, and 2025. *Δdensity* > 1.0 indicates that *b.current* is higher than *b.baseline*, and therefore there was an increase in biomass at grid square in the current year compared to the baseline year. *Δdensity* = 1.0 indicates that *b.current* and *b.baseline* are equal, and therefore there was no change in biomass at grid square in the current year compared to the baseline year. *Δdensity* < 1.0 indicates that *b.current* is lower than *b.baseline*, and therefore there was a decrease in biomass at grid square in the current year compared to the baseline year.

3.6. Biological sampling

Random samples of up to 100 individuals of each species were collected in each station and measured to the lowest 1 cm for finfish and to the lowest 0.5 cm for squid species. Dorsal mantle length was measured for Argentine shortfin squid and Patagonian squid (Calamari *D. gahi*). Total length was measured for common hake, kingclip, red cod (*Salilota australis*), rock cod, southern blue whiting, southern hake (*Merluccius australis*), and Patagonian toothfish. Pre-anal length was measured for banded whiptail grenadier (*Coelorinchus fasciatus*) and hoki. For finfish, macroscopic assessment of sex and maturity were conducted following an eight-stage maturity scale (Brickle et al. 2005, modified from Nikolsky 1963): 1, immature; 3, early developing; 4, late developing; 5, ripe; 6, running; 7, spent; 8, recovering spent; 2, resting. Except for Patagonian toothfish and rock cod, the finfish species assessed in this study are multiple batch spawners (Macchi et al. 2021; Brickle et al. 2006). Stage 2 (resting) denotes a post-spawning condition and is therefore presented last in developmental sequence. For squid, macroscopic assessment of sex and maturity were conducted following a six-stage maturity scale (Lipinski 1979): 1, young; 2, immature; 3, preparatory; 4, maturing; 5, mature; 6, spent.

The sampling of fish and squid was prioritised (sharks and skates included, although data on these taxa are not presented in the current report). Benthos sorting was conducted either concurrently with or following the sampling of the primary commercial species. Occasionally, small juvenile fish were encountered within the benthos samples after completing the processing of the 100 random samples, and therefore these were not included within the random samples.

3.7. Length composition

3.7.1. Length-weight relationship.

Length and weight data were retrieved from the FIFD database, records with missing length or weight values, or with length or weight values ≤ 0 were removed. Length measurements were rounded to the lower 0.5 cm for squids, and to the lower 1.0 cm for finfish. To capture the smaller range of sizes, individuals recorded as juveniles were randomly assigned to either female or male with equal probability (50:50) using a fixed random seed to ensure reproducibility.

Length-weight relationships were fitted separately for each species using the standard power function (Le Cren 1951):

$$W = a \cdot L^b$$

this was estimated via log-linearisation, fitting ordinary least squares regression of the form:

$$ln(W) = ln(a) + b \cdot ln(L)$$

where W is total weight (g), L is length (cm), a is the condition factor, and b is the allometric growth coefficient (Froese 2006).

An initial length-weight model was fitted per species, and observations with absolute standardised residuals exceeding 2.5 were excluded (Froese 2006). Biologically implausible lengths were also excluded, which arose mainly from the wrong length type being recorded (e.g., total length instead of pre-anal length for grenadiers and hoki) or from data entry errors. Fewer than 2% of length records were removed per species, resulting in between 5,462 (banded whiptail grenadier) and 309,052 (Argentine shortfin squid) length-weight records retained for further analyses. Final length-weight parameters were estimated by refitting the model on the cleaned dataset, and the fitted power curves were overlaid on scatter plots of the observed data for each species (Appendix I). Plots were produced using the *ggplot2* (Wickham 2016) and the *patchwork* packages (Pedersen 2024) in R (version 4.5.1; R Core Team 2025). Final length-weight parameters were used to calculate weight (g) from length (cm) for each species random samples collected during the surveys.

3.7.2. Overall length composition

Biomass-at-length distributions were constructed at the species, survey, and sex levels (all years pooled), and for each species × year × sex combination. Extrapolation of sample weight-at-length class to total biomass estimate was done by summing the weight of individuals in each length class and calculating the proportion of the weight in each length class to the total sample weight. This proportion was then applied to the biomass estimate to obtain an extrapolated biomass per length class, and per sex in length class.

3.7.3. Comparative length composition at the survey and sex levels

The proportional biomass-at-length distribution was computed to assess differences in the size composition between groundfish and calamari pre-season surveys, and between sexes. Overlap between pairs of biomass-at-length distributions (groundfish vs. calamari pre-season surveys; females vs. males) was calculated following Swanson et al. (1974):

$$O = \left(1 - \frac{1}{2}\sum_{i=1}^{n} |p_{1i} - p_{2i}|\right) \times 100$$

where O is the overlap index (%), p_{1i} is the proportional biomass in length class i for group 1, p_{2i} is the proportional biomass in length class i for group 2, n is the total number of length classes, $\sum_{i=1}^{n} | p_{1i} - p_{2i} |$ is the sum of absolute differences across all length classes. The overlap index ranges from 0% (no overlap between distributions) to 100% (complete overlap).

Differences in the biomass-weighted mean length between groups were assessed using a weighted permutation test (10,000 permutations), in which the observed difference in biomass-weighted mean lengths between the two groups was compared against a null distribution generated by randomly permuting group labels while retaining the original biomass weights (Manly 2007). A fixed random seed was used to ensure reproducibility. The p-value was calculated as the proportion of permuted differences equal to or exceeding the absolute observed difference in weighted means, providing a two-tailed test of significance that requires no distributional assumptions.

For each species, survey, and sex biomass-at-length distribution, the biomass-weighted mean length was computed using the proportional biomass of each length class as weights, with its uncertainty expressed as the standard error of the weighted mean. The effective sample size (n_{eff}) was calculated as the inverse of the sum of squared biomass proportions ($n_{eff} = 1/\sum p_i^2$), which accounts for the unequal weighting of length classes and provides a more appropriate denominator for the standard error of the weighted mean than the raw count of length classes (Kish 1965). The standard error of the weighted mean was then computed as $SE = SD/\sqrt{n_{eff}}$. Biomass-weighted quantiles were calculated at the 0th, 2.5th, 50th, 97.5th, and 100th percentiles of the length distribution using proportional biomass as weights. Standard errors for all percentile estimates were derived by bootstrap resampling with replacement (10,000 resamples; Efron & Tibshirani 1993), with weights renormalised after each resample and the standard deviation of the bootstrap distribution taken as the standard error. All length metrics were rounded down to the nearest 0.5 cm for squids, and to the nearest 1.0 cm for finfish. Weighted quantiles and mean were calculated using the *Hmisc* package (Harrell 2024) in R (version 4.5.1; R Core Team 2025).

3.7.4. Yearly length composition

The yearly composition of biomass at length-class was analysed for each species. The biomass-weighted mean length, quantiles at the 0th, 2.5th, 50th, 97.5th, and 100th percentiles of the length distribution, and standard errors were calculated as per the previous section. To calculate modal length, GAM (Wood 2017) was fitted to the binned biomass-at-length class data (biomass per 0.5 cm length class for squids, and per 1.0 cm length class for finfish) using a Gaussian error distribution, with length class as the smooth predictor term:

$$B \sim s(length, k)$$

where *B* is the biomass per length class, *s* denotes a thin-plate regression spline (Wood 2003), and *k* is the maximum number of knots, set adaptively between 3 and 15 based on the number of unique length classes available per group. The modal length was extracted as the length class corresponding to the peak of the fitted GAM smooth. All GAMs were fitted by REML using the *mgcv* package (Wood 2011) in R (version 4.5.1; R Core Team 2025).

3.8. Sex and maturity composition

Biomass was extrapolated for each sex category (juvenile, female, male, and undetermined) for each species in every year, and expressed as a percentage of the total annual biomass for the species. Overall sex composition for each species was summarised as the mean annual proportion ± SE across the time series.

Sexual maturity composition was determined for each species, year and sex, with only females and males included. Individual weights were summed by maturity stage for each sex within each year and expressed as a percentage of the total sampled weight for that sex. Maturity stage proportions were additionally applied to the annual biomass estimate for each species to extrapolate biomass by maturity stage.

4. Results and Discussion

4.1. Bottom trawl stations

A total of 882 bottom trawls were conducted during the July groundfish and calamari pre-season surveys in 2017, 2020, and 2022–2026. In groundfish surveys, a range of 33 to 84 trawls were conducted, with catches between 32 and 163 t considering only the species assessed in this report. In calamari pre-season surveys, a range of 47 to 64 trawls were conducted, with catches between 147 and 644 t considering only the species assessed in this report.

In 2026, a total of 84 trawls (163 t) were conducted in the groundfish survey aboard the *F.V.* Argos Vigo (ZDLU1), and 64 trawls (325 t) were conducted in the calamari pre-season survey aboard the *F.V.* Sil (ZDLR1; Table III).

4.2. Biomass estimates

For several species in July 2026, the 10,000 biomass sample iterations showed a Gaussian distribution (Fig. 2). For these species, the deterministic, mean, and median biomass estimates were in close agreement, indicating that the biomass distributions were approximately symmetrical and that any of the three biomass estimates can be considered reliable (Fig. 2). For Patagonian squid and Patagonian toothfish, the deterministic (146,260 t and 6,965 t, respectively) diverged from the mean (97,190 t and 10,161 t, respectively) and the median (97,820 t and 10,363 t, respectively) estimates. For banded whiptail grenadier, southern blue whiting and southern hake, the 10,000 biomass samples had multimodal distributions, and the deterministic value was considerably below the mean and the median biomass estimates due to left-skewed biomass distribution. In these cases, where the biomass distribution was skewed, the median was considered the most appropriate estimate as it is robust to extreme values and represents more appropriately the central tendency. Therefore, the median was selected to describe patterns of biomass through time and biomass-related calculations for all species, as for February parallel demersal surveys from 2010, 2011, and 2015–2026 (Ramos 2026).

Biomass estimates from the July parallel demersal surveys conducted in 2017, 2020, and 2022–2026 were as low as 59.30 t (34.75 – 81.80 t) for the Argentine shortfin squid in 2022 and as high as 752,687.46 t (514,497.46 – 990,071.28 t) for common hake in 2022. In 2026, the lowest estimate of biomass was for southern blue whiting with 923.60 t (318.59 – 1,273.75 t), and the highest estimate of biomass was for common hake with 662,873.79 t (586,286.16 – 760,614.12 t; Table IV).

Of the 11 species assessed, four species exhibited signs of increasing biomass (Argentine shortfin squid, common hake, Patagonian toothfish, and southern hake), three species exhibited signs of decreasing biomass (hoki, Patagonian squid, and red cod), and four species did not exhibit temporal biomass trends (banded whiptail grenadier, kingclip, rock cod, and southern blue whiting; Table V).

Table III. July groundfish and calamari pre-season surveys information. Catches per survey and combined total include Argentine shortfin squid, banded whiptail grenadier, common hake, hoki, kingclip, Patagonian squid, Patagonian toothfish, red cod, rock cod, southern blue whiting, and southern hake.

Year	Groundfish survey				Calamari pre-season survey				Total	
	Vessel (Callsign)	No. of trawls	Trawls excluded	Catch (t)	Vessel (Callsign)	No. of trawls	Trawls excluded	Catch (t)	No. of trawls	Catch (t)
2017	Castelo (ZDLT1)	74	NA	37.65	Igueldo (ZDLE1)	59	930-933	460.61	133	498.26
2020	Castelo (ZDLT1)	33	3179-3195	32.43	Beagle F.I. (ZDLZ)	55	NA	643.92	88	676.35
2022	Castelo (ZDLT1)	63	NA	79.28	Argos Pereira (ZDLO1)	59	NA	488.19	122	567.47
2023	Castelo (ZDLT1)	70	NA	71.65	Montelourido (ZDLC4)	56	NA	358.45	126	430.1
2024	Castelo (ZDLT1)	76	NA	109.58	Robin M. Lee (ZDLZ1)	47	NA	146.52	123	256.1
2025	Argos Vigo (ZDLU1)	82	NA	144.84	Prion (ZDLS4)	60	NA	368.75	142	513.59
2026	Argos Vigo (ZDLU1)	84	NA	162.74	Sil (ZDLR1)	64	NA	324.7	148	487.44

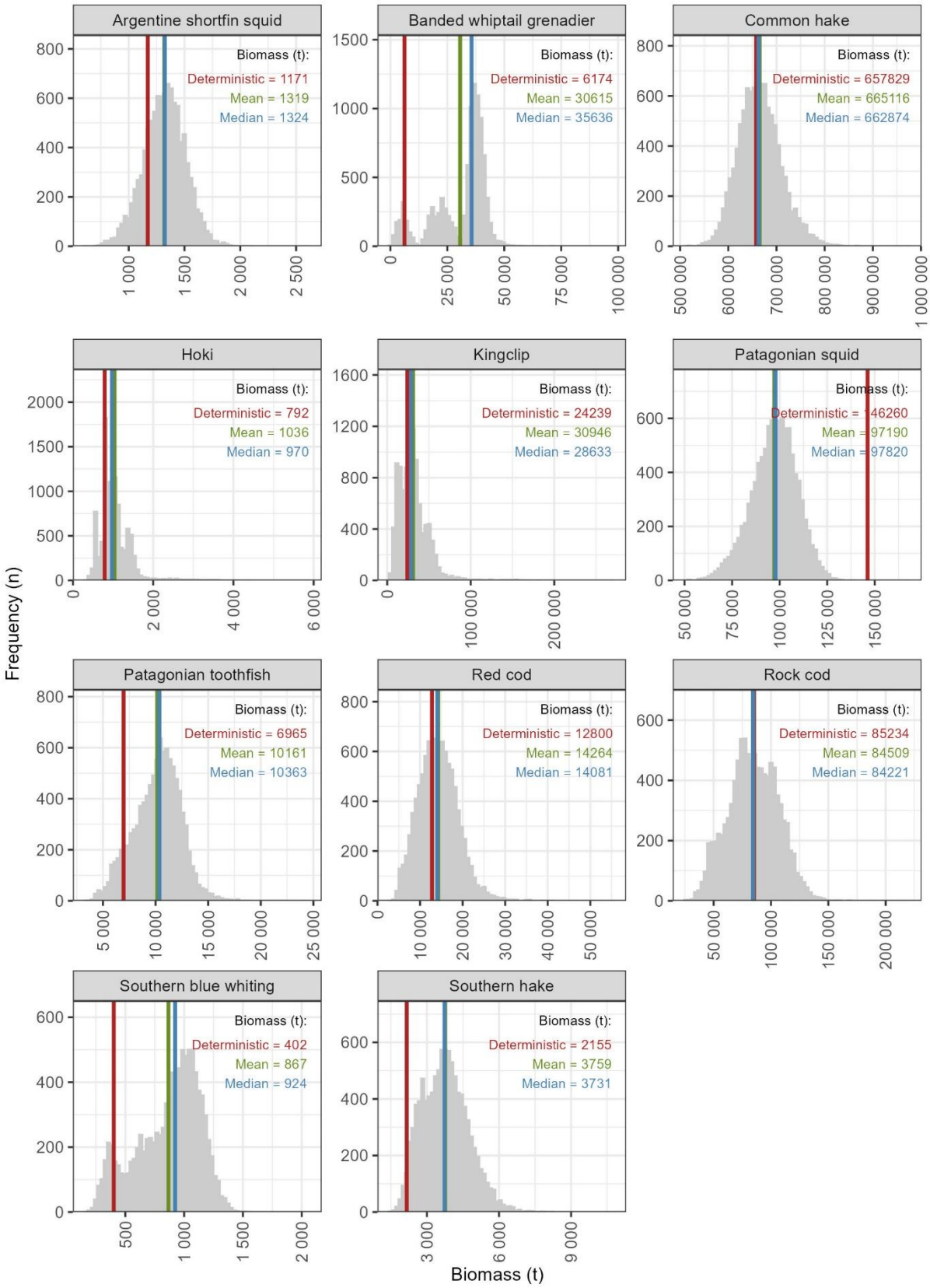

Fig. 2. Biomass (t) distribution of the 10,000 bootstrap samples estimated from July 2026 groundfish and calamari pre-season surveys conducted in Falkland Islands waters. Deterministic, mean, and median biomasses are indicated by the red, green, and blue vertical lines, respectively.

Table IV. Biomass estimates (t; median) of main commercial species during the July 2017, 2020, and 2022–2026 groundfish and calamari pre-season surveys in Falkland Islands waters. The 95% confidence intervals are indicated in parentheses.

Year	Argentine shortfin squid	Banded whiptail grenadier	Common hake	Hoki
2017	140.98 (92.98-191.07)	91.46 (2.99-235.54)	116485.35 (94883.33-149313.91)	85477.47 (26258.16-159761.23)
2020	60.45 (32.70-86.69)	15411.90 (848.25-22931.73)	363223.52 (241976.86-494774.17)	41280.57 (7619.52-64130.09)
2022	59.30 (34.75-81.80)	12220.06 (3388.30-16623.02)	752687.46 (514497.46-990071.28)	2546.38 (155.50-4916.82)
2023	100.93 (56.71-139.63)	95.36 (13.95-137.16)	390348.32 (287297.91-474558.82)	946.52 (432.78-2014.46)
2024	346.58 (216.33-482.69)	2112.14 (363.50-3353.74)	590438.07 (490165.40-699467.03)	2657.99 (881.37-4834.04)
2025	728.30 (415.47-1007.14)	11010.13 (3817.99-15225.75)	713098.27 (508225.35-907855.14)	3685.84 (808.34-7827.01)
2026	1323.96 (941.62-1670.18)	35636.30 (3410.47-44377.82)	662873.79 (586286.16-760614.12)	970.16 (535.38-1938.16)

Table IV. *continued*

Year	Kingclip	Patagonian squid	Patagonian toothfish	Red cod
2017	19021.55 (5170.30-33657.94)	344472.91 (247893.93-435232.46)	1323.17 (1060.57-1597.51)	12079.24 (6420.61-17896.36)
2020	35502.58 (20331.17-50260.38)	277792.59 (211454.59-364202.28)	7745.96 (2613.27-9762.09)	39343.25 (6320.91-68377.24)
2022	18685.80 (8635.13-40125.23)	215027.95 (176919.40-256330.86)	1249.57 (803.53-1685.00)	27347.06 (4607.76-46783.62)
2023	28655.49 (7630.35-65456.91)	135962.61 (107499.58-161883.97)	510.28 (335.03-669.12)	37433.94 (4422.53-77296.16)
2024	33582.21 (6923.31-82590.52)	75242.93 (63743.43-85857.67)	2117.95 (1422.84-2645.95)	25373.79 (9768.25-38396.31)
2025	61942.50 (5669.78-140754.91)	125153.80 (101861.17-149299.02)	9825.53 (7891.53-11348.41)	20832.07 (12034.34-30481.08)
2026	28633.11 (8154.03-69826.45)	97819.97 (71807.92-119014.17)	10363.00 (5695.34-14137.75)	14080.62 (6079.20-23963.28)

Table IV. *continued*

Year	Rock cod	Southern blue whiting	Southern hake
2017	50826.44 (32112.03-66518.09)	1556.92 (338.45-2675.77)	511.89 (213.85-716.95)
2020	5778.33 (4279.70-7473.88)	9229.48 (505.15-13409.20)	200.18 (1.74-391.60)
2022	52263.40 (19950.60-91307.58)	415.68 (184.60-753.75)	687.89 (0.00-866.85)
2023	31140.60 (12630.26-46731.41)	1314.07 (572.04-2201.07)	101.52 (0.00-269.56)
2024	49433.33 (24664.36-71873.45)	325.09 (203.98-440.72)	287.62 (128.37-432.01)
2025	90882.26 (49956.90-138520.77)	324.10 (73.39-496.23)	1146.05 (549.18-1639.73)
2026	84220.92 (44498.95-124881.03)	923.60 (318.59-1273.75)	3730.83 (2180.52-5755.89)

Table V. Indicators of change in biomass in 2026 relative to the 2017, 2025, and the 2023–2025 mean biomasses, and over the period 2017 to 2026, derived from July groundfish and calamari pre-season surveys in Falkland Islands waters. Indicators 2026 vs 2017, 2026 vs 2025, and 2026 vs 2023–2025 mean are ratios of biomass and represent the magnitude of change. Increases and decreases are indicated by + and −, respectively*. Significant results are shown in bold: Holm-adjusted $p < 0.017$ for the three year-to-baseline comparisons (Holm 1979), and $p < 0.05$ for the GAM trend.

Species	Biomass 2017 (t)	Biomass 2025 (t)	Biomass 2023–2025 mean (t)	Biomass 2026 (t)	2026 vs 2017	2026 vs 2025	2026 vs 2023–2025 mean	GAM 2017–2026 (*p* value)
Argentine shortfin squid	140.98	728.30	391.94	1323.96	**+9.39**	**+1.82**	**+3.38**	**0.002; +**
Banded whiptail grenadier	91.46	11010.13	4405.88	35636.30	**+389.66**	+3.24	+8.09	0.318
Common hake	116485.35	713098.27	564628.22	662873.79	**+5.69**	-0.930	+1.17	**0.015; +**
Hoki	85477.47	3685.84	2430.12	970.16	**-0.011**	-0.263	-0.399	**0.004; -**
Kingclip	19021.55	61942.50	41393.40	28633.11	+1.51	-0.462	-0.692	0.286
Patagonian squid	344472.91	125153.80	112119.78	97819.97	**-0.284**	-0.782	-0.872	**0.008; -**
Patagonian toothfish	1323.17	9825.53	4151.25	10363.00	**+7.83**	+1.05	**+2.50**	**0.023; +**
Red cod	12079.24	20832.07	27879.93	14080.62	+1.17	-0.676	-0.505	**0.043; -**
Rock cod	50826.44	90882.26	57152.07	84220.92	+1.66	-0.927	+1.47	0.185
Southern blue whiting	1556.92	324.10	654.42	923.60	-0.593	+2.85	+1.41	0.193
Southern hake	511.89	1146.05	511.73	3730.83	**+7.29**	**+3.26**	**+7.29**	**0.037; +**

* For interpretation, the value -0.930 for common hake in 2026 vs 2025 indicates that the 2026 biomass was 93% of the 2025 biomass, a 7% decrease (100-93 = 7; negative symbol indicating the decrease). In contrast, the positive value +5.69 for common hake in 2026 vs 2017 indicates that the 2026 biomass was 5.69 times the 2017 biomass

4.3. Species summaries

4.3.1. Argentine shortfin squid (*Illex argentinus*)

4.3.1.1. Temporal patterns of abundance

On average, 62% of the total Argentine shortfin squid catches in the time series were from groundfish surveys and 38% were from calamari pre-season surveys. The lowest catch was reported in 2020 (0.014 t). The highest catch was reported in 2026 (0.212 t), representing a nearly ten-fold increase relative to the 2017 catch (0.022 t), a 7% increase relative to the 2025 catch (0.198 t), and a nearly two-fold increase relative to the 2023–2025 mean catch (0.090 t; Fig. 3a; Appendix II).

The highest densities occurred in 2026 (mean ± SE: 5.34 ± 1.00 kg/km²), representing a nearly eight-fold increase relative to the 2017 densities (0.68 ± 0.14 kg/km²), a 25% increase relative to the 2025 densities (4.29 ± 1.51 kg/km²), and a nearly three-fold increase relative to the 2023–2025 mean (2.12 ± 0.57 kg/km²; Fig. 3b).

The highest biomass in the time series was estimated for 2026 (1,323.96 t; CI = 941.62–1,670.18 t), representing a nearly a nine-fold increase relative to the 2017 levels (140.98 t; CI = 92.98–191.07 t), a nearly two-fold increase relative to the 2025 biomass (728.30 t; CI = 415.47–1,007.14 t), and a nearly three-fold increase relative to the 2023–2025 mean (391.94 t), with all comparisons being statistically significant ($p < 0.05$; Fig. 3c; Table IV–V; Appendix III–IV). Analysis of the full time series revealed a strong and significant increasing trend in biomass (GAM: edf = 3.94, F = 640.37, p = 0.002), with the fitted model explaining 99.9% of the deviance (R^2 adj. = 0.998; Fig. 3c; Appendix V).

4.3.1.2. Spatial patterns of abundance

In 2026, *I. argentinus* was distributed in small densities mainly through the west, and the highest density (102 kg/km^2) was observed to the north-west at approximately 50°S and 61.7°W, near the western limit of the FICZ. Similar patterns of spatial distribution were observed in 2017, 2024 and 2025, with the main aggregations further south at approximately 51°S and 62°W near the 200 m isobath. The highest density in the full time series was reported in 2025 (201 kg/km^2; Fig. 4).

Analysis of the spatial change in density revealed minor density increase over the survey area, with the main increase in the west. Densities in 2026 relative to 2017 increased through the west in the FICZ/FOCZ and in discrete areas of the ‘Loligo Box’. Densities in 2026 relative to 2025, and relative to the 2023–2025 mean, increased in patchy areas to the north-west in the FICZ and in the south of the ‘Loligo Box’. Densities declined near the western limit of the FICZ and in discrete areas along the ‘Loligo Box’ (Fig. 5).

4.3.1.3. Length composition

Across all survey years combined, dorsal mantle length of the Argentine shortfin squid was in the range of 4.5 to 35.0 cm; however, 95% of the estimated biomass was comprised of individuals between 8.0 and 32.5 cm, with median and mean lengths (± SE) of 12.5 ± 0.94 cm and 14.0 ± 1.23 cm, respectively (Fig. 6a).

The distribution of biomass proportions by size class exhibited a 40% overlap between the groundfish and calamari pre-season surveys. Individuals from the groundfish survey (mean ± SE: 13.5 ± 1.30 cm) were significantly smaller than those from the calamari pre-season survey (mean ± SE: 16.5 ± 0.87 cm; p = 0.032). In the groundfish survey, 95% of the biomass of Argentine shortfin squid was comprised of individuals between 8.0 and 33.0 cm (median ± SE: 12.0 ± 0.87 cm). In the calamari pre-season survey, 95% of the biomass was comprised of individuals between 11.5 and 26.5 cm (median ± SE: 16.0 ± 0.73 cm; Fig. 6b).

The distribution of biomass proportions by size class exhibited a 91% overlap between females and males. The permutation analysis revealed that females (mean ± SE: 15.0 ± 1.38 cm) were significantly larger than males (mean ± SE: 12.0 ± 0.70 cm; p = 0.023). For females, 95% of the biomass was comprised of individuals between 8.0 and 33.5 cm (median ± SE: 12.5 ± 1.08 cm). For males, 95% of the biomass was comprised of individuals between 8.0 and 19.0 cm (median ± SE: 12.0 ± 0.86 cm; Fig. 6c).

Through the time series, the distribution of the biomass-at-length class was broad and multimodal, with the smallest length-group exhibiting a modal length at 9.5–12.0 cm. Additional length-groups may have been present at larger sizes but they were not clearly distinguished because of overlap in size distributions and due to the small number of individuals (Fig. 7). In 2026, dorsal mantle length was in the range of 5.5 to 35.0 cm; however, 95% of the biomass was comprised of individuals between 8.0 and 33.0 cm, with median and mean lengths (± SE) of 11.5 ± 0.56 cm and 13.5 ± 1.09 cm, respectively. For females, 95% of the biomass was comprised of individuals between 8.0 and 33.0 cm, with median and mean lengths (± SE) of 12.0 ± 0.98 cm and 15.5 ± 1.80 cm, respectively. For males, 95% of the biomass was comprised of individuals between 8.0 and 16.5 cm, with median and mean lengths (± SE) of 11.5 ± 0.76 cm and 11.5 ± 0.65 cm, respectively (Fig. 7).

Analysis of the full time series revealed non-significant temporal trends in either mean (GAM: edf = 4.86, F = 83.59, p = 0.083, R^2 adj. = 0.986, DE = 99.7%) or median (GAM: edf = 1.00, F = 3.27, p = 0.130, R^2 adj. = 0.248, DE = 39.5%) dorsal mantle length. Despite the absence of a statistically significant trend, the fitted smooths captured moderate interannual variability for mean length, with both mean and median lengths declining from approximately 15.0 cm in 2017 to 11.5–13.5 cm in 2026 (Fig. 8).

4.3.1.4. Sex and maturity composition

The sex composition of Argentine shortfin squid was consistently dominated by females (mean ± SE: 58.7 ± 1.0%), followed by males (41.1 ± 1.1%), and juveniles (0.1 ± 0.1%; recorded only in 2020 and 2025) throughout the time series. In 2026, the sex composition consisted of 55% females and 45% males (Fig. 9).

Maturity composition was similar for females and males throughout the time series. Females were predominantly young or immature in most years (≥ 69%); preparatory females were ≤ 23%, and maturing and mature females rarely exceeded 14% combined. Males were predominantly young or immature in most years (47–100%); maturing or mature males generally occurred in low proportions (≤ 15%), except for 2020 (39%; Fig. 10).

4.3.1.5. Discussion

Across the full time series, biomass of Argentine shortfin squid increased significantly in July parallel surveys, in contrast with the lack of trend in February surveys (Ramos 2026) and with the flat, non-significant trend in commercial CPUE from 1984–2019 (LOESS-smoothed; Arkhipkin et al. 2022a). It must be noted that this species is primarily captured by commercial jiggers during the first half of the year when it is more abundant in Falkland Islands waters (Falkland Islands Government 2026). The July increase in biomass was driven by a higher proportion of females (~ 59%) than males (~ 41%), predominantly young, immature, and of small size; a composition that remained consistent throughout the time series. Size at recruitment and at maturity also showed no significant change in the commercial fishery over 1984–2019 (Arkhipkin et al. 2022a), indicating size stability.

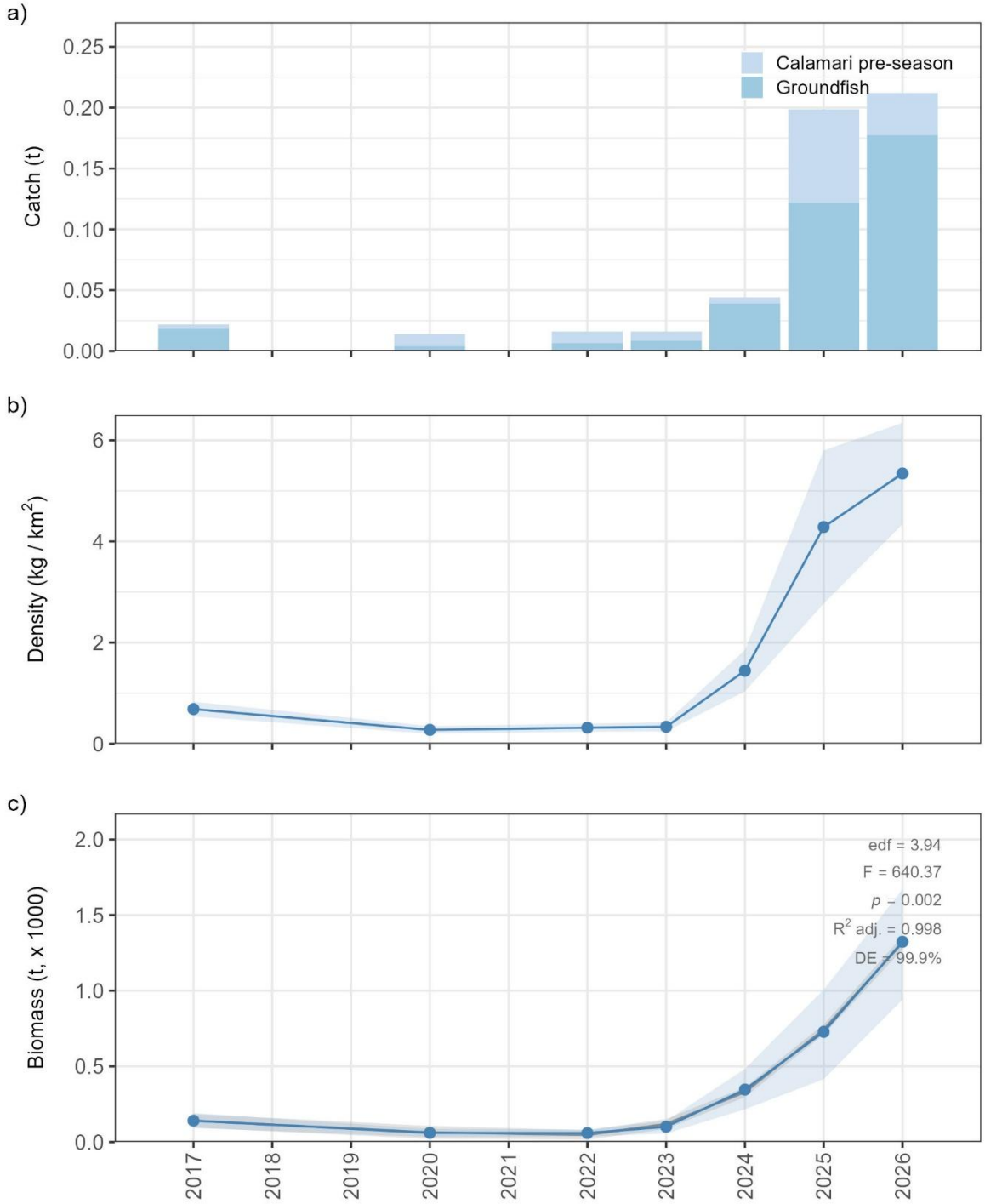

Fig. 3. Abundance of Argentine shortfin squid (*Illex argentinus*) during July groundfish and calamari pre-season surveys conducted in Falkland Islands waters in 2017, 2020, and 2022–2026. (a) Catch per survey, (b) annual mean density ± SE represented by the blue line and shaded region, respectively, and (c) estimated biomass, where the blue line and shaded region represent the median and 95% pointwise confidence interval derived from 10,000 bootstrap biomass estimates, and the grey line and shaded region represent the fitted Generalised Additive Model (GAM) smooth and its 95% pointwise confidence interval.

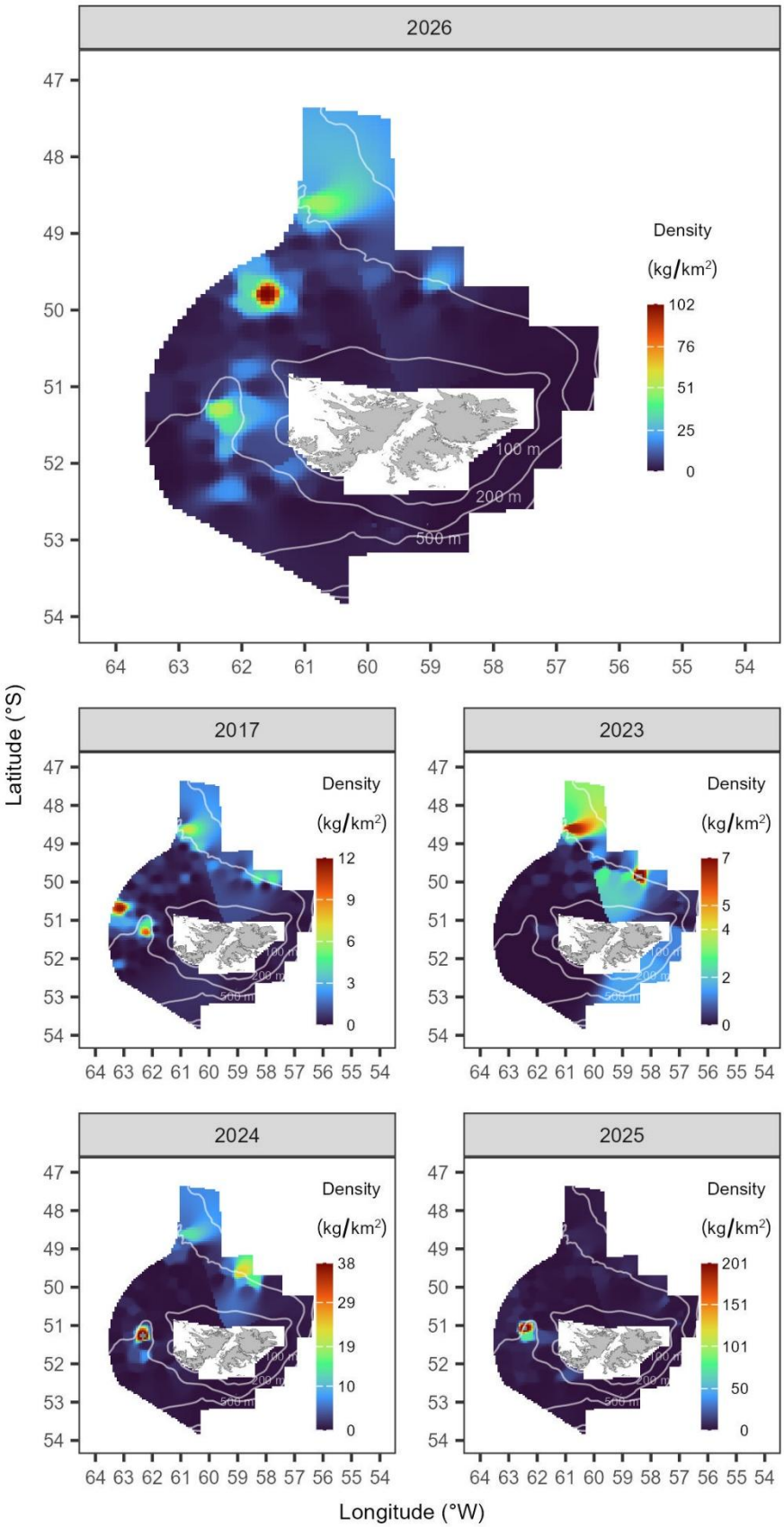

Fig. 4. Density distribution of the Argentine shortfin squid (*Illex argentinus*) derived from the July 2026 groundfish and calamari pre-season surveys in Falkland Islands waters, compared with the first year of the time series (2017) and the three preceding years (2023–2025). Colour scales are specific to each year. Isobaths at 100 m, 200 m, and 500 m are shown.

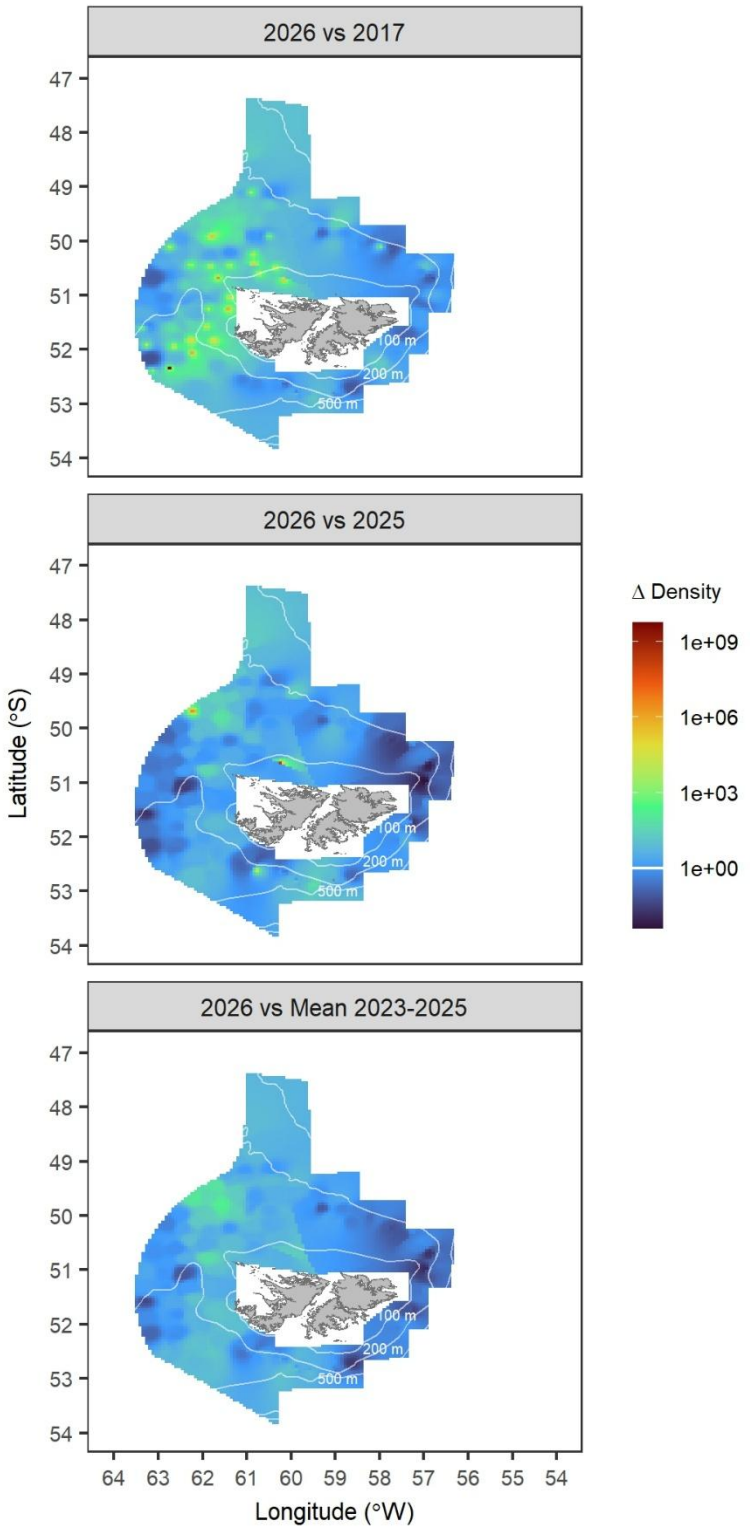

Fig. 5. Spatial change in density of the Argentine shortfin squid (*Illex argentinus*) derived from the July 2026 groundfish and calamari pre-season surveys in Falkland Islands waters, relative to the first year of the time series (2017), the previous year (2025), and the mean of the three preceding years (2023–2025). The spatial change in density is expressed as the ratio of density (kg/km^2) in 2026 relative to the density in the baseline year (2017, 2025, 2023–2025 mean). Isobaths at 100 m, 200 m, and 500 m are shown. The colour scale is $\log_{10}$-transformed to aid visualisation, with increases in density indicated above the horizontal white line towards dark red, and decreases in density indicated below the horizontal white line towards dark blue.

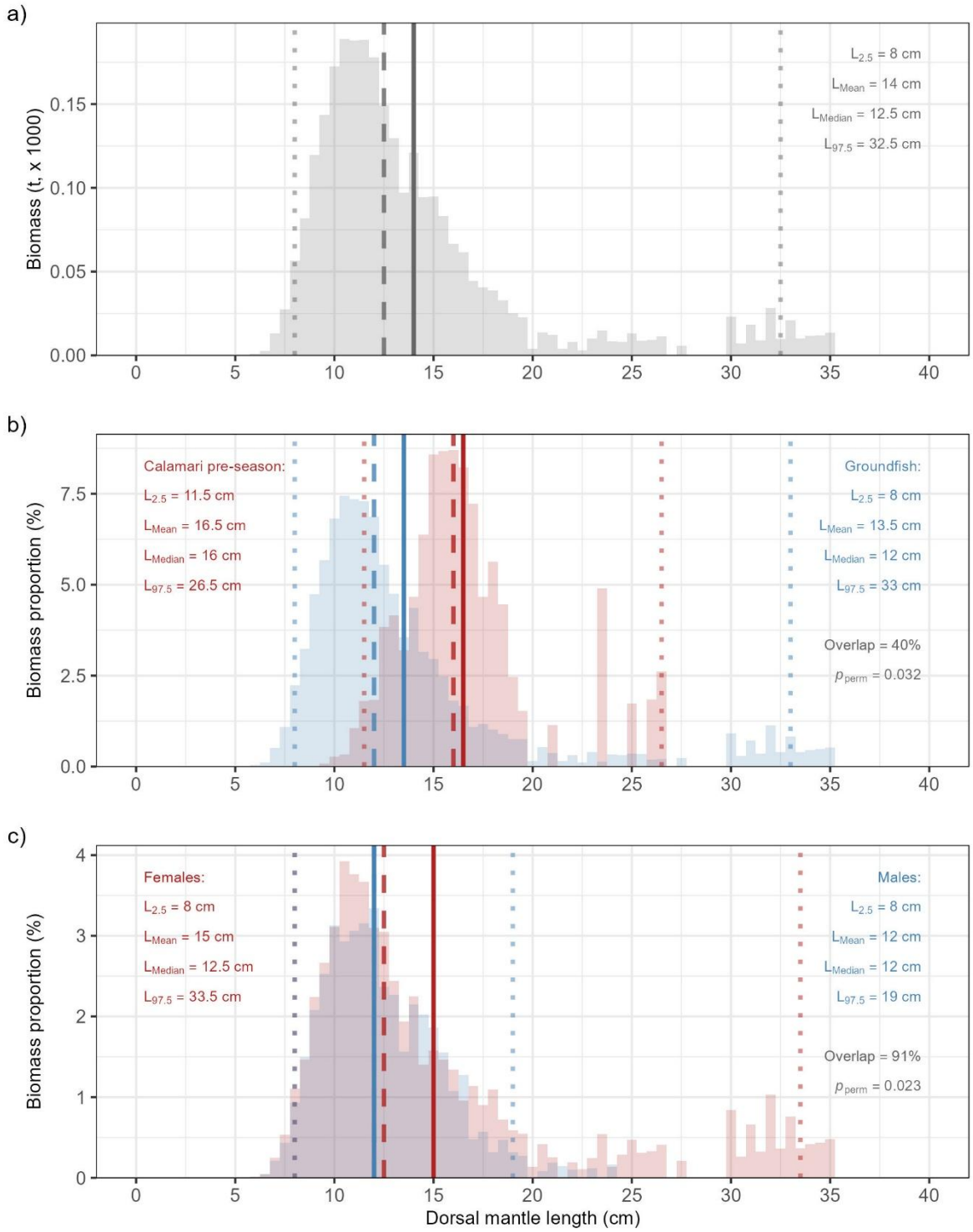

Fig. 6. Biomass-at-length class composition of Argentine shortfin squid (*Illex argentinus*) across all years combined, based on July groundfish and calamari pre-season surveys conducted in Falkland Islands waters in 2017, 2020, and 2022–2026. a) Overall biomass-at-length frequency distribution. b) Overlap in biomass-at-length distributions between calamari pre-season (red) and groundfish (blue) surveys. c) Overlap in biomass-at-length distributions between females (red) and males (blue). Solid vertical lines indicate the mean length (L_{Mean}), dashed lines the median length (L_{Median}), and dotted lines the 2.5th and 97.5th length percentiles ($L_{2.5}$ and $L_{97.5}$, respectively). p_{perm} is the significance of the weighted permutation test to assess differences between groups.

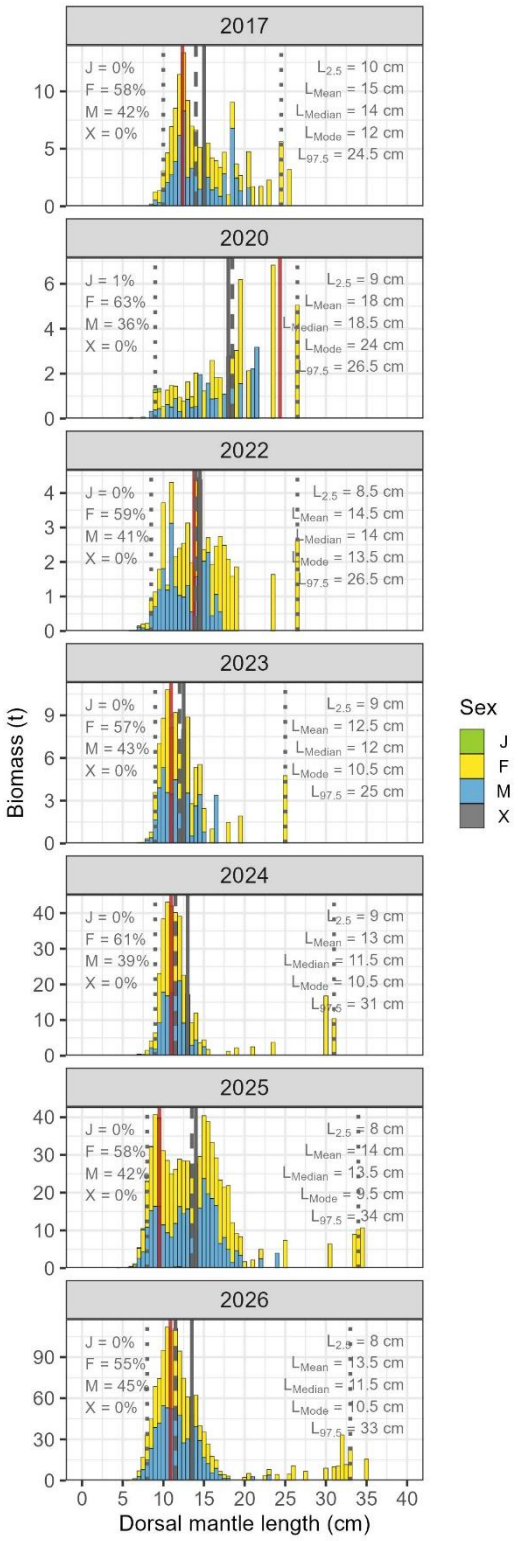

Fig. 7. Annual biomass-at-length class composition of Argentine shortfin squid (*Illex argentinus*) during July groundfish and calamari pre-season surveys conducted in Falkland Islands waters in 2017, 2020, and 2022–2026. Stacked bars represent biomass (t) per 0.5 cm length class, partitioned by sex (J = juvenile; F = female; M = male; X = undetermined), with the proportion of total annual biomass for each sex indicated in the upper left of each panel. Vertical lines indicate the mean length (L_{Mean}, grey solid), median length (L_{Median}, grey dashed), modal length (L_{Mode}, red solid), and 2.5th and 97.5th percentiles ($L_{2.5}$ and $L_{97.5}$, grey dotted) of the biomass-weighted length distribution. Note the different y-axis scales among years.

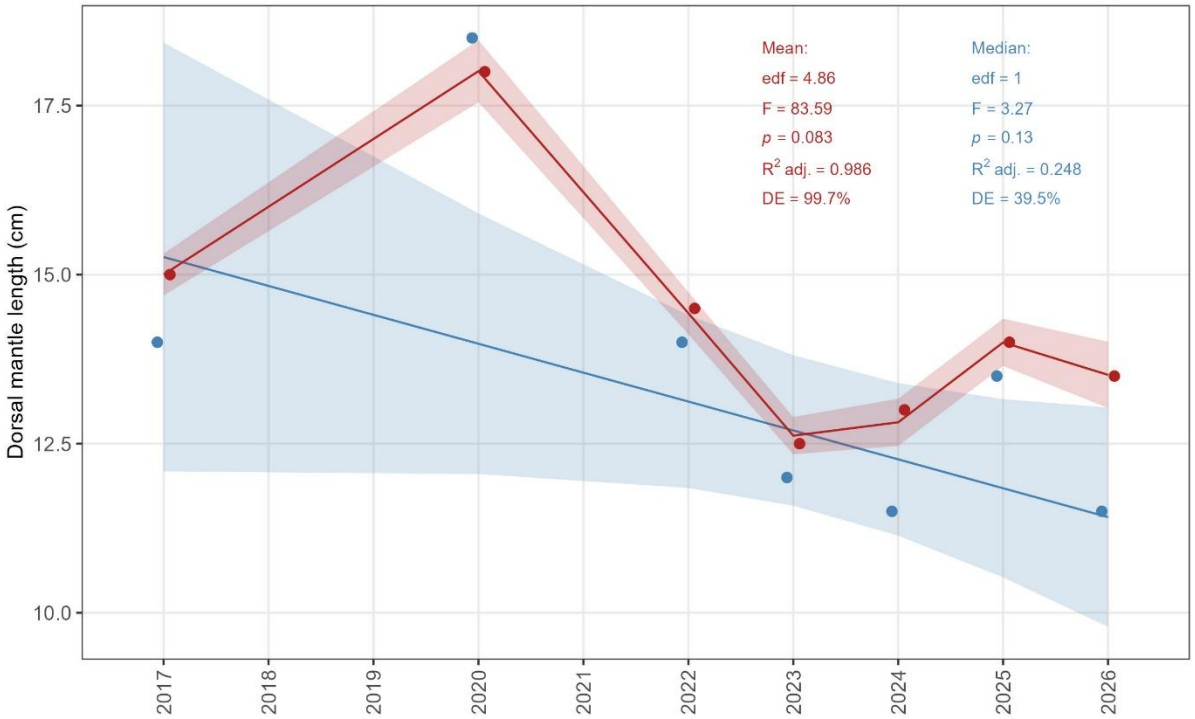

Fig. 8. Median (blue) and mean (red) dorsal mantle length of Argentine shortfin squid (*Illex argentinus*) during July groundfish and calamari pre-season surveys conducted in Falkland Islands waters in 2017, 2020, and 2022–2026. The line and shaded region represent the fitted Generalised Additive Model (GAM) smooth and its 95% pointwise confidence interval.

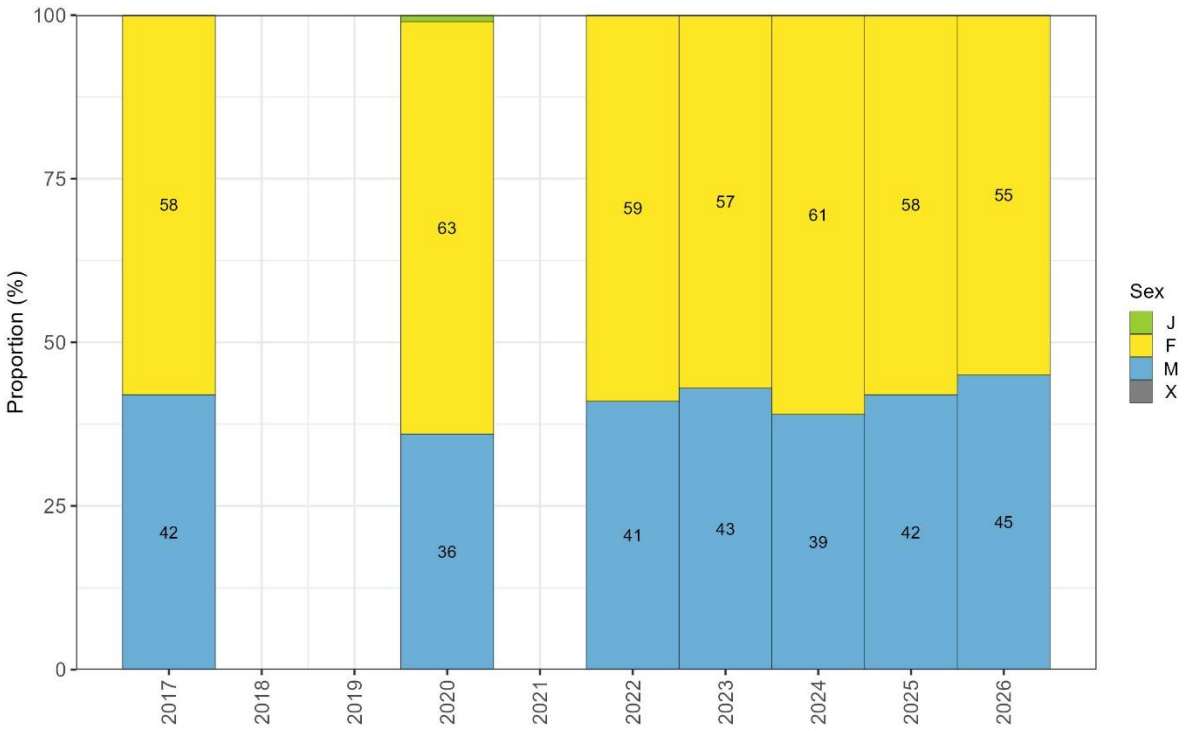

Fig. 9. Proportion by sex (J = juvenile; F = female; M = male; X = undetermined) of Argentine shortfin squid (*Illex argentinus*) during July groundfish and calamari pre-season surveys conducted in Falkland Islands waters in 2017, 2020, and 2022–2026. Labels for proportions < 3% are omitted.

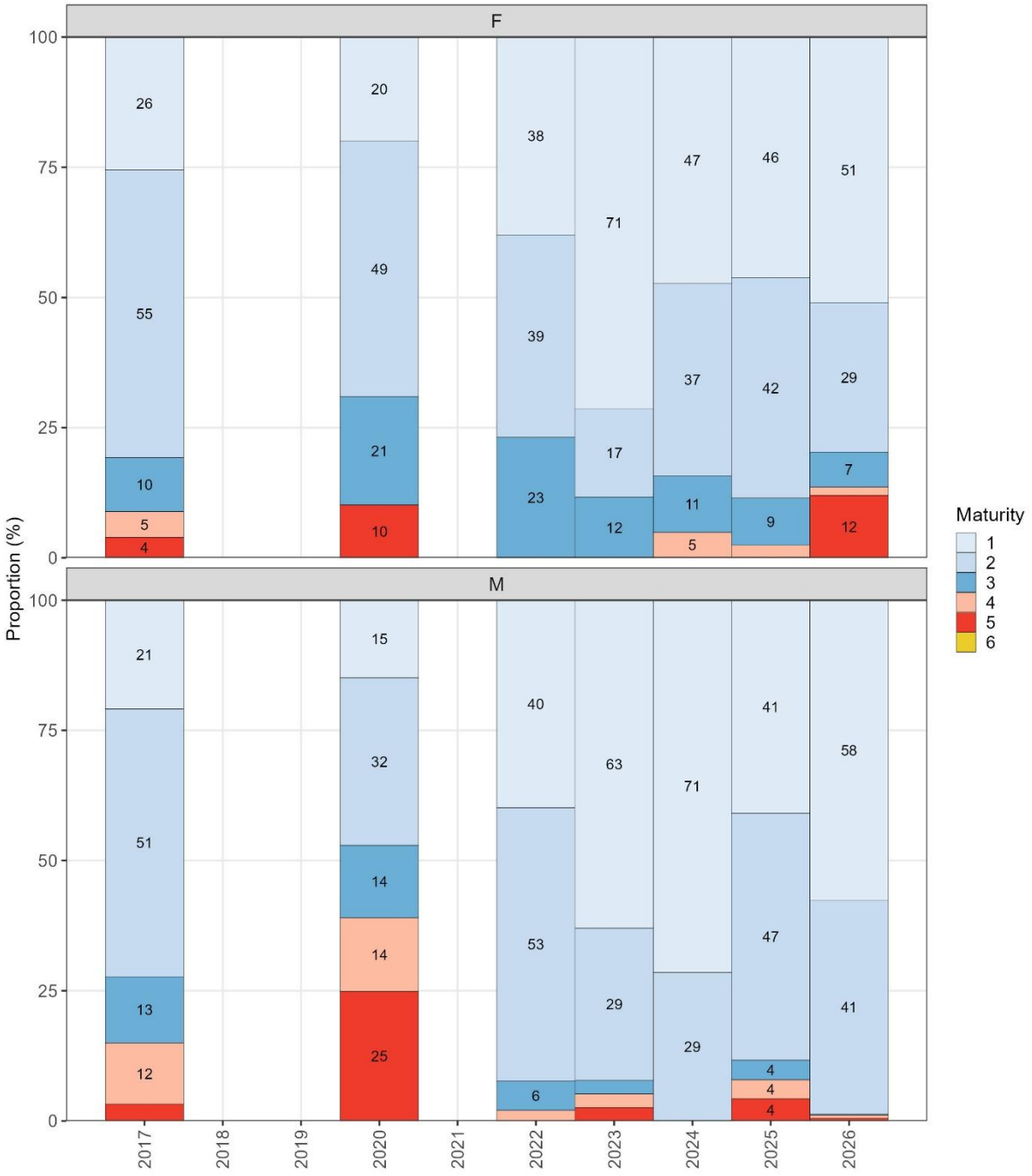

Fig. 10. Proportion by sexual maturity (1, young; 2, immature; 3, preparatory; 4, maturing; 5, mature; 6, spent) of Argentine shortfin squid (*Illex argentinus*) during July groundfish and calamari pre-season surveys conducted in Falkland Islands waters in 2017, 2020, and 2022–2026. Labels for proportions < 3% are omitted.

4.3.2. Banded whiptail grenadier (*Coelorinchus fasciatus*)

4.3.2.1. Temporal patterns of abundance

Catch and abundance had moderate inter-annual variability likely due to the patchy distribution of this species, resulting in wide confidence intervals for density and biomass. On average, 79% of the catches in the time series were from groundfish surveys and 21% were from calamari pre-season surveys. The catch in 2026 (0.71 t) represented a 42-fold increase relative to the 2017 catch (0.02 t), a 35% decrease relative to the 2025 catch (1.10 t), and a 46% increase relative to the 2023–2025 mean catch (0.49 t; Fig. 11a; Appendix II).

The highest densities occurred in 2020 (mean ± SE: 37.99 ± 22.38 kg/km²). Densities in 2026 (19.61 ± 9.91 kg/km²) represented a nearly thirty-fold increase relative to the 2017 levels (0.65 ± 0.57 kg/km²), a 45% decrease relative to the 2025 densities (35.65 ± 16.58 kg/km²), and a 28% increase relative to the 2023–2025 mean densities (15.36 ± 6.16 kg/km²; Fig. 11b).

The highest biomass in the time series was estimated for 2026 (35,636.30 t; CI = 3,410.47–44,377.82 t), representing a statistically significant 390-fold increase relative to the 2017 biomass (91.46 t; CI = 2.99–235.54 t; $p < 0.001$), a non-significant three-fold increase relative to the 2025 biomass (11,010.13 t; CI = 3,817.99–15,225.75 t; $p > 0.05$), and a non-significant eight-fold increase relative to the 2023–2025 mean (4,405.88 t; $p > 0.05$; Fig. 11c; Table IV–V; Appendix III–IV). Analysis of the full time series revealed a non-significant temporal trend in biomass (GAM: edf = 1.00, F = 1.23, p = 0.318), with the model explaining only 9.5% of the deviance (R^2 adj. = 0.126), reflecting moderate interannual variability and no consistent directional change over the time series (Fig. 11c; Appendix V).

4.3.2.2. Spatial patterns of abundance

The south below 51.5°S and between 59–62°W was the main area of distribution for banded whiptail grenadier across survey years (Fig. 12). The highest density in the time series was calculated for 2022 (1,853 kg/km^2) near the south-west limit of the FICZ. In 2026, the main aggregations (1,091 kg/km^2) occurred to the south of West Falkland, at approximately 53°S and 61°W.

In 2026, densities increased to the south-west in the FICZ relative to 2017, 2023, and 2024, but decreased relative to 2025, which highest density (1,507 kg/km^2) was located to the south of West Falkland (Fig. 13). The increase in posterior densities noted to the north-east may be an artifact of the axial loop that resulted in the projection of densities in areas where this species was not caught, and should be interpreted with caution (Fig. 13).

4.3.2.3. Length composition

Across all survey years combined, the size structure of banded whiptail grenadier was in the range of 3 to 16 cm pre-anal length; however, 95% of the estimated biomass was comprised of individuals between 6 and 12 cm, with median and mean lengths (± SE) of 8 ± 0.92 cm and 8 ± 0.79 cm, respectively (Fig. 14a).

The distribution of biomass proportions by size class exhibited a 69% overlap between the groundfish and calamari pre-season surveys, with no significant differences between the

groundfish survey (mean ± SE: 8 ± 0.78 cm) and the calamari pre-season survey (mean ± SE: 10 ± 1.63 cm; $p > 0.05$). In the groundfish survey, 95% of the biomass of banded whiptail grenadier was comprised of individuals between 6 and 12 cm (median ± SE: 8 ± 0.92 cm). In the calamari pre-season survey, 95% of the biomass was comprised of individuals between 6 and 13 cm (median ± SE: 12 ± 0.72 cm; Fig. 14b).

The distribution of biomass proportions by size class exhibited a 69% overlap between females and males. The permutation analysis revealed non-significant differences between females (mean ± SE: 9.0 ± 0.76 cm) and males (mean ± SE: 7.0 ± 0.94 cm; $p > 0.05$). For females, 95% of the biomass was comprised of individuals between 6 and 13 cm (median ± SE: 9 ± 0.91 cm). For males, 95% of the biomass was comprised of individuals between 6 and 12 cm (median ± SE: 7 ± 0.79 cm; Fig. 14c).

The distribution of biomass-at-length was unimodal and generally consistent across years at 7–9 cm, with the mean and median pre-anal lengths at 8–10 cm. In 2026, lengths were in the range of 3 to 12 cm; however, 95% of the biomass was comprised of individuals between 6 and 12 cm, with median and mean lengths (± SE) of 8 ± 0.73 cm and 8 ± 0.62 cm, respectively. For females, 95% of the biomass was comprised of individuals between 7 and 12 cm, with median and mean lengths (± SE) of 9 ± 0.82 cm and 8 ± 0.72 cm, respectively. For males, 95% of the biomass was comprised of individuals between 6 and 9 cm, with median and mean lengths (± SE) of 7 ± 0.67 cm and 7 ± 0.67 cm, respectively (Fig. 15).

Analysis of the full time series revealed non-significant temporal trends in either mean (GAM: edf = 1.00, F = 0.59, p = 0.477, R^2 adj. = -0.078, DE = 10.6%) or median (GAM: edf = 1.36, F = 1.12, p = 0.471, R^2 adj. = 0.099, DE = 30.3%) pre-anal length (Fig. 16).

4.3.2.4. Sex and maturity composition

The sex composition of banded whiptail grenadier was strongly dominated by females (mean ± SE: 79.1 ± 2.4%), followed by males (19.1 ± 2.1%), and individuals of undetermined sex (1.7 ± 0.9%) throughout the time series. Sex composition had moderate interannual variability, with the female proportion ranging from 70% in 2024 to 88% in 2017, and the male proportion ranging from 12% in 2017 to 29% in 2024. In 2026, the sex composition consisted of 84% females (above the full time series average), 14% males, and 1.7% individuals of undetermined sex (Fig. 17).

Maturity composition was dominated by post-spawning individuals (resting) in both sexes in most years. Females were characterised by a substantial post-spawning component throughout the time series (> 48%). Males were predominantly in the resting stage (≥ 52%), except in 2026 when early developing individuals were dominant (73%). Late developing, ripe and running individuals rarely exceeded 25%, except for 2020 (40%; Fig. 18).

4.3.2.5. Discussion

Across the full time series, banded whiptail grenadier biomass showed no significant temporal trend, reflecting moderate interannual variability rather than a consistent directional change. July biomass was consistently lower than February biomass, although February also showed moderate interannual variability with no clear trend (Ramos 2026). Female biomass was dominated by post-spawning individuals (> 48%), suggesting spawning

does not occur in July (or February; Ramos 2026), or occurs outside the survey area at this time of year; body size remained consistent throughout the time series. Comparison of biomass estimates with external data is limited given the scarcity of species-level information for grenadiers in Falkland Islands waters. The only stock assessment conducted for grenadiers in Falkland Islands waters (Winter & Lee 2018) produced contrasting results depending on the method applied; CMSY indicated higher biomass in 2017 relative to 1988, while OCOM indicated the opposite. In the commercial bottom trawl fisheries, banded whiptail grenadier accounts for approximately 68.3% of total grenadier catches in Falkland Islands waters, of which over 85% are discarded (Winter & Lee 2018), pointing to potentially substantial unreported mortality with implications for the long-term abundance of this species.

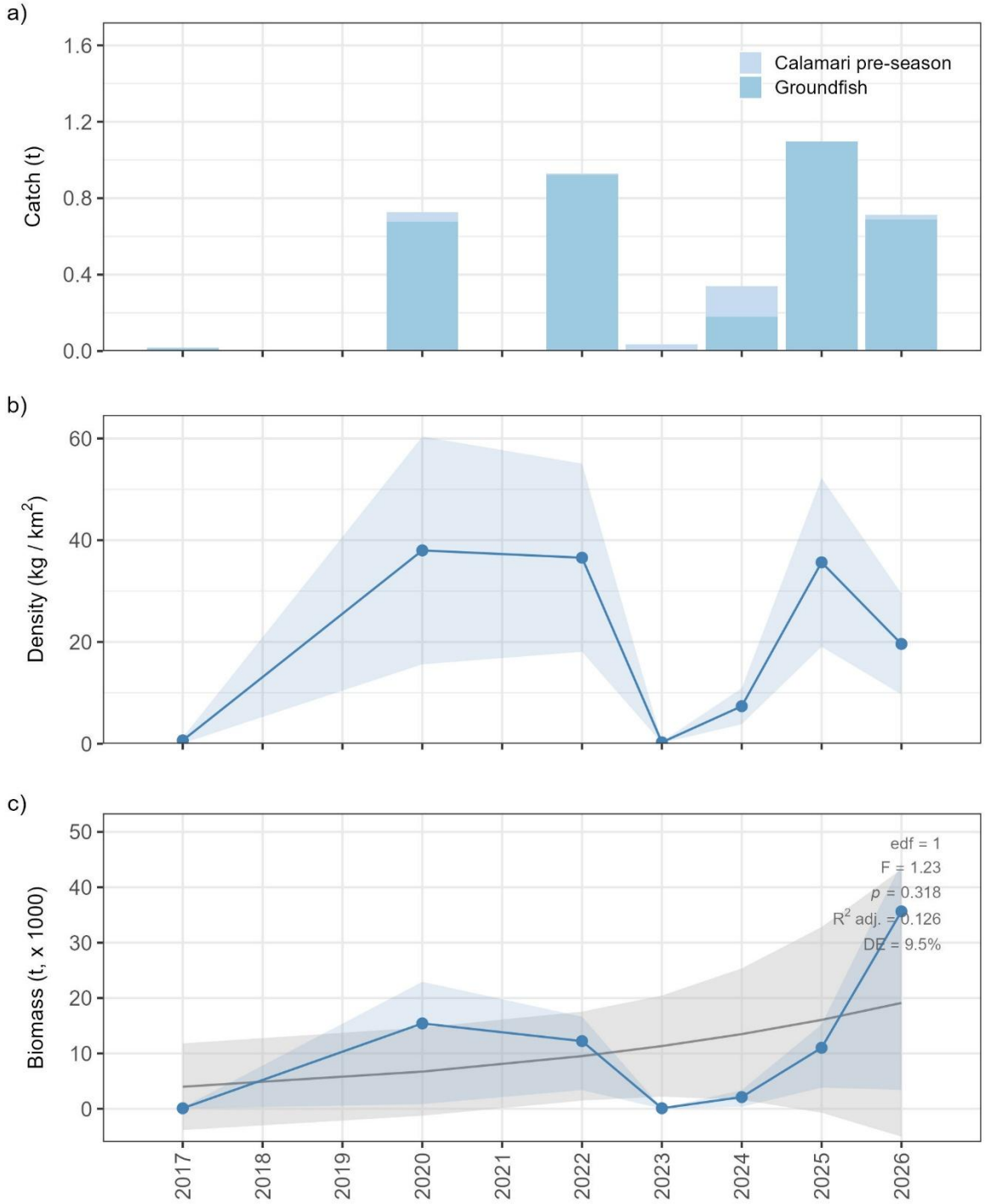

Fig. 11. Abundance of banded whiptail grenadier (*Coelorinchus fasciatus*) during July groundfish and calamari pre-season surveys conducted in Falkland Islands waters in 2017, 2020, and 2022–2026. (a) Catch per survey, (b) annual mean density ± SE represented by the blue line and shaded region, respectively, and (c) estimated biomass, where the blue line and shaded region represent the median and 95% pointwise confidence interval derived from 10,000 bootstrap biomass estimates, and the grey line and shaded region represent the fitted Generalised Additive Model (GAM) smooth and its 95% pointwise confidence interval.

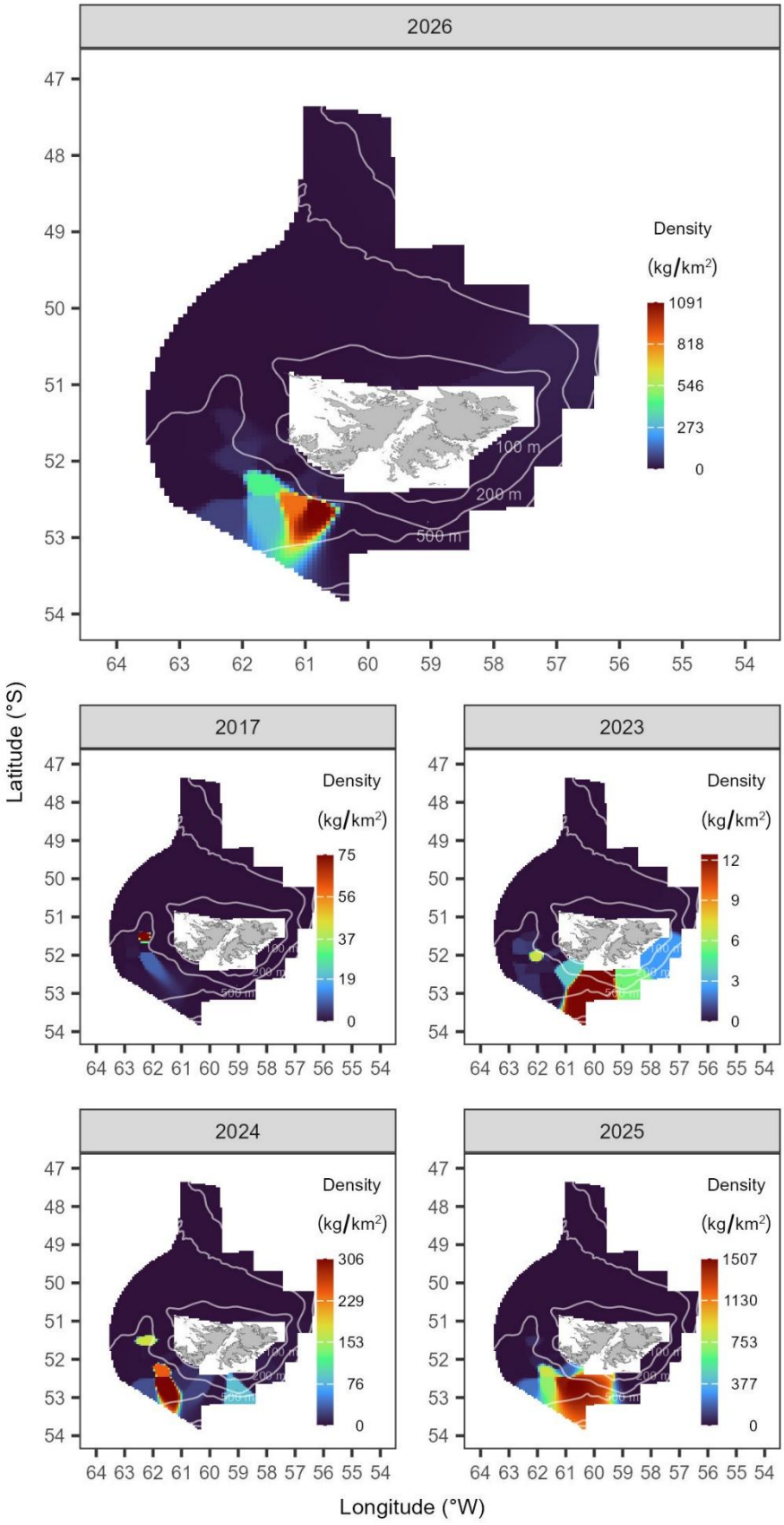

Fig. 12. Distribution and abundance of banded whiptail grenadier (*Coelorinchus fasciatus*) derived from the July 2026 groundfish and calamari pre-season surveys in Falkland Islands waters, compared with the first year of the time series (2017) and the three preceding years (2023–2025). Colour scales are specific to each year. Isobaths at 100 m, 200 m, and 500 m are shown.

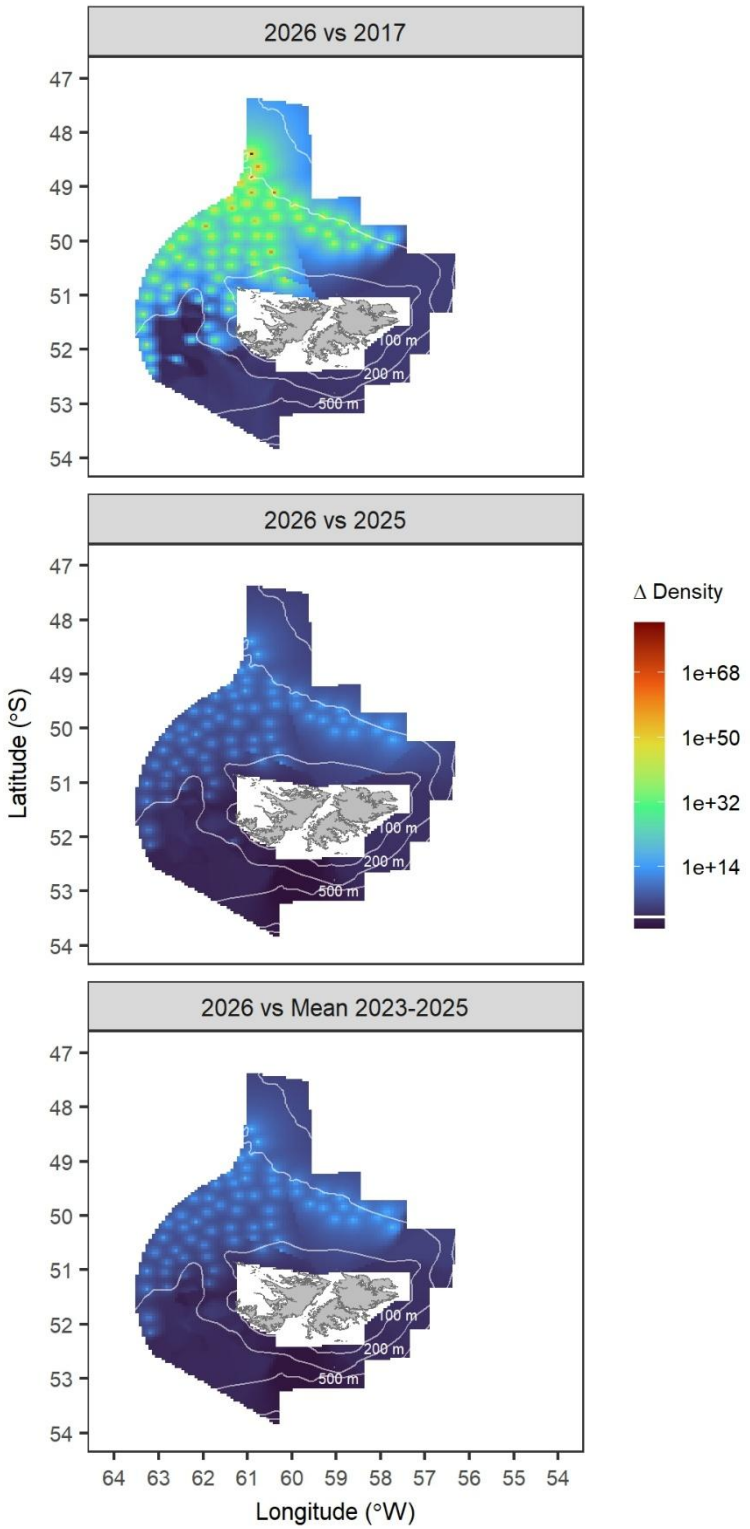

Fig. 13. Spatial change in density of banded whiptail grenadier (*Coelorinchus fasciatus*) derived from the July 2026 groundfish and calamari pre-season surveys in Falkland Islands waters, relative to the first year of the time series (2017), the previous year (2025), and the mean of the three preceding years (2023–2025). The spatial change in density is expressed as the ratio of density (kg/km^2) in 2026 relative to the density in the baseline year (2017, 2025, 2023–2025 mean). Isobaths at 100 m, 200 m, and 500 m are shown. The colour scale is $\log_{10}$-transformed to aid visualisation, with increases in density indicated above the horizontal white line towards dark red, and decreases in density indicated below the horizontal white line towards dark blue.

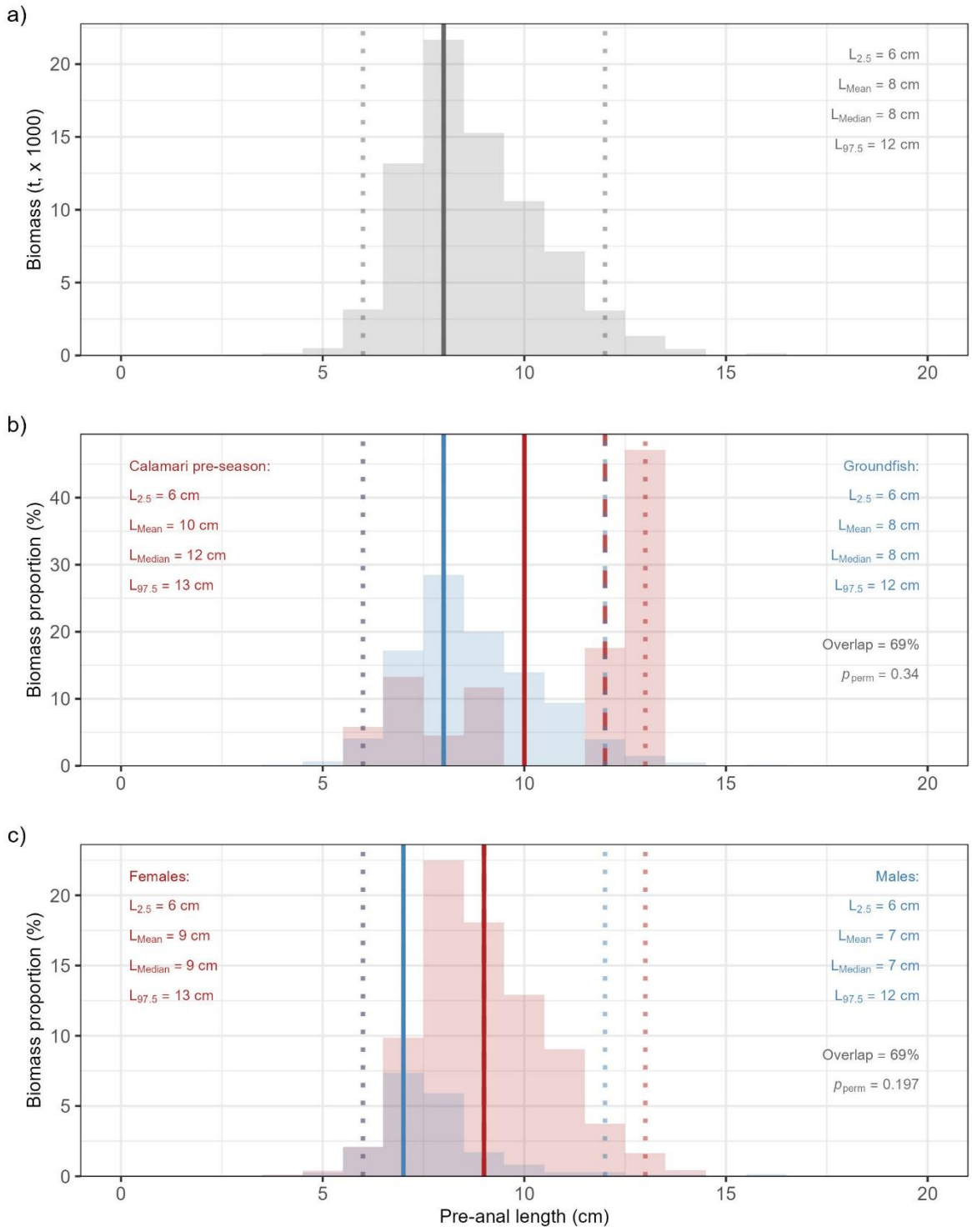

Fig. 14. Biomass-at-length class composition of banded whiptail grenadier (*Coelorinchus fasciatus*) across all years combined, based on July groundfish and calamari pre-season surveys conducted in Falkland Islands waters in 2017, 2020, and 2022–2026. a) Overall biomass-at-length frequency distribution. b) Overlap in biomass-at-length distributions between calamari pre-season (red) and groundfish (blue) surveys. c) Overlap in biomass-at-length distributions between females (red) and males (blue). Solid vertical lines indicate the mean length (L_{Mean}), dashed lines the median length (L_{Median}), and dotted lines the 2.5th and 97.5th length percentiles ($L_{2.5}$ and $L_{97.5}$, respectively). p_{perm} is the significance of the weighted permutation test to assess differences between groups.

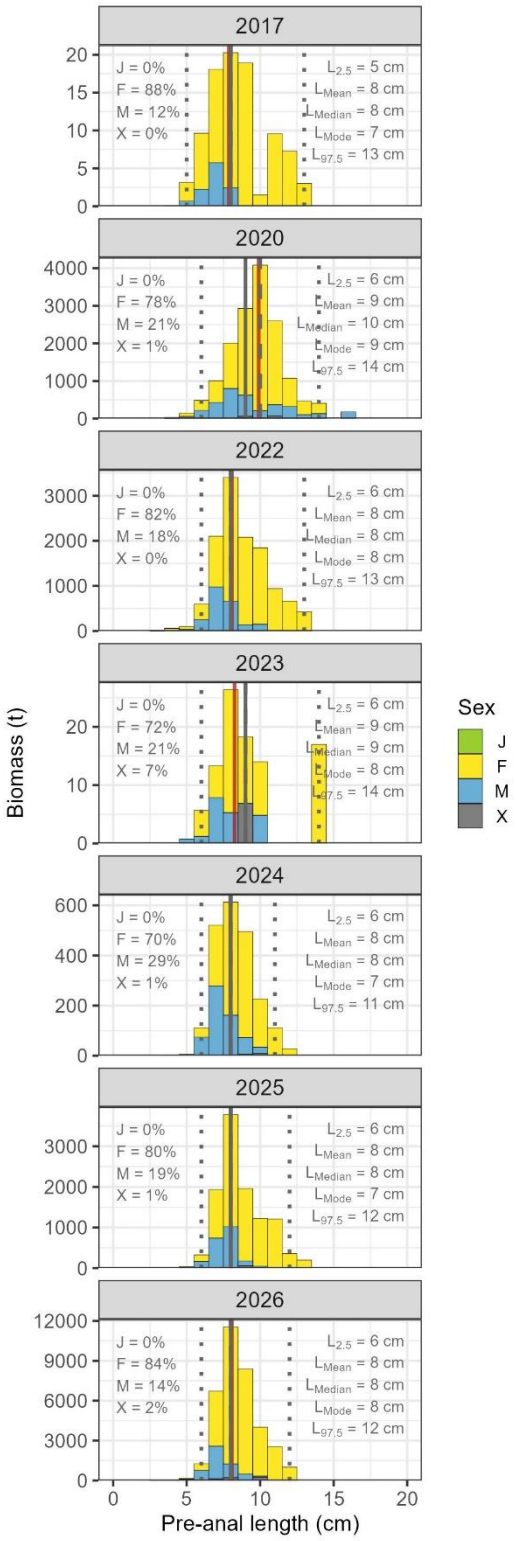

Fig. 15. Annual biomass-at-length class composition of banded whiptail grenadier (*Coelorinchus fasciatus*) during July groundfish and calamari pre-season surveys conducted in Falkland Islands waters in 2017, 2020, and 2022–2026. Stacked bars represent biomass (t) per 1.0 cm length class, partitioned by sex (J = juvenile; F = female; M = male; X = undetermined), with the proportion of total annual biomass for each sex indicated in the upper left of each panel. Vertical lines indicate the mean length (L_{Mean}, grey solid), median length (L_{Median}, grey dashed), modal length (L_{Mode}, red solid), and 2.5th and 97.5th percentiles ($L_{2.5}$ and $L_{97.5}$, grey dotted) of the biomass-weighted length distribution. Note the different y-axis scales among years.

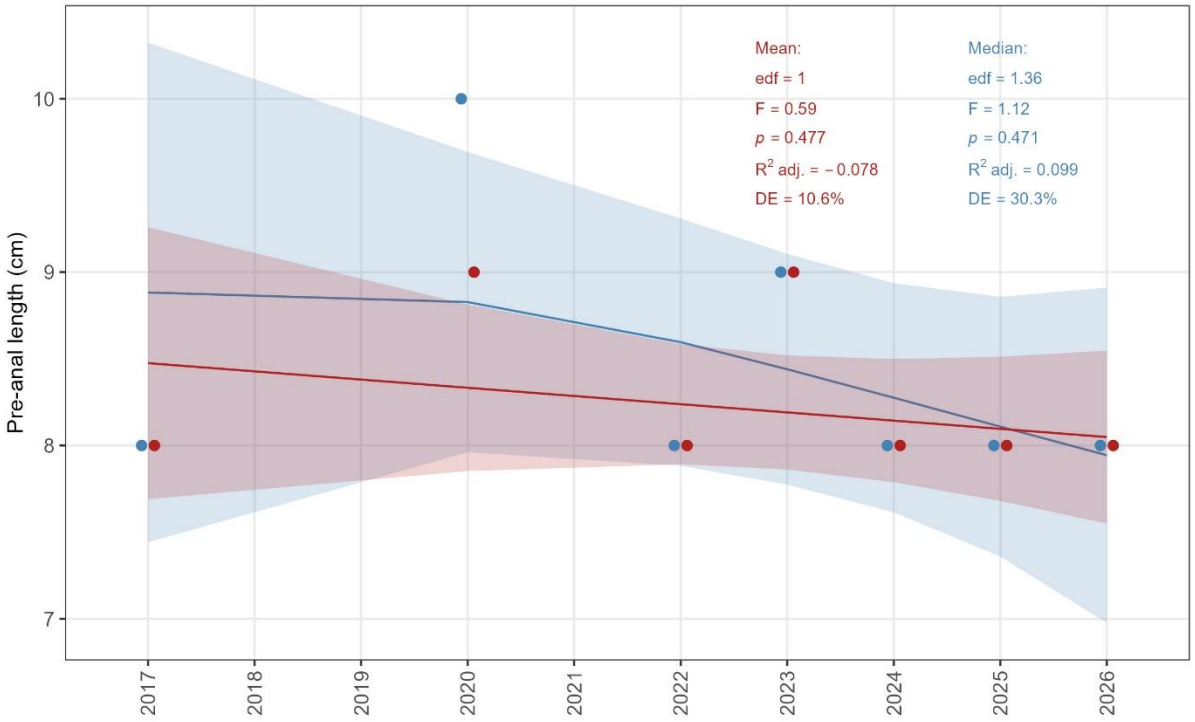

Fig. 16. Median (blue) and mean (red) pre-anal length of banded whiptail grenadier (*Coelorinchus fasciatus*) during July groundfish and calamari pre-season surveys conducted in Falkland Islands waters in 2017, 2020, and 2022–2026. The line and shaded region represent the fitted Generalised Additive Model (GAM) smooth and its 95% pointwise confidence interval.

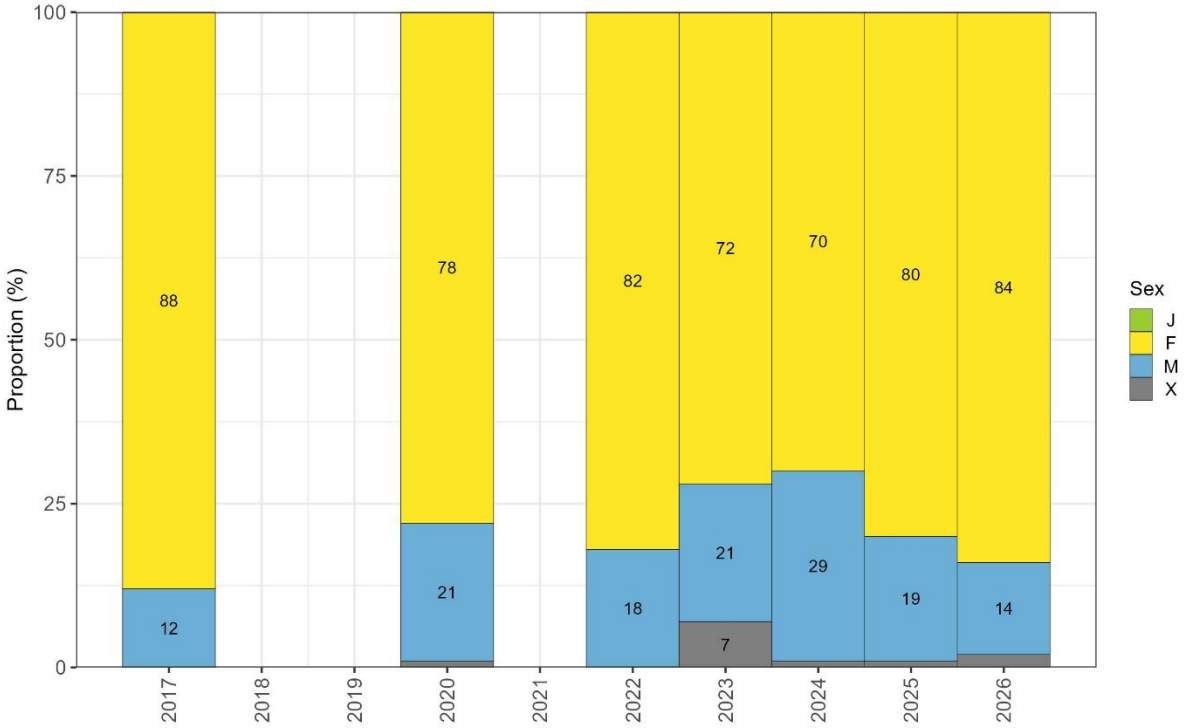

Fig. 17. Proportion by sex (J = juvenile; F = female; M = male; X = undetermined) of banded whiptail grenadier (*Coelorinchus fasciatus*) during July groundfish and calamari pre-season surveys conducted in Falkland Islands waters in 2017, 2020, and 2022–2026. Labels for proportions < 3% are omitted.

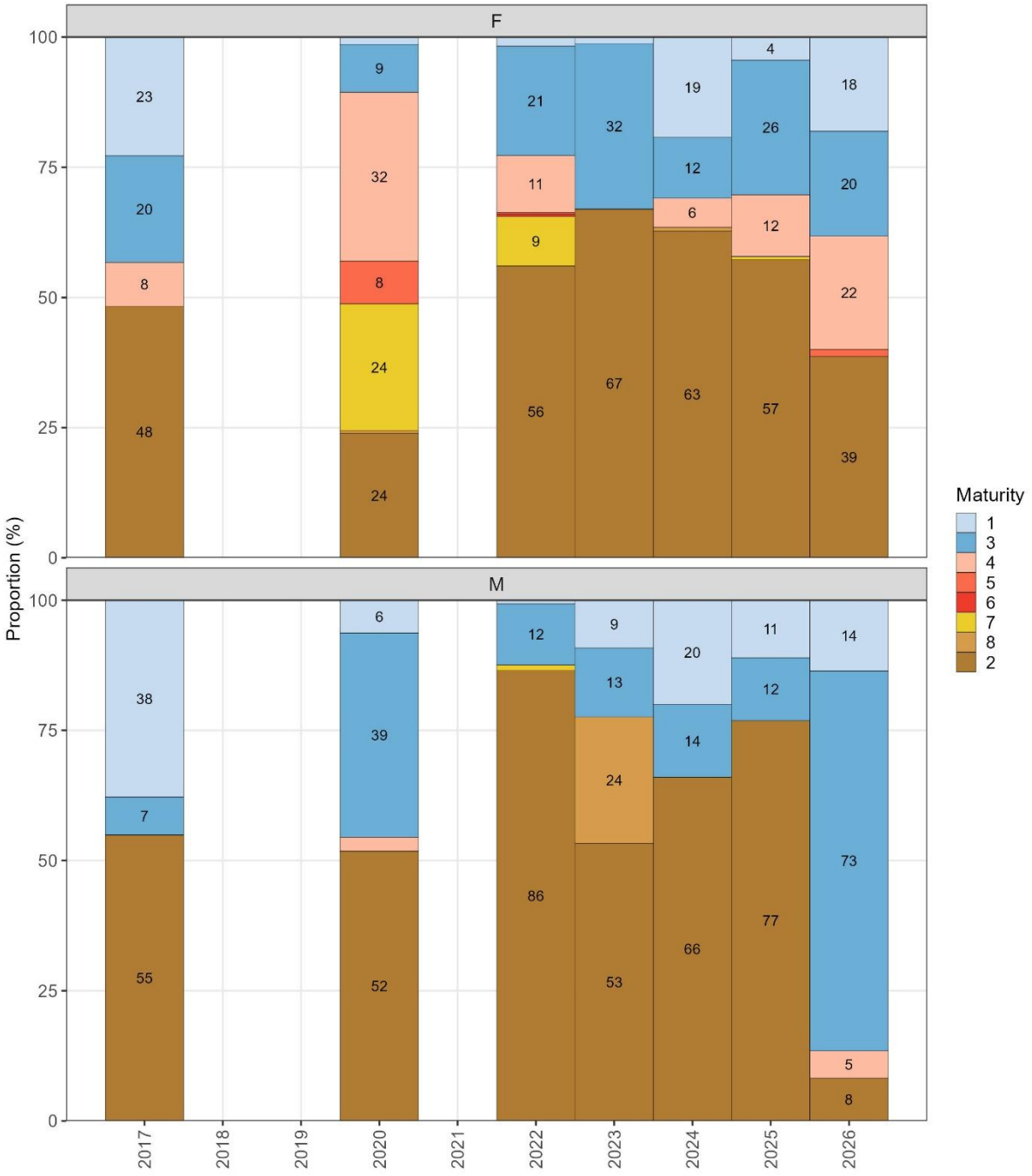

Fig. 18. Proportion by sexual maturity (1, immature; 3, early developing; 4, late developing; 5, ripe; 6, running; 7, spent; 8, recovering spent; 2, resting) of banded whiptail grenadier (*Coelorinchus fasciatus*) during July groundfish and calamari pre-season surveys conducted in Falkland Islands waters in 2017, 2020, and 2022–2026. Maturity stages ordered by developmental sequence. Labels for proportions < 3% are omitted.

4.3.3. Common hake (*Merluccius hubbsi*)

4.3.3.1. Temporal patterns of abundance

On average, 50% of the common hake catches in the time series were from groundfish surveys and 50% were from calamari pre-season surveys. The highest catch was reported in 2025 (250.81 t). The second highest catch was reported in 2026 (243.80 t), and represented a nearly nine-fold increase relative to the 2017 catch (26.65 t), a 3% decrease relative to the 2025 catch, and a 42% increase relative to the 2023–2025 mean catch (171.49 t; Fig. 19a; Appendix II).

The highest densities in the time series occurred in 2026 (mean ± SE: 4,180.76 ± 470.26 kg/km²), and represented a nearly six-fold increase relative to the 2017 densities (705.83 ± 106.94 kg/km²), a 9% increase relative to the 2025 densities (3,822.03 ± 585.92 kg/km²), and a 34% increase relative to the 2023–2025 mean densities (3,130.01 ± 266.90 kg/km²; Fig. 19b).

The biomass of common hake in 2026 (662,873.79 t; CI = 586,286.16–760,614.12 t) was the third highest biomass in the time series, and represented a significant six-fold increase relative to 2017 levels (116,485.35 t; CI = 94,883.33–149,313.91 t; $p < 0.001$), a non-significant 7% decrease relative to 2025 levels (713,098.27 t; CI = 508,225.35–907,855.14 t; $p > 0.05$), and a non-significant 17% increase relative to the 2023–2025 mean (564,628.22 t; $p > 0.05$; Fig. 19c; Table IV–V; Appendix III–IV). Analysis of the full time series revealed a significant increasing trend in biomass (GAM: edf = 2.05, F = 14.14, p = 0.015), with the model explaining 86.4% of the deviance (R^2 adj. = 0.624; Fig. 19c; Appendix V).

4.3.3.2. Spatial patterns of abundance

In 2026, common hake was mainly distributed through the west in the FICZ, and its highest density (30,836 kg/km^2) occurred to the north-west within a wider area of relatively high densities located north of 51.5°S and west of 61.5°W. In 2017 and in 2023–2025 the highest densities were observed to the north and to the south-west, with the highest density in the time series occurring in 2025 (56,903 kg/km^2; Fig. 20).

Analysis of the spatial change in density revealed an overall increase in densities through the survey area in 2026 relative to 2017, with predominant increase to the west near the limit of the FICZ and to the north-east around the 200 m isobath, as well as to the south in the 'Loligo Box'. Densities in 2026 increased through the west in the FICZ and decreased along the 'Loligo Box' relative to 2025, and relative to the 2023–2025 mean (Fig. 21).

4.3.3.3. Length composition

Across all survey years combined, total length of common hake was in the range of 20 to 88 cm; however, 95% of the estimated biomass was comprised of individuals between 35 and 71 cm, with median and mean lengths (± SE) of 47 ± 2.35 cm and 49 ± 1.76 cm, respectively (Fig. 22a).

The distribution of biomass proportions by size class exhibited a 72% overlap between the groundfish and calamari pre-season surveys. Individuals from the groundfish survey (mean ± SE: 47 ± 1.82 cm) were significantly smaller than those from the calamari pre-season survey (mean ± SE: 53 ± 1.64 cm; p = 0.008). In the groundfish survey, 95% of the biomass of

common hake was comprised of individuals between 35 and 70 cm (median ± SE: 45 ± 2.17 cm). In the calamari pre-season survey, 95% of the biomass of common hake was comprised of individuals between 39 and 72 cm (median ± SE: 52 ± 2.43 cm; Fig. 22b).

The distribution of biomass proportions by size class exhibited a 64% overlap between females and males. The permutation analysis revealed that females (mean ± SE: 50 ± 1.70 cm) were significantly larger than males (mean ± SE: 39 ± 1.05 cm; $p < 0.001$). For females, 95% of the biomass was comprised of individuals between 36 and 72 cm (median ± SE: 49 ± 2.30 cm). For males, 95% of the biomass was comprised of individuals between 34 and 47 cm (median ± SE: 39 ± 1.22 cm; Fig. 22c).

Through the time series, the size structure of common hake was broad and with several length groups that are not clearly distinguished because of size overlap. Main modal length decreased from 46 cm in 2017 to 41 cm in 2022–2026 (Fig. 23). In 2026, lengths were in the range of 30 to 82 cm; however, 95% of the biomass was comprised of individuals between 36 and 69 cm, with median and mean lengths (± SE) of 45 ± 1.68 cm and 47 ± 1.57 cm, respectively. For females, 95% of the biomass was comprised of individuals between 38 and 70 cm, with median and mean lengths (± SE) of 46 ± 2.04 cm and 48 ± 1.78 cm, respectively. For males, 95% of the biomass was comprised of individuals between 35 and 45 cm, with median and mean lengths (± SE) of 39 ± 1.13 cm and 39 ± 0.94 cm, respectively (Fig. 23).

Analysis of the full time series revealed a significant decline in mean length (GAM: edf = 2.14, $F = 17.36$, $p = 0.01$, R^2 adj. = 0.881, DE = 92.4%), decreasing from 54 cm in 2017 to 47 cm in 2026, with the steepest decline occurring between 2017 and 2022 and a relative stabilisation thereafter (Fig. 24). Median length also had a declining trend (GAM: edf = 2.22, $F = 30.17$, $p = 0.003$, R^2 adj. = 0.93, DE = 95.6%) from 54 cm in 2017 to 45 cm in 2026. Mean lengths were consistently higher than median lengths throughout the time series, reflecting a right-skewed length distribution due to the presence of larger individuals, particularly in recent years (Fig. 23).

4.3.3.4. Sex and maturity composition

The sex composition of common hake was dominated by females (mean ± SE: 85.9 ± 1.3%), followed by males (14.1 ± 1.3%) throughout the time series, consistent with the larger size of females compared to males. In 2026, the sex composition consisted of 84% females and 16% males (Fig. 25).

Maturity composition differed between sexes throughout the time series. Females had a substantial post-spawning component (spent, recovering spent, and resting), reaching 90% of the female biomass in 2022. Early developing females were dominant in 2026 (51%). Males had contrasting maturity composition across years. Post-spawning males were dominant (≥ 95%) in 2017 and 2022; however, late developing males were dominant since 2023. Ripe or running individuals were scarce in both sexes (≤ 12%; Fig. 26).

4.3.3.5. Discussion

Across the full time series, common hake biomass in Falkland Islands waters showed a significant increasing trend, consistent with that observed in February (Ramos 2026). These results align with commercial trawler CPUE in the FICZ/FOCZ, which peaked in 2021 (Ramos

& Winter 2022a; no post-2021 indices are available), and with the southern stock (south of 41°S) in Argentine waters, which increased from the late 2000s to a maximum in 2023 (Santos et al. 2024), suggesting the increase in Falkland Islands waters may reflect a broader regional trend in common hake abundance. The increasing abundance in July was driven by females (~ 86%) and mainly in post-spawning maturity stage, with a shift toward early developing individuals in July 2026. The predominance of post-spawning individuals across most of the time series, in both July and February (Ramos 2026), agrees with spawning grounds identified outside Falkland Islands waters, on the Argentine continental shelf (Macchi et al. 2010; Arkhipkin et al. 2015). Marked interannual shifts in maturity-stage composition may reflect environmental variability or inconsistencies in the FIFD maturity scale, which has recently been described in more detail (Soeth 2026) and will continue to be refined. Common hake abundance is typically higher from May to September in Falkland Islands waters (Ramos & Winter 2022a), making July surveys particularly informative for stock assessment, and ahead of the finfish and calamari fisheries during the second half of the year.

In contrast with the increasing biomass trend, both mean and median total length declined significantly in July parallel surveys, consistent with the size decline observed in February surveys (Ramos 2026), indicating that the increase in biomass is due to the increase in number of individuals.

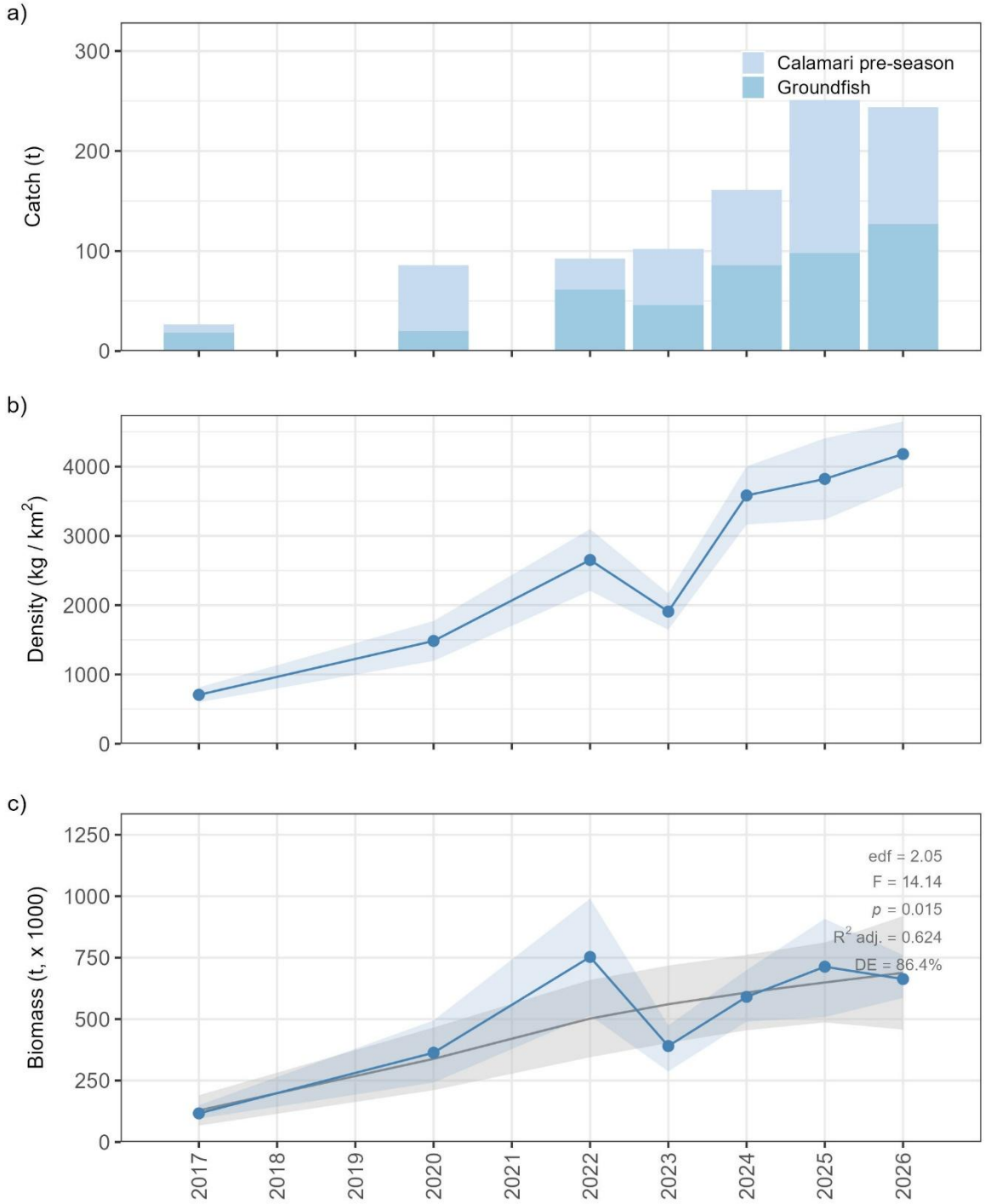

Fig. 19. Abundance of common hake (*Merluccius hubbsi*) during July groundfish and calamari pre-season surveys conducted in Falkland Islands waters in 2017, 2020, and 2022–2026. (a) Catch per survey, (b) annual mean density ± SE represented by the blue line and shaded region, respectively, and (c) estimated biomass, where the blue line and shaded region represent the median and 95% pointwise confidence interval derived from 10,000 bootstrap biomass estimates, and the grey line and shaded region represent the fitted Generalised Additive Model (GAM) smooth and its 95% pointwise confidence interval.

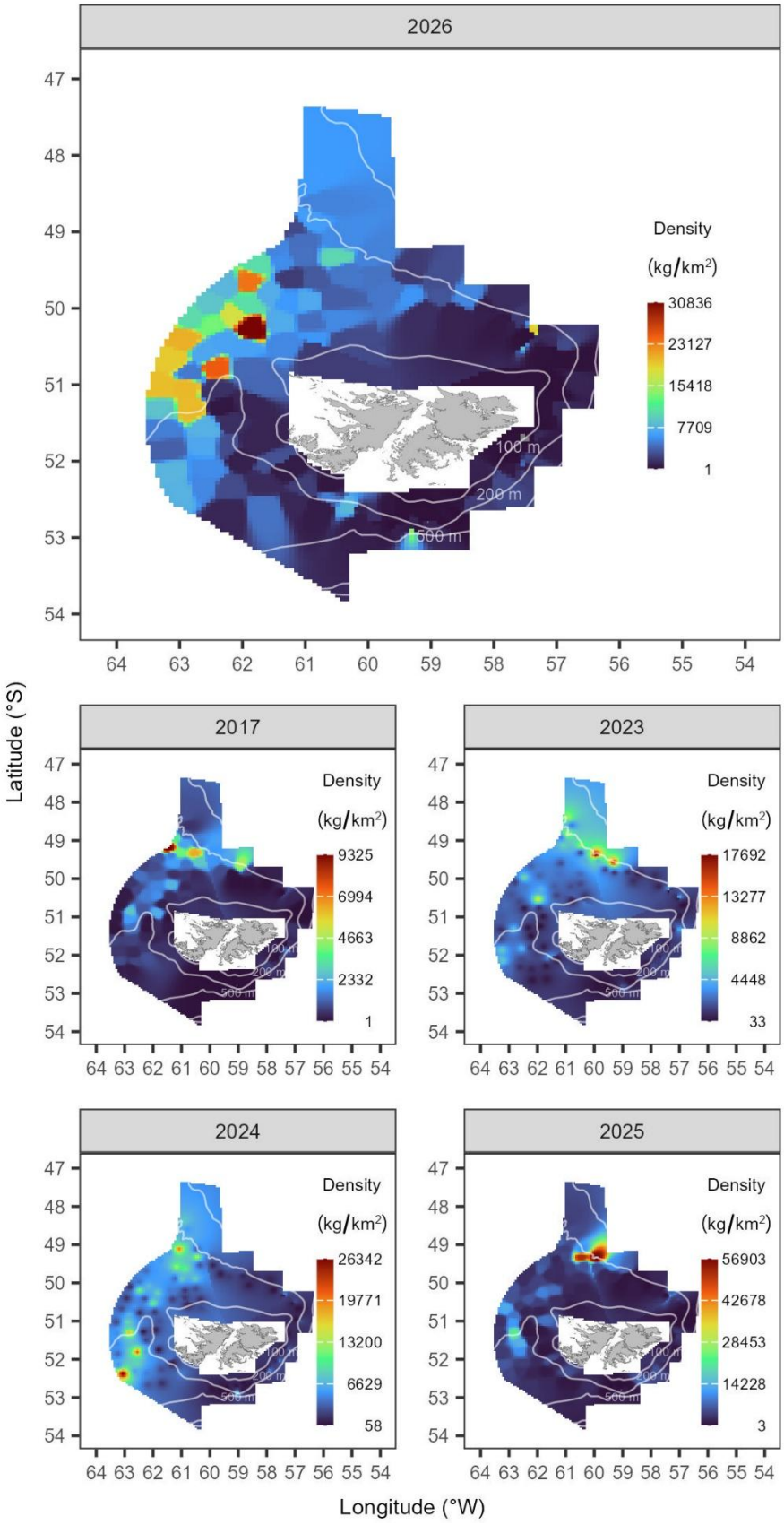

Fig. 20. Distribution and abundance of common hake (*Merluccius hubbsi*) derived from the July 2026 groundfish and calamari pre-season surveys in Falkland Islands waters, compared with the first year of the time series (2017) and the three preceding years (2023–2025). Colour scales are specific to each year. Isobaths at 100 m, 200 m, and 500 m are shown.

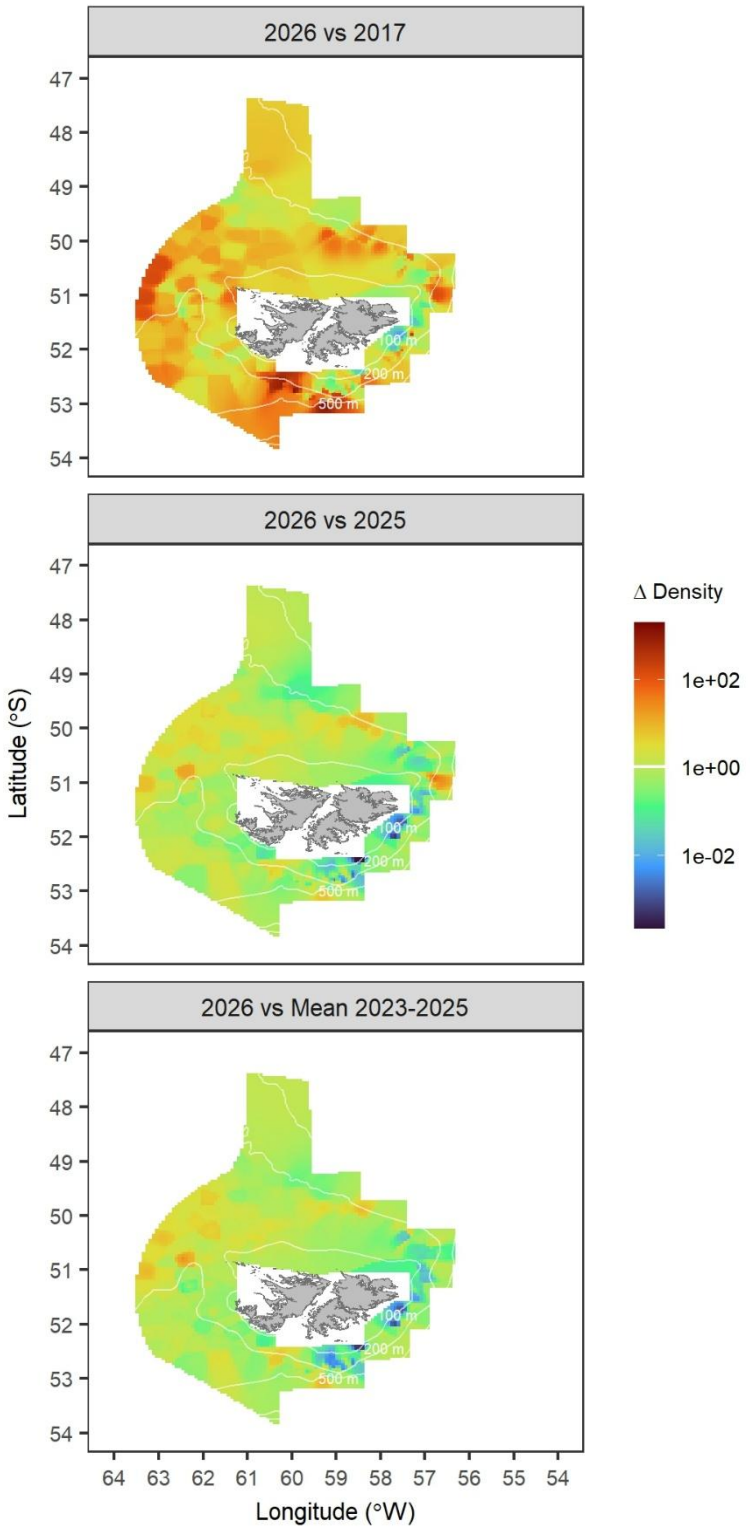

Fig. 21. Spatial change in density of common hake (*Merluccius hubbsi*) derived from the July 2026 groundfish and calamari pre-season surveys in Falkland Islands waters, relative to the first year of the time series (2017), the previous year (2025), and the mean of the three preceding years (2023–2025). The spatial change in density is expressed as the ratio of density (kg/km^2) in 2026 relative to the density in the baseline year (2017, 2025, 2023–2025 mean). Isobaths at 100 m, 200 m, and 500 m are shown. The colour scale is $\log_{10}$-transformed to aid visualisation, with increases in density indicated above the horizontal white line towards dark red, and decreases in density indicated below the horizontal white line towards dark blue.

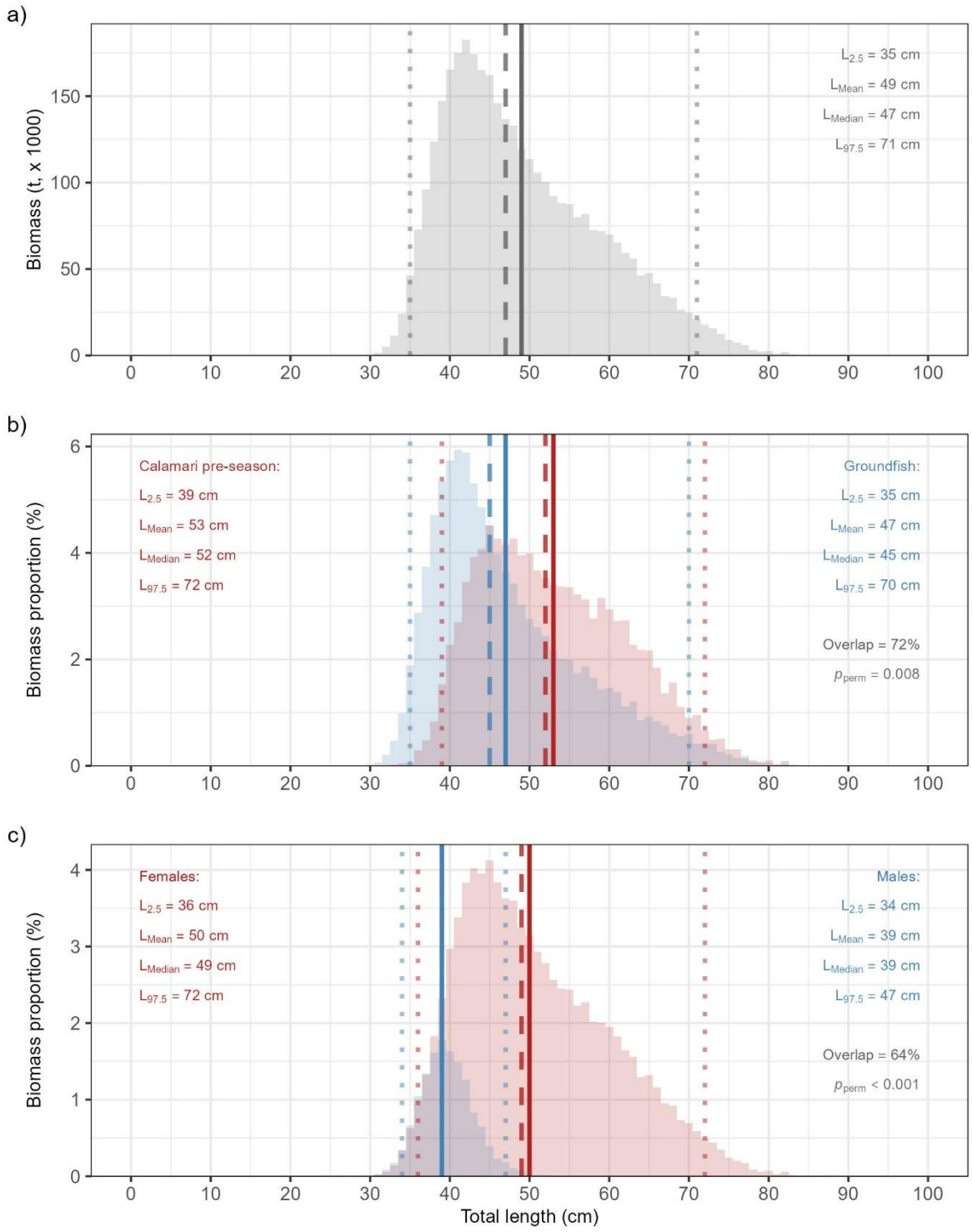

Fig. 22. Biomass-at-length class composition of common hake (*Merluccius hubbsi*) across all years combined, based on July groundfish and calamari pre-season surveys conducted in Falkland Islands waters in 2017, 2020, and 2022–2026. a) Overall biomass-at-length frequency distribution. b) Overlap in biomass-at-length distributions between calamari pre-season (red) and groundfish (blue) surveys. c) Overlap in biomass-at-length distributions between females (red) and males (blue). Solid vertical lines indicate the mean length (L_{Mean}), dashed lines the median length (L_{Median}), and dotted lines the 2.5th and 97.5th length percentiles ($L_{2.5}$ and $L_{97.5}$, respectively). p_{perm} is the significance of the weighted permutation test to assess differences between groups.

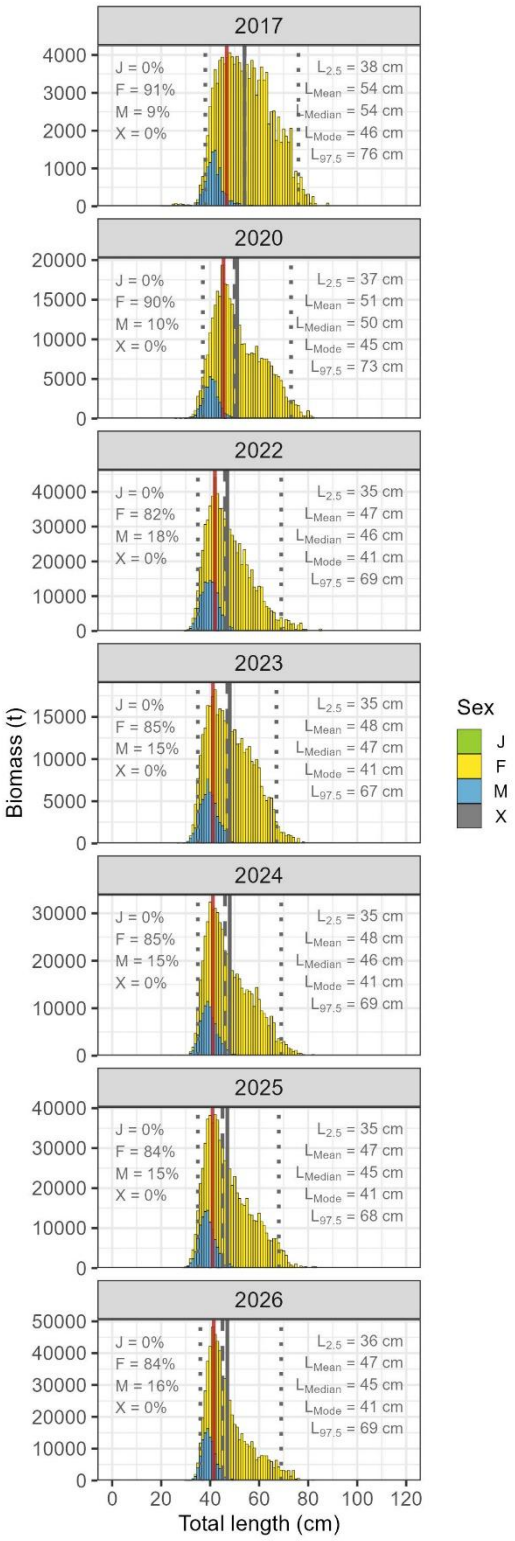

Fig. 23. Annual biomass-at-length class composition of common hake (*Merluccius hubbsi*) during July groundfish and calamari pre-season surveys conducted in Falkland Islands waters in 2017, 2020, and 2022–2026. Stacked bars represent biomass (t) per 1.0 cm length class, partitioned by sex (J = juvenile; F = female; M = male; X = undetermined), with the proportion of total annual biomass for each sex indicated in the upper left of each panel. Vertical lines indicate the mean length (L_{Mean}, grey solid), median length (L_{Median}, grey dashed), modal length (L_{Mode}, red solid), and 2.5th and 97.5th percentiles ($L_{2.5}$ and $L_{97.5}$, grey dotted) of the biomass-weighted length distribution. Note the different y-axis scales among years.

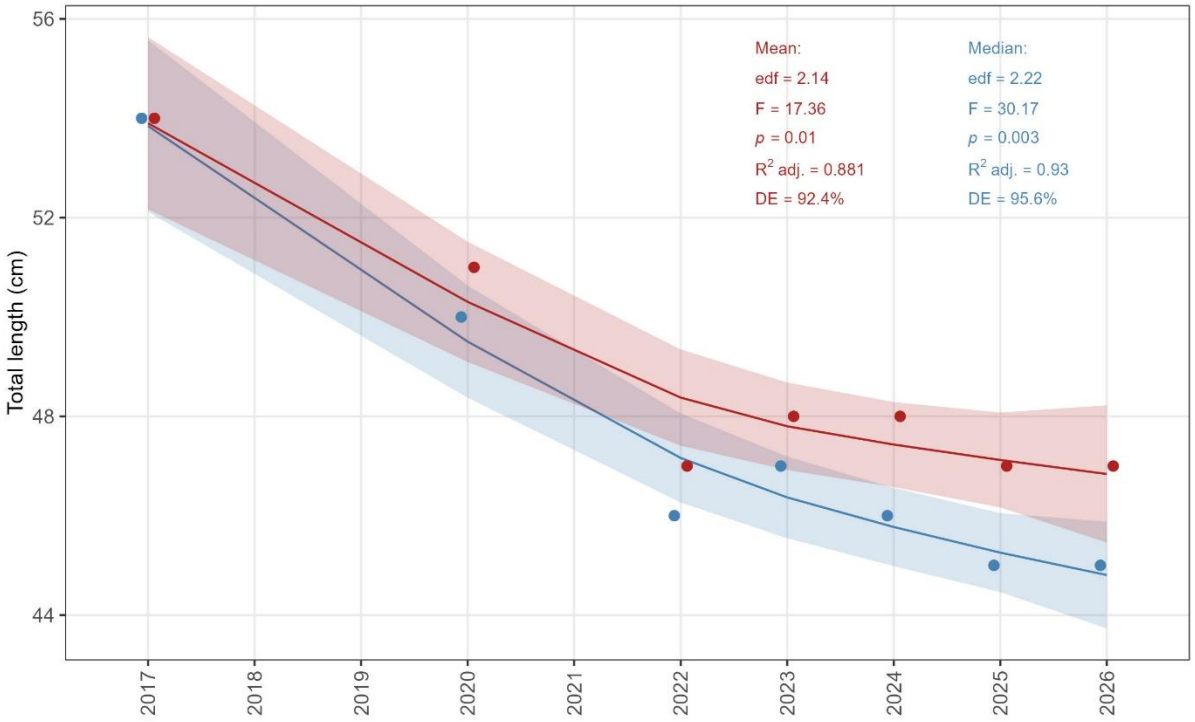

Fig. 24. Median (blue) and mean (red) total length of common hake (*Merluccius hubbsi*) during July groundfish and calamari pre-season surveys conducted in Falkland Islands waters in 2017, 2020, and 2022–2026. The line and shaded region represent the fitted Generalised Additive Model (GAM) smooth and its 95% pointwise confidence interval.

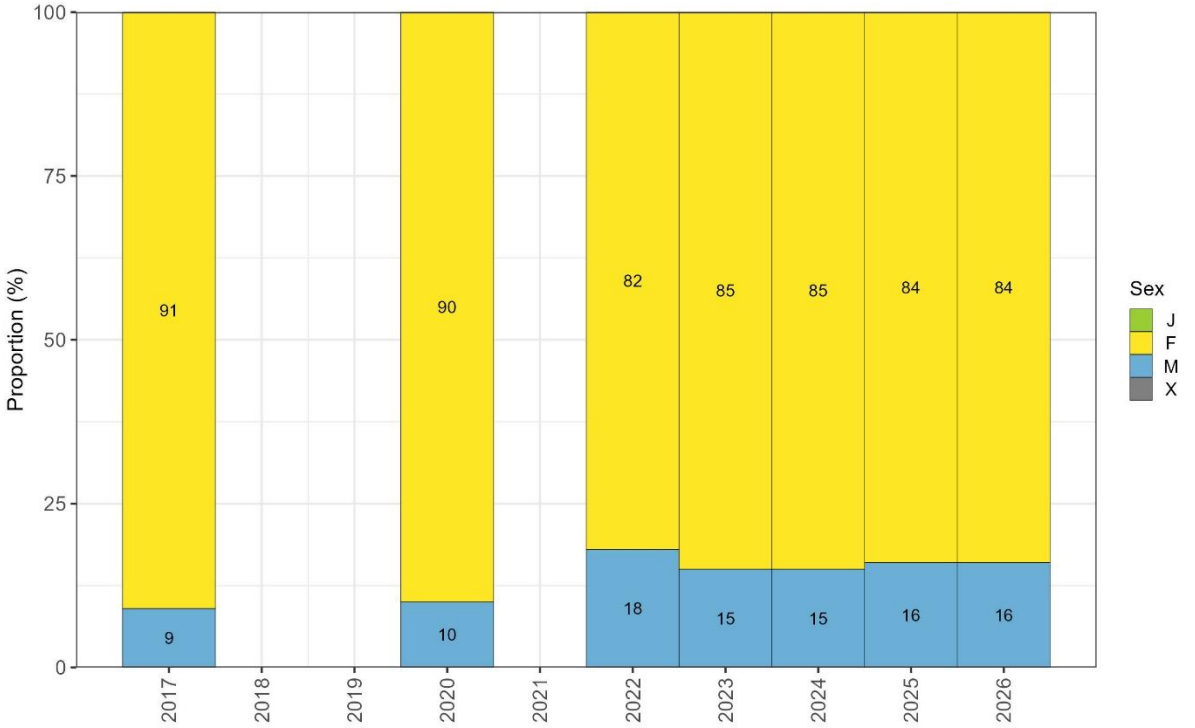

Fig. 25. Proportion by sex (J = juvenile; F = female; M = male; X = undetermined) of common hake (*Merluccius hubbsi*) during July groundfish and calamari pre-season surveys conducted in Falkland Islands waters in 2017, 2020, and 2022–2026. Labels for proportions < 3% are omitted.

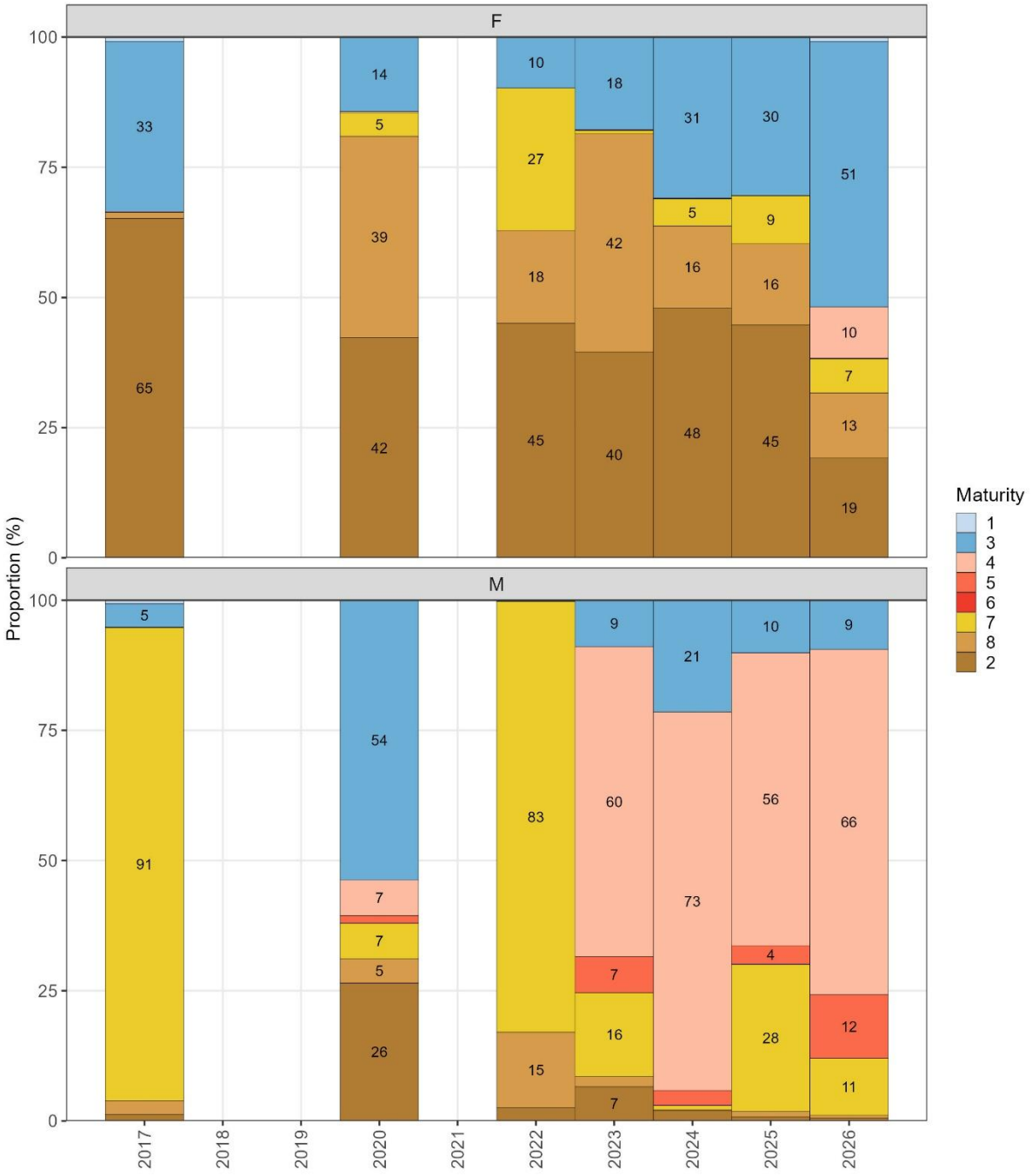

Fig. 26. Proportion by sexual maturity (1, immature; 3, early developing; 4, late developing; 5, ripe; 6, running; 7, spent; 8, recovering spent; 2, resting) of common hake (*Merluccius hubbsi*) during July groundfish and calamari pre-season surveys conducted in Falkland Islands waters in 2017, 2020, and 2022–2026. Maturity stages ordered by developmental sequence. Labels for proportions < 3% are omitted.

4.3.4. Hoki (*Macruronus magellanicus*)

4.3.4.1. Temporal patterns of abundance

On average, 67% of the total hoki catches in the time series were from groundfish surveys and 33% from calamari pre-season surveys. Hoki catch in 2026 (0.05 t) corresponded to < 1% of the 2017 catch (114.72 t), 10% of the 2025 catch (0.49 t), and 9% of the 2023–2025 mean catch (0.54 t; Fig. 27a; Appendix II).

The highest densities occurred in 2017 (mean ± SE: 1,267.56 ± 753.04 kg/km²). Densities in 2026 (1.35 ± 0.80 kg/km²) were the lowest in the time series and corresponded to < 1% of the 2017 densities, represented a 92% decrease relative to the 2025 densities (16.12 ± 10.38 kg/km²), and an 89% decrease relative to the 2023–2025 mean densities (12.43 ± 4.25 kg/km²; Fig. 27b).

The highest biomass in the time series was estimated for 2017 (85,477.47 t; CI = 26,258.16–159,761.23 t). Biomass declined over the following years and has remained at low levels. Hoki biomass in 2026 (970.16 t; CI = 535.38–1,938.16 t) was the second lowest in the time series and corresponded to a significant 99% decrease relative to 2017 levels ($p < 0.001$), a non-significant 74% decrease relative to 2025 levels (3,685.84 t; CI = 808.34–7,827.01 t), and a non-significant 60% decrease relative to the 2023–2025 mean (2,430.12 t; $p > 0.05$; Fig. 27c; Table IV–V; Appendix III–IV). Analysis of the full time series revealed a significant declining trend in biomass (GAM: edf = 1.00, F = 25.85, p = 0.004), with the model explaining 80.8% of the deviance (R^2 adj. = 0.875; Fig. 27c; Appendix V).

4.3.4.2. Spatial patterns of abundance

In 2026, hoki aggregations were located to the south-west, with the highest density (116 kg/km^2) at around 52.3°S and 61.7°W. Similar patterns were observed in previous years, except for 2017 when the highest density in the time series (84,055 kg/km^2) occurred to the east in the 'Loligo Box' (Fig. 28).

Analysis of the spatial change in density revealed an overall decrease in densities through the survey area in 2026 relative to 2017, 2025, and the 2023–2025 mean densities (Fig. 29). The increase in posterior densities noted to the north may be an artifact of the axial loop that resulted in the projection of densities in areas where hoki were not caught, and should be interpreted with caution (Fig. 29).

4.3.4.3. Length composition

Across all survey years combined, pre-anal length of hoki was in the range of 8 to 36 cm; however, 95% of the estimated biomass was comprised of individuals between 13 and 30 cm, with median and mean lengths (± SE) of 20 ± 1.56 cm and 19 ± 1.20 cm, respectively (Fig. 30a).

The distribution of biomass proportions by size class exhibited an 80% overlap between the groundfish and calamari pre-season surveys, with no significant differences between the groundfish survey (mean ± SE: 19 ± 1.21 cm) and the calamari pre-season survey (19 ± 1.22 cm; $p > 0.05$). In the groundfish survey, 95% of the biomass of hoki was comprised of individuals between 13 and 30 cm (median ± SE: 20 ± 1.56 cm). In the calamari pre-season

survey, 95% of the biomass was comprised of individuals between 14 and 29 cm (median ± SE: 19 ± 1.69 cm; Fig. 30b).

The distribution of biomass proportions by size class exhibited an 91% overlap between females and males. The permutation analysis revealed non-significant differences between females (mean ± SE: 20 ± 1.20 cm) and males (mean ± SE: 19 ± 1.19 cm; $p > 0.05$). For females, 95% of the biomass was comprised of individuals between 14 and 30 cm (median ± SE: 20 ± 1.54 cm). For males, 95% of the biomass was comprised of individuals between 13 and 29 cm (median ± SE: 19 ± 1.57 cm; Fig. 30c).

The size structure of hoki was broad and multimodal throughout the time series. Several length-groups were present and not clearly distinguished because of size overlap in most years. The main modal length increased from 14 cm in 2017 to 23 cm in 2020, and decreased over the following years to 20 cm in 2026 (Fig. 31). In 2026, pre-anal lengths were in the range of 8 to 31 cm; however, 95% of the biomass was comprised of individuals between 19 and 31 cm, with median and mean lengths (± SE) of 22 ± 0.87 cm and 22 ± 0.89 cm, respectively. For females, 95% of the individuals were between 17 and 31 cm, with median and mean lengths (± SE) of 22 ± 1.42 cm and 23 ± 1.37 cm, respectively. For males, 95% of the biomass was comprised of individuals between 19 and 27 cm, with median and mean lengths (± SE) of 21 ± 1.23 cm and 21 ± 1.07 cm, respectively (Fig. 31).

Analysis of the full time series revealed positive but non-significant temporal trends in mean (GAM: edf = 1.00, F = 1.36, p = 0.295, R^2 adj. = 0.056, DE = 21.4%) and median (GAM: edf = 1.00, F = 2.11, p = 0.206, R^2 adj. = 0.170, DE = 29.6%) pre-anal lengths. Both mean and median pre-anal lengths were approximately 16–17 cm in 2017 and increased to approximately 21–22 cm in 2026 (Fig. 32).

4.3.4.4. Sex and maturity composition

The sex composition of hoki was dominated by females (mean ± SE: 57.4 ± 2.4%), followed by males (42.6 ± 2.4%) throughout the time series. Sex composition had moderate interannual variability; female proportion ranged from 48% in 2026 to 65% in 2020 and 2022, and male proportion ranged from 35% in 2020 to 52% in 2026 (Fig. 33).

Maturity composition was dominated by post-spawning individuals (resting) in both sexes in most survey years. Resting individuals were predominant for females (68–96%) and for males (42–85%) in most years, except for 2017, 2023, and 2026 when immature and early developing individuals combined had a relatively higher contribution (≥ 64% for females, and ≥ 58% for males). Ripe and running individuals were not observed throughout the time series (Fig. 34).

4.3.4.5. Discussion

Analysis of the full time series revealed a significant declining trend in hoki biomass during July parallel surveys, with wide confidence intervals in the earlier years; note that hoki abundance is lower in Falkland Islands waters at this time of year (Falkland Islands Government 2026). This decline is consistent with a data-poor stock assessment of commercial catch data, which estimated 2018 biomass at approximately 13% of the 1987 level (Ramos & Winter 2019). At a broader regional scale, Zavatteri & Giussi (2022) reported

that hoki biomass in Argentine and adjacent waters peaked in 2000, declined sharply to a minimum in 2016, and recovered modestly in 2017–2019, a pattern consistent with the low biomass observed in February surveys around 2016–2017 (Ramos 2026). No biomass estimates are available from Falkland Islands commercial data since 2019 (Ramos & Winter 2022c), limiting more recent fishery–survey comparisons. Females contributed a higher proportion of biomass than males (~ 57% females, and ~ 43% males), and most individuals were at resting maturity, consistent with February parallel surveys (Ramos 2026) and indicating that hoki do not spawn within the survey area in either July or February.

Mean and median pre-anal length both increased from 2017 to 2026, although non-significantly, consistent with a similar increase in February surveys from 2020 to 2026 (Ramos 2026). While abundance has remained low in recent years in both survey periods, size composition appears to be shifting back towards larger individuals. This may be linked to the year-round closed area established in the south-western FICZ (south of 52.5°S, west of 60.5°W) since December 2023 to reduce Patagonian toothfish bycatch (FIFD, *unpublished internal document*), which overlaps with areas of historically higher hoki occurrence and may be easing fishing pressure and aiding stock recovery.

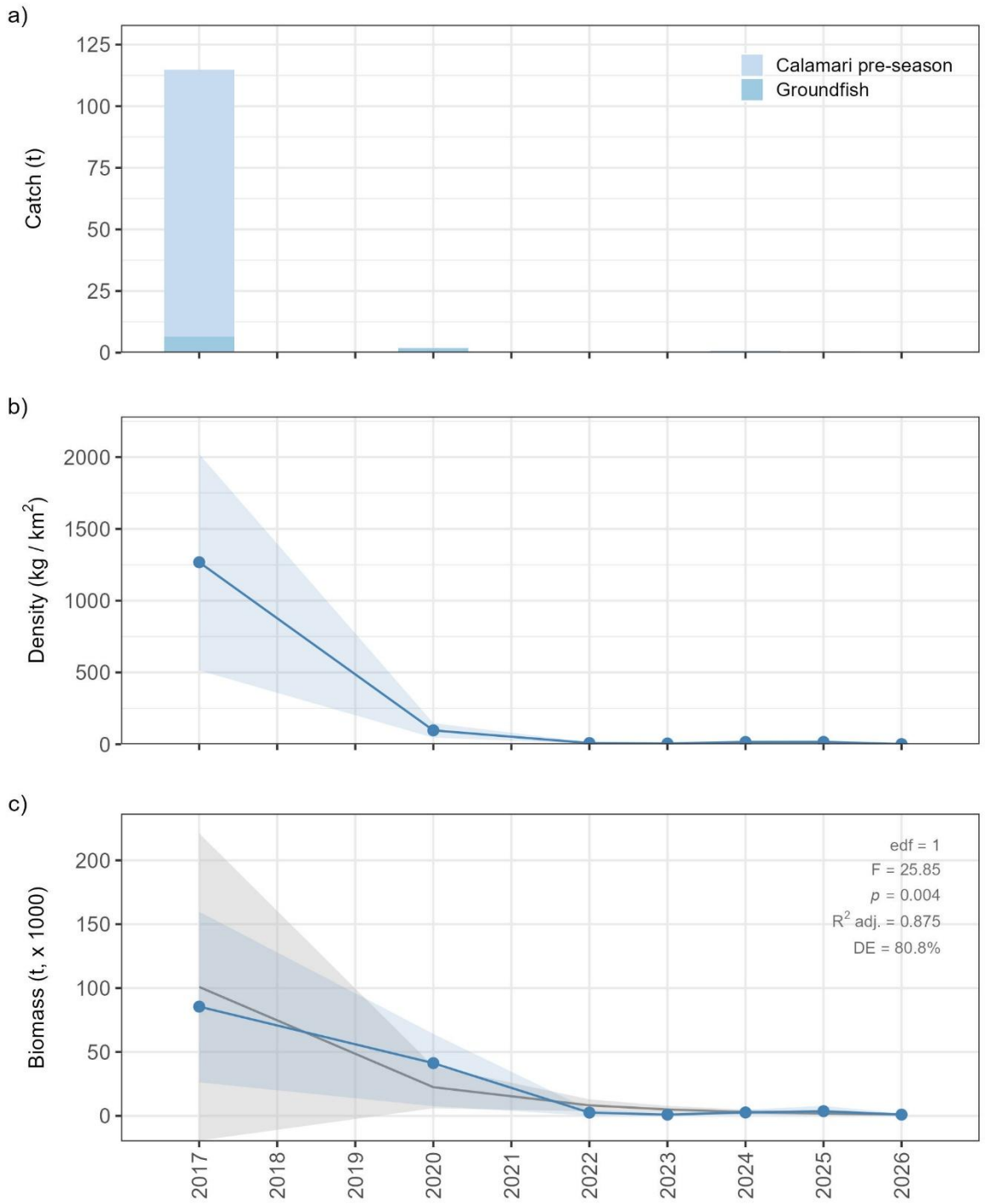

Fig. 27. Abundance of hoki (*Macruronus magellanicus*) during July groundfish and calamari pre-season surveys conducted in Falkland Islands waters in 2017, 2020, and 2022–2026. (a) Catch per survey, (b) annual mean density ± SE represented by the blue line and shaded region, respectively, and (c) estimated biomass, where the blue line and shaded region represent the median and 95% pointwise confidence interval derived from 10,000 bootstrap biomass estimates, and the grey line and shaded region represent the fitted Generalised Additive Model (GAM) smooth and its 95% pointwise confidence interval.

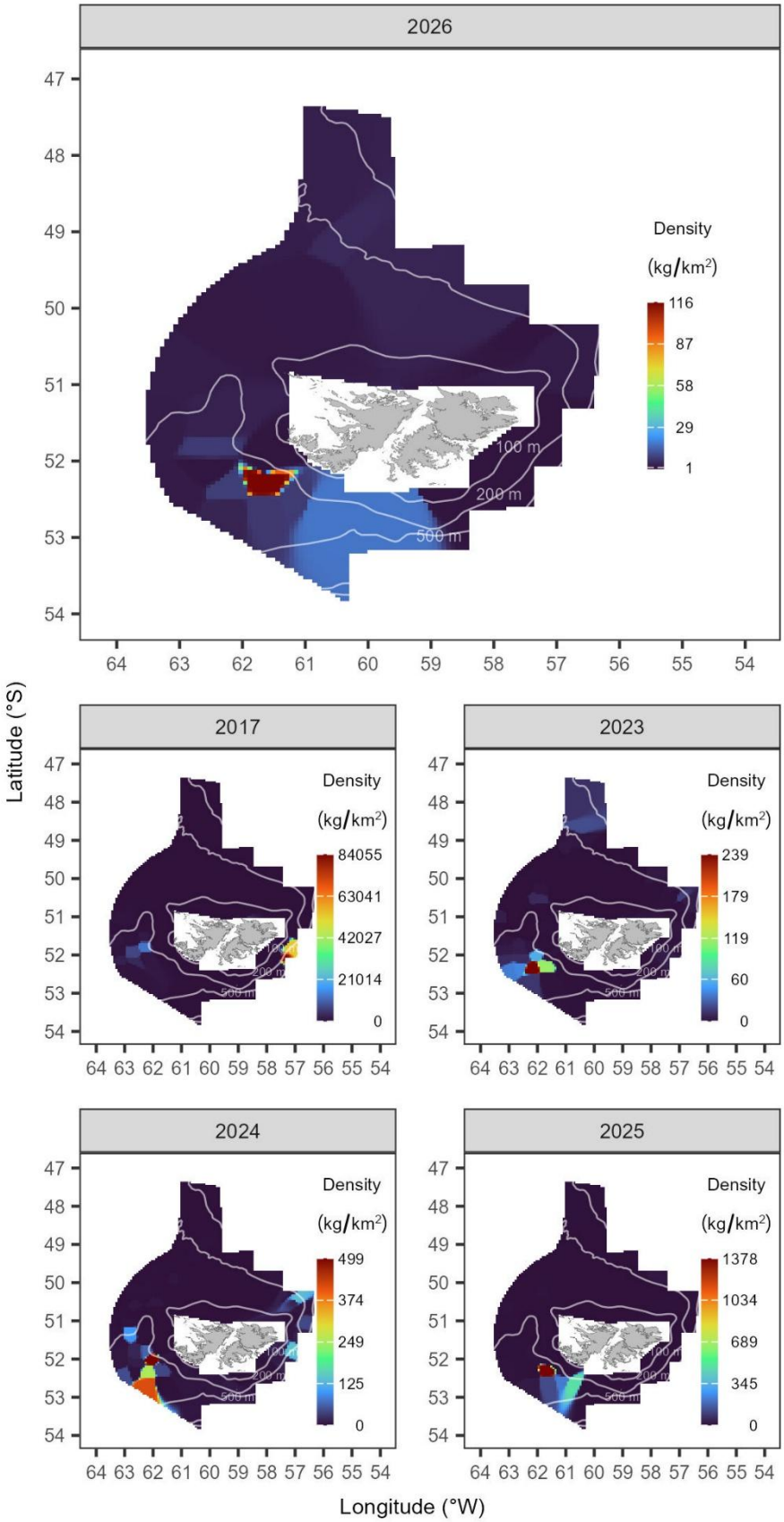

Fig. 28. Distribution and abundance of hoki (*Macruronus magellanicus*) derived from the July 2026 groundfish and calamari pre-season surveys in Falkland Islands waters, compared with the first year of the time series (2017) and the three preceding years (2023–2025). Colour scales are specific to each year. Isobaths at 100 m, 200 m, and 500 m are shown.

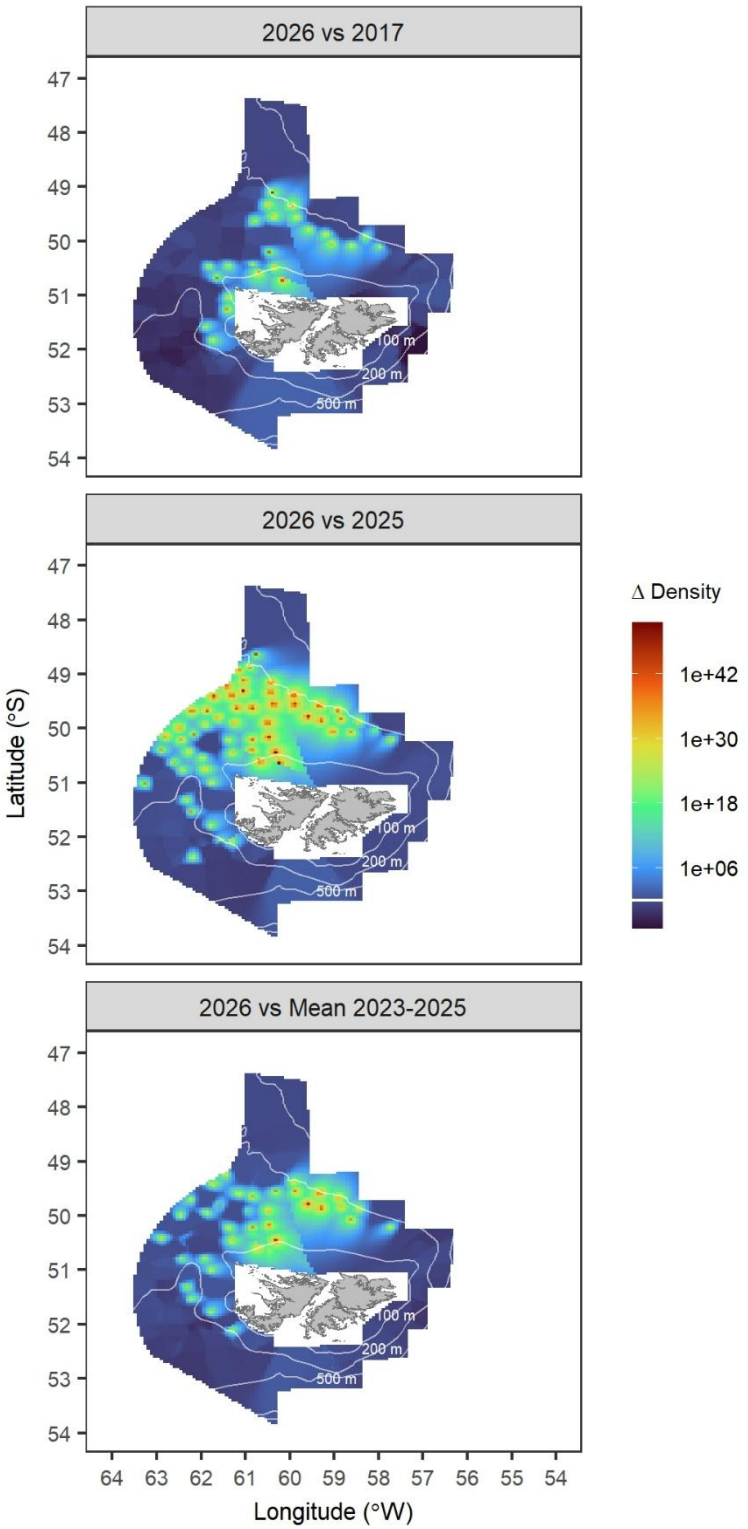

Fig. 29. Spatial change in density of hoki (*Macruronus magellanicus*) derived from the July 2026 groundfish and calamari pre-season surveys in Falkland Islands waters, relative to the first year of the time series (2017), the previous year (2025), and the mean of the three preceding years (2023–2025). The spatial change in density is expressed as the ratio of density (kg/km^2) in 2026 relative to the density in the baseline year (2017, 2025, 2023–2025 mean). Isobaths at 100 m, 200 m, and 500 m are shown. The colour scale is $\log_{10}$-transformed to aid visualisation, with increases in density indicated above the horizontal white line towards dark red, and decreases in density indicated below the horizontal white line towards dark blue.

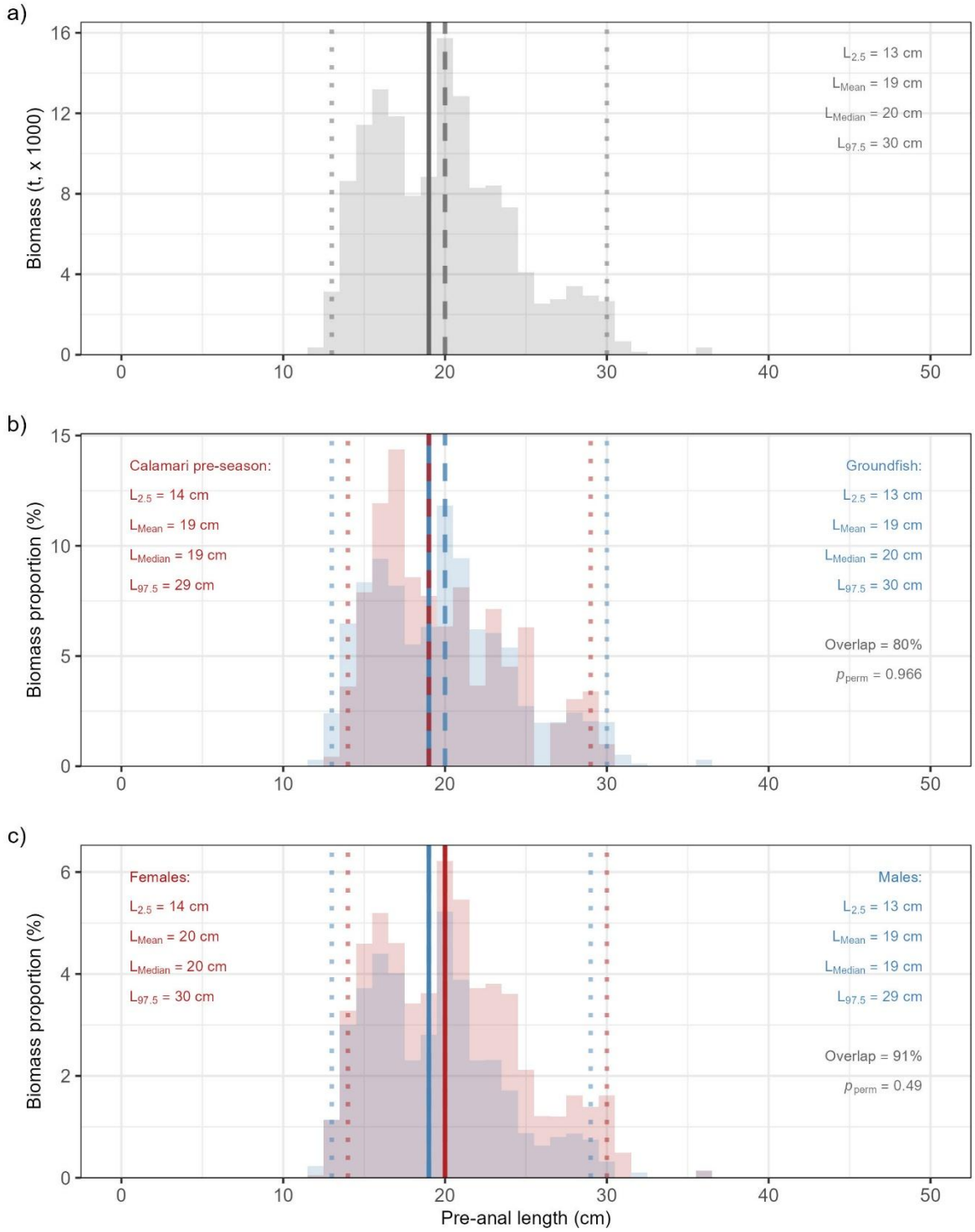

Fig. 30. Biomass-at-length class composition of hoki (*Macruronus magellanicus*) across all years combined, based on July groundfish and calamari pre-season surveys conducted in Falkland Islands waters in 2017, 2020, and 2022–2026. a) Overall biomass-at-length frequency distribution. b) Overlap in biomass-at-length distributions between calamari pre-season (red) and groundfish (blue) surveys. c) Overlap in biomass-at-length distributions between females (red) and males (blue). Solid vertical lines indicate the mean length (L_{Mean}), dashed lines the median length (L_{Median}), and dotted lines the 2.5th and 97.5th length percentiles ($L_{2.5}$ and $L_{97.5}$, respectively). p_{perm} is the significance of the weighted permutation test to assess differences between groups.

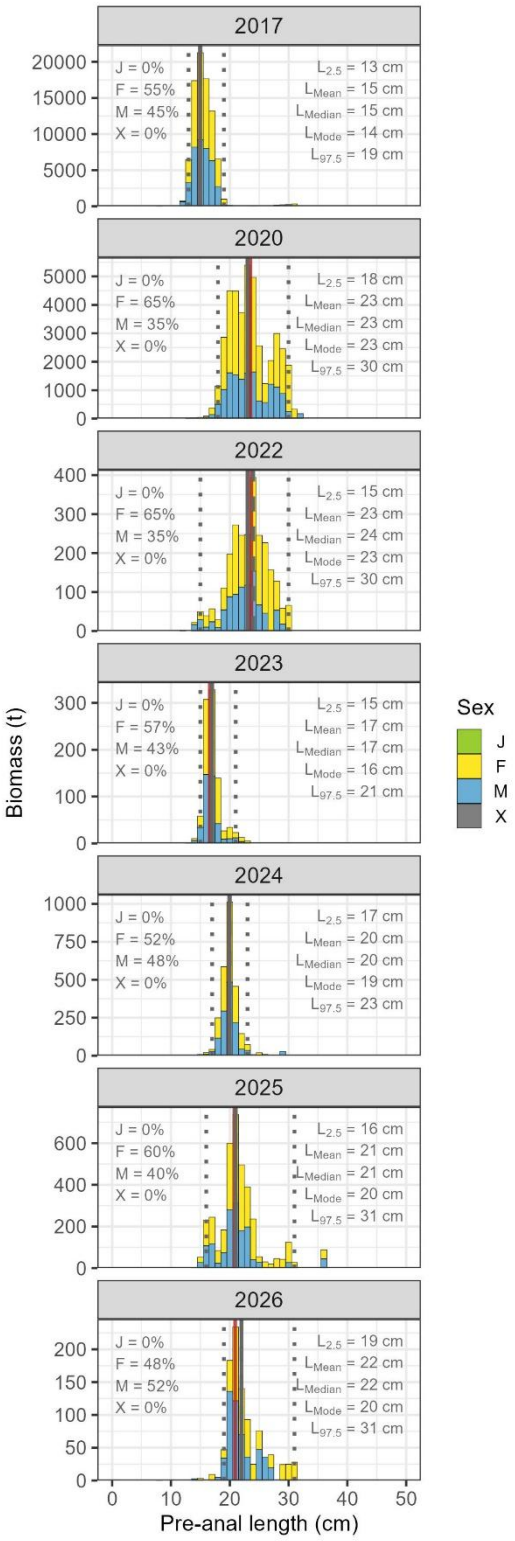

Fig. 31. Annual biomass-at-length class composition of hoki (*Macruronus magellanicus*) during July groundfish and calamari pre-season surveys conducted in Falkland Islands waters in 2017, 2020, and 2022–2026. Stacked bars represent biomass (t) per 1.0 cm length class, partitioned by sex (J = juvenile; F = female; M = male; X = undetermined), with the proportion of total annual biomass for each sex indicated in the upper left of each panel. Vertical lines indicate the mean length (L_{Mean}, grey solid), median length (L_{Median}, grey dashed), modal length (L_{Mode}, red solid), and 2.5th and 97.5th percentiles ($L_{2.5}$ and $L_{97.5}$, grey dotted) of the biomass-weighted length distribution. Note the different y-axis scales among years.

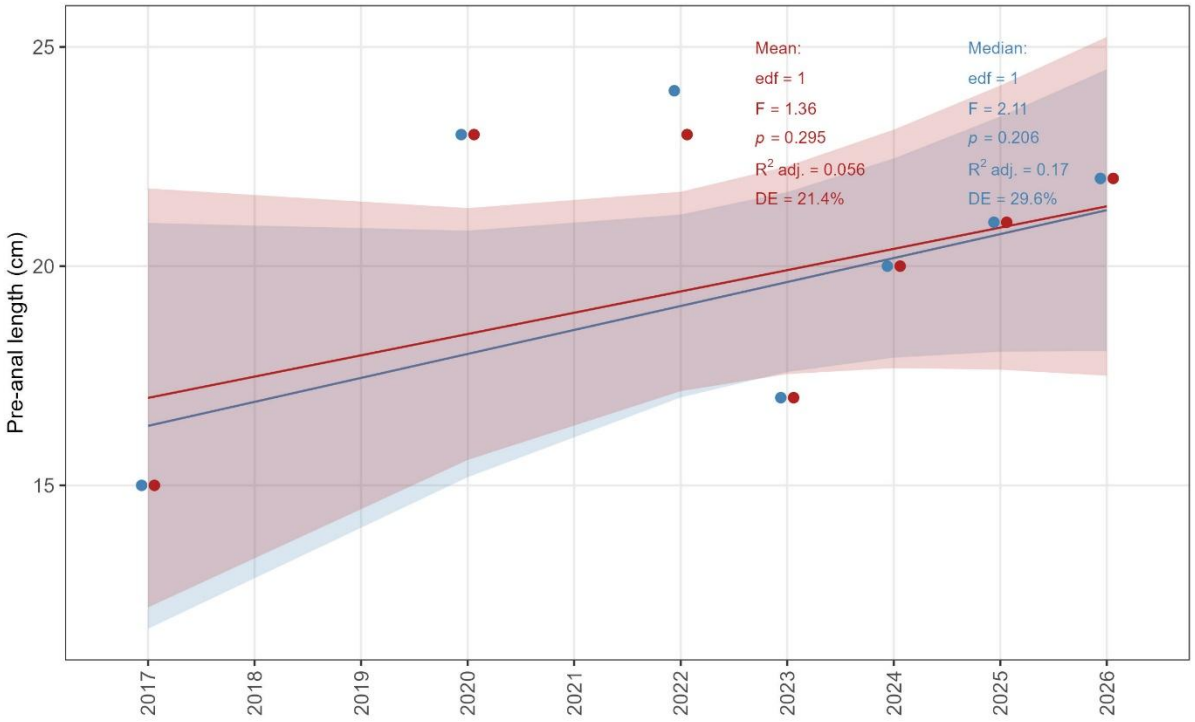

Fig. 32. Median (blue) and mean (red) pre-anal length of hoki (*Macruronus magellanicus*) during July groundfish and calamari pre-season surveys conducted in Falkland Islands waters in 2017, 2020, and 2022–2026. The line and shaded region represent the fitted Generalised Additive Model (GAM) smooth and its 95% pointwise confidence interval.

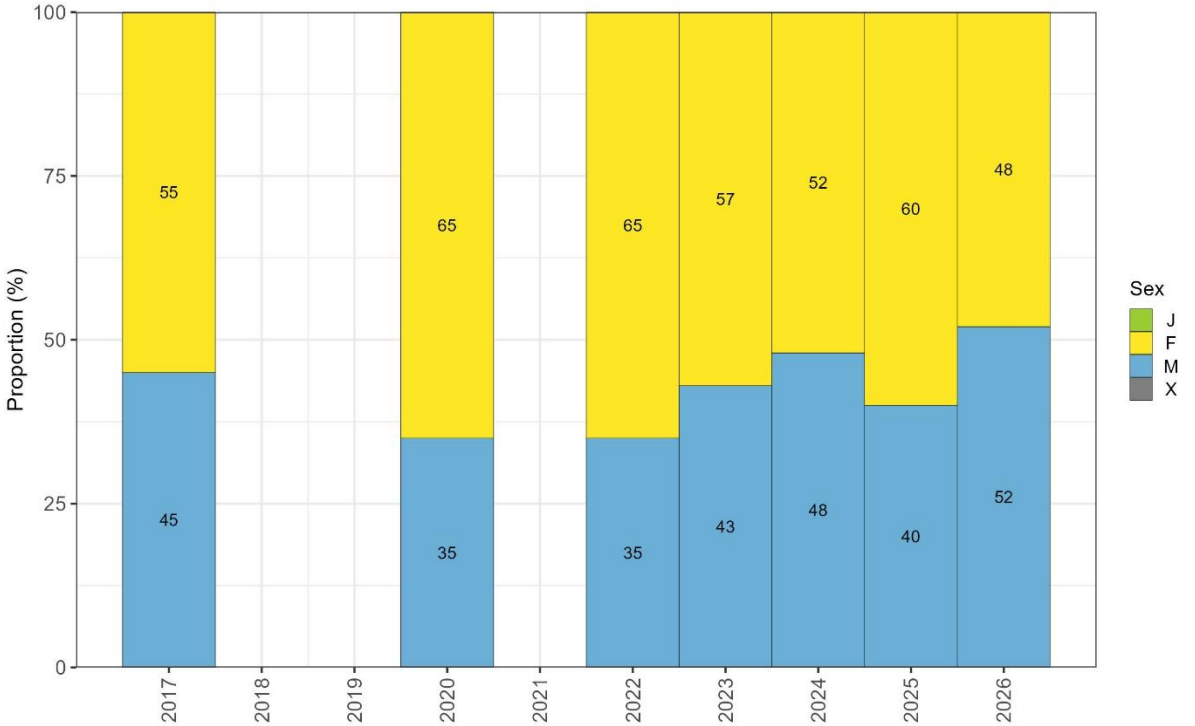

Fig. 33. Proportion by sex (J = juvenile; F = female; M = male; X = undetermined) of hoki (*Macruronus magellanicus*) during July groundfish and calamari pre-season surveys conducted in Falkland Islands waters in 2017, 2020, and 2022–2026. Labels for proportions < 3% are omitted.

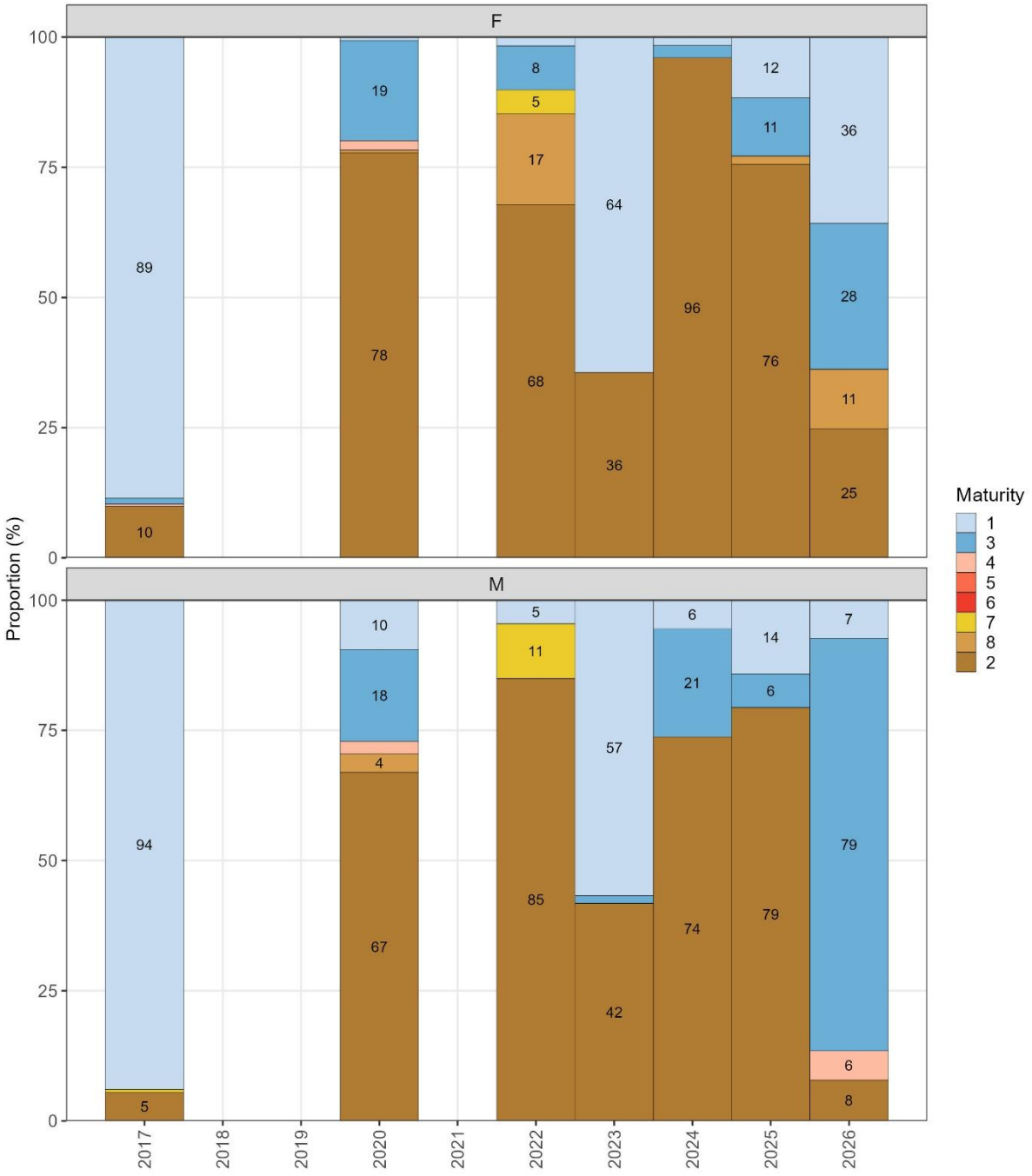

Fig. 34. Proportion by sexual maturity (1, immature; 3, early developing; 4, late developing; 5, ripe; 6, running; 7, spent; 8, recovering spent; 2, resting) of hoki (*Macruronus magellanicus*) during July groundfish and calamari pre-season surveys conducted in Falkland Islands waters in 2017, 2020, and 2022–2026. Maturity stages ordered by developmental sequence. Labels for proportions < 3% are omitted.

4.3.5. Kingclip (*Genypterus blacodes*)

4.3.5.1. Temporal patterns of abundance

On average, 93% of the total kingclip catches in the time series were from groundfish surveys and 7% from calamari pre-season surveys. The highest catch occurred in 2025 (12.42 t). Catch in 2026 (3.09 t) was the third lowest in the time series and corresponded to 74% of the 2017 catch (4.16 t), 25% of the 2025 catch, and 40% of the 2023–2025 mean (7.75 t; Fig. 35a; Appendix II).

The highest densities were recorded in 2025 (mean ± SE: 402.32 ± 278.85 kg/km²; although with wide confidence intervals). Densities in 2026 (87.99 ± 38.39 kg/km²) represented a 37% decrease relative to the 2017 densities (140.30 ± 64.04 kg/km²), a 78% decrease relative to the 2025 densities, and a 66% decrease relative to the 2023–2025 mean densities (265.48 ± 113.33 kg/km²; Fig. 35b).

Kingclip biomass was highest in 2025 (61,942.50 t; CI = 5,669.78–140,754.91 t; although with wide confidence intervals). Biomass in 2026 (28,633.11 t; CI = 8,154.03–69,826.45 t) was the third lowest in the time series, representing a 51% increase relative to 2017 levels (19,021.55 t; CI = 5,170.30–33,657.94 t) but a 54% decrease relative to 2025 levels and a 31% decrease relative to the 2023–2025 mean biomass (41,393.40 t); however, these were not significant changes in biomass ($p > 0.05$; Fig. 35c; Table IV–V; Appendix III–IV). Analysis of the full time series revealed a non-significant trend (GAM: edf = 1.00, F = 1.43, p = 0.286), with the model explaining only 22.3% of the deviance (R^2 adj. = 0.018; Fig. 35c; Appendix V).

4.3.5.2. Spatial patterns of abundance

In 2026, the highest density (4,689 kg/km^2) of kingclip occurred to the west of West Falkland at approximately 52°S and 61–62°W, with a secondary aggregation at approximately 50.5°S and 62.3°W. Similar patterns of spatial distribution were observed in 2023–2025, with the highest density in the time series recorded in 2025 (37,550 kg/km^2). In 2017, the highest density occurred at approximately 50.5°S and 62.3°W (Fig. 36).

Analysis of the spatial change in density revealed an overall decrease in densities through the survey area in 2026 relative to 2017, 2025, and the 2023–2025 mean, with minor increases to the north (Fig. 37).

4.3.5.3. Length composition

Across all survey years combined, total length of kingclip was in the range of 26 to 121 cm; however, 95% of the estimated biomass was comprised of individuals between 49 and 105 cm, with median and mean lengths (± SE) of 78 ± 2.79 cm and 77 ± 2.04 cm (Fig. 38a).

The distribution of biomass proportions by size class exhibited a 64% overlap between the groundfish and calamari pre-season surveys, with no significant differences between the groundfish survey (mean ± SE: 77 ± 2.04 cm) and the calamari pre-season survey (mean ± SE: 74 ± 2.45 cm; $p > 0.05$). In the groundfish survey, 95% of the biomass of kingclip was comprised of individuals between 49 and 105 cm (median ± SE: 78 ± 2.79 cm). In the calamari pre-season survey, 95% of the biomass was comprised of individuals between 54 and 103 cm (median ± SE: 70 ± 3.48 cm; Fig. 38b).

The distribution of biomass proportions by size class exhibited an 82% overlap between females and males.

The permutation analysis revealed that females (mean ± SE: 80 ± 2.06 cm) were significantly larger than males (mean ± SE: 71 ± 2.00 cm; $p < 0.001$). This difference in size structure was in part due to the presence of females > 70 cm that were not as abundant for males. For females, 95% of the biomass was comprised of individuals between 51 and 106 cm (median ± SE: 82 ± 2.56 cm). For males, 95% of the biomass was comprised of individuals between 46 and 99 cm (median ± SE: 71 ± 2.39 cm; Fig. 38c).

Through the time series, the size structure of kingclip was broad and multimodal. Several length-groups were present and not clearly distinguished because of size overlap. The main modal length increased from 73 cm in 2017 to 89 cm in 2026 (Fig. 39). In 2026, lengths were in the range of 33 to 121 cm; however, 95% of the biomass was comprised of individuals between 59 and 106 cm, with median and mean lengths (± SE) of 88 ± 1.84 cm and 86 ± 1.79 cm, respectively. For females, 95% of the biomass was comprised of individuals between 63 and 106 cm, with median and mean lengths (± SE) of 89 ± 1.94 cm and 88 ± 1.99 cm, respectively. For males, 95% of the biomass was comprised of individuals between 45 and 103 cm, with median and mean lengths (± SE) of 79 ± 2.14 cm and 78 ± 2.21 cm, respectively (Fig. 39).

Strongly significant non-linear trends were observed for the mean (GAM: edf = 2.36, $F = 22.69$, $p = 0.006$, R^2 adj. = 0.914, DE = 94.8%) and the median (GAM: edf = 2.71, $F = 19.59$, $p = 0.018$, R^2 adj. = 0.913, DE = 95.2%) lengths. Both mean and median lengths were approximately 69 cm in 2017, remained relatively stable through to 2020, and increased to approximately 85–87 cm in 2026 (Fig. 40).

4.3.5.4. Sex and maturity composition

The sex composition of kingclip was consistently dominated by females (mean ± SE: 66.9 ± 3.1%), followed by males (33.1 ± 1.3%) throughout the time series; individuals of undetermined sex accounted for negligible proportions (< 1%). Interannual variability in sex composition was moderate, with the female proportion ranging from 58% in 2020 to 80% in 2026, and the male proportion ranging from 20% in 2026 to 42% in 2020 (Fig. 41).

Maturity composition was dominated by post-spawning individuals (resting) in both sexes in most years. For females, resting individuals were predominant (58–93%) between 2017 and 2025. For males, resting individuals were predominant (≥ 56%) in most years, except for 2026. Late developing, ripe, and running individuals were reported in small proportions (< 9% combined). In 2026, sex composition departed from this pattern and was characterised by a shift towards immature and early developing individuals (Fig. 42).

4.3.5.5. Discussion

Kingclip biomass has remained relatively low in Falkland Islands waters during July parallel surveys, comparable with levels observed in recent February surveys (Ramos 2026). Biomass was comprised mostly of females (~ 67%), and mainly at resting maturity stage, indicating that spawning does not occur within the survey area in either July or February (Ramos 2026). These low biomass levels are consistent with declining CPUE in the Falkland

Islands finfish fishery since 2013 (García 2024) and with analyses of Argentine survey and fishery data showing an overall biomass decline from 1987 to 2021, a period of stability from 2014 to 2017, and a gradual increase thereafter (Di Marco 2022). The biomass trends observed in the July and February surveys may thus reflect broader regional dynamics.

Despite low biomass levels, both mean and median total length showed significant increasing trends, corresponding with the size increase observed in February surveys since 2021 (Ramos 2026). Because kingclip are caught at relatively small sizes in the Falkland Islands and stock status remains below the limit reference point, harvesting closer to 80 cm has been recommended to improve fishing mortality and yield per recruit and facilitate stock recovery (García 2025). The frequent presence of large individuals (70–95 cm) in recent February and July surveys indicates that such animals are available in the FICZ/FOCZ, and the recovery of mean and median length beyond 80 cm may point to an improving size structure that could support more selective harvesting strategies. Further work is needed to evaluate whether restricting fishing in specific grid squares or adjusting fishing gear could reduce catches of small individuals and further support stock recovery.

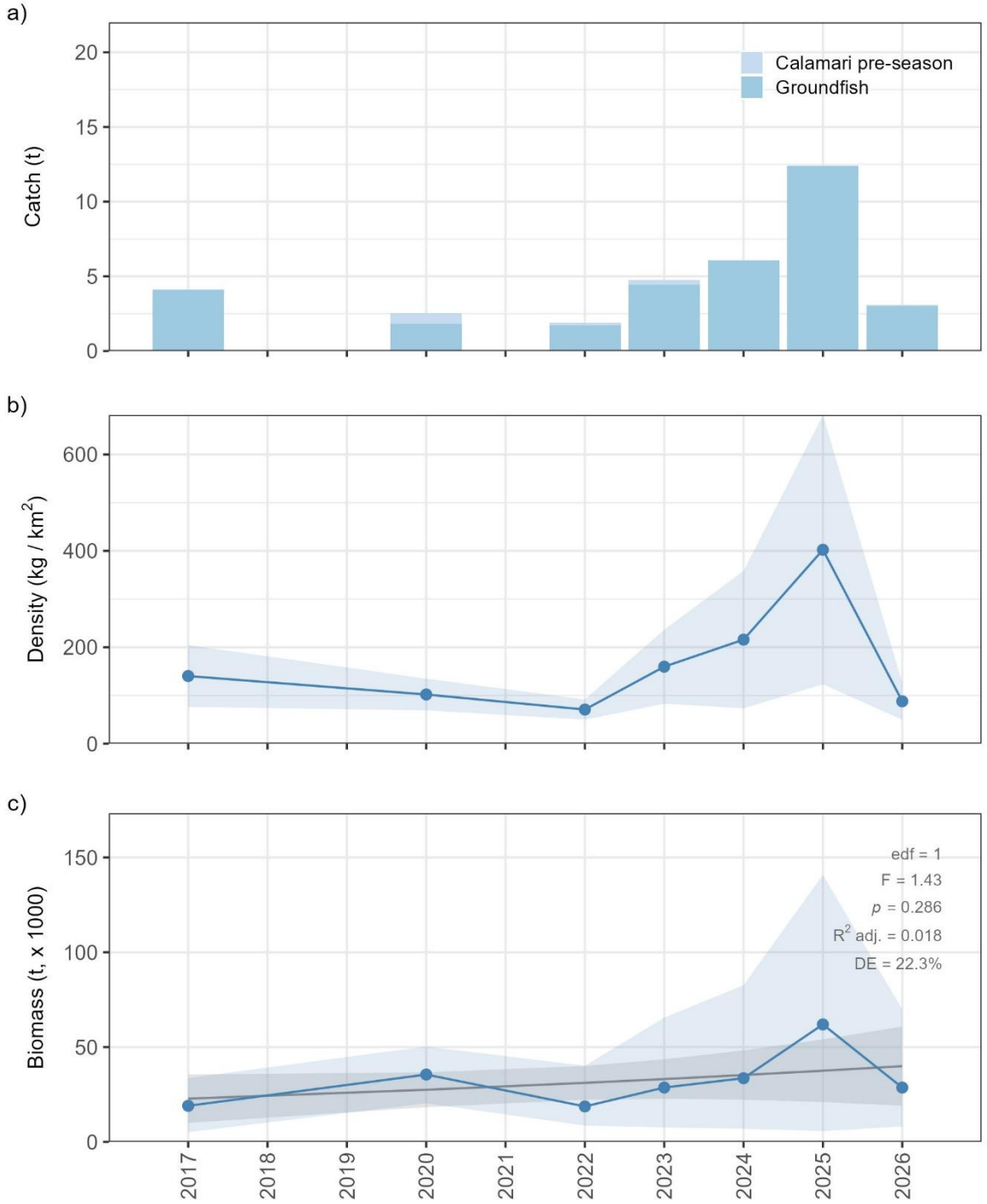

Fig. 35. Abundance of kingclip (*Genypterus blacodes*) during July groundfish and calamari pre-season surveys conducted in Falkland Islands waters in 2017, 2020, and 2022–2026. (a) Catch per survey, (b) annual mean density ± SE represented by the blue line and shaded region, respectively, and (c) estimated biomass, where the blue line and shaded region represent the median and 95% pointwise confidence interval derived from 10,000 bootstrap biomass estimates, and the grey line and shaded region represent the fitted Generalised Additive Model (GAM) smooth and its 95% pointwise confidence interval.

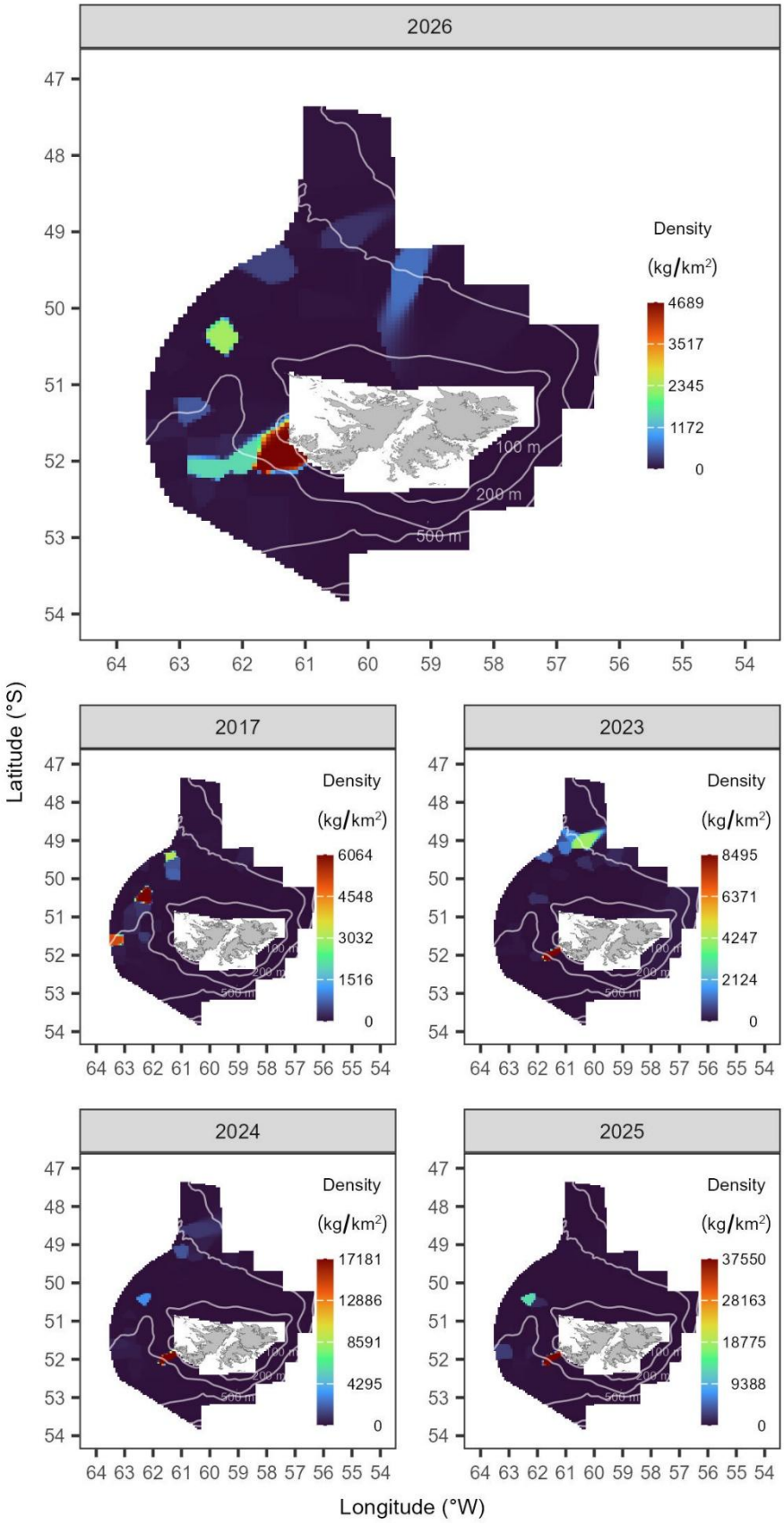

Fig. 36. Distribution and abundance of kingclip (*Genypterus blacodes*) derived from the July 2026 groundfish and calamari pre-season surveys in Falkland Islands waters, compared with the first year of the time series (2017) and the three preceding years (2023–2025). Colour scales are specific to each year. Isobaths at 100 m, 200 m, and 500 m are shown.

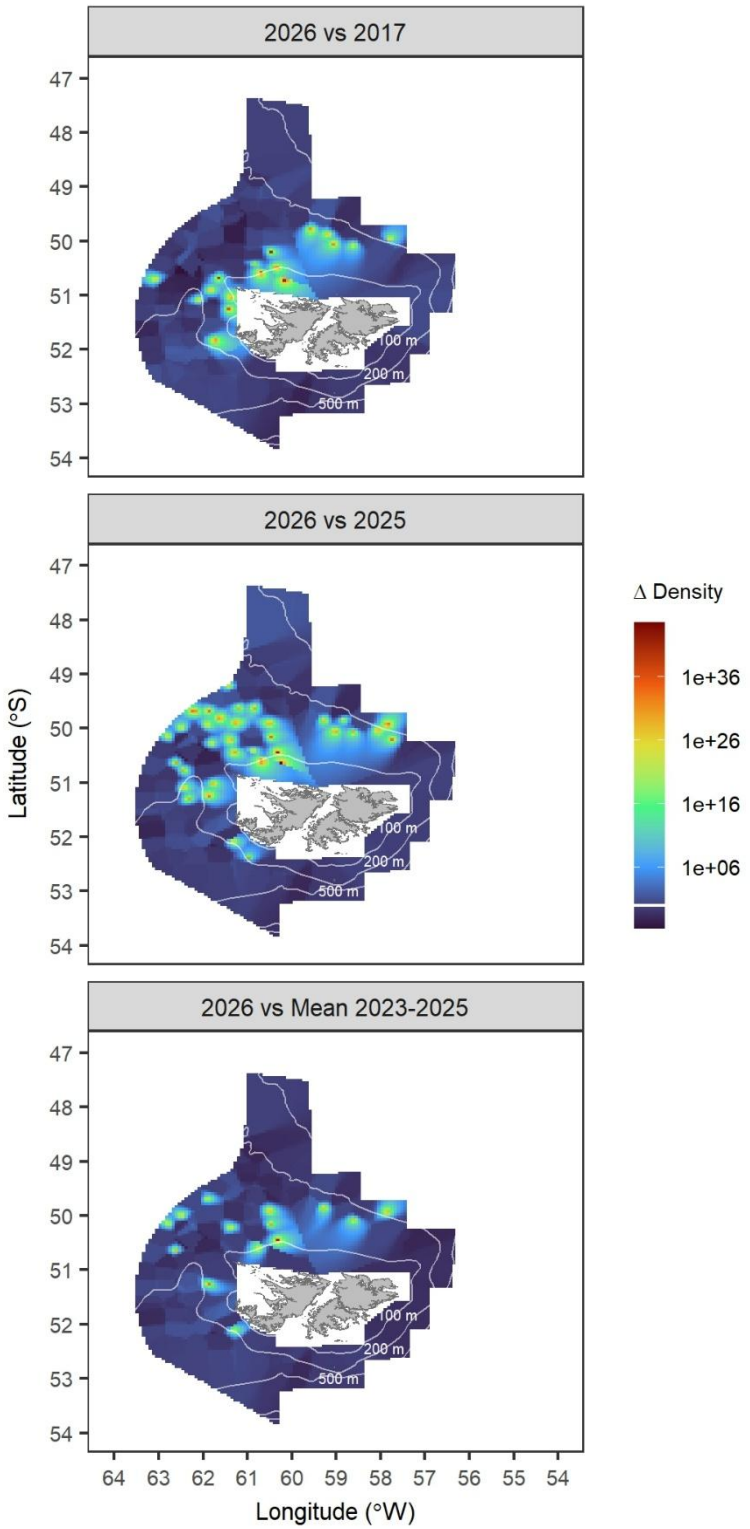

Fig. 37. Spatial change in density of kingclip (*Genypterus blacodes*) derived from the July 2026 groundfish and calamari pre-season surveys in Falkland Islands waters, relative to the first year of the time series (2017), the previous year (2025), and the mean of the three preceding years (2023–2025). The spatial change in density is expressed as the ratio of density (kg/km^2) in 2026 relative to the density in the baseline year (2017, 2025, 2023–2025 mean). Isobaths at 100 m, 200 m, and 500 m are shown. The colour scale is $\log_{10}$-transformed to aid visualisation, with increases in density indicated above the horizontal white line towards dark red, and decreases in density indicated below the horizontal white line towards dark blue.

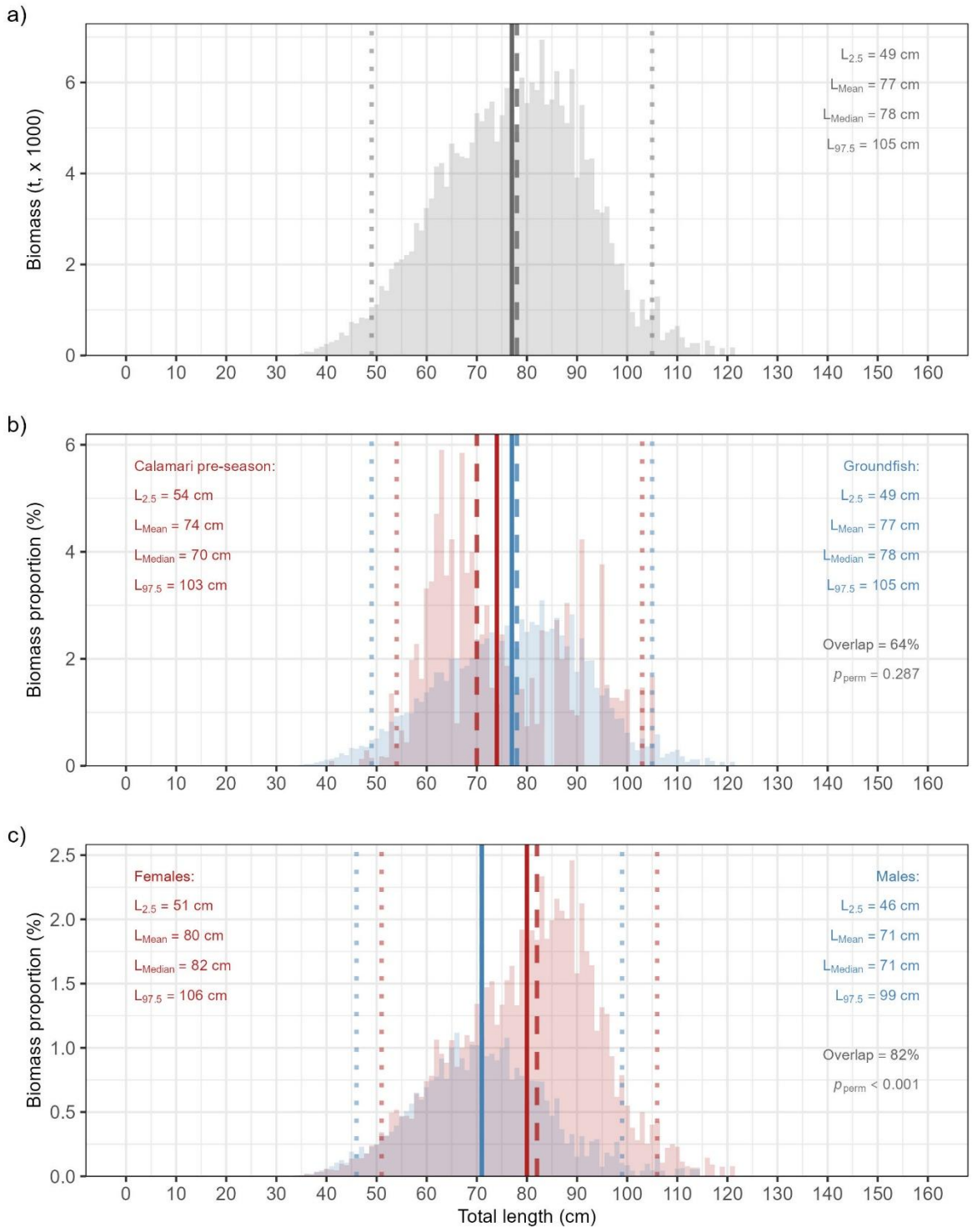

Fig. 38. Biomass-at-length class composition of kingclip (*Genypterus blacodes*) across all years combined, based on July groundfish and calamari pre-season surveys conducted in Falkland Islands waters in 2017, 2020, and 2022–2026. a) Overall biomass-at-length frequency distribution. b) Overlap in biomass-at-length distributions between calamari pre-season (red) and groundfish (blue) surveys. c) Overlap in biomass-at-length distributions between females (red) and males (blue). Solid vertical lines indicate the mean length (L_{Mean}), dashed lines the median length (L_{Median}), and dotted lines the 2.5th and 97.5th length percentiles ($L_{2.5}$ and $L_{97.5}$, respectively). p_{perm} is the significance of the weighted permutation test to assess differences between groups.

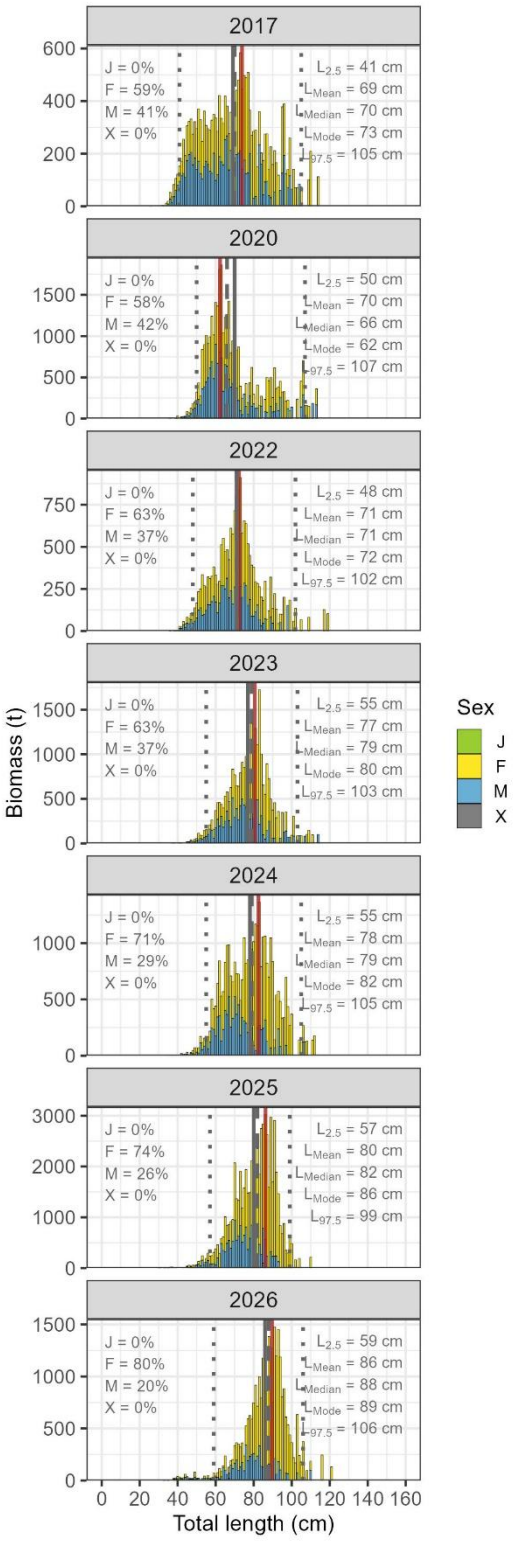

Fig. 39. Annual biomass-at-length class composition of kingclip (*Genypterus blacodes*) during July groundfish and calamari pre-season surveys conducted in Falkland Islands waters in 2017, 2020, and 2022–2026. Stacked bars represent biomass (t) per 1.0 cm length class, partitioned by sex (J = juvenile; F = female; M = male; X = undetermined), with the proportion of total annual biomass for each sex indicated in the upper left of each panel. Vertical lines indicate the mean length (L_{Mean}, grey solid), median length (L_{Median}, grey dashed), modal length (L_{Mode}, red solid), and 2.5th and 97.5th percentiles ($L_{2.5}$ and $L_{97.5}$, grey dotted) of the biomass-weighted length distribution. Note the different y-axis scales among years.

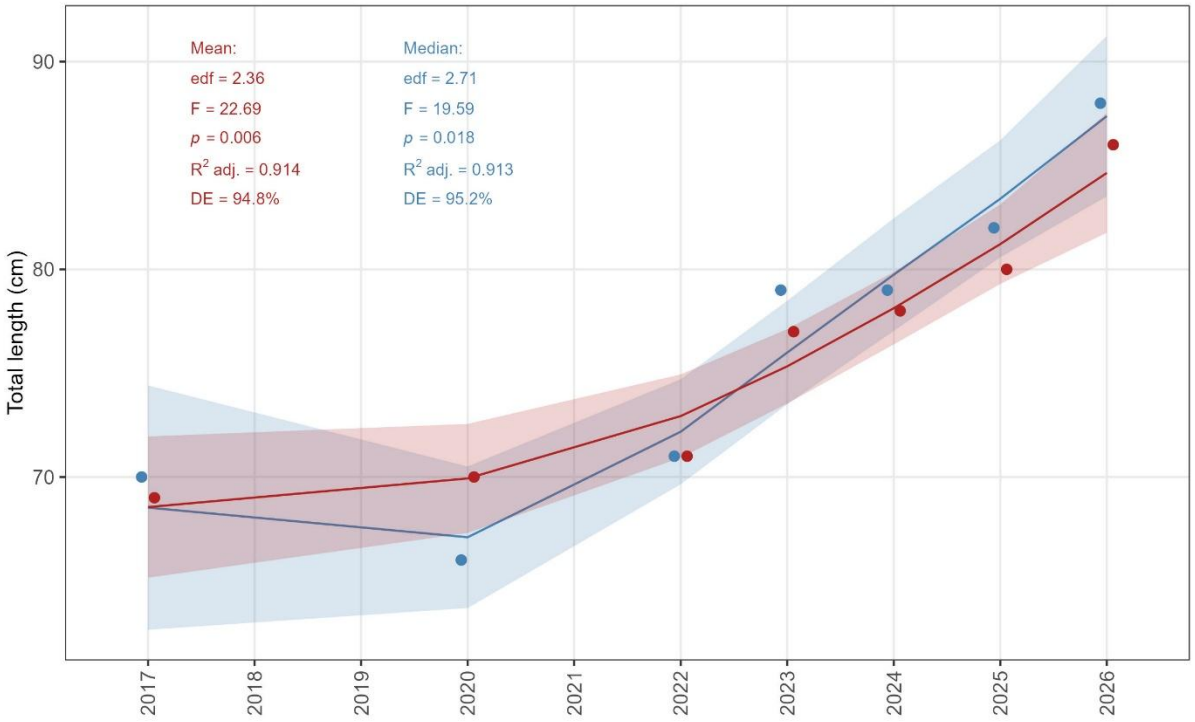

Fig. 40. Median (blue) and mean (red) total length of kingclip (*Genypterus blacodes*) during July groundfish and calamari pre-season surveys conducted in Falkland Islands waters in 2017, 2020, and 2022–2026. The line and shaded region represent the fitted Generalised Additive Model (GAM) smooth and its 95% pointwise confidence interval.

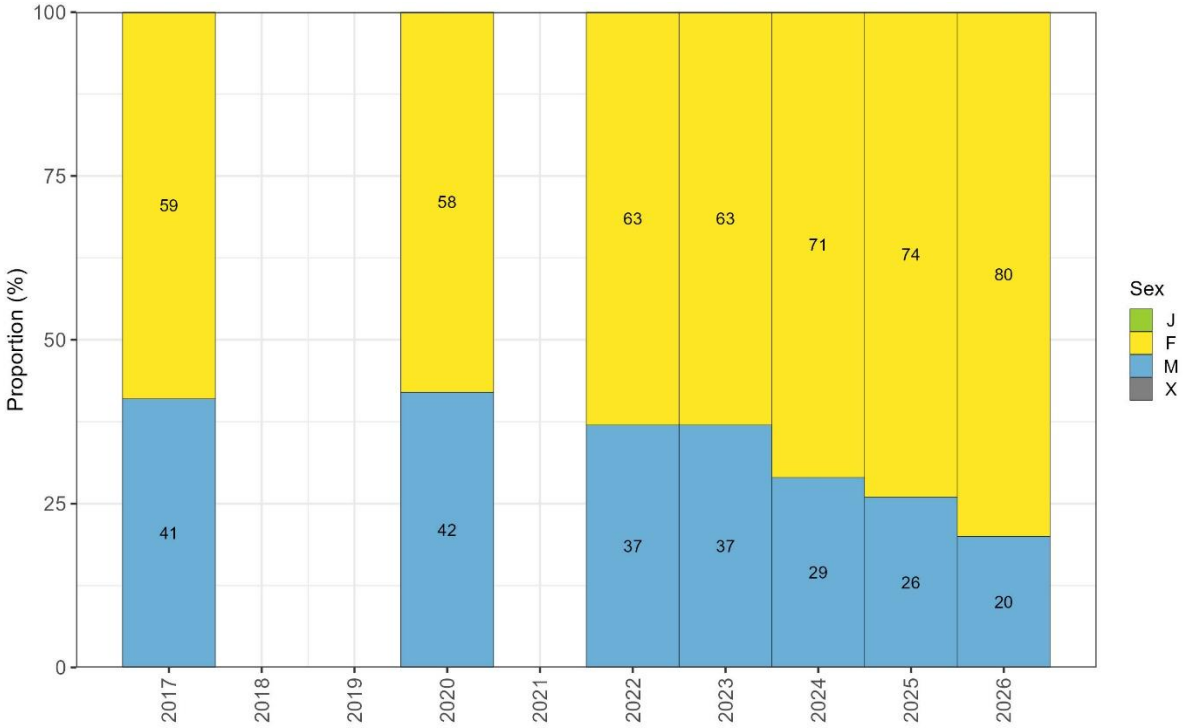

Fig. 41. Proportion by sex (J = juvenile; F = female; M = male; X = undetermined) of kingclip (*Genypterus blacodes*) during July groundfish and calamari pre-season surveys conducted in Falkland Islands waters in 2017, 2020, and 2022–2026. Labels for proportions < 3% are omitted.

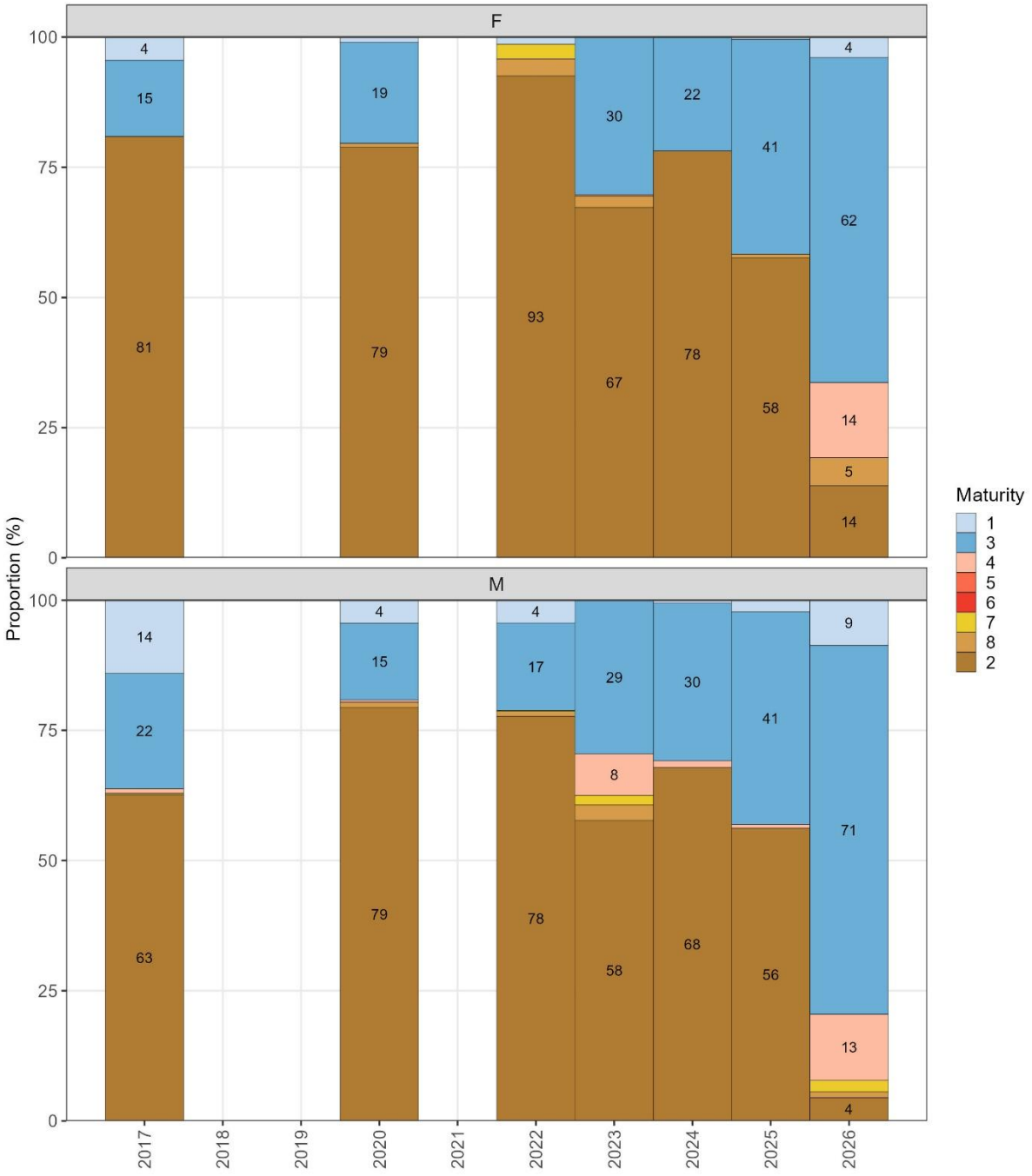

Fig. 42. Proportion by sexual maturity (1, immature; 3, early developing; 4, late developing; 5, ripe; 6, running; 7, spent; 8, recovering spent; 2, resting) of kingclip (*Genypterus blacodes*) during July groundfish and calamari pre-season surveys conducted in Falkland Islands waters in 2017, 2020, and 2022–2026. Maturity stages ordered by developmental sequence. Labels for proportions < 3% are omitted.

4.3.6. Patagonian squid (*Doryteuthis gahi*)

4.3.6.1. Temporal patterns of abundance

On average, 3.5% of the Patagonian squid catches in the time series were from groundfish surveys and 96.5% from calamari pre-season surveys. Catches increased from 2017 (316 t) to 2020 (580 t) but decreased over the following years and reached the lowest catch in 2024 (55 t). The third lowest catch in the time series was reported in 2026 (210 t) and represented a 33% decrease relative to the 2017 catch, a 2% increase relative to 2025 catch (206 t), and a 12% increase relative to the 2023–2025 mean catch (187 t; Fig. 43a; Appendix II).

The highest densities were recorded in 2020 (mean ± SE: 5,538.19 ± 1,835.03 kg/km²). Densities in 2026 (1,131.38 ± 212.90 kg/km²) were the second lowest in the time series and represented a 58% decrease relative to the 2017 densities (2,708.03 ± 557.35 kg/km²), a 4% decrease relative to the 2025 densities (1,179.63 ± 145.40 kg/km²), and a 2% decrease relative to the 2023–2025 mean densities (1,159.04 ± 139.43 kg/km²; Fig. 43b).

Patagonian squid biomass was highest in 2017 (344,472.91 t; CI = 247,893.93–435,232.46 t), declined over the following years and reached the lowest level in 2024 (75,242.93 t; CI = 63,743.43–85,857.67 t). Biomass in 2026 (97,819.97 t; CI = 71,807.92–119,014.17 t) was the second lowest in the time series and represented a significant 72% decrease relative to 2017 levels ($p < 0.001$), a non-significant 22% decrease relative to 2025 levels (125,153.80 t; CI = 101,861.17–149,299.02 t; $p > 0.05$), and a non-significant 13% decrease relative to the 2023–2025 mean biomass (112,119.78 t; $p > 0.05$; Fig. 43c; Table IV–V; Appendix III–IV). Analysis of the full time series revealed a significant declining trend in biomass (GAM: edf = 1.00, F = 18.09, p = 0.008), with the model explaining 76.4% of the deviance (R^2 adj. = 0.806; Fig. 43c; Appendix V).

4.3.6.2. Spatial patterns of abundance

In 2026, the highest densities (17,821 kg/km²) were recorded to the south within the 'Loligo Box' at approximately 53°S and 59–60°W (Fig. 44), consistent with previous years. The highest density in the time series was calculated for 2020 (117,582 kg/km²) in the same area.

Analysis of the spatial change in density revealed an overall decrease in the 'Loligo Box' but an increase in patchy areas to the west in the FICZ in 2026 relative to 2017, 2025, and the 2023–2025 mean (Fig. 45).

4.3.6.3. Length composition

Across all survey years combined, dorsal mantle length of Patagonian squid was in the range of 3.0 to 35.0 cm; however, 95% of the estimated biomass was comprised of individuals between 7.5 and 18.5 cm, with median and mean lengths (± SE) of 11.5 ± 0.68 cm and 11.5 ± 0.70 cm, respectively (Fig. 46a).

The distribution of biomass proportions by size class exhibited a 77% overlap between the groundfish and calamari pre-season surveys, with no significant differences between the groundfish survey (mean ± SE: 11.0 ± 0.71 cm) and the calamari pre-season survey (mean ± SE: 12.0 ± 0.70 cm; $p > 0.05$). In the groundfish survey, 95% of the biomass of Patagonian squid was comprised of individuals between 6.5 and 18.0 cm (median ± SE: 11.0 ± 0.73 cm).

In the calamari pre-season survey, 95% of the biomass was comprised of individuals between 8.5 and 18.5 cm (median ± SE: 12.0 ± 0.67 cm; Fig. 46b).

The distribution of biomass proportions by size class exhibited a 92% overlap between females and males, with no significant differences between females (mean ± SE: 11.0 ± 0.60 cm) and males (mean ± SE: 12.0 ± 0.74 cm; $p > 0.05$). For females, 95% of the biomass was comprised of individuals between 7.5 and 15.5 cm (median ± SE: 11.0 ± 0.65 cm). For males, 95% of the biomass was comprised of individuals between 7.5 and 20.0 cm (median ± SE: 12.0 ± 0.72 cm (Fig. 46c).

The size structure was mostly unimodal, with modal length decreasing from 13.5 cm in 2017 to 11.0 cm in 2026. In 2026, dorsal mantle lengths were in the range of 4.0 to 29.5 cm; however, 95% of the biomass was comprised of individuals between 6.5 and 17.0 cm, with median and mean lengths (± SE) of 11.5 ± 0.48 cm and 11.5 ± 0.47 cm, respectively. For females, 95% of the individuals were between 6.5 and 15.0 cm, with median and mean lengths (± SE) of 11.0 ± 0.63 cm and 10.5 ± 0.59 cm, respectively. For males, 95% of the biomass was comprised of individuals between 6.5 and 18.0 cm, with median and mean lengths (± SE) of 12.0 ± 0.68 cm and 12.0 ± 0.70 cm, respectively (Fig. 47).

Analysis of the full time series revealed a non-significant temporal trend in mean dorsal mantle length (GAM: edf = 1.85, $F = 5.77$, $p = 0.063$, R^2 adj. = 0.672, DE = 77.4%). In contrast, median dorsal mantle length decreased significantly (GAM: edf = 2.55, $F = 12.64$, $p = 0.033$, R^2 adj. = 0.863, DE = 92.2%). The fitted smooths for mean and median lengths showed similar patterns, decreasing from 13.0–13.5 cm in 2017 to 11.0–11.5 cm in 2026 (Fig. 48).

Analysis of the spatial distribution of median length revealed that the largest individuals occurred in 2017, and these were less evident over the following survey years. Large individuals were mainly distributed to the south within the 'Loligo Box', although these were also observed to the west in the FICZ in 2017, 2023, 2024, and 2026, likely associated with deeper stations (> 200 m depth). Small individuals were generally distributed to the west, between the 100 m and the 200 m isobaths (Appendix VI).

4.3.6.4. Sex and maturity composition

The sex composition of Patagonian squid was relatively consistent and comprised of 52.3 ± 1.7% (mean ± SE) males and 47.7 ± 1.7% females throughout the time series. Juveniles and individuals of undetermined sex were recorded in negligible proportions (< 1%). In 2017 and 2026, the sex composition had the lowest proportion of females (43%; Fig. 49).

Maturity composition was different between females and males throughout the time series. For females, preparatory individuals were predominant in 2017 (62%) but there was a shift towards immature individuals since 2020 (56–91%); maturing and mature females combined contributed < 10% in each year. Males had a greater representation of preparatory (23–54%), and of maturing and mature stages combined (35–73%; Fig. 50).

4.3.6.5. Discussion

Patagonian squid biomass declined significantly in July parallel surveys from 2017 to 2026, driven mainly by a decline in abundance in the southern 'Loligo Box'. This contrasts with February parallel surveys, which showed no significant temporal trend in biomass (Ramos

2026). Biomass estimates reported here differ in magnitude from those of the July calamari pre-season survey alone, as the latter uses a smaller 'Loligo Box' area and accounts for habitat preference; however, the declining trend is consistent between the two.

While first-season abundance has remained generally consistent in recent years, the second season has experienced persistently low abundances. The July 2024 pre-season survey yielded the lowest calamari biomass estimate since 2006 (Winter et al. 2025), prompting cancellation of the 2024 second season; this was apparently linked to a northward displacement of *D. gahi* driven by strong, colder oceanic currents, which caused the fleet to fish in international waters north of the FOCZ (Falkland Islands Government 2025). The July 2025 survey yielded the sixth-lowest biomass estimate since 2006 (Winter et al. 2025), and the 2025 second season yielded the fifth-lowest catch since 2006, excluding 2024 (Skeljo & Winter 2025). The July 2026 survey yielded the third-lowest biomass estimate since 2006 (Chemshirova et al. *in prep.*), and the 2026 second season yielded the lowest catch since 2006, excluding 2024 (Skeljo & Winter *in prep.*), prompting an early end to the fishing season.

This divergence between first- and second-season availability requires attention, as persistent declines in second-season abundance could reflect environmental effects, earlier spawning migration, shifts in recruit distribution, or reduced inter-season survival, all with implications for fishery management. The declining trend in median dorsal mantle length, together with the lower proportion of females in July 2026 and the shift towards immature rather than preparatory individuals since 2020, may indicate that the spring-spawning cohort is shifting towards smaller and later maturing individuals in recent years.

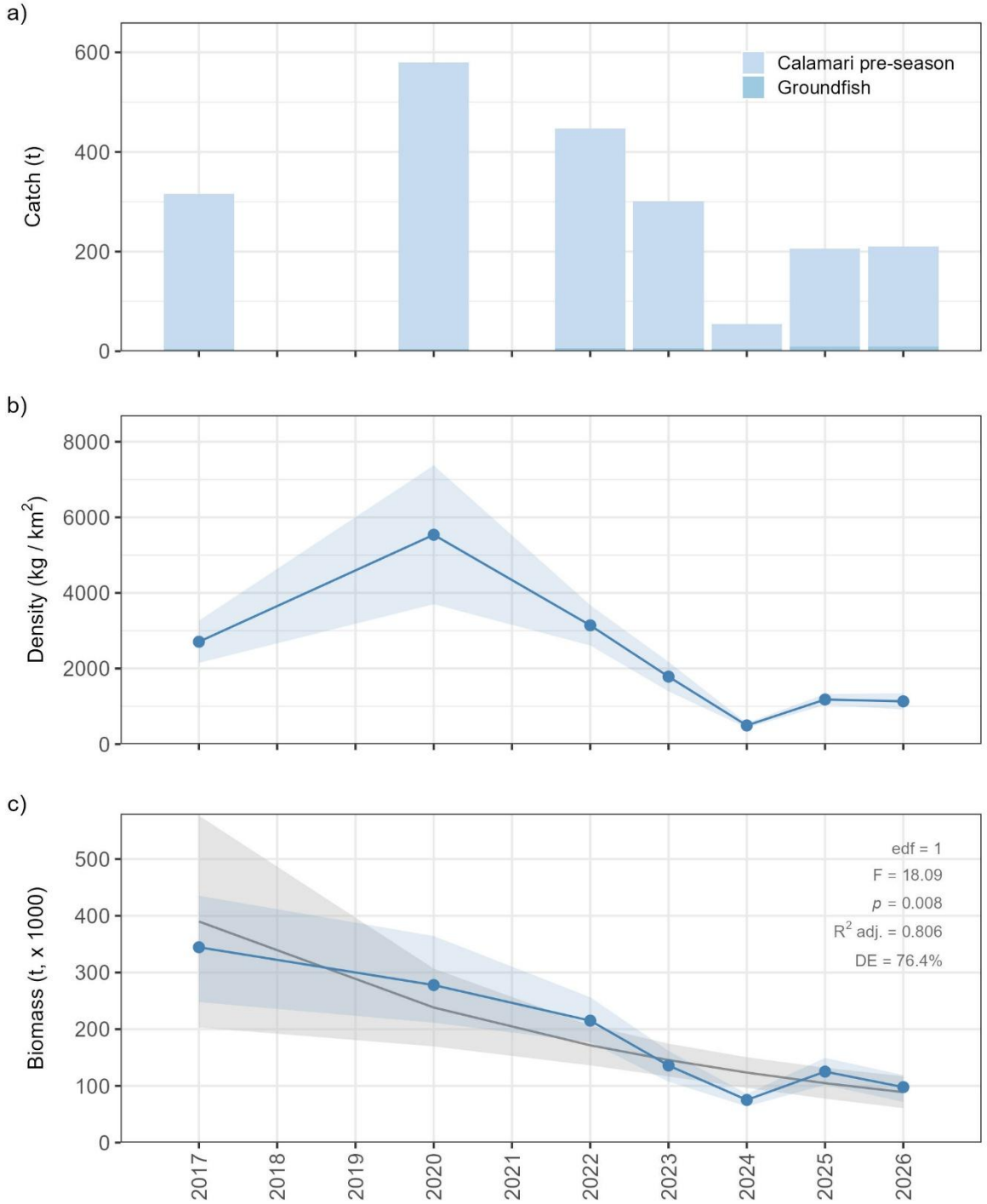

Fig. 43. Abundance of Patagonian squid (*Doryteuthis gahi*) during July groundfish and calamari pre-season surveys conducted in Falkland Islands waters in 2017, 2020, and 2022–2026. (a) Catch per survey, (b) annual mean density ± SE represented by the blue line and shaded region, respectively, and (c) estimated biomass, where the blue line and shaded region represent the median and 95% pointwise confidence interval derived from 10,000 bootstrap biomass estimates, and the grey line and shaded region represent the fitted Generalised Additive Model (GAM) smooth and its 95% pointwise confidence interval.

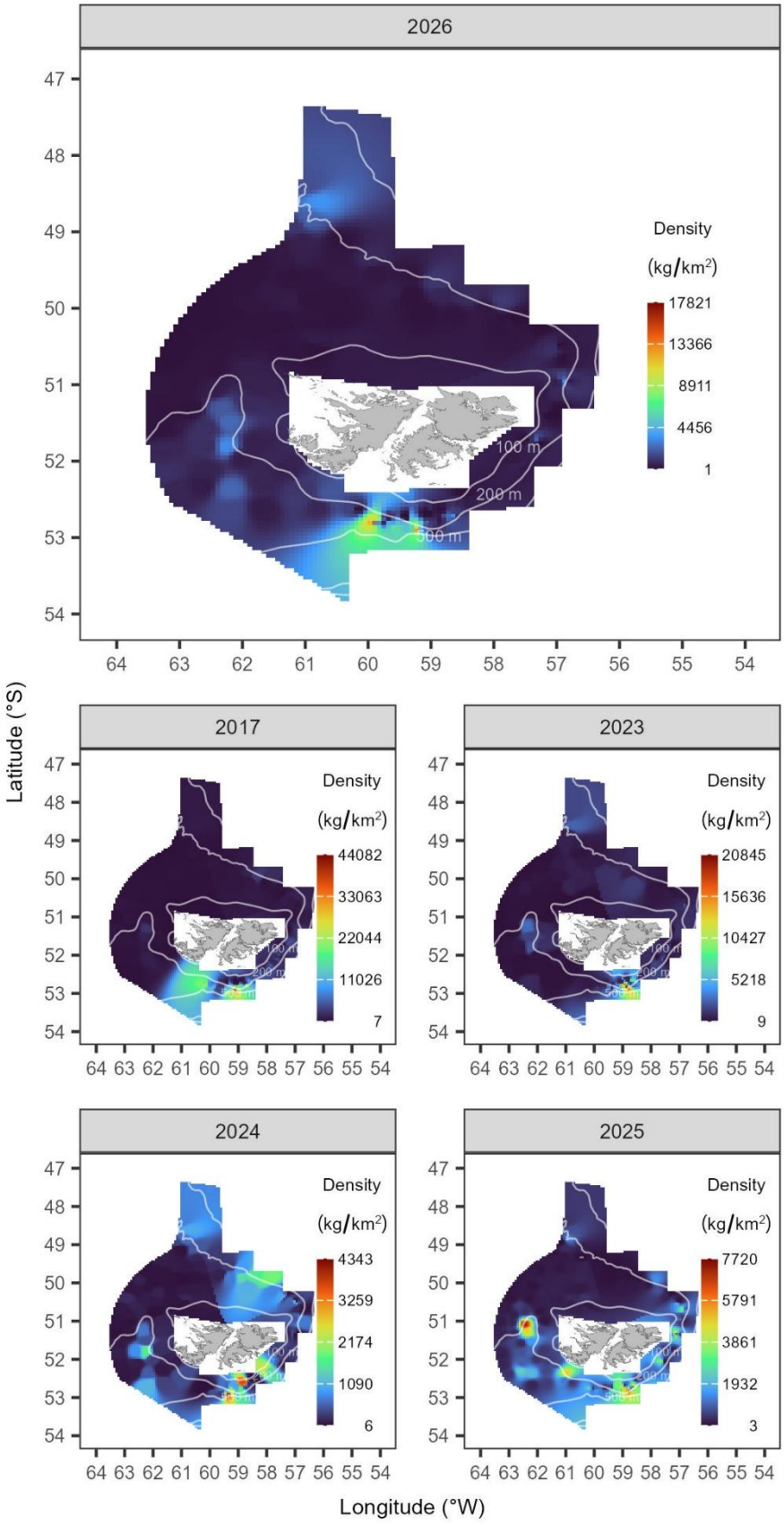

Fig. 44. Distribution and abundance of the Patagonian squid (*Doryteuthis gahi*) derived from the July 2026 groundfish and calamari pre-season surveys in Falkland Islands waters, compared with the first year of the time series (2017) and the three preceding years (2023–2025). Colour scales are specific to each year. Isobaths at 100 m, 200 m, and 500 m are shown.

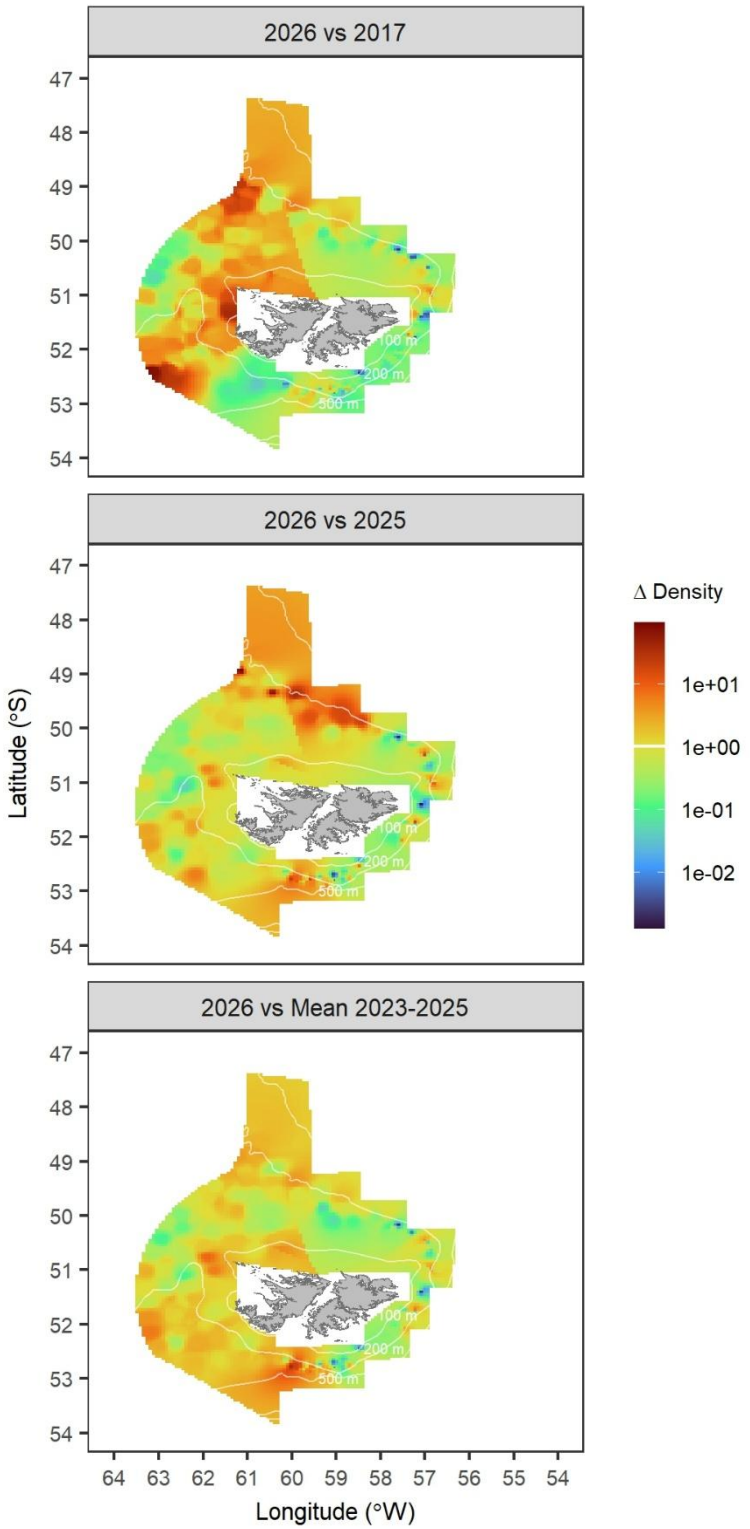

Fig. 45. Spatial change in density of the Patagonian squid (*Doryteuthis gahi*) derived from the July 2026 groundfish and calamari pre-season surveys in Falkland Islands waters, relative to the first year of the time series (2017), the previous year (2025), and the mean of the three preceding years (2023–2025). The spatial change in density is expressed as the ratio of density (kg/km^2) in 2026 relative to the density in the baseline year (2017, 2025, 2023–2025 mean). Isobaths at 100 m, 200 m, and 500 m are shown. The colour scale is $\log_{10}$-transformed to aid visualisation, with increases in density indicated above the horizontal white line towards dark red, and decreases in density indicated below the horizontal white line towards dark blue.

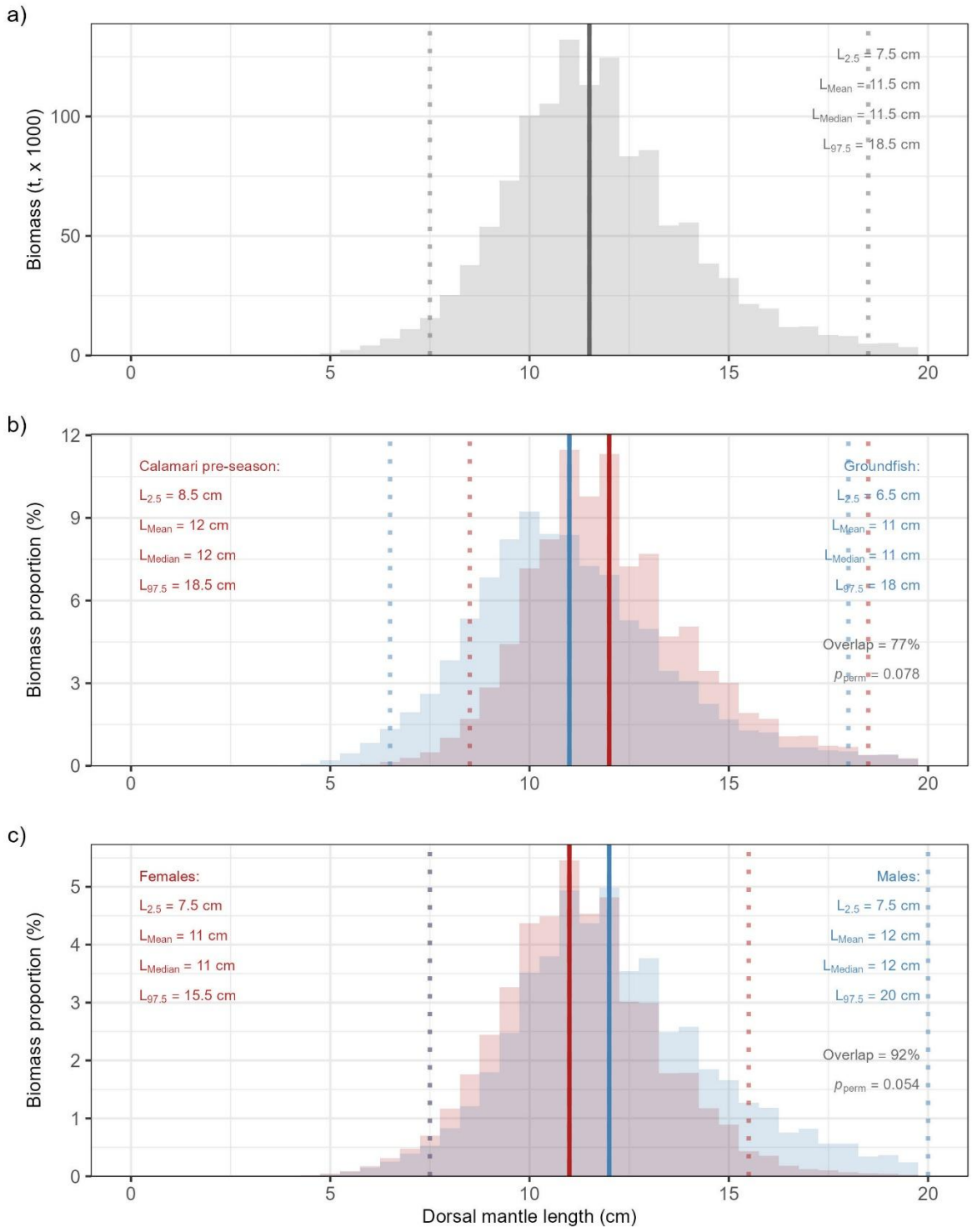

Fig. 46. Biomass-at-length class composition of the Patagonian squid (*Doryteuthis gahi*) across all years combined, based on July groundfish and calamari pre-season surveys conducted in Falkland Islands waters in 2017, 2020, and 2022–2026. a) Overall biomass-at-length frequency distribution. b) Overlap in biomass-at-length distributions between calamari pre-season (red) and groundfish (blue) surveys. c) Overlap in biomass-at-length distributions between females (red) and males (blue). Solid vertical lines indicate the mean length (L_{Mean}), dashed lines the median length (L_{Median}), and dotted lines the 2.5th and 97.5th length percentiles ($L_{2.5}$ and $L_{97.5}$, respectively). p_{perm} is the significance of the weighted permutation test to assess differences between groups.

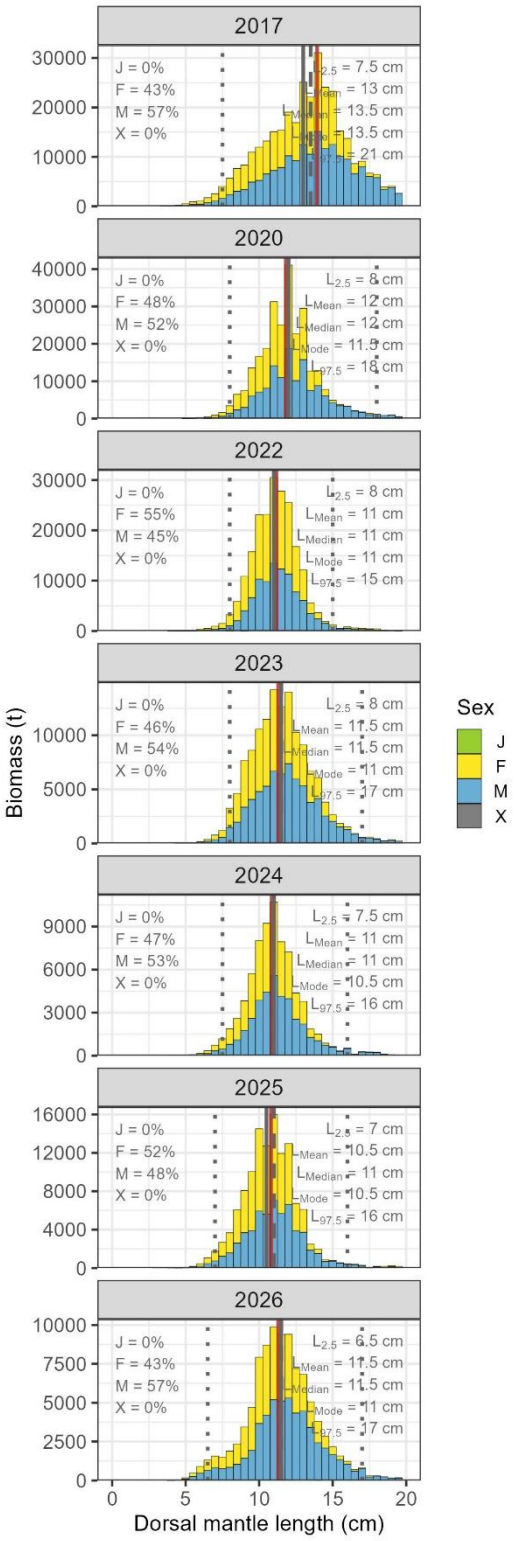

Fig. 47. Annual biomass-at-length class composition of the Patagonian squid (*Doryteuthis gahi*) during July groundfish and calamari pre-season surveys conducted in Falkland Islands waters in 2017, 2020, and 2022–2026. Stacked bars represent biomass (t) per 0.5 cm length class, partitioned by sex (J = juvenile; F = female; M = male; X = undetermined), with the proportion of total annual biomass for each sex indicated in the upper left of each panel. Vertical lines indicate the mean length (L_{Mean}, grey solid), median length (L_{Median}, grey dashed), modal length (L_{Mode}, red solid), and 2.5th and 97.5th percentiles ($L_{2.5}$ and $L_{97.5}$, grey dotted) of the biomass-weighted length distribution. Note the different y-axis scales among years.

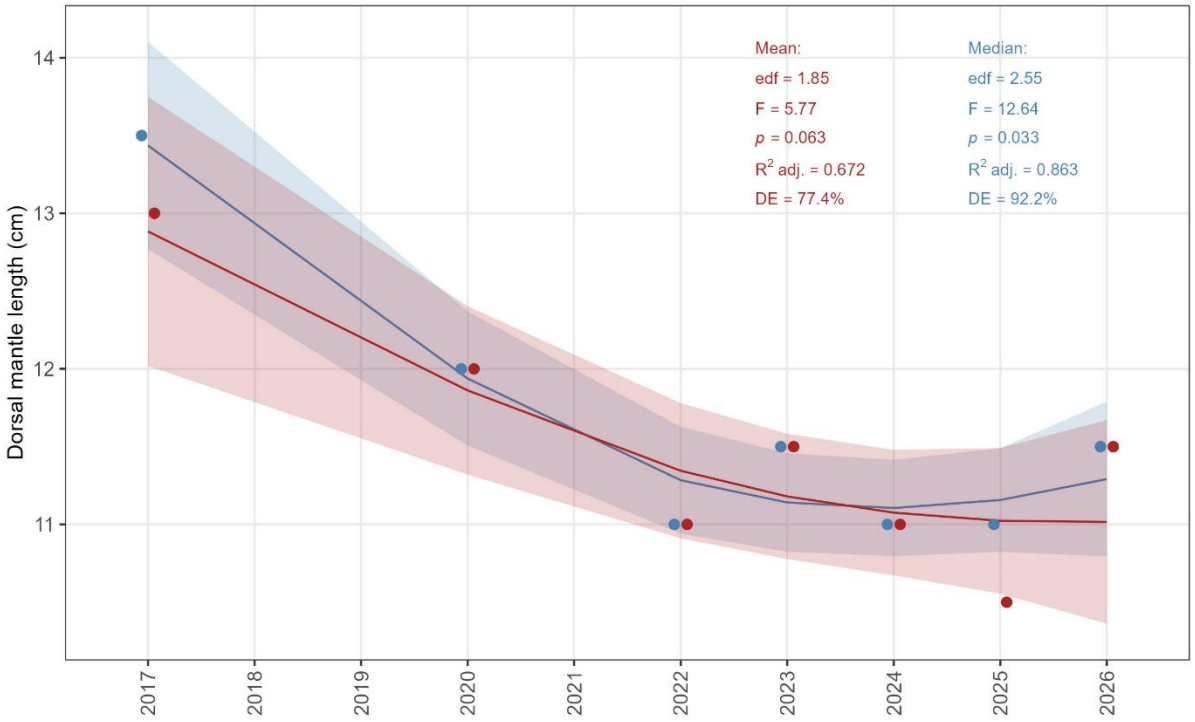

Fig. 48. Median (blue) and mean (red) dorsal mantle length of the Patagonian squid (*Doryteuthis gahi*) during July groundfish and calamari pre-season surveys conducted in Falkland Islands waters in 2017, 2020, and 2022–2026. The line and shaded region represent the fitted Generalised Additive Model (GAM) smooth and its 95% pointwise confidence interval.

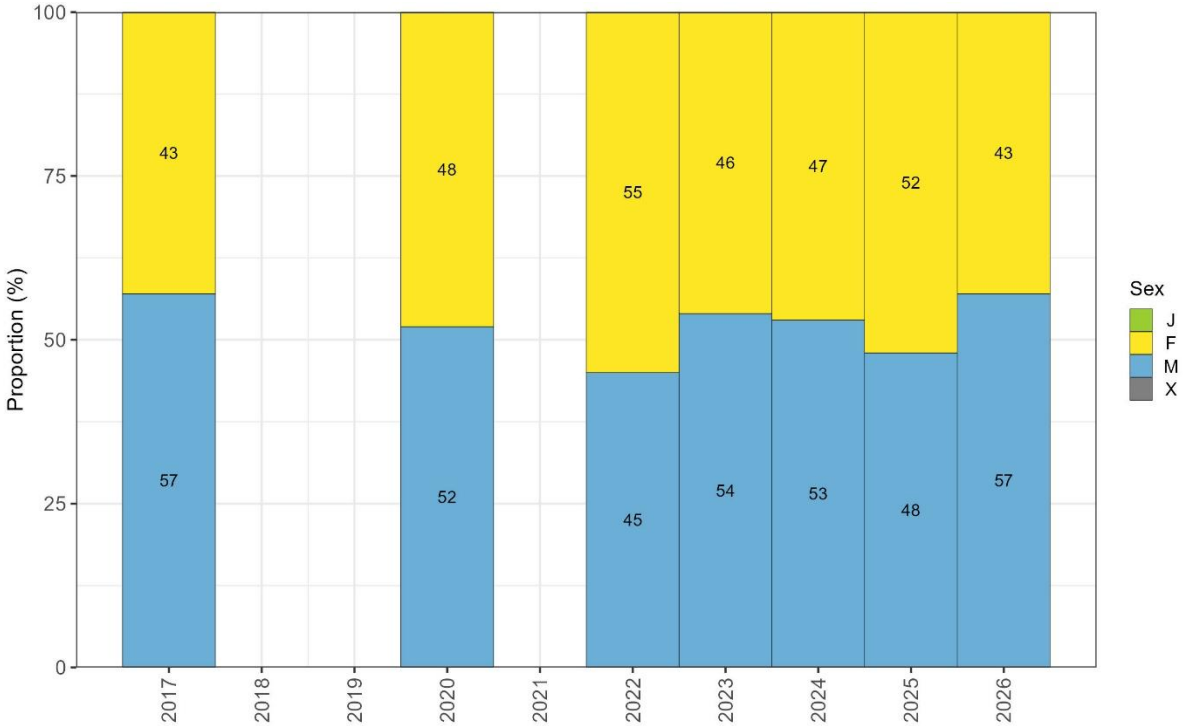

Fig. 49. Proportion by sex (J = juvenile; F = female; M = male; X = undetermined) of the Patagonian squid (*Doryteuthis gahi*) during July groundfish and calamari pre-season surveys conducted in Falkland Islands waters in 2017, 2020, and 2022–2026. Labels for proportions < 3% are omitted.

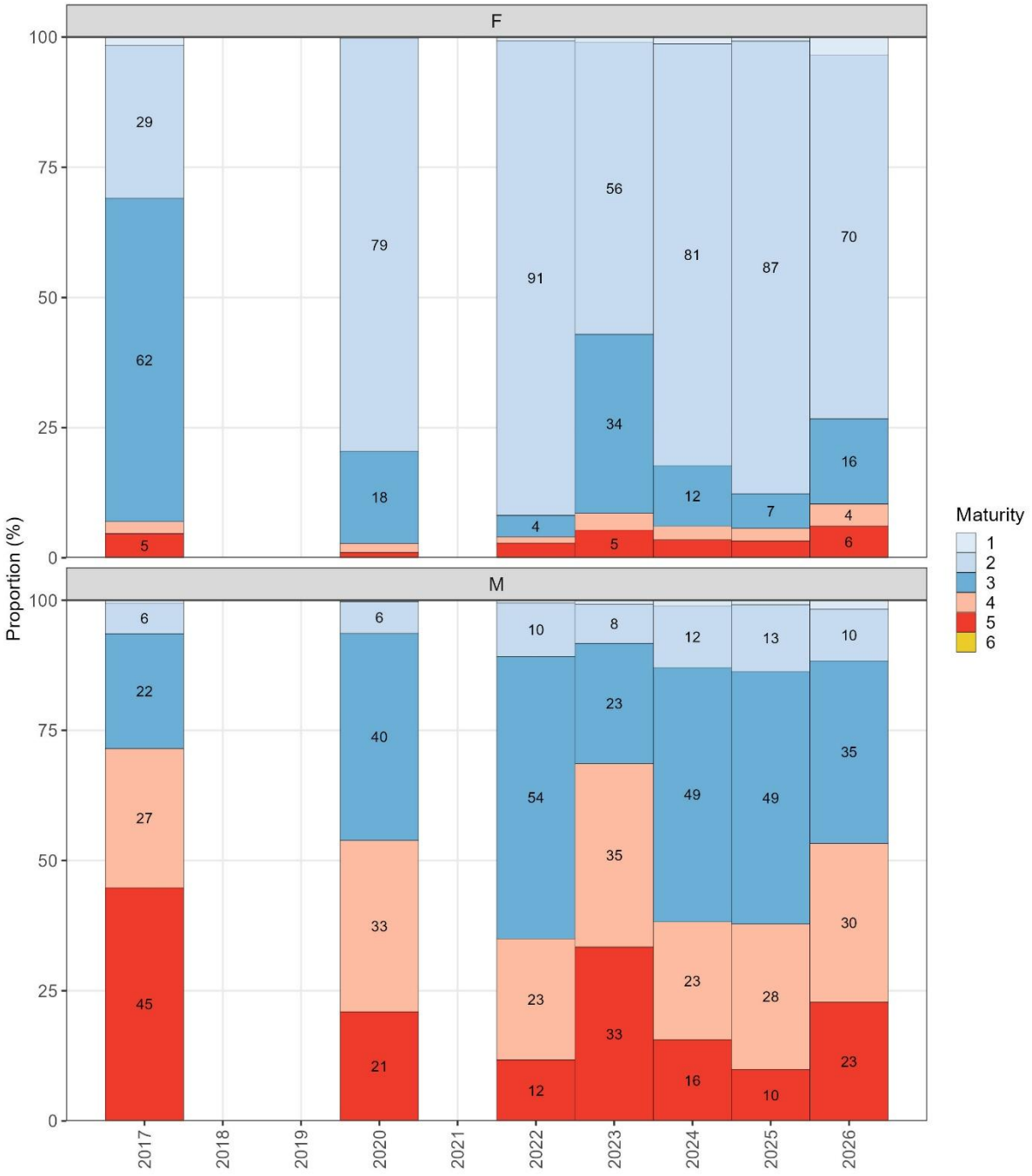

Fig. 50. Proportion by sexual maturity (1, young; 2, immature; 3, preparatory; 4, maturing; 5, mature; 6, spent) of the Patagonian squid (*Doryteuthis gahi*) during July groundfish and calamari pre-season surveys conducted in Falkland Islands waters in 2017, 2020, and 2022–2026. Labels for proportions < 3% are omitted.

4.3.7. Patagonian toothfish (*Dissostichus eleginoides*)

4.3.7.1. Temporal patterns of abundance

On average, 35% of the total Patagonian toothfish catches in the time series were from groundfish surveys and 65% from calamari pre-season surveys. The second highest catch was reported in 2026 (2.26 t) and represented approximately a three-fold increase relative to the 2017 catch (0.65 t), a 41% decrease relative to the 2025 catch (3.83 t), and a 32% increase relative to the 2023–2025 mean catch (1.71 t; Fig. 51a; Appendix II).

The second highest densities were recorded in 2026 (mean ± SE: 35.18 ± 9.23 kg/km²), representing an approximately four-fold increase relative to the 2017 densities (8.70 ± 1.29 kg/km²), a 33% decrease relative to the 2025 densities (52.28 ± 7.13 kg/km²), and a 48% increase relative to the 2023–2025 mean densities (23.72 ± 2.9 kg/km²; Fig. 51b).

The highest biomass in the time series was estimated for 2026 (10,363.00 t; CI = 5,695.34–14,137.75 t), representing a significant eight-fold increase relative to 2017 levels (1,323.17 t; CI = 1,060.57–1,597.51 t; $p < 0.001$), a non-significant 5% increase relative to 2025 (9,825.53 t; CI = 7,891.53–11,348.41 t; $p > 0.05$), and a significant three-fold increase relative to the 2023–2025 mean biomass (4,151.25 t; $p = 0.007$; Fig. 51c; Table IV–V; Appendix III–IV). Analysis of the full time series revealed a significant non-linear trend in biomass (GAM: edf = 3.94, F = 43.11, $p = 0.023$), with the model explaining 98.7% of the deviance (R^2 adj. = 0.921), indicating a strong and consistent increase in recent years (Fig. 51c; Appendix V).

4.3.7.2. Spatial patterns of abundance

In 2026, the highest concentration (1,020 kg/km²; the highest in the time series) of Patagonian toothfish was detected to the south-west in the FICZ at approximately 52°S and 62.5°W, and a secondary concentration was detected to the north-west at approximately 50.5°S and 61.7°W. In previous survey years, Patagonian toothfish distribution was also higher to the south-west in the FICZ (Fig. 52).

Densities increased in 2026 mainly through the west in the FICZ relative to 2017. In contrast, densities decreased in 2026 relative to 2025 and the 2023–2025 mean, mainly due to the overall higher densities observed during 2025 over the survey area (Fig. 53).

4.3.7.3. Length composition

Across all survey years combined, total length of Patagonian toothfish was in the range of 12 to 100 cm; however, 95% of the estimated biomass was comprised of individuals between 34 and 84 cm, with median and mean lengths (± SE) of 52 ± 2.49 cm and 54 ± 2.08 cm, respectively (Fig. 54a).

The distribution of biomass proportions by size class exhibited a 62% overlap between the groundfish and calamari pre-season surveys. Individuals from the groundfish survey (mean ± SE: 58 ± 1.93 cm) were significantly larger than those from the calamari pre-season survey (mean ± SE: 50 ± 2.28 cm; $p < 0.001$). In the groundfish survey, 95% of the biomass of Patagonian toothfish was comprised of individuals between 39 and 85 cm (median ± SE: 58 ± 2.75 cm). In the calamari pre-season survey, 95% of the biomass was comprised of individuals between 24 and 81 cm (median ± SE: 48 ± 1.79 cm; Fig. 54b).

The distribution of biomass proportions by size class exhibited an 87% overlap between females and males. The permutation analysis revealed that females (mean ± SE: 56 ± 2.10 cm) were significantly larger than males (mean ± SE: 51 ± 1.98 cm; p = 0.036). This difference was in part due to individuals > 45 cm that were more abundant for females compared to males. For females, 95% of the biomass was comprised of individuals between 36 and 87 cm (median ± SE: 54 ± 2.81 cm). For males, 95% of the biomass was comprised of individuals between 33 and 76 cm (median ± SE: 50 ± 1.99 cm; Fig. 54c).

Through the time series, the size structure of Patagonian toothfish was broad and multimodal, with several length-groups not clearly distinguished because of size overlap. A small group with modal length at approximately 22 cm was present in several years (Fig. 55). In 2026, lengths were in the range of 19 to 85 cm; however, 95% of the biomass was comprised of individuals between 47 and 79 cm, with median and mean lengths (± SE) of 60 ± 1.68 cm and 60 ± 1.28 cm, respectively. For females, 95% of the biomass was comprised of individuals between 48 and 83 cm, with median and mean lengths (± SE) of 62 ± 1.95 cm and 61 ± 1.70 cm, respectively. For males, 95% of the biomass was comprised of individuals between 45 and 76 cm, with median and mean lengths (± SE) of 56 ± 2.17 cm and 57 ± 1.74 cm, respectively (Fig. 55).

Both mean (GAM: edf = 4.21, F = 15.52, p = 0.061, R^2 adj. = 0.922, DE = 97.7%) and median (GAM: edf = 3.68, F = 4.2, p = 0.208, R^2 adj. = 0.729, DE = 89.6%) total lengths had non-significant, complex and fluctuating temporal trends. Both mean and median total length were approximately 45–48 cm in 2017, increased to a maximum of 60 cm in 2020–2022, declined to 48–52 cm in 2024–2025, and increased again to 60 cm in 2026 (Fig. 56). This oscillatory pattern may reflect recruitment pulses.

4.3.7.4. Sex and maturity composition

The sex composition of Patagonian toothfish was consistently dominated by females (mean ± SE: 61.7 ± 1.7%), followed by males (37.9 ± 1.8%), and juveniles (0.4 ± 0.4%; recorded in 2017, 2020, 2022, and 2025) throughout the time series. In 2026, the sex composition consisted of 63% females and 37% males (Fig. 57).

Maturity composition consisted of immature and “resting” individuals throughout the time series (Fig. 58). For Patagonian toothfish, “resting” individuals are effectively immature individuals, given that the groundfish and calamari pre-season surveys conducted with bottom trawl do not capture adult individuals, which instead are primarily caught with longlines at greater depths. Early developing individuals were reported in 2025 and 2026, and contributed < 10% in either sex.

4.3.7.5. Discussion

The significant non-linear biomass trend of Patagonian toothfish in Falkland Islands waters reflects a complex but increasing pattern in recent years. The relatively high biomass estimated in July 2026 is consistent with high biomass recorded in February 2026 (Ramos 2026). This increase may be attributable in part to the growth of recruits detected in 2022–2023, coupled with reduced fishing pressure following the all-year-round closure of fishing grid squares to the south-west of the FICZ (south of 52.5°S and west of 60.5°W) since

December 2023 (FIFD, *unpublished internal document*). It is important to note that the groundfish and calamari pre-season surveys do not effectively sample adult Patagonian toothfish, which are primarily caught with longlines at greater depths; consequently, the biomass estimates presented here are not representative of the adult stock and should be interpreted as an index of juvenile and sub-adult abundance from bottom trawl surveys. The "resting" maturity stage should be revised and corrected accordingly to appropriately describe the juvenile and sub-adult components of this stock.

The oscillatory trends in both mean and median total length may indicate recruitment pulses at irregular intervals. The recent decline in mean and median length in 2024–2025, followed by a partial recovery in 2026 was also noted in February parallel surveys (Ramos 2026), and may reflect the presence of a cohort of larger individuals or continued growth of the 2022–2023 recruits.

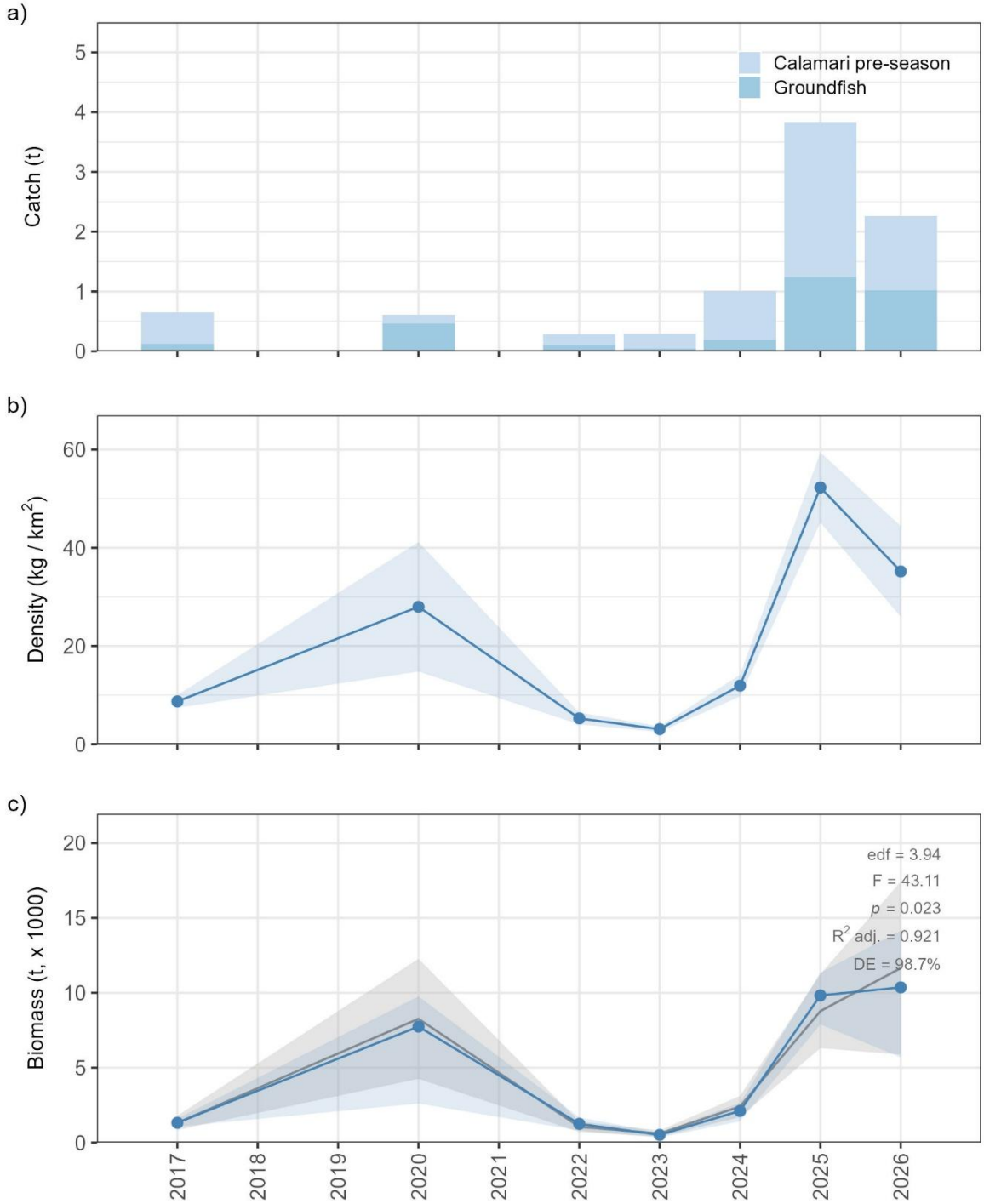

Fig. 51. Abundance of Patagonian toothfish (*Dissostichus eleginoides*) during July groundfish and calamari pre-season surveys conducted in Falkland Islands waters in 2017, 2020, and 2022–2026. (a) Catch per survey, (b) annual mean density ± SE represented by the blue line and shaded region, respectively, and (c) estimated biomass, where the blue line and shaded region represent the median and 95% pointwise confidence interval derived from 10,000 bootstrap biomass estimates, and the grey line and shaded region represent the fitted Generalised Additive Model (GAM) smooth and its 95% pointwise confidence interval.

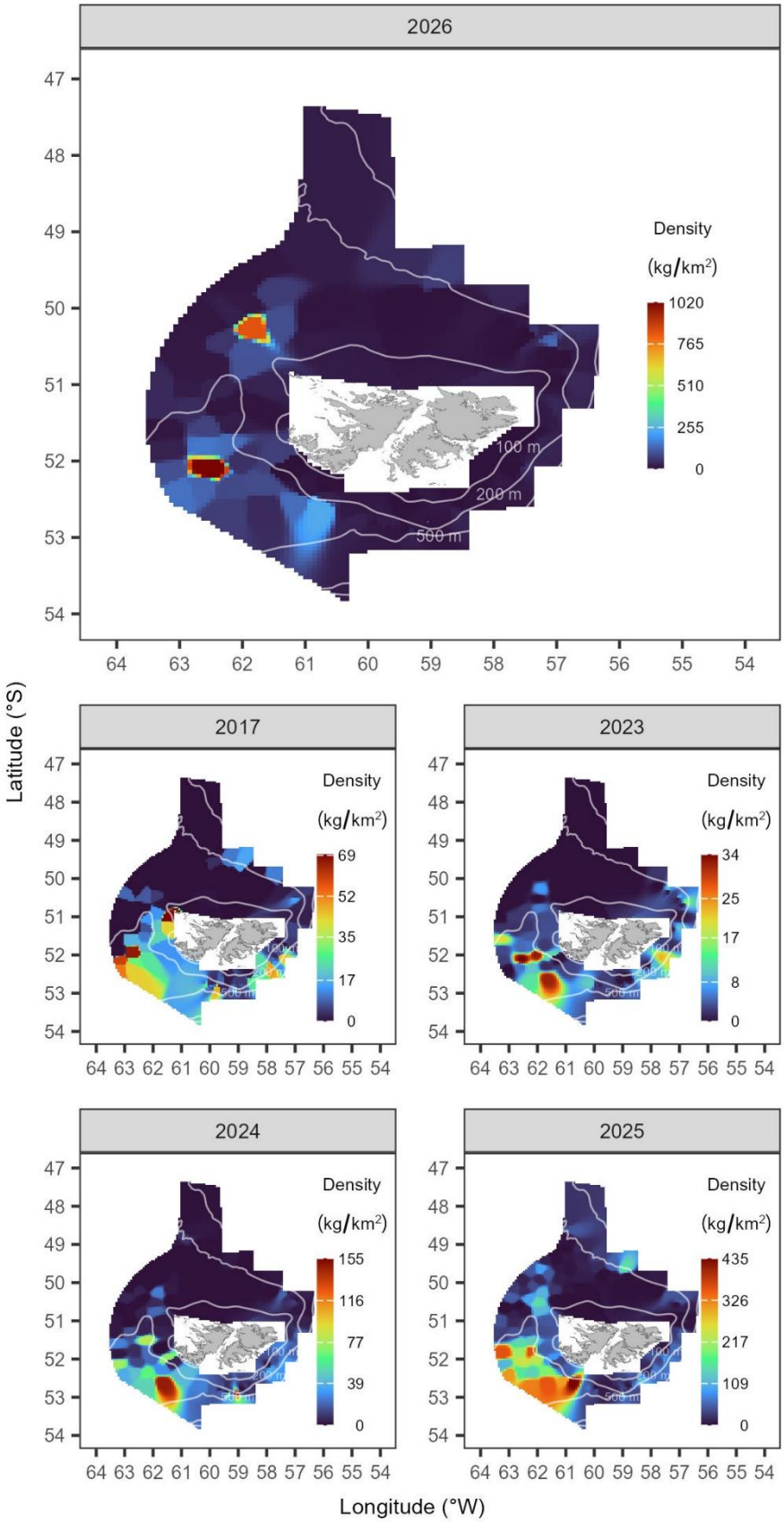

Fig. 52. Distribution and abundance of Patagonian toothfish (*Dissostichus eleginoides*) derived from the July 2026 groundfish and calamari pre-season surveys in Falkland Islands waters, compared with the first year of the time series (2017) and the three preceding years (2023–2025). Colour scales are specific to each year. Isobaths at 100 m, 200 m, and 500 m are shown.

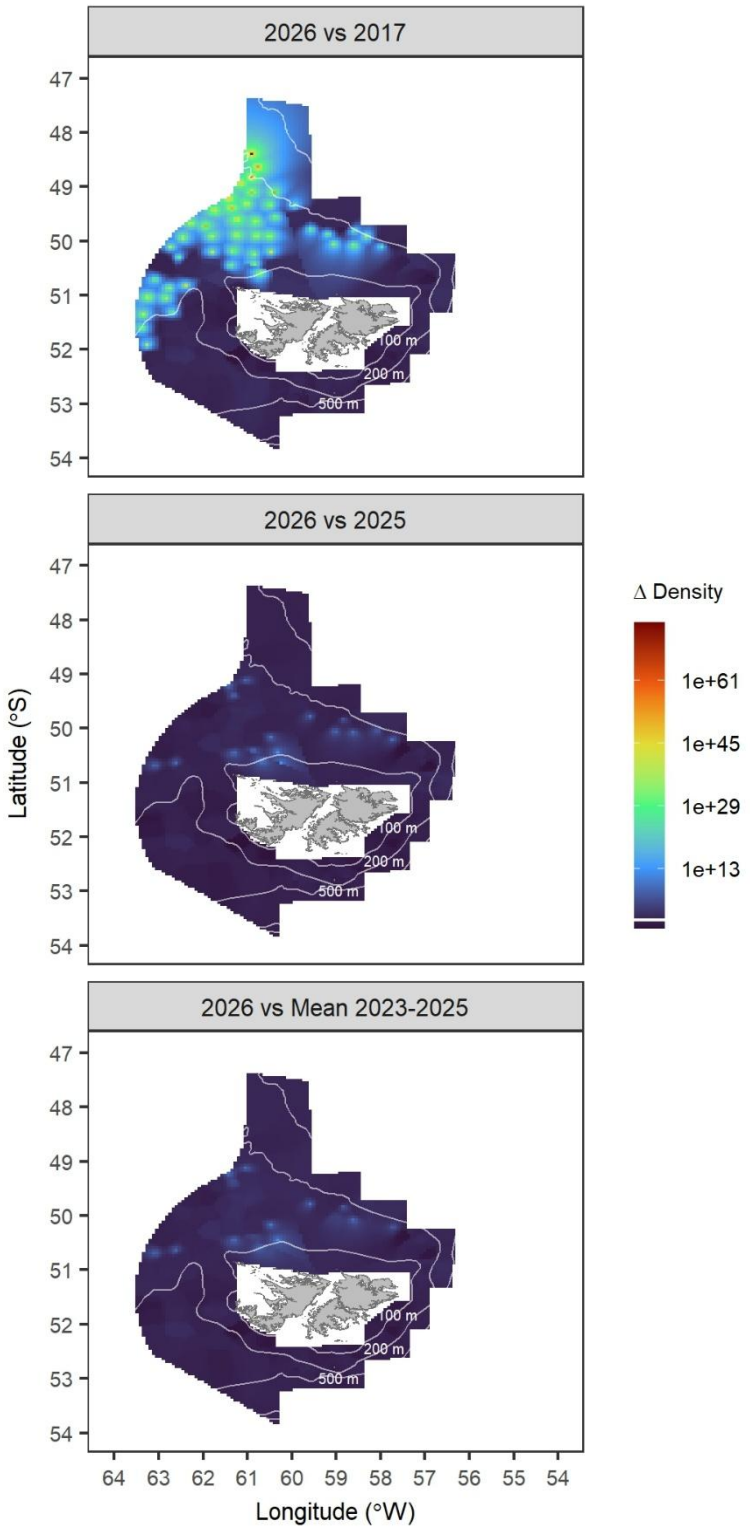

Fig. 53. Spatial change in density of Patagonian toothfish (*Dissostichus eleginoides*) derived from the July 2026 groundfish and calamari pre-season surveys in Falkland Islands waters, relative to the first year of the time series (2017), the previous year (2025), and the mean of the three preceding years (2023–2025). The spatial change in density is expressed as the ratio of density (kg/km^2) in 2026 relative to the density in the baseline year (2017, 2025, 2023–2025 mean). Isobaths at 100 m, 200 m, and 500 m are shown. The colour scale is $\log_{10}$-transformed to aid visualisation, with increases in density indicated above the horizontal white line towards dark red, and decreases in density indicated below the horizontal white line towards dark blue.

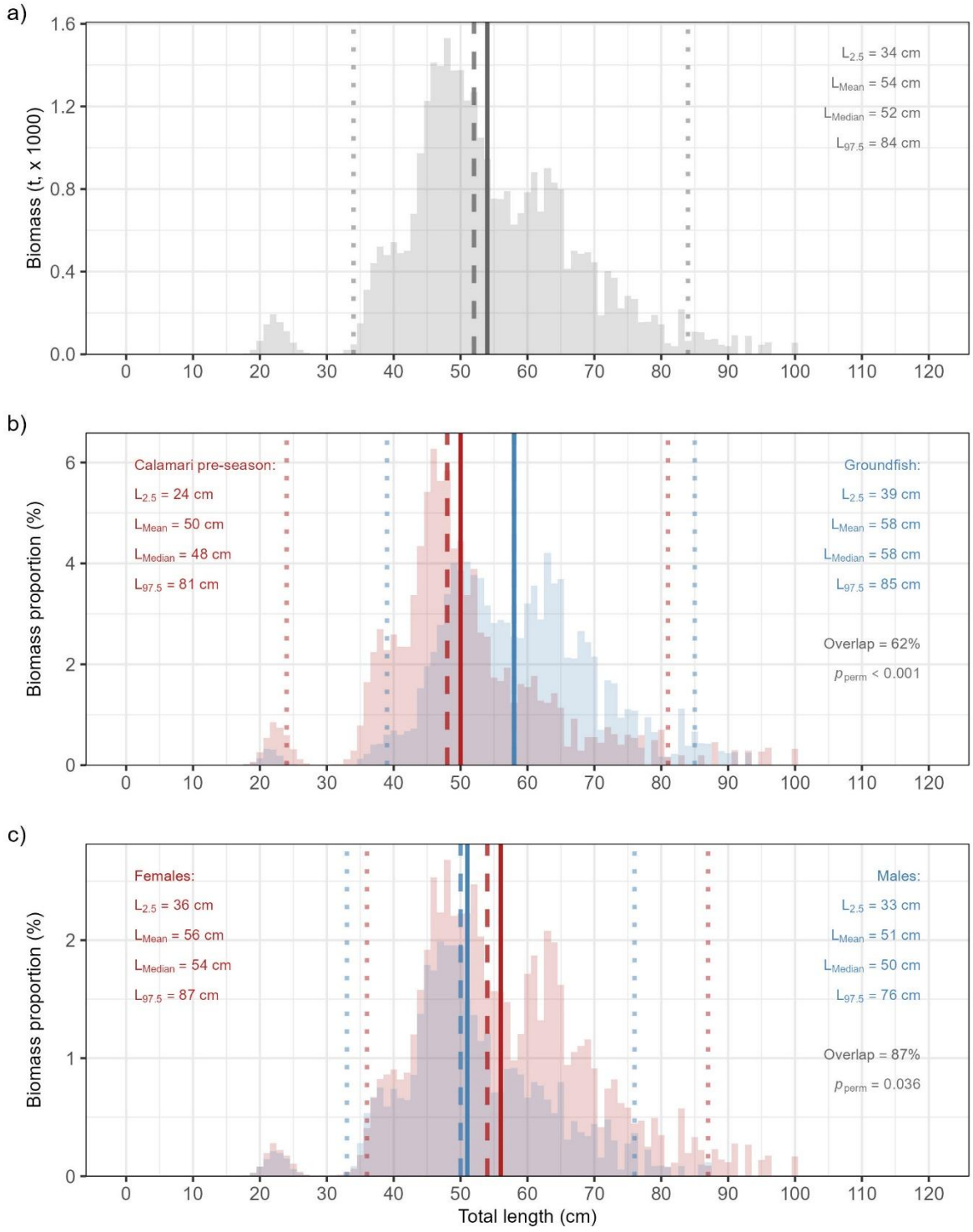

Fig. 54. Biomass-at-length class composition of Patagonian toothfish (*Dissostichus eleginoides*) across all years combined, based on July groundfish and calamari pre-season surveys conducted in Falkland Islands waters in 2017, 2020, and 2022–2026. a) Overall biomass-at-length frequency distribution. b) Overlap in biomass-at-length distributions between calamari pre-season (red) and groundfish (blue) surveys. c) Overlap in biomass-at-length distributions between females (red) and males (blue). Solid vertical lines indicate the mean length (L_{Mean}), dashed lines the median length (L_{Median}), and dotted lines the 2.5th and 97.5th length percentiles ($L_{2.5}$ and $L_{97.5}$, respectively). p_{perm} is the significance of the weighted permutation test to assess differences between groups.

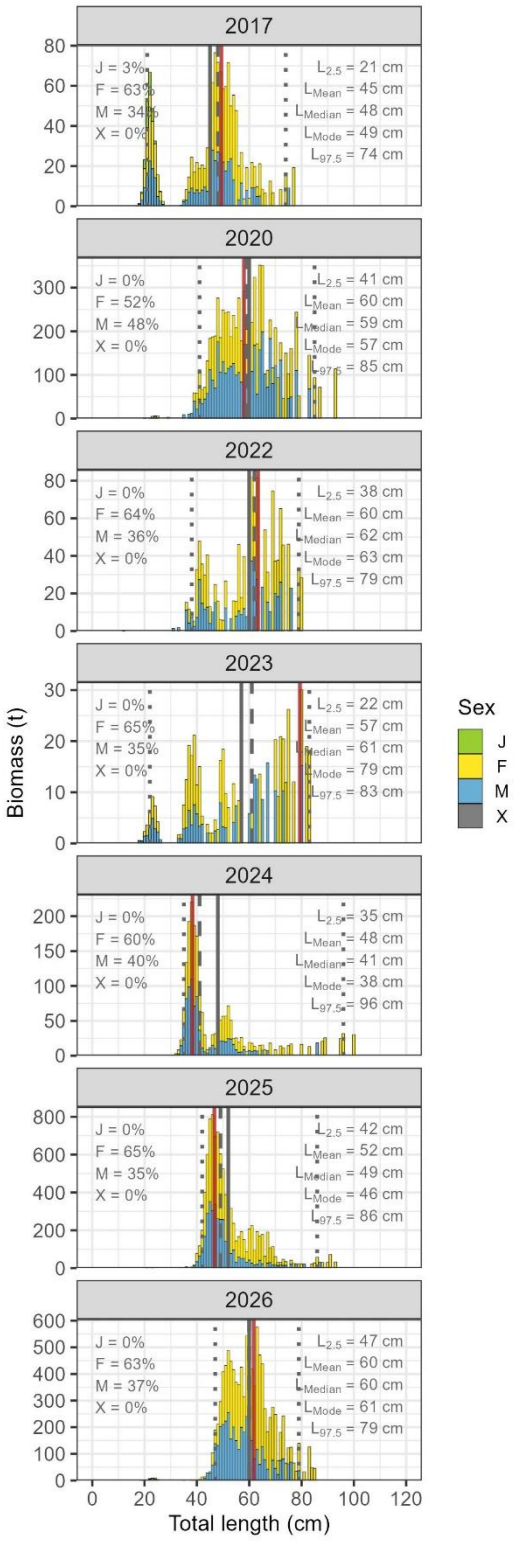

Fig. 55. Annual biomass-at-length class composition of Patagonian toothfish (*Dissostichus eleginoides*) during July groundfish and calamari pre-season surveys conducted in Falkland Islands waters in 2017, 2020, and 2022–2026. Stacked bars represent biomass (t) per 1.0 cm length class, partitioned by sex (J = juvenile; F = female; M = male; X = undetermined), with the proportion of total annual biomass for each sex indicated in the upper left of each panel. Vertical lines indicate the mean length (L_{Mean}, grey solid), median length (L_{Median}, grey dashed), modal length (L_{Mode}, red solid), and 2.5th and 97.5th percentiles ($L_{2.5}$ and $L_{97.5}$, grey dotted) of the biomass-weighted length distribution. Note the different y-axis scales among years.

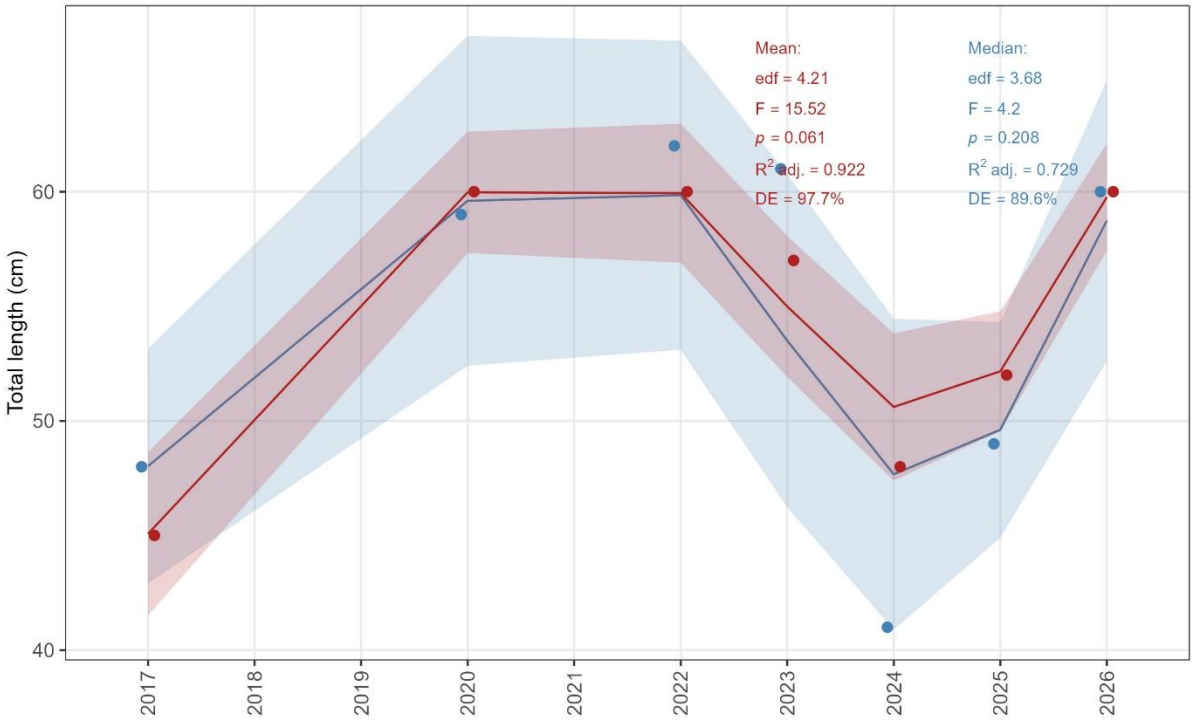

Fig. 56. Median (blue) and mean (red) total length of Patagonian toothfish (*Dissostichus eleginoides*) during July groundfish and calamari pre-season surveys conducted in Falkland Islands waters in 2017, 2020, and 2022–2026. The line and shaded region represent the fitted Generalised Additive Model (GAM) smooth and its 95% pointwise confidence interval.

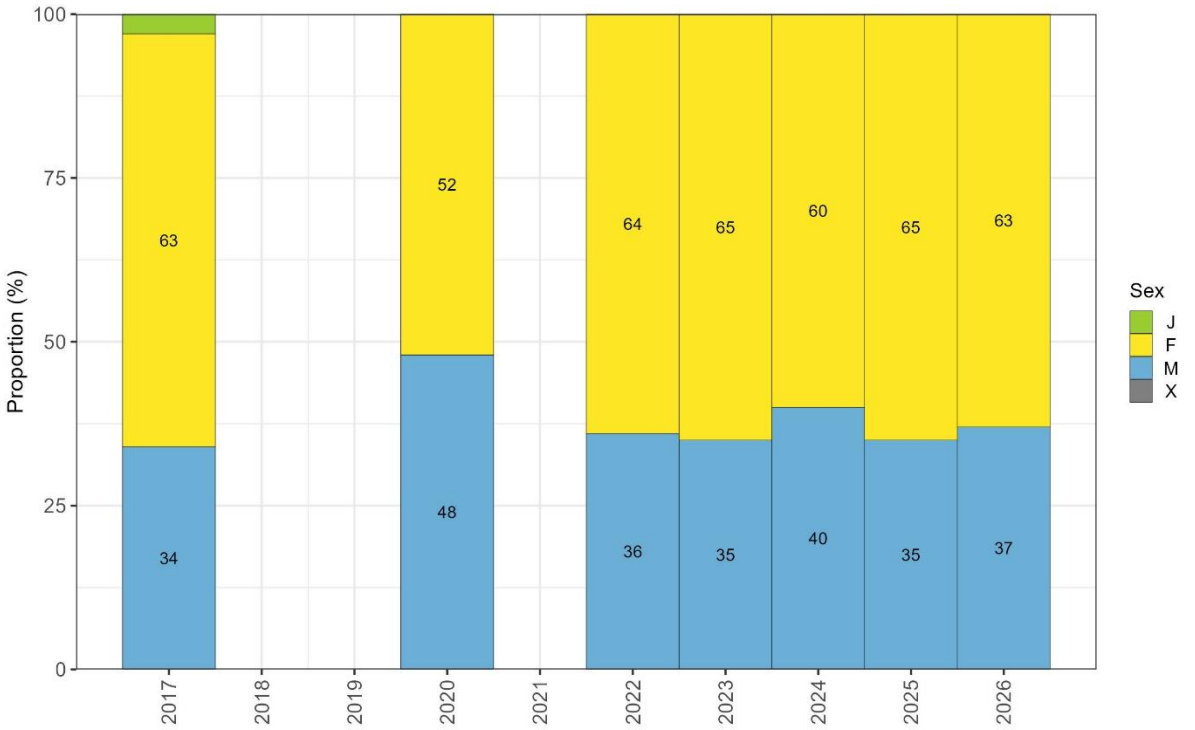

Fig. 57. Proportion by sex (J = juvenile; F = female; M = male; X = undetermined) of Patagonian toothfish (*Dissostichus eleginoides*) during July groundfish and calamari pre-season surveys conducted in Falkland Islands waters in 2017, 2020, and 2022–2026. Labels for proportions < 3% are omitted.

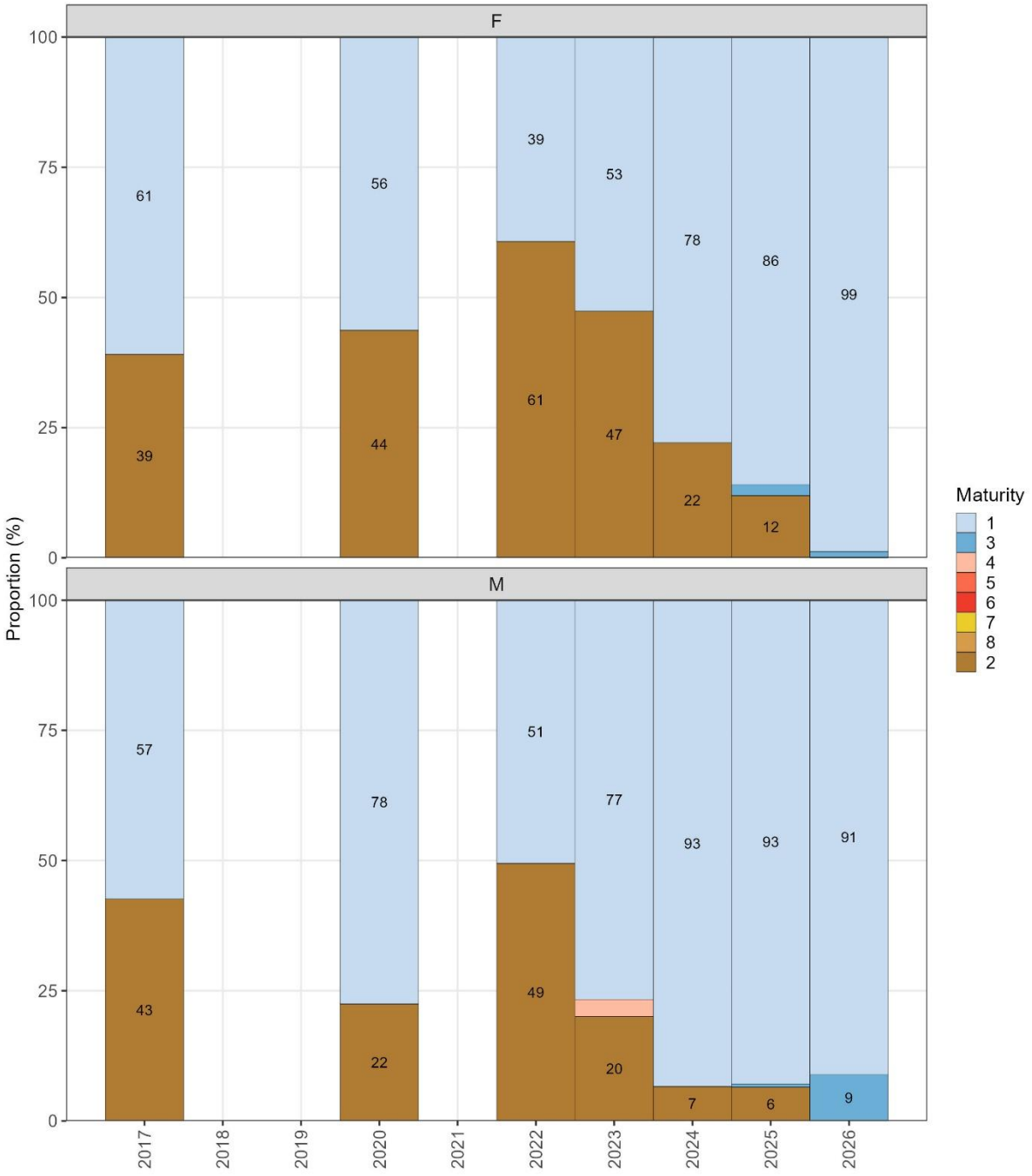

Fig. 58. Proportion by sexual maturity (1, immature; 3, early developing; 4, late developing; 5, ripe; 6, running; 7, spent; 8, recovering spent; 2, resting) of Patagonian toothfish (*Dissostichus eleginoides*) during July groundfish and calamari pre-season surveys conducted in Falkland Islands waters in 2017, 2020, and 2022–2026. Maturity stages ordered by developmental sequence. Labels for proportions < 3% are omitted.

4.3.8. Red cod (*Salilota australis*)

4.3.8.1. Temporal patterns of abundance

On average, 65% of the total red cod catches in the time series were from groundfish surveys and 35% from calamari pre-season surveys. The catch in 2026 (4.32 t) was the third lowest in the time series, and corresponded to a 69% increase relative to the 2017 catch (2.56 t) but represented a 37% decrease relative to the 2025 catch (6.90 t) and a 39% decrease relative to the 2023–2025 mean catch (7.08 t; Fig. 59a; Appendix II).

Densities in 2026 (mean ± SE: 85.91 ± 35.46 kg/km²) represented a 24% increase relative to the 2017 densities (69.21 ± 20.62 kg/km²) but a 24% decrease relative to the 2025 densities (112.63 ± 32.02 kg/km²) and a 53% decrease relative to the 2023–2025 mean densities (183.73 ± 81.77 kg/km²; Fig. 59b).

Red cod biomass was highest in 2020 (39,343.25 t; CI = 6,320.91–68,377.24 t; although with wide confidence intervals). Biomass in 2026 (14,080.62 t; CI = 6,079.20–23,963.28 t) was the second lowest in the time series, corresponding to a 17% increase relative to 2017 levels (12,079.24 t; CI = 6,420.61–17,896.36 t), a 32% decrease relative to 2025 levels (20,832.07 t; CI = 12,034.34–30,481.08 t) and a 49% decrease relative to the 2023–2025 mean biomass (27,879.93 t). These were non-significant changes in biomass ($p > 0.05$; Fig. 59c; Table IV–V; Appendix III–IV). In contrast, analysis of the full time series revealed a significant declining trend in biomass in recent years (GAM: edf = 2.81, F = 10.29, p = 0.043), with the model explaining 91.2% of the deviance (R^2 adj. = 0.649); however, this trend must be interpreted with caution given the high inter-annual variability in biomass and the wide confidence intervals (Fig. 59c; Appendix V).

4.3.8.2. Spatial patterns of abundance

In 2026, the highest densities (3,761 kg/km^2) occurred to the north-west limit of the FICZ at approximately 50°S and 63°W, and to the south-west at approximately 52°S and 62.5°W (Fig. 60). Through the time series, red cod occurred in patchy aggregations mainly to the west in the FICZ, with the highest density in the time series calculated for 2023 (30,885 kg/km2) to the north-west limit of the FICZ at approximately 49.5°S and 62°W.

Analysis of the spatial change in density revealed an overall decrease in densities in 2026 through the survey area, although with increases in distinct areas mainly to the north, relative to 2017, 2025, and the 2023–2025 mean (Fig. 61).

4.3.8.3. Length composition

Across all survey years combined, total length of red cod was in the range of 8 to 84 cm; however, 95% of the estimated biomass was comprised of individuals between 21 and 76 cm, with median and mean lengths (± SE) of 49 ± 2.48 cm and 48 ± 2.08 cm, respectively (Fig. 62a).

The distribution of biomass proportions by size class exhibited a 47% overlap between the groundfish and calamari pre-season surveys. Individuals from the groundfish survey (mean ± SE: 46 ± 2.04 cm) were significantly smaller than those from the calamari pre-season survey (mean ± SE: 63 ± 2.02 cm; $p < 0.001$). In the groundfish survey, 95% of the biomass of

red cod was comprised of individuals between 21 and 74 cm (median ± SE: 48 ± 2.49 cm). In the calamari pre-season survey, 95% of the biomass was comprised of individuals between 35 and 80 cm (median ± SE: 66 ± 2.68 cm; Fig. 62b).

The distribution of biomass proportions by size class exhibited an 80% overlap between females and males. The permutation analysis revealed that females (mean ± SE: 51 ± 2.08 cm) were significantly larger than males (mean ± SE: 42 ± 2.00 cm; p = 0.001). This difference was in part due to individuals > 40 cm that were more abundant for females compared to males. For females, 95% of the biomass was comprised of individuals between 22 and 78 cm (median ± SE: 52 ± 2.56 cm). For males, 95% of the biomass was comprised of individuals between 20 and 68 cm (median ± SE: 43 ± 2.70 cm; Fig. 62c).

Through the time series, the size structure of red cod was broad and multimodal, with several length-groups not clearly distinguished because of size overlap. The main modal length ranged between 23 and 56 cm, suggesting that more than one length-group was dominant in the time series. Few recruits were in the range of 15 to 18 cm in 2025 and 2026; a group of relatively small individuals of approximately 20 cm was evident most years (Fig. 63). In 2026, lengths were in the range of 9 to 84 cm; however, 95% of the biomass was comprised of individuals between 20 and 76 cm, with median and mean lengths (± SE) of 54 ± 2.01 cm and 52 ± 2.05 cm, respectively. For females, 95% of the biomass was comprised of individuals between 21 and 77 cm, with median and mean lengths (± SE) of 57 ± 2.58 cm and 55 ± 2.44 cm, respectively. For males, 95% of the biomass was comprised of individuals between 19 and 72 cm, with median and mean lengths (± SE) of 45 ± 3.64 cm and 42 ± 2.65 cm, respectively (Fig. 63).

Strongly significant and positive trends were observed for the mean (GAM: edf = 1.00, F = 43.84, p = 0.001, R^2 adj. = 0.877, DE = 89.8%) and the median (GAM: edf = 4.58, F = 76.48, p = 0.087, R^2 adj. = 0.984, DE = 99.6%) lengths. Both mean and median lengths were approximately 41–43 cm in 2017 and increased to approximately 52–54 cm in 2026 (Fig. 64).

4.3.8.4. Sex and maturity composition

The sex composition of red cod was consistently dominated by females (mean ± SE: 69.1 ± 1.8%), followed by males (30.7 ± 1.7%) throughout the time series. Individuals of undetermined sex accounted for a negligible 0.1 ± 0.1%, and juveniles occurred in even smaller amounts. In 2026, the sex composition was characterised by the highest proportion of females in the time series (76%; Fig. 65).

Maturity composition was contrasting between females and males. Females were characterised by individuals in resting stage most years (≥ 55%); immature and early developing individuals accounted for ≤ 32%, and late developing, ripe and running individuals ≤ 16%, except for 2026 with late developing individuals being dominant (42%). For males, immature and early developing individuals were predominant in most years (48–65%), except for 2023 (26%) when late developing, ripe, and running individuals accounted for 60%. Post-spawning (spent, recovering spent, and resting) males contributed 14–43% in most years, except for 2026 (2%; Fig. 66).

4.3.8.5. Discussion

The significant declining trend in red cod biomass in Falkland Islands waters in recent years is consistent with the recent downward trend in February parallel surveys (Ramos 2026), declining CPUE from finfish-licensed vessels in the FICZ (Ramos & Winter 2022d), and the low spawning biomass reported from a survey in September 2022 covering the spawning ground south and south-west of West Falkland (Arkhipkin et al. 2022b). The commercial fishery has shown significant CPUE fluctuations, with peaks in 1996 and 2011 followed by a sustained decline since 2013 (Ramos & Winter 2022d; FIFD, *unpublished data*). At a regional scale, red cod biomass in Argentine waters also declined from 1980 to 2015, with the 2023 biomass representing 58% of the 1980 level despite a slow recovery since 2015 (Troccoli et al. 2024), suggesting that the declining trend observed in Falkland Islands waters may reflect broader regional trends.

The significant increase in mean total length is consistent with the marginally non-significant increase in median length in July parallel surveys, and with both mean and median length trends in February parallel surveys since 2017 (Ramos 2026), indicating that size composition may be shifting as biomass declined in recent years. Given this sustained biomass decline, and that females mostly in post-spawning stages comprise a higher proportion of the biomass, the closure of red cod spawning grounds south and south-west of West Falkland since 2010 (Ramos & Winter 2022d) remains an important conservation measure that should be maintained, and additional management measures may be necessary.

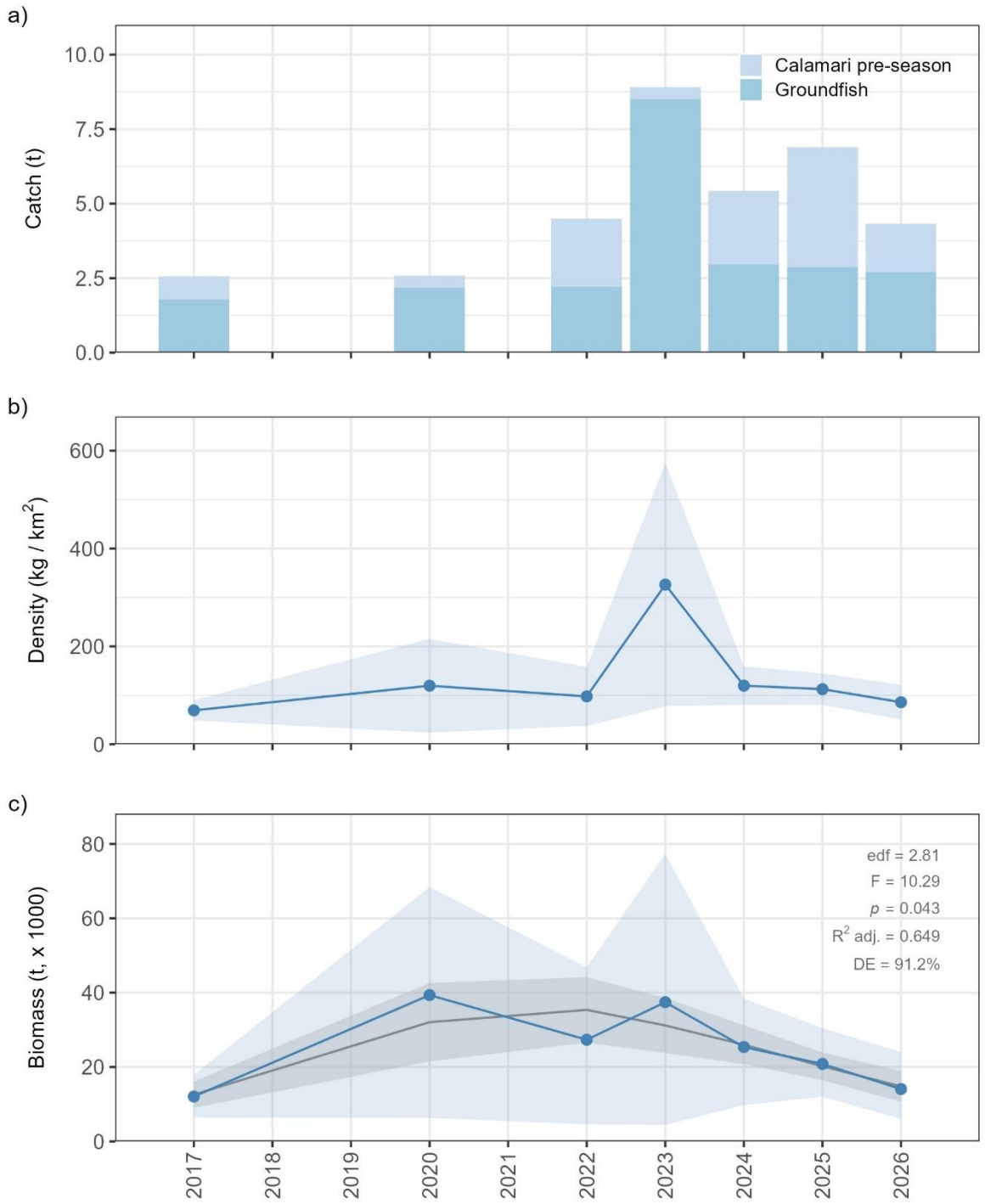

Fig. 59. Abundance of red cod (*Salilota australis*) during July groundfish and calamari pre-season surveys conducted in Falkland Islands waters in 2017, 2020, and 2022–2026. (a) Catch per survey, (b) annual mean density ± SE represented by the blue line and shaded region, respectively, and (c) estimated biomass, where the blue line and shaded region represent the median and 95% pointwise confidence interval derived from 10,000 bootstrap biomass estimates, and the grey line and shaded region represent the fitted Generalised Additive Model (GAM) smooth and its 95% pointwise confidence interval.

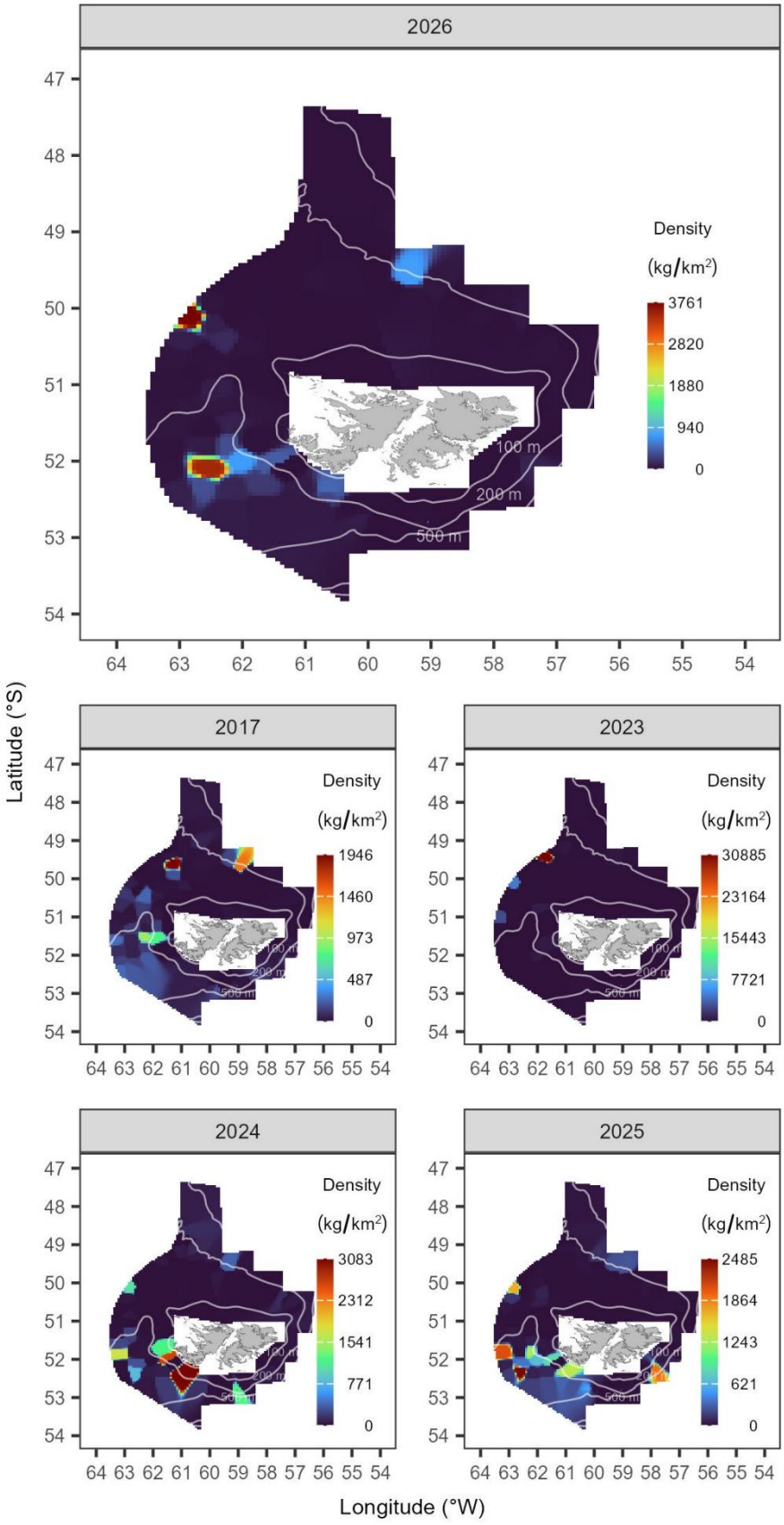

Fig. 60. Distribution and abundance of red cod (*Salilota australis*) derived from the July 2026 groundfish and calamari pre-season surveys in Falkland Islands waters, compared with the first year of the time series (2017) and the three preceding years (2023–2025). Colour scales are specific to each year. Isobaths at 100 m, 200 m, and 500 m are shown.

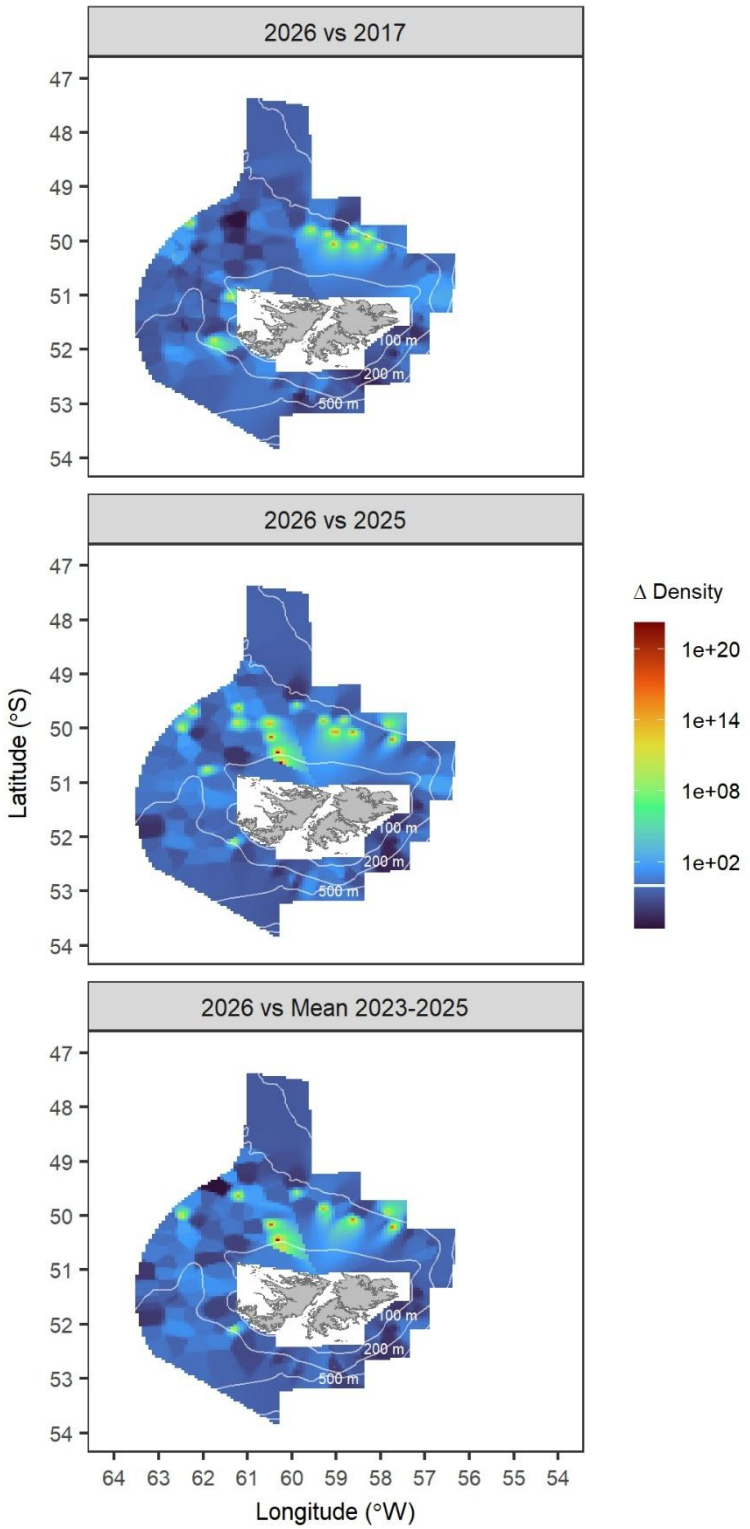

Fig. 61. Spatial change in density of red cod (*Salilota australis*) derived from the July 2026 groundfish and calamari pre-season surveys in Falkland Islands waters, relative to the first year of the time series (2017), the previous year (2025), and the mean of the three preceding years (2023–2025). The spatial change in density is expressed as the ratio of density (kg/km^2) in 2026 relative to the density in the baseline year (2017, 2025, 2023–2025 mean). Isobaths at 100 m, 200 m, and 500 m are shown. The colour scale is $\log_{10}$-transformed to aid visualisation, with increases in density indicated above the horizontal white line towards dark red, and decreases in density indicated below the horizontal white line towards dark blue.

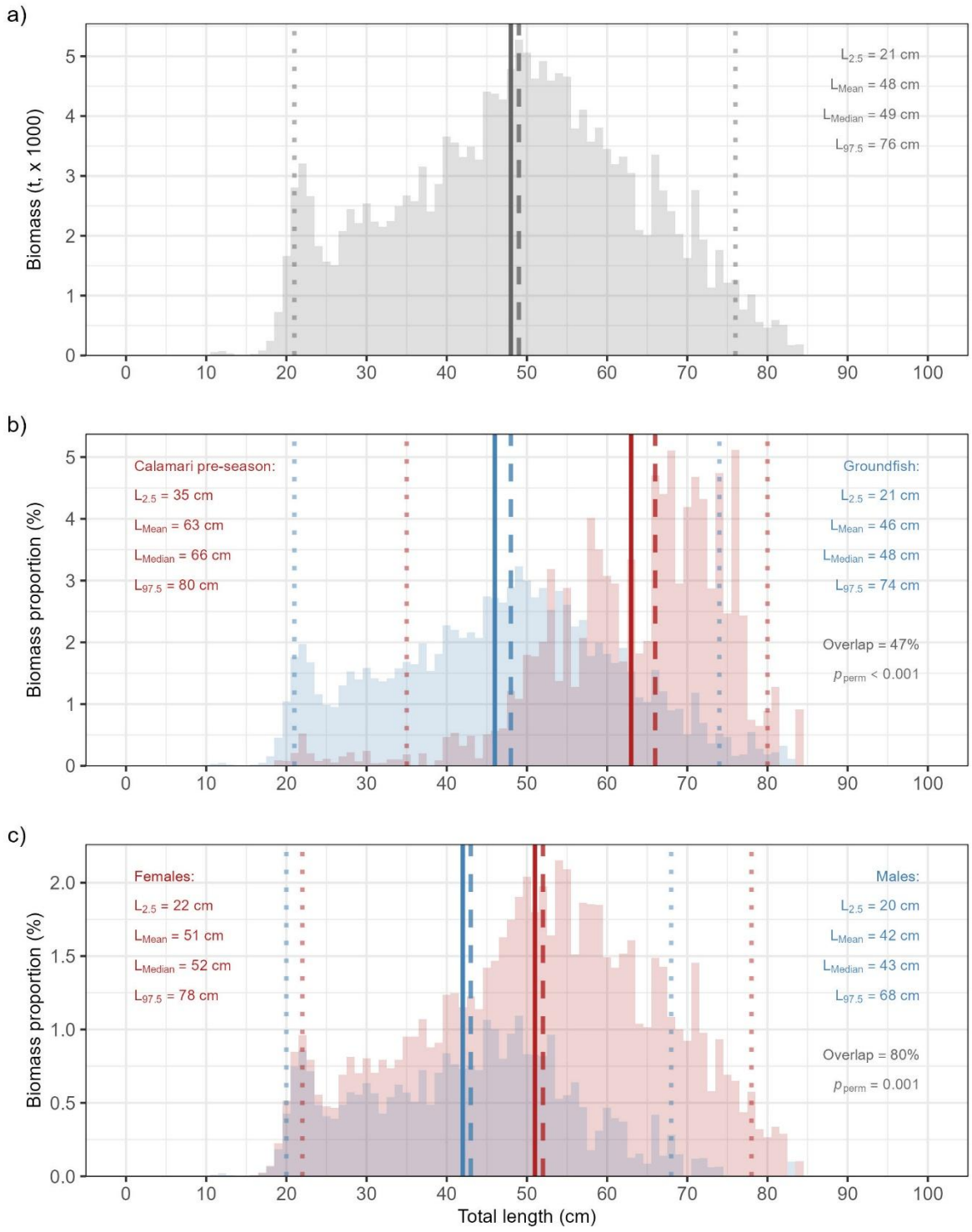

Fig. 62. Biomass-at-length class composition of red cod (*Salilota australis*) across all years combined, based on July groundfish and calamari pre-season surveys conducted in Falkland Islands waters in 2017, 2020, and 2022–2026. a) Overall biomass-at-length frequency distribution. b) Overlap in biomass-at-length distributions between calamari pre-season (red) and groundfish (blue) surveys. c) Overlap in biomass-at-length distributions between females (red) and males (blue). Solid vertical lines indicate the mean length (L_{Mean}), dashed lines the median length (L_{Median}), and dotted lines the 2.5th and 97.5th length percentiles ($L_{2.5}$ and $L_{97.5}$, respectively). p_{perm} is the significance of the weighted permutation test to assess differences between groups.

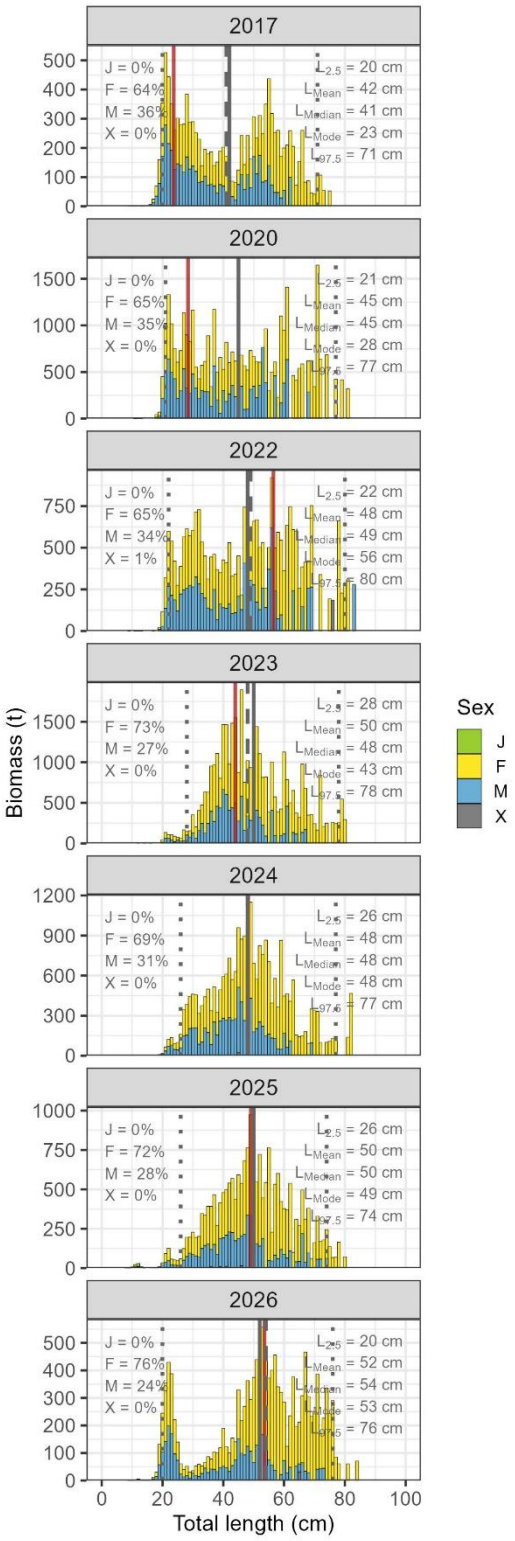

Fig. 63. Annual biomass-at-length class composition of red cod (*Salilota australis*) during July groundfish and calamari pre-season surveys conducted in Falkland Islands waters in 2017, 2020, and 2022–2026. Stacked bars represent biomass (t) per 1.0 cm length class, partitioned by sex (J = juvenile; F = female; M = male; X = undetermined), with the proportion of total annual biomass for each sex indicated in the upper left of each panel. Vertical lines indicate the mean length (L_{Mean}, grey solid), median length (L_{Median}, grey dashed), modal length (L_{Mode}, red solid), and 2.5th and 97.5th percentiles ($L_{2.5}$ and $L_{97.5}$, grey dotted) of the biomass-weighted length distribution. Note the different y-axis scales among years.

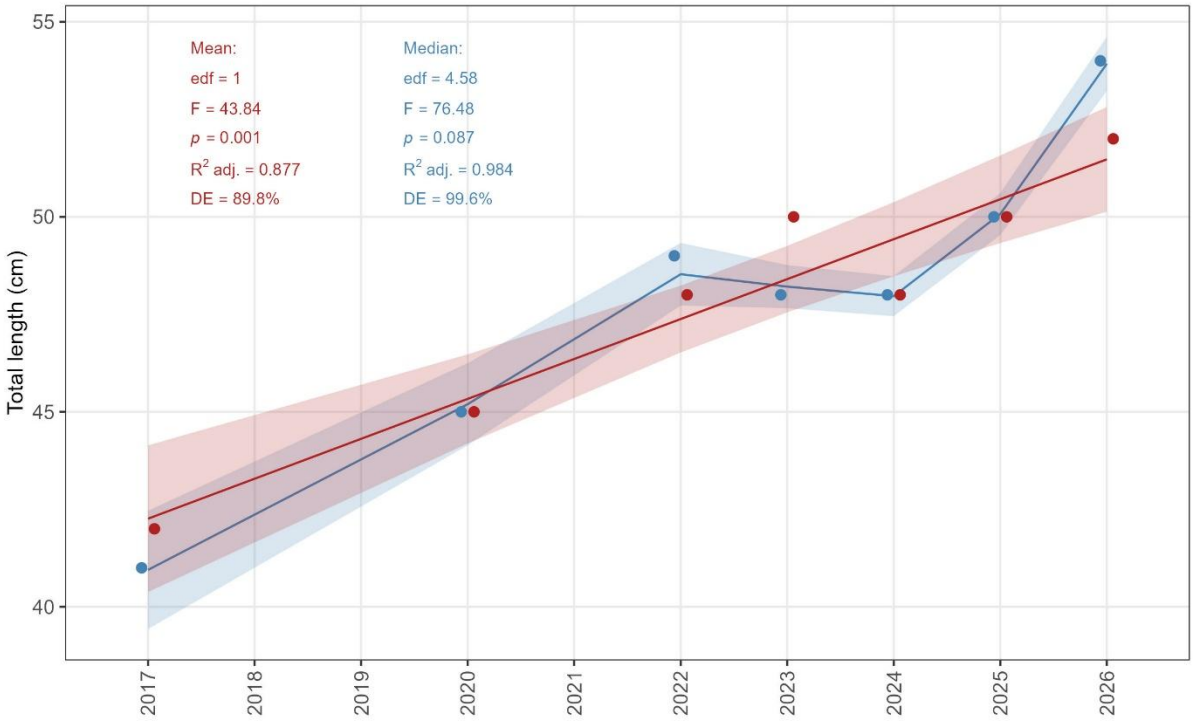

Fig. 64. Median (blue) and mean (red) total length of red cod (*Salilota australis*) during July groundfish and calamari pre-season surveys conducted in Falkland Islands waters in 2017, 2020, and 2022–2026. The line and shaded region represent the fitted Generalised Additive Model (GAM) smooth and its 95% pointwise confidence interval.

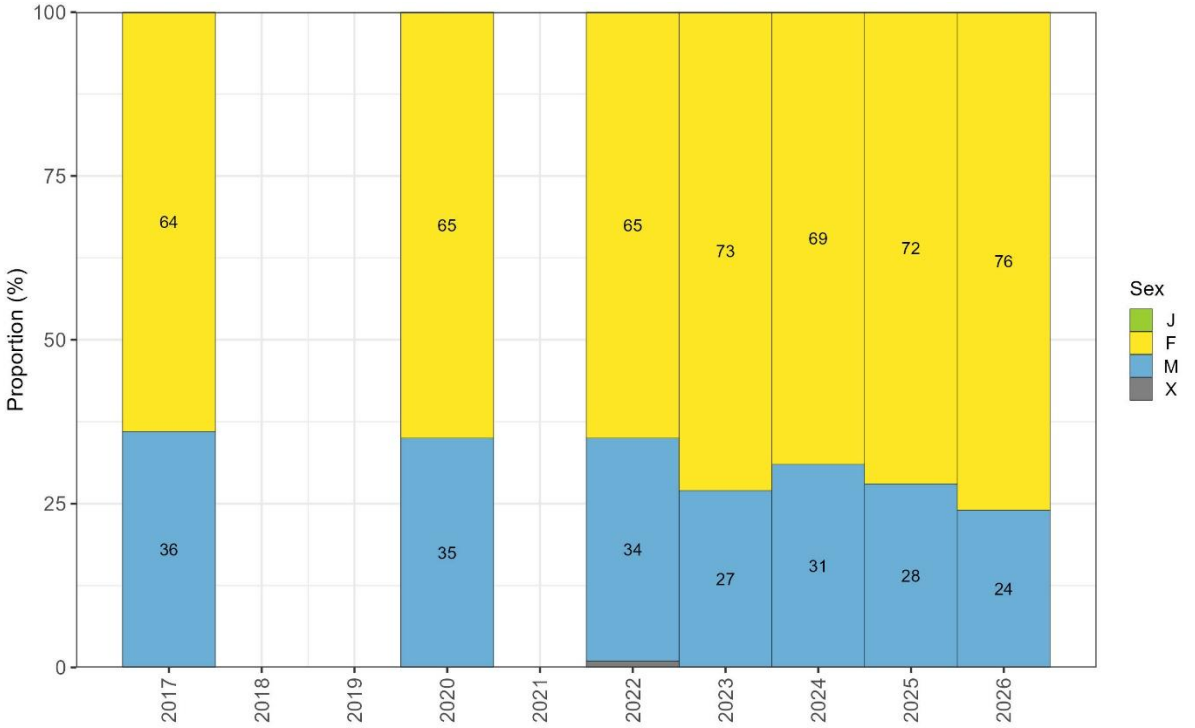

Fig. 65. Proportion by sex (J = juvenile; F = female; M = male; X = undetermined) of red cod (*Salilota australis*) during July groundfish and calamari pre-season surveys conducted in Falkland Islands waters in 2017, 2020, and 2022–2026. Labels for proportions < 3% are omitted.

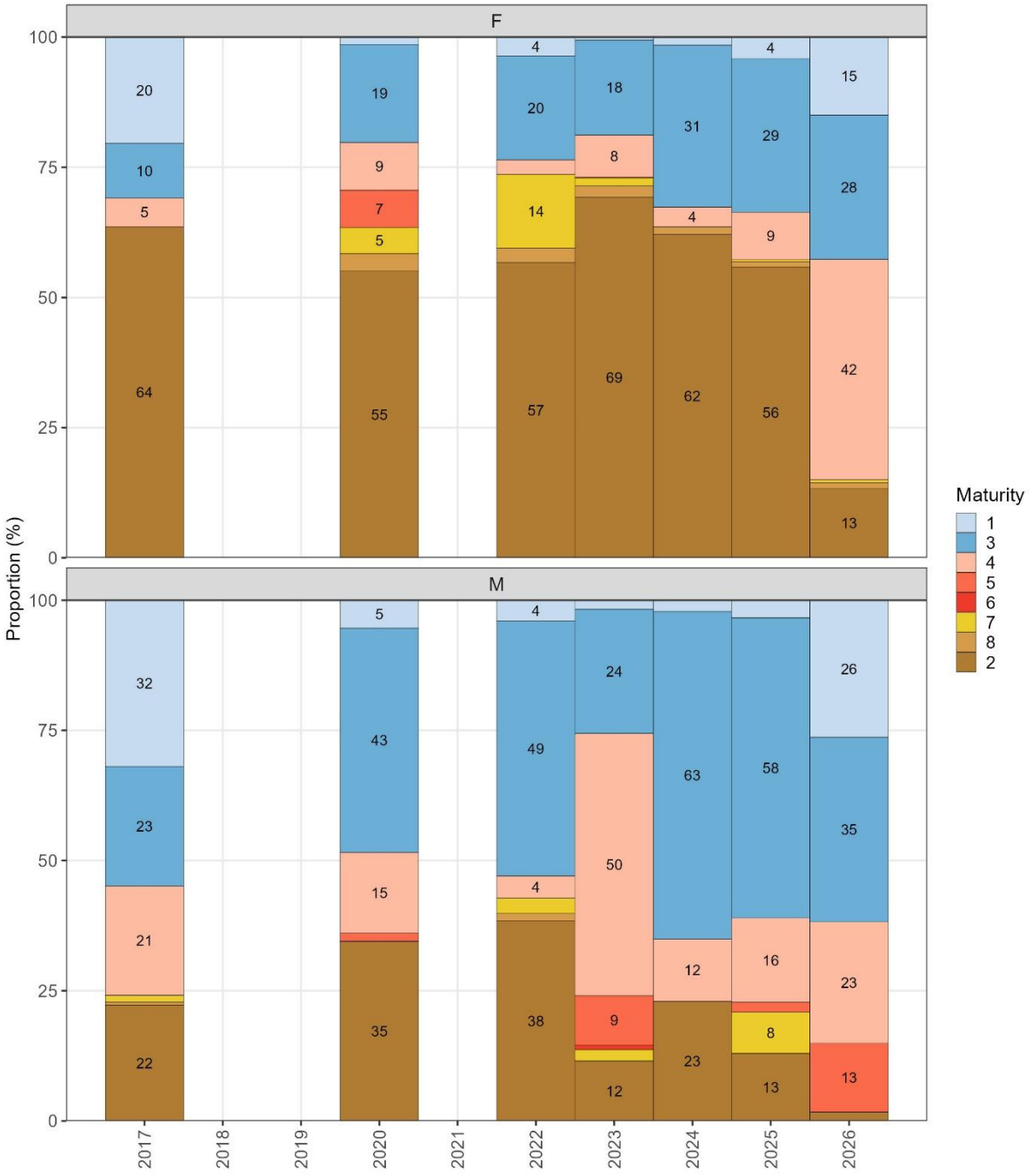

Fig. 66. Proportion by sexual maturity (1, immature; 3, early developing; 4, late developing; 5, ripe; 6, running; 7, spent; 8, recovering spent; 2, resting) of red cod (*Salilota australis*) during July groundfish and calamari pre-season surveys conducted in Falkland Islands waters in 2017, 2020, and 2022–2026. Maturity stages ordered by developmental sequence. Labels for proportions < 3% are omitted.

4.3.9. Rock cod (*Patagonotothen ramsayi*)

4.3.9.1. Temporal patterns of abundance

On average, 42% of the total rock cod catches in the time series were from groundfish surveys and 58% from calamari pre-season surveys. The catch in 2026 (22.54 t) represented a 32% decrease relative to the 2017 catch (32.91 t; the highest catch in the time series), a 29% decrease relative to the 2025 catch (31.80 t), and a 1% decrease relative to the 2023–2025 mean catch (22.77 t; Fig. 67a; Appendix II).

The highest densities were recorded in 2025 (mean ± SE: 679.64 ± 297.51 kg/km²; although with wide confidence intervals). Densities in 2026 (548.63 ± 190.96 kg/km²) represented a 71% increase relative to the 2017 densities (321.23 ± 58.94 kg/km²) but a 19% decrease relative to the 2025 densities and an 18% increase relative to the 2023–2025 mean densities (466.41 ± 128.67 kg/km²; Fig. 67b).

Rock cod biomass in 2026 (84,220.92 t; CI = 44,498.95–124,881.03 t) was the second highest in the time series, corresponding to a 66% increase relative to 2017 levels (50,826.44 t; CI = 32,112.03–66,518.09 t), a 7% decrease relative to 2025 levels (90,882.26 t; CI = 49,956.90–138,520.77 t), and a 47% increase relative to the 2023–2025 mean biomass (57,152.07 t). However, these were non-significant changes in biomass ($p > 0.05$; Fig. 67c; Table IV–V; Appendix III–IV). Analysis of the full time series revealed a non-significant increasing trend in biomass (GAM: edf = 2.31, F = 3.20, p = 0.185), with the model explaining 60.2% of the deviance (R^2 adj. = 0.63; Fig. 67c; Appendix V).

4.3.9.2. Spatial patterns of abundance

In 2026, the highest density of rock cod (21,657 kg/km^2) occurred to the north-west limit of the FICZ at approximately 50.3°S and 63°W. A secondary patch of high density was observed at approximately 50.2°S and 62°W. The highest densities were also observed from 2023 to 2025 to the north-west in the FICZ (Fig. 68), and the highest density in the time series was calculated for 2025 (41,295 kg/km^2).

Densities increased in the north-west and decreased mainly along the 'Loligo Box' in 2026 relative to 2017. Similar changes but of less magnitude were observed in 2026 relative to 2025 and relative to the 2023–2025 mean (Fig. 69).

4.3.9.3. Length composition

Across all survey years combined, total length of rock cod was in the range of 4 to 39 cm; however, 95% of the estimated biomass was comprised of individuals between 14 and 32 cm, with median and mean lengths (± SE) of 23 ± 1.51 cm and 22 ± 1.19 cm, respectively (Fig. 70a).

The distribution of biomass proportions by size class exhibited a 77% overlap between the groundfish and calamari pre-season surveys, with no significant differences between the groundfish survey (mean ± SE: 23 ± 1.18 cm) and the calamari pre-season survey (mean ± SE: 20 ± 1.17 cm; $p > 0.05$). In the groundfish survey, 95% of the biomass of rock cod was comprised of individuals between 15 and 32 cm (median ± SE: 24 ± 1.37 cm). In the calamari pre-season survey, 95% of the biomass was comprised of individuals between 13 and 30 cm (median ± SE: 21 ± 1.71 cm; Fig. 70b).

The distribution of biomass proportions by size class exhibited a 93% overlap between females and males, with no significant differences between females (mean ± SE: 23 ± 1.21 cm) and males (mean ± SE: 21 ± 1.14 cm; $p > 0.05$). For females, 95% of the biomass was comprised of individuals between 14 and 33 cm (median ± SE: 24 ± 1.48 cm). For males, 95% of the biomass was comprised of individuals between 14 and 30 cm (median ± SE: 22 ± 1.58 cm; Fig. 70c).

Through the time series, the size structure of rock cod was broad and multimodal, with at least two length-groups that were not clearly distinguished because of size overlap. A small length-group was observed at about 15 cm, and a larger length-group at 22–25 cm. Different length-groups were dominant in the time series (Fig. 71). In 2026, lengths were in the range of 7 to 38 cm; however, 95% of the biomass was comprised of individuals between 15 and 32 cm, with median and mean lengths (± SE) of 23 ± 1.03 cm and 22 ± 0.81 cm, respectively. For females, 95% of the biomass was comprised of individuals between 15 and 33 cm, with median and mean lengths (± SE) of 23 ± 1.54 cm and 23 ± 1.19 cm, respectively. For males, 95% of the biomass was comprised of individuals between 15 and 30 cm, with median and mean lengths (± SE) of 22 ± 1.33 cm and 22 ± 1.11 cm, respectively (Fig. 71).

Analysis of the full time series revealed non-significant trends in both mean (GAM: edf = 1.00, $F = 5.97$, $p = 0.058$, R^2 adj. = 0.453, DE = 54.4%) and median (GAM: edf = 1.00, $F = 4.3$, $p = 0.093$, R^2 adj. = 0.350, DE = 46.3%) total lengths. Mean and median lengths remained at approximately 21–23 cm throughout the time series (Fig. 72).

4.3.9.4. Sex and maturity composition

The sex composition of rock cod was consistent and comprised of 55.1 ± 1.0% (mean ± SE) females, 44.9 ± 1.0% males, and negligible proportions of juveniles and individuals of undetermined sex throughout the time series. The 2026 and the 2024 sex compositions were similar, and had the lowest proportions of females in the time series (Fig. 73).

Maturity composition in rock cod was different between females and males. Females were predominantly in late developing stage (28–55%); immature and early developing females accounted for 20–49%, and post-spawning (mainly resting) females contributed a further 18–28%. Males were characterised by resting individuals (42–51%), immature and early developing individuals (33–49%), and late developing and ripe individuals (2–18%); running males were not reported throughout the time series (Fig. 74).

4.3.9.5. Discussion

The pattern of rock cod biomass is consistent between July and February parallel surveys from 2017 to 2026, with a moderate increase since approximately 2020 (Ramos 2026). However, the July parallel surveys began in 2017 and therefore cover only the end of the decline evident in the February surveys from 2010 to 2020 (Ramos 2026). This decline is consistent with decreasing biomass estimates from the commercial fishery from 2005 to 2019 (Winter 2020) and decreasing CPUE from 2011 to 2020 (Ramos & Winter 2023a). The stabilisation observed in recent years in both survey series and in commercial CPUE since 2020 (Ramos & Winter 2023a) suggests the rate of decline is slowing and the stock may be recovering slowly. An apparent shift in geographic distribution, inferred from increasing out-

of-zone catches, may have contributed to the reduced abundance observed between 2016 and 2018 (Winter 2021).

The non-significant increase in mean and median length observed in July parallel surveys is consistent with the gradual increase in mean length in February surveys since 2022 (Ramos 2026). However, the February surveys capture a longer-term decline in both mean and median length, indicating a shift towards smaller individuals in the population from 2010 to 2026. This is consistent with the rise in rock cod discard rates in Falkland Islands fisheries, from an average of 13% annually during 2010–2015 to 72% during 2016–2024, with up to 94% reported in 2021 (Falkland Islands Government, *unpublished data*). The Patagonian squid fishery has accounted for the majority of rock cod catches and discards since 2016 (Ramos & Winter 2023a), where rock cod are typically discarded due to their small size. Since most discarded individuals have not yet reproduced and survival rates of discarded fish are low, this removes future reproductive potential from the population and represents a source of unaccounted mortality not fully captured in stock assessments (Guillen et al. 2018). Rock cod remains a permitted catch under finfish vessel licences, with no conservation measures beyond a TAC in place across Falkland Islands fisheries, including the Patagonian squid fishery (Falkland Islands Government 2026). Given the sustained biomass decline, the shift towards smaller individuals, and high discard rates, measures to address the incidental capture and discard of rock cod may be needed to prevent further deterioration and support stock recovery.

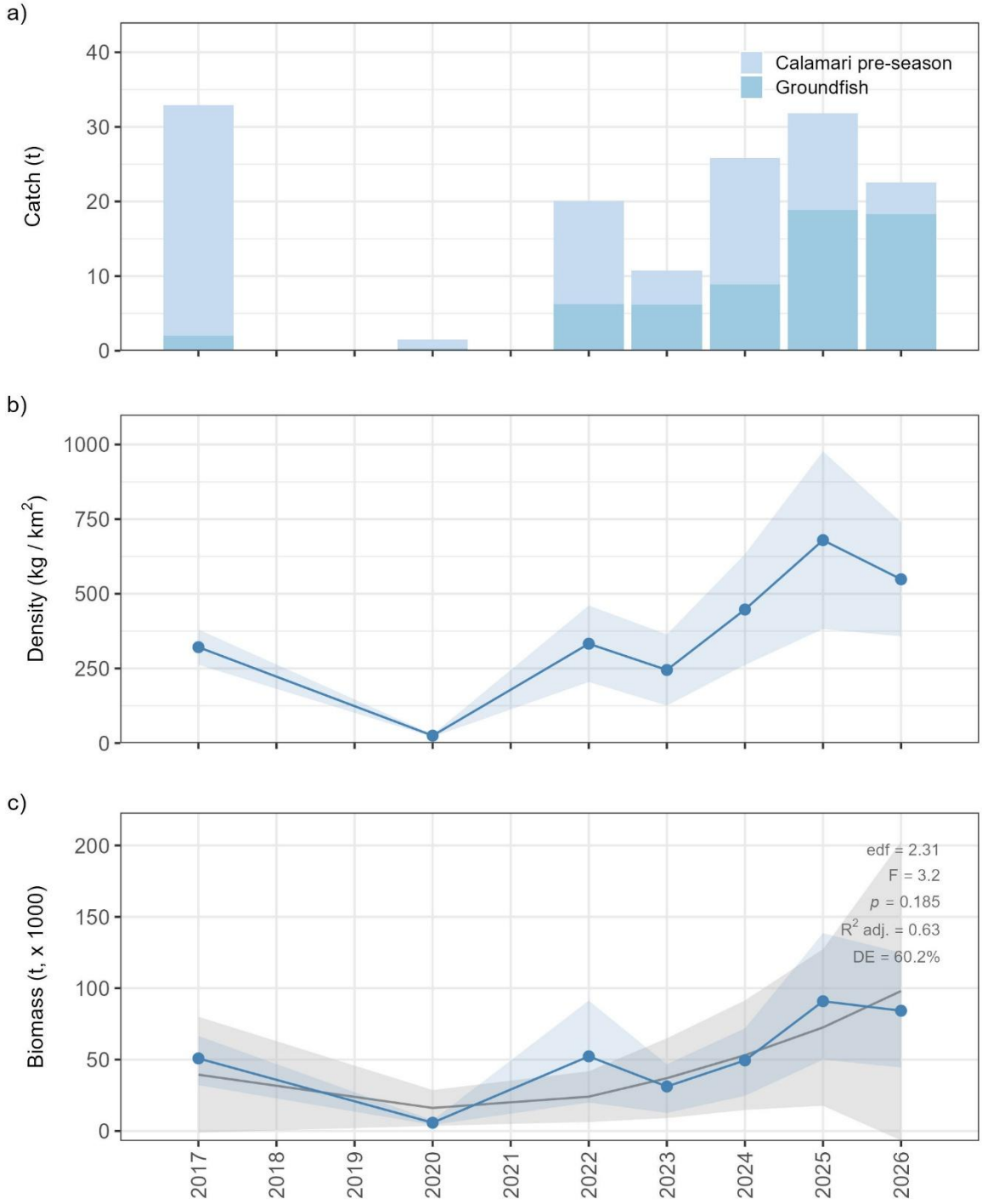

Fig. 67. Abundance of rock cod (*Patagonotothen ramsayi*) during July groundfish and calamari pre-season surveys conducted in Falkland Islands waters in 2017, 2020, and 2022–2026. (a) Catch per survey, (b) annual mean density ± SE represented by the blue line and shaded region, respectively, and (c) estimated biomass, where the blue line and shaded region represent the median and 95% pointwise confidence interval derived from 10,000 bootstrap biomass estimates, and the grey line and shaded region represent the fitted Generalised Additive Model (GAM) smooth and its 95% pointwise confidence interval.

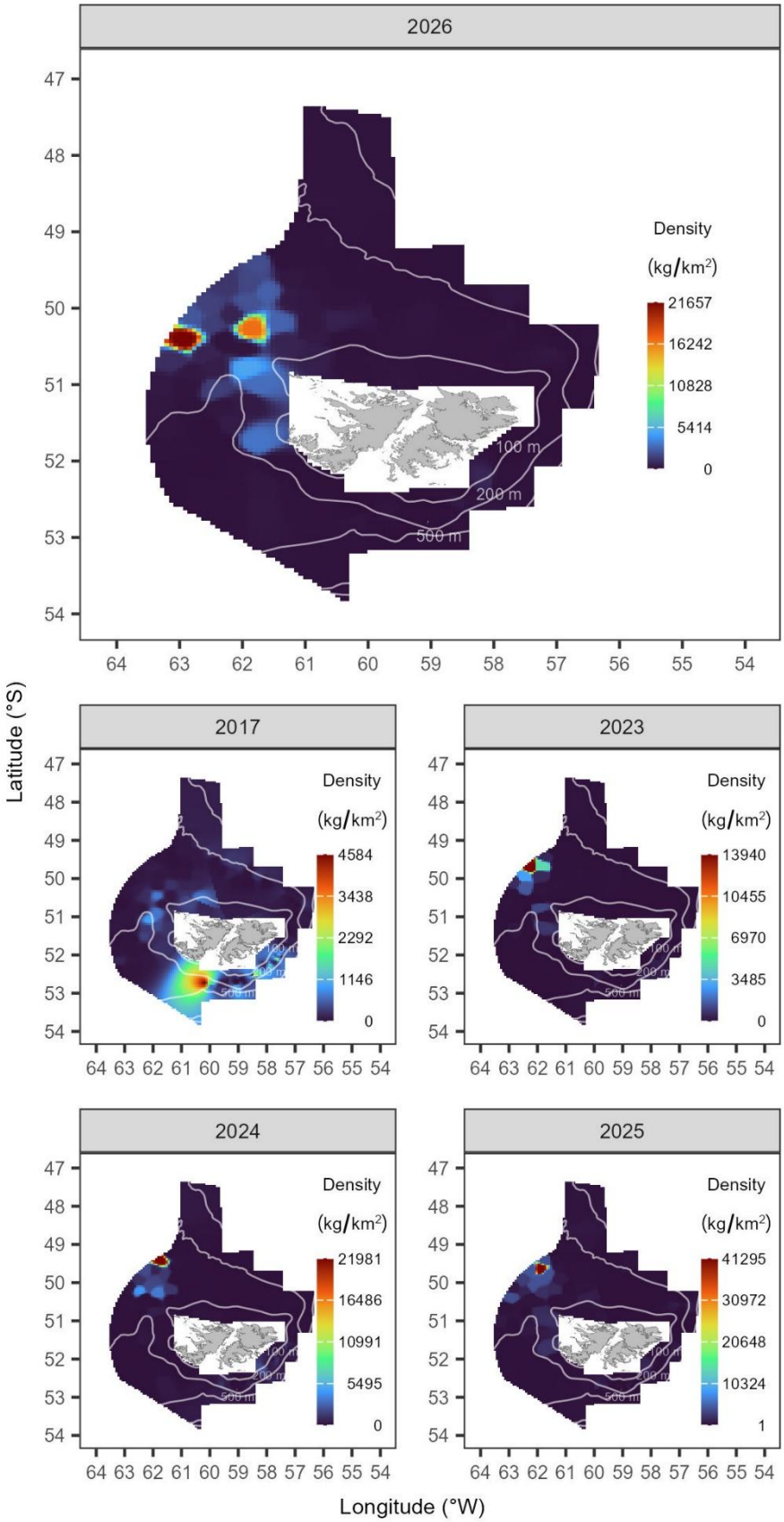

Fig. 68. Distribution and abundance of rock cod (*Patagonotothen ramsayi*) derived from the July 2026 groundfish and calamari pre-season surveys in Falkland Islands waters, compared with the first year of the time series (2017) and the three preceding years (2023–2025). Colour scales are specific to each year. Isobaths at 100 m, 200 m, and 500 m are shown.

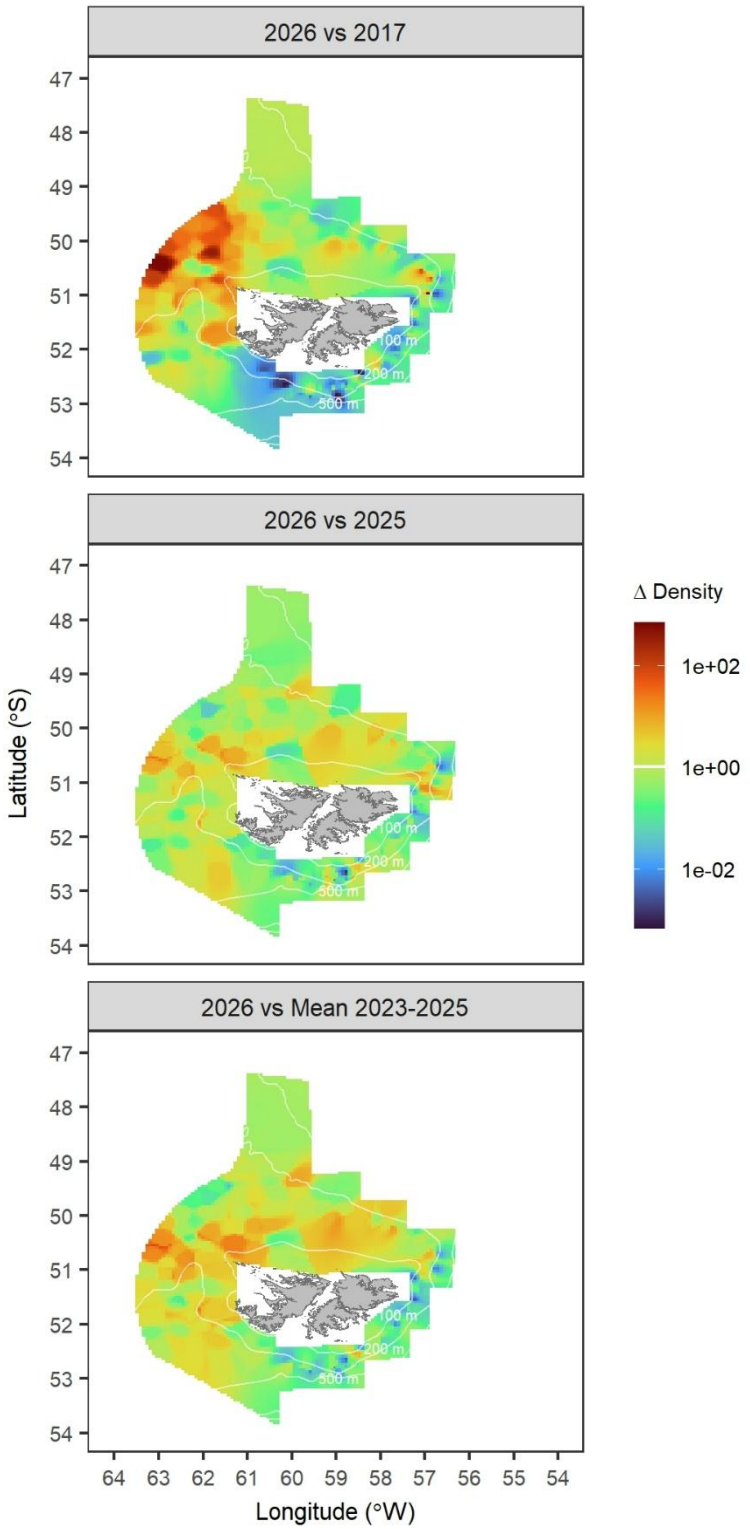

Fig. 69. Spatial change in density of rock cod (*Patagonotothen ramsayi*) derived from the July 2026 groundfish and calamari pre-season surveys in Falkland Islands waters, relative to the first year of the time series (2017), the previous year (2025), and the mean of the three preceding years (2023–2025). The spatial change in density is expressed as the ratio of density (kg/km^2) in 2026 relative to the density in the baseline year (2017, 2025, 2023–2025 mean). Isobaths at 100 m, 200 m, and 500 m are shown. The colour scale is $\log_{10}$-transformed to aid visualisation, with increases in density indicated above the horizontal white line towards dark red, and decreases in density indicated below the horizontal white line towards dark blue.

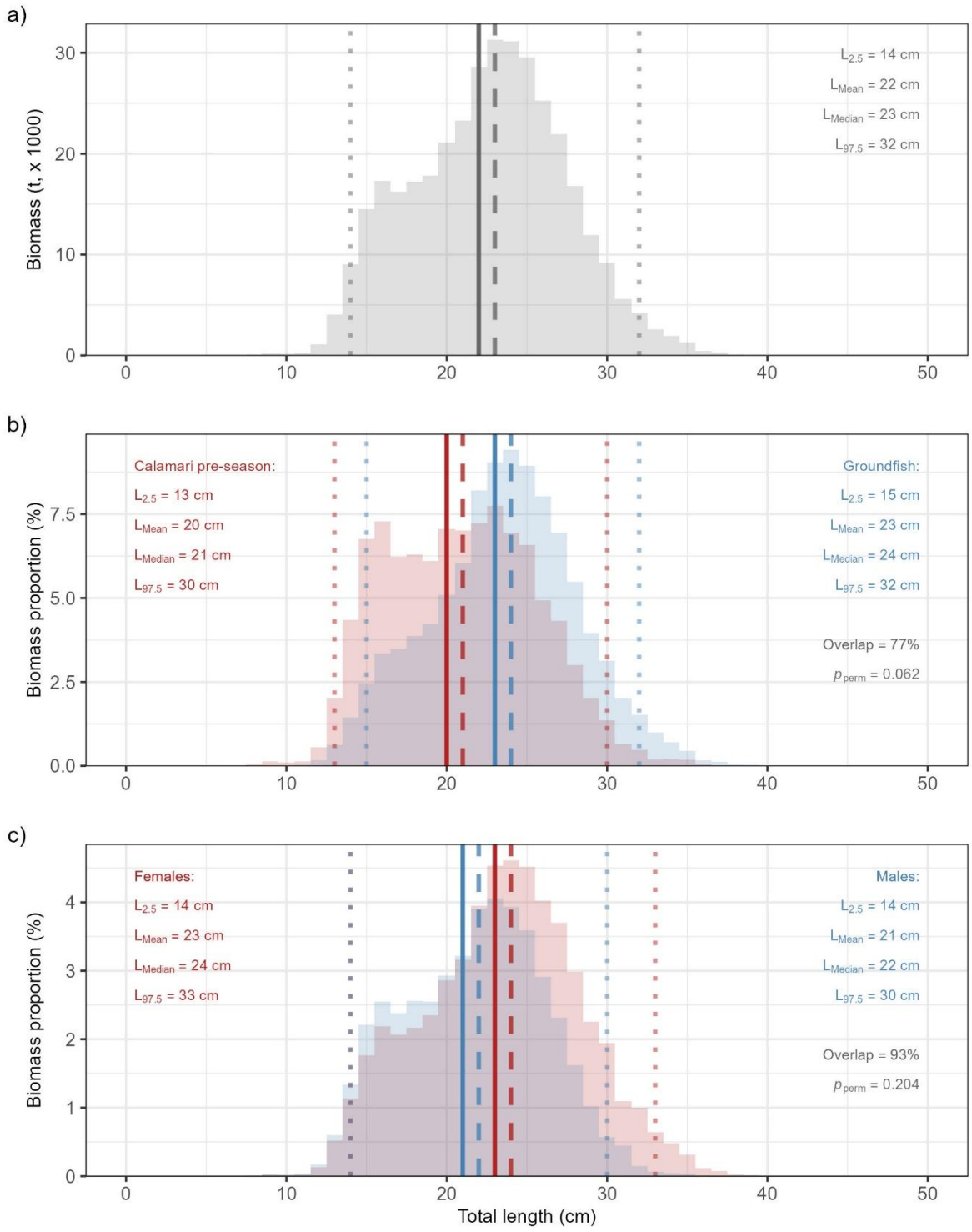

Fig. 70. Biomass-at-length class composition of rock cod (*Patagonotothen ramsayi*) across all years combined, based on July groundfish and calamari pre-season surveys conducted in Falkland Islands waters in 2017, 2020, and 2022–2026. a) Overall biomass-at-length frequency distribution. b) Overlap in biomass-at-length distributions between calamari pre-season (red) and groundfish (blue) surveys. c) Overlap in biomass-at-length distributions between females (red) and males (blue). Solid vertical lines indicate the mean length (L_{Mean}), dashed lines the median length (L_{Median}), and dotted lines the 2.5th and 97.5th length percentiles ($L_{2.5}$ and $L_{97.5}$, respectively). p_{perm} is the significance of the weighted permutation test to assess differences between groups.

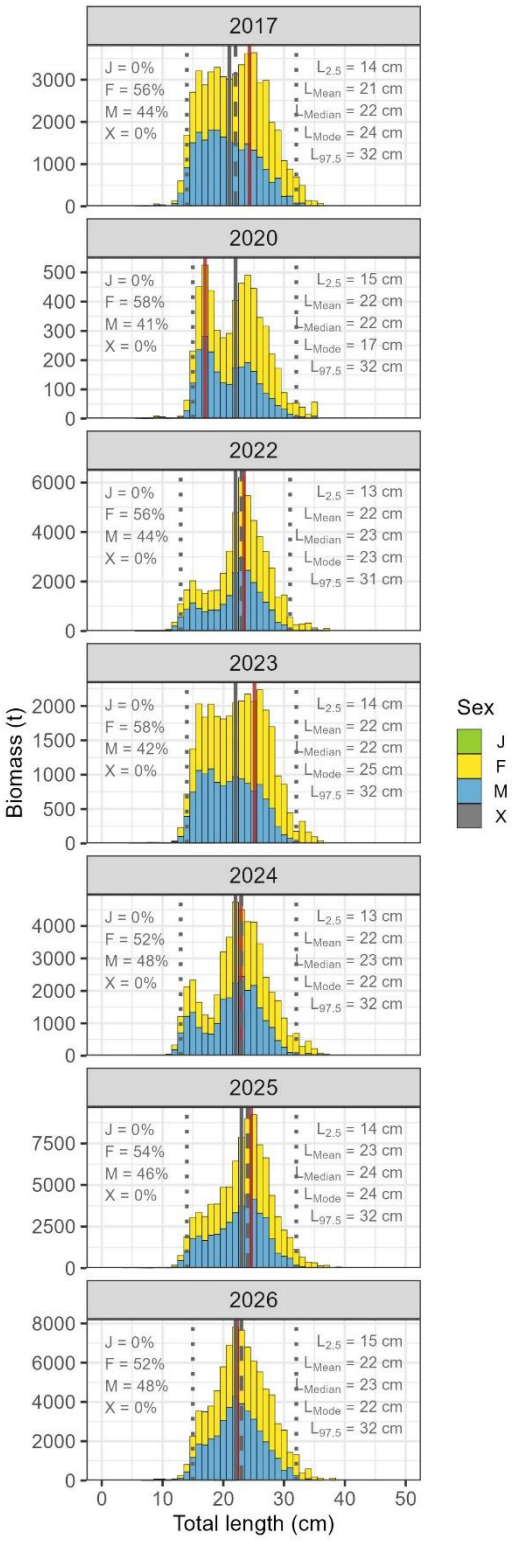

Fig. 71. Annual biomass-at-length class composition of rock cod (*Patagonotothen ramsayi*) during July groundfish and calamari pre-season surveys conducted in Falkland Islands waters in 2017, 2020, and 2022–2026. Stacked bars represent biomass (t) per 1.0 cm length class, partitioned by sex (J = juvenile; F = female; M = male; X = undetermined), with the proportion of total annual biomass for each sex indicated in the upper left of each panel. Vertical lines indicate the mean length (L_{Mean}, grey solid), median length (L_{Median}, grey dashed), modal length (L_{Mode}, red solid), and 2.5th and 97.5th percentiles ($L_{2.5}$ and $L_{97.5}$, grey dotted) of the biomass-weighted length distribution. Note the different y-axis scales among years.

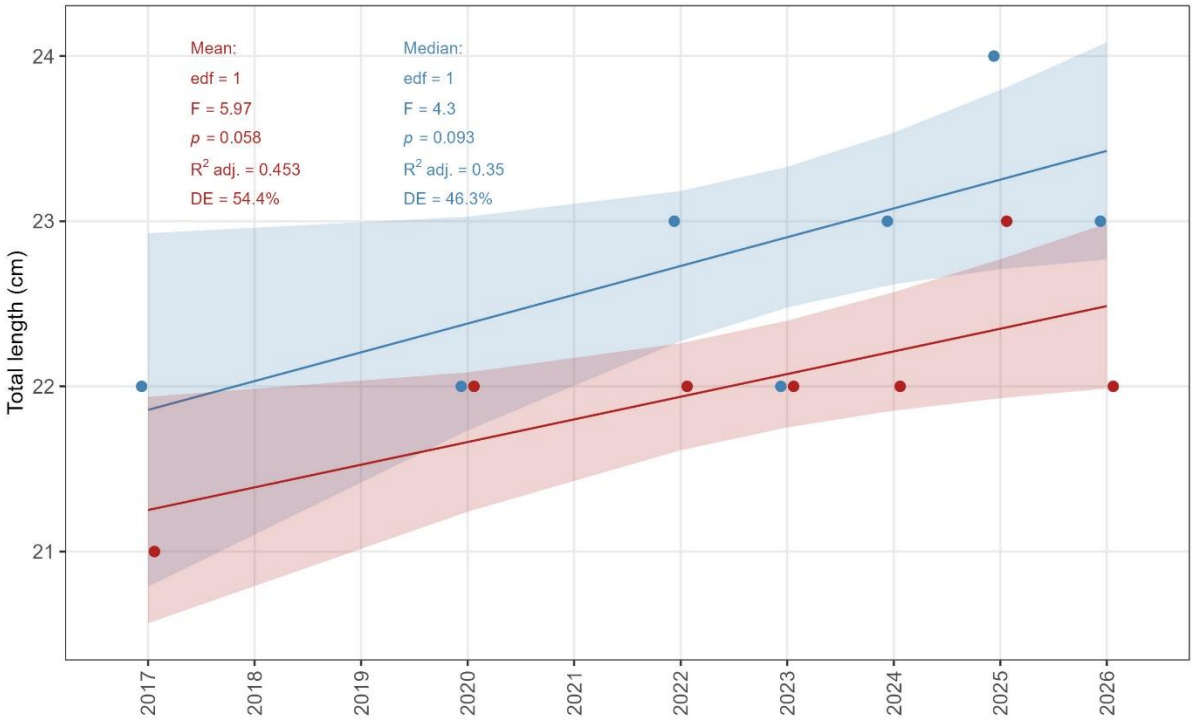

Fig. 72. Median (blue) and mean (red) total length of rock cod (*Patagonotothen ramsayi*) during July groundfish and calamari pre-season surveys conducted in Falkland Islands waters in 2017, 2020, and 2022–2026. The line and shaded region represent the fitted Generalised Additive Model (GAM) smooth and its 95% pointwise confidence interval.

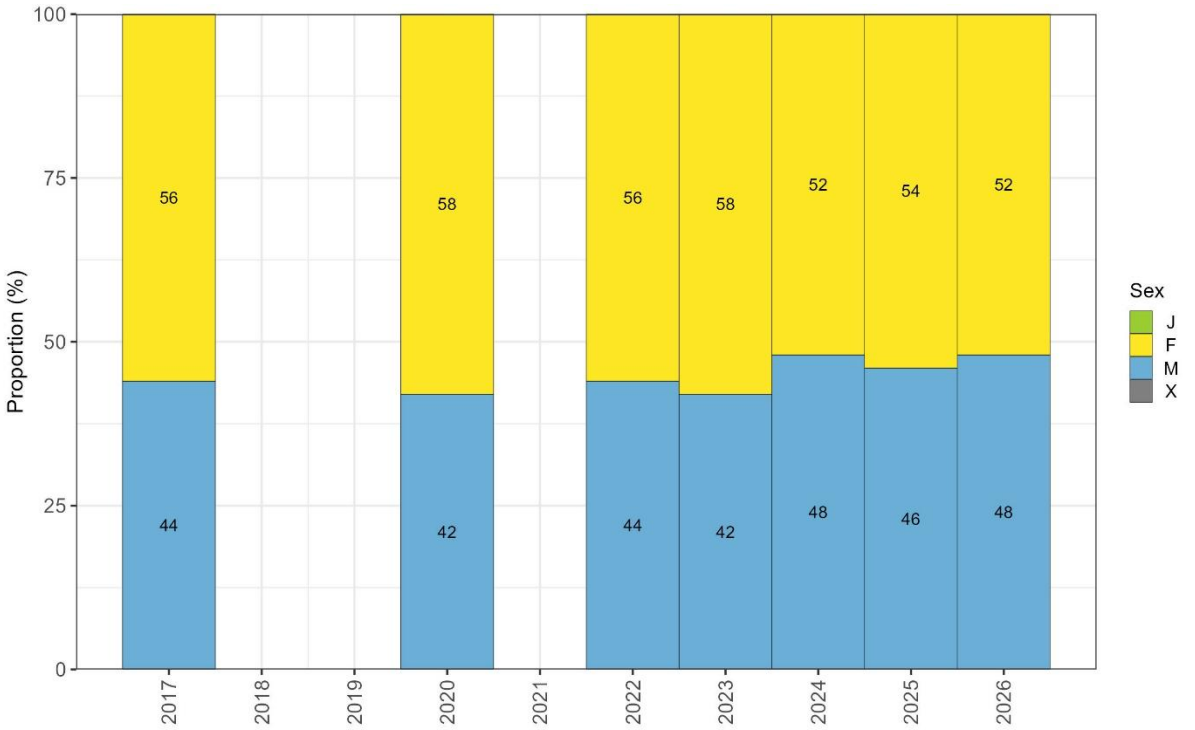

Fig. 73. Proportion by sex (J = juvenile; F = female; M = male; X = undetermined) of rock cod (*Patagonotothen ramsayi*) during July groundfish and calamari pre-season surveys conducted in Falkland Islands waters in 2017, 2020, and 2022–2026. Labels for proportions < 3% are omitted.

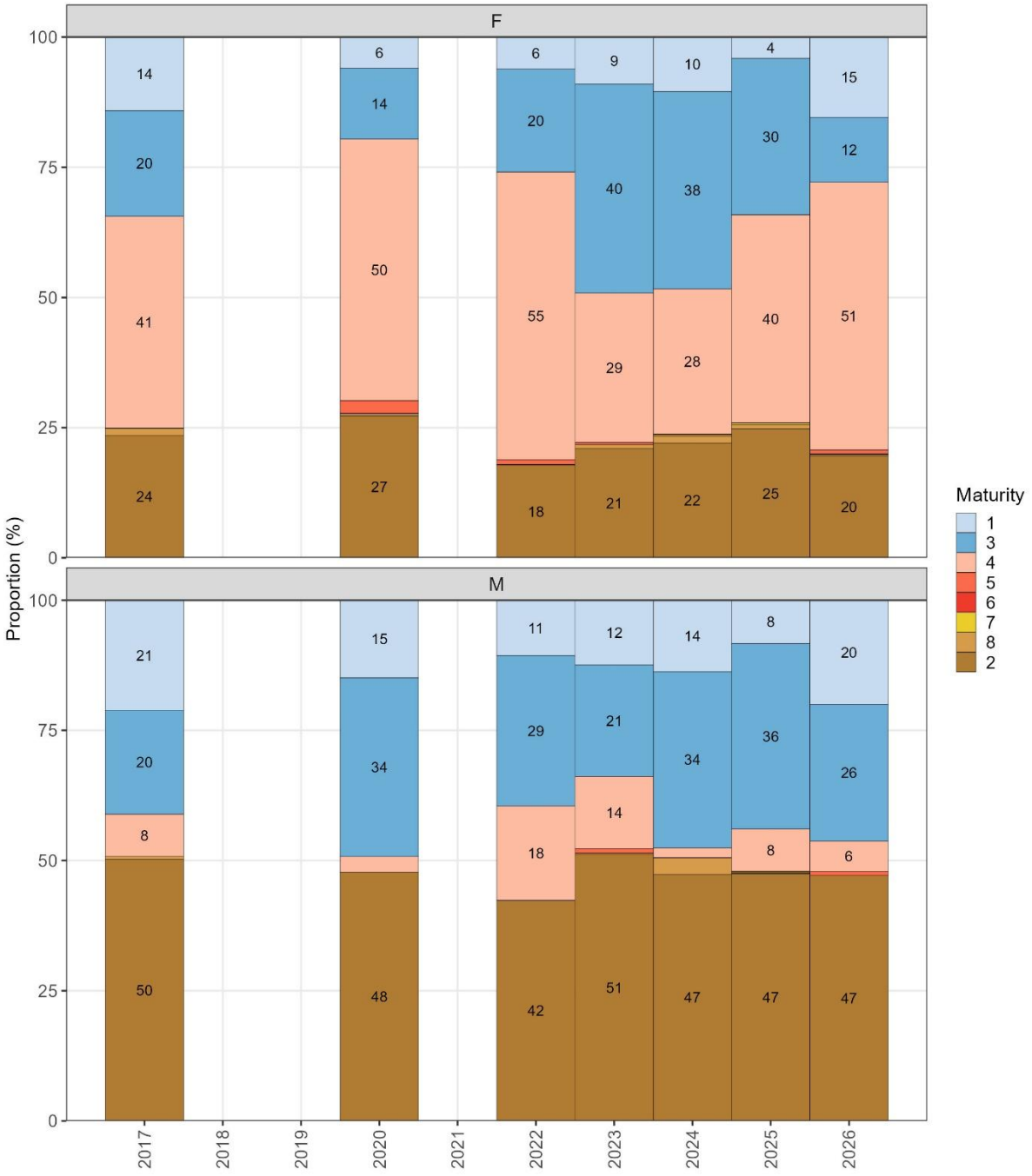

Fig. 74. Proportion by sexual maturity (1, immature; 3, early developing; 4, late developing; 5, ripe; 6, running; 7, spent; 8, recovering spent; 2, resting) of rock cod (*Patagonotothen ramsayi*) during July groundfish and calamari pre-season surveys conducted in Falkland Islands waters in 2017, 2020, and 2022–2026. Maturity stages ordered by developmental sequence. Labels for proportions < 3% are omitted.

4.3.10. Southern blue whiting (*Micromesistius australis*)

4.3.10.1. Temporal patterns of abundance

On average, 42% of the total southern blue whiting catches in the time series were from groundfish surveys and 58% from calamari pre-season surveys. The catch in 2026 (0.04 t) represented a 94% decrease relative to the 2017 catch (0.70 t) and relative to the 2023–2025 mean catch (0.70 t), and it was similar to the catch in 2025 (0.04 t; Fig. 75a; Appendix II).

The highest densities were recorded in 2020 (mean ± SE: 35.57 ± 20.88 kg/km²; although with wide confidence intervals). Densities in 2026 (1.15 ± 0.40 kg/km²) represented an 88% decrease relative to the 2017 densities (9.59 ± 5.14 kg/km²), a 4% increase relative to the 2025 densities (1.11 ± 0.52 kg/km²), and a 74% decrease relative to the 2023–2025 mean densities (4.35 ± 2.05 kg/km²; Fig. 75b).

Southern blue whiting biomass peaked in 2020 (9,229.48 t; CI = 505.15–13,409.20 t). Biomass in 2026 (923.60 t; CI = 318.59–1,273.75 t) represented a 41% decrease relative to 2017 levels (1,556.92 t; CI = 338.45–2,675.77 t) but represented a nearly three-fold increase relative to 2025 levels (324.10 t; CI = 73.39–496.23 t), and a 41% increase relative to the 2023–2025 mean biomass (654.42 t). These were non-significant changes in biomass ($p > 0.05$; Fig. 75c; Table IV–V; Appendix III–IV). Analysis of the full time series revealed a non-significant temporal trend in biomass (GAM: edf = 1.51, F = 2.52, p = 0.193), with the model explaining 52.3% of the deviance (R^2 adj. = -0.371; Fig. 75c; Appendix V).

4.3.10.2. Spatial patterns of abundance

In 2026, southern blue whiting occurred to the south-west in the FICZ, with the highest density (46 kg/km^2) at approximately 52.7°S and 61°W. Higher densities occurred to the north-east in 2017 (665 kg/km^2), to the south of East Falkland in 2023 (784 kg/km^2), to the east of East Falkland in 2024 (80 kg/km^2), and to the south of West Falkland in 2025 (68 kg/km^2; Fig. 76). The highest density in the time series was calculated for 2020 to the south of East Falkland (1,288 kg/km^2).

Densities in 2026 decreased through the survey area, except for the north and west in the FICZ relative to 2017, 2025, and the 2023–2025 mean (Fig. 77). The increase in posterior densities noted to the north-west in 2026 relative to 2017 may be an artifact of the axial loop that resulted in the projection of densities in areas where this species was not caught and should be interpreted with caution (Fig. 77).

4.3.10.3. Length composition

Across all survey years combined, total length of southern blue whiting was in the range of 9 to 63 cm; however, 95% of the estimated biomass was comprised of individuals between 16 and 60 cm, with median and mean lengths (± SE) of 43 ± 3.58 cm and 39 ± 2.79 cm, respectively (Fig. 78a).

The distribution of biomass proportions by size class exhibited a 53% overlap between the groundfish and calamari pre-season surveys, with no significant differences between the groundfish survey (mean ± SE: 39 ± 2.85 cm) and the calamari pre-season survey (mean ± SE: 36 ± 3.39 cm; $p > 0.05$). In the groundfish survey, 95% of the biomass of southern blue whiting

was comprised of individuals between 16 and 59 cm (median ± SE: 43 ± 3.43 cm). In the calamari pre-season survey, 95% of the biomass was comprised of individuals between 16 and 63 cm (median ± SE: 31 ± 8.60 cm; Fig. 78b).

The distribution of biomass proportions by size class exhibited an 82% overlap between females and males. The permutation analysis revealed non-significant differences between females (mean ± SE: 42 ± 2.94 cm) and males (mean ± SE: 39 ± 2.65 cm; $p > 0.05$). For females, 95% of the biomass was comprised of individuals between 16 and 61 cm (median ± SE: 48 ± 3.51 cm). For males, 95% of the biomass was comprised of individuals between 16 and 58 cm (median ± SE: 42 ± 2.97 cm; Fig. 78c).

Through the time series, the size structure of southern blue whiting was broad and multimodal, with some length-groups not clearly distinguished because of size overlap (Fig. 79). In 2026, lengths were in the range of 14 to 61 cm; however, 95% of the biomass was comprised of individuals between 16 and 61 cm, with median and mean lengths (± SE) of 52 ± 5.98 cm and 43 ± 4.02 cm, respectively. For females, 95% of the biomass was comprised of individuals between 17 and 61 cm, with median and mean lengths (± SE) of 56 ± 8.38 cm and 46 ± 6.17 cm, respectively. For males, 95% of the biomass was comprised of individuals between 16 and 56 cm, with median and mean lengths (± SE) of 50 ± 11.42 cm and 40 ± 5.36 cm, respectively (Fig. 79).

Analysis of the full time series revealed statistically significant increasing trends in both mean (GAM: edf = 3.21, $F = 9.91$, $p = 0.048$, R^2 adj. = 0.856, DE = 93%) and median (GAM: edf = 2.62, $F = 20.26$, $p = 0.018$, R^2 adj. = 0.872, DE = 94.7%) total lengths. Both mean and median lengths increased from approximately 20 cm in 2017 to approximately 42–52 cm in 2026. Observed values revealed considerable interannual variability, likely in part due to the limited number of individuals caught (Fig. 80).

4.3.10.4. Sex and maturity composition

The sex composition of southern blue whiting was dominated by males (mean ± SE: 57.4 ± 5.6%), followed by females (34.6 ± 4.2%), juveniles (7.9 ± 7.2%; highest at 51% in 2017 but < 3% in 2020 and 2025), and individuals of undetermined sex (with a negligible 0.1 ± 0.1%) throughout the time series. In 2026, the sex composition was characterised by the highest proportion of females in the time series (49%; Fig. 81).

Maturity similar between sexes. Females were predominantly immature or early developing in most years (≥ 49% combined), except for 2026 when late developing individuals were dominant (67%); post-spawning (spent, recovering spent, and resting) females were observed in relatively high proportions in 2022, and 2024–2025 (32–51%). For males, immature and early developing individuals were predominant in most years (≥ 55%), except for 2026 when late developing individuals accounted for 57%; post-spawning males were observed in relatively high proportions in 2022 (28%) and 2024 (56%; Fig. 82).

4.3.10.5. Discussion

The absence of a significant temporal trend and the low biomass levels of southern blue whiting observed in July parallel surveys are consistent with February parallel surveys (Ramos 2026), and with the stock's low abundance following heavy exploitation in the Southwest

Atlantic since the early 1990s and its collapse in 2009 (Navarro et al. 2014; Falkland Islands Government 2026). A no-fishing area established south-west of the Falkland Islands from 1 July to 15 October in 2007 for S-licensed vessels that targeted southern blue whiting and hoki (Falkland Islands Government 2026), and the absence of S-licence fishing since 2017 may have provided some protection. However, the Falkland Islands contributed only ~4% of the catch shared with Argentina and ~2.5% of the total catch shared among Argentina, Chile, and the Falkland Islands from 2017 to 2024 (Ramos & Winter 2023c; Falkland Islands Government 2026; Government of Argentina, www.magyp.gob.ar), suggesting the persistently low biomass in Falkland Islands waters reflects cumulative fishing pressure across multiple EEZs rather than conditions within the Falkland Islands zone alone.

The increase in mean and median length in July parallel surveys is consistent with the apparent increase in median length in February parallel surveys from 2017 to 2026 (Ramos 2026), although high interannual variability and anomalously low values in July 2023 and February 2022–2023 limit interpretation of size composition trends.

Continued protection of the spawning ground south of the Falkland Islands (Shubnikov et al. 1969; Pájaro & Macchi 2001; Macchi et al. 2005) remains essential, particularly given the influence of the Falkland Current intensity on its size and location (Arkhipkin et al. 2009, 2012). Any resumption of directed fishing on this stock should be approached cautiously as it may negatively affect the recovery of the stock.

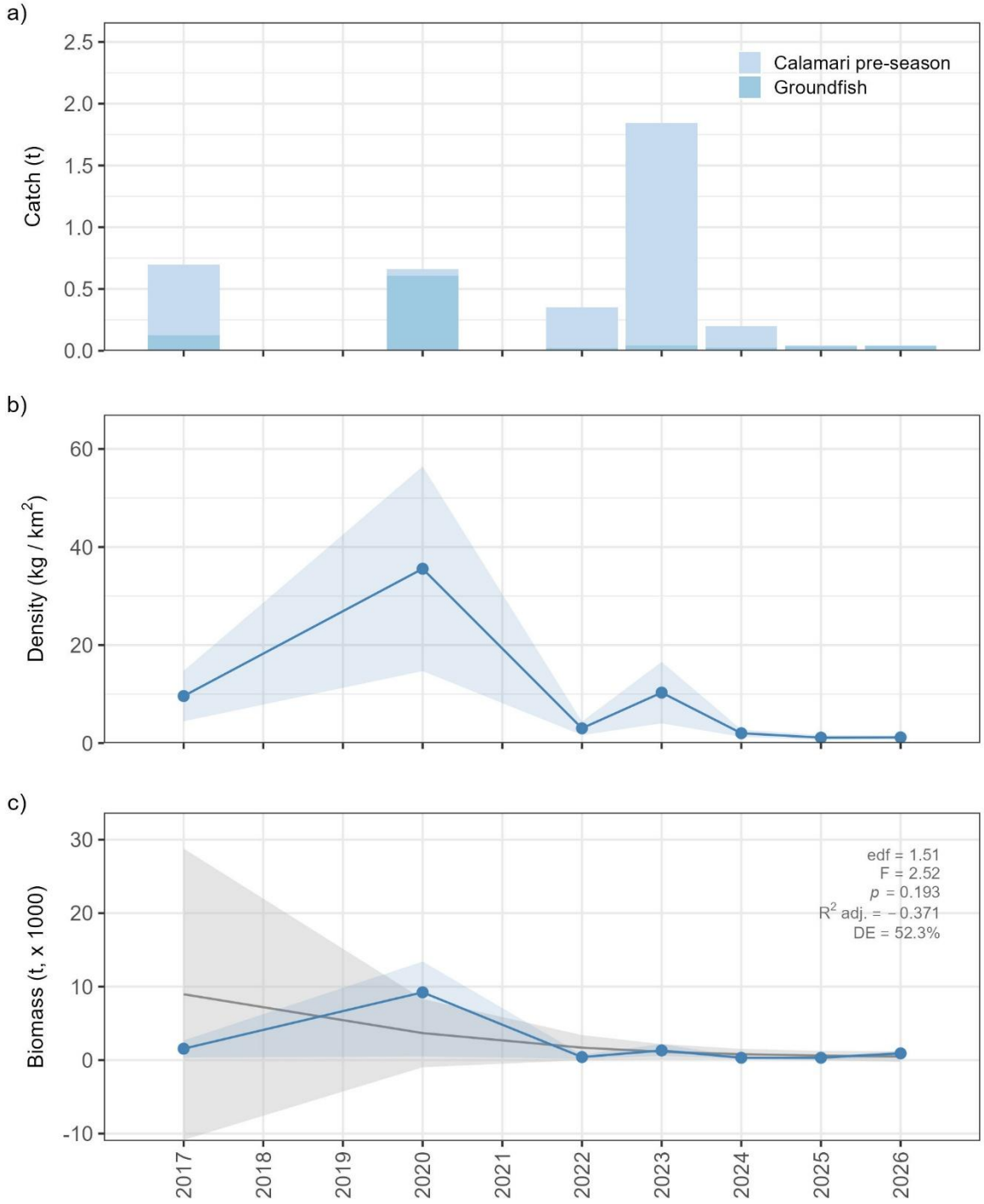

Fig. 75. Abundance of southern blue whiting (*Micromesistius australis*) during July groundfish and calamari pre-season surveys conducted in Falkland Islands waters in 2017, 2020, and 2022–2026. (a) Catch per survey, (b) annual mean density ± SE represented by the blue line and shaded region, respectively, and (c) estimated biomass, where the blue line and shaded region represent the median and 95% pointwise confidence interval derived from 10,000 bootstrap biomass estimates, and the grey line and shaded region represent the fitted Generalised Additive Model (GAM) smooth and its 95% pointwise confidence interval.

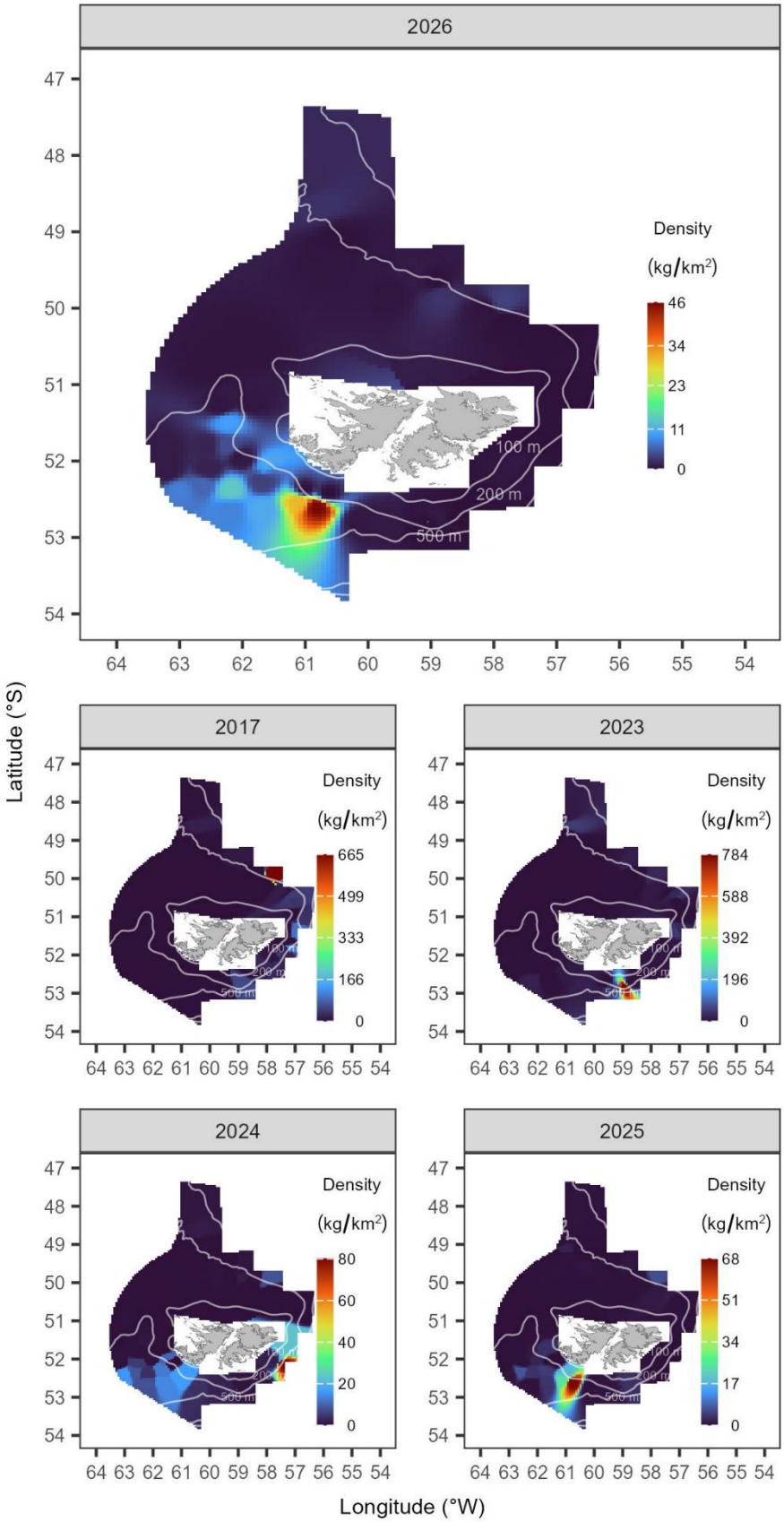

Fig. 76. Distribution and abundance of southern blue whiting (*Micromesistius australis*) derived from the July 2026 groundfish and calamari pre-season surveys in Falkland Islands waters, compared with the first year of the time series (2017) and the three preceding years (2023–2025). Colour scales are specific to each year. Isobaths at 100 m, 200 m, and 500 m are shown.

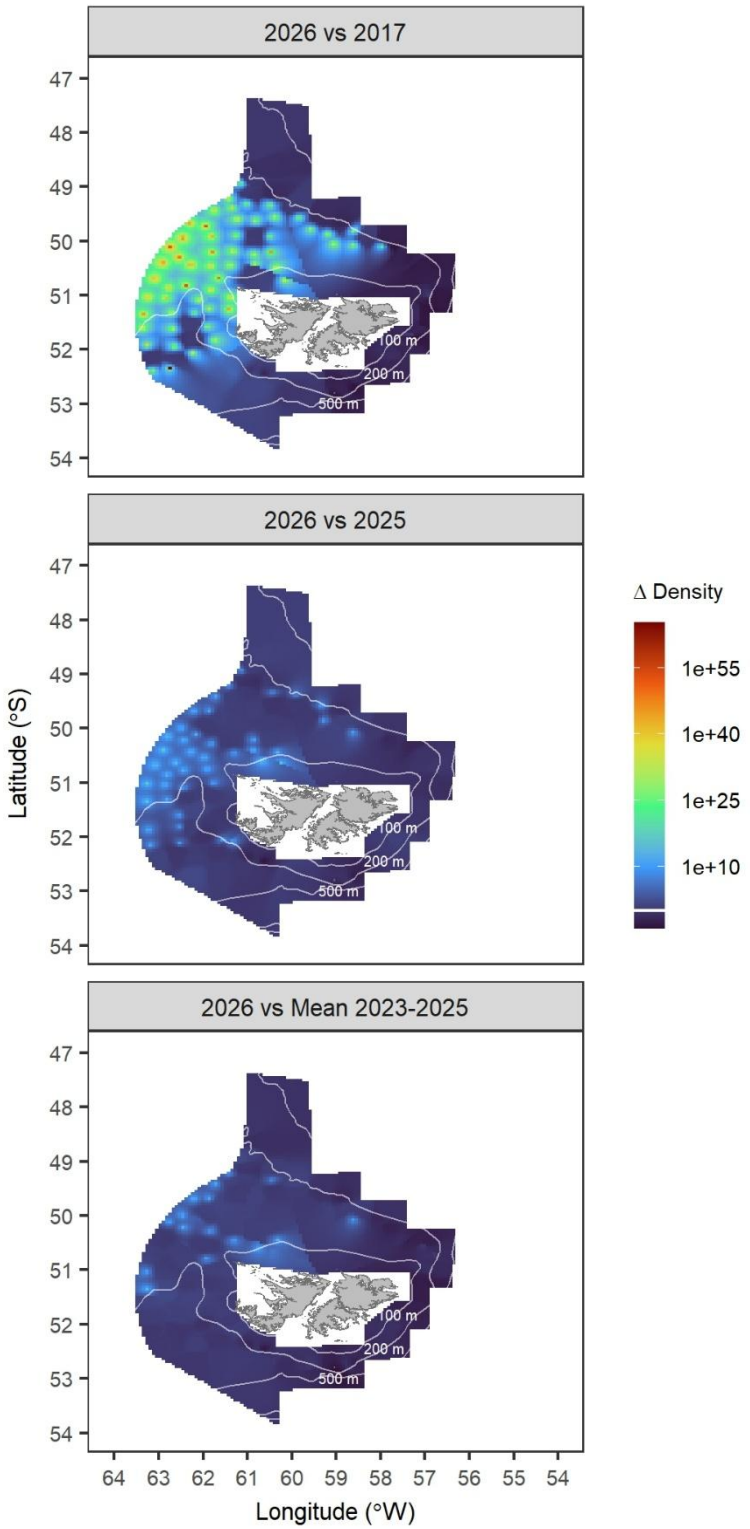

Fig. 77. Spatial change in density of southern blue whiting (*Micromesistius australis*) derived from the July 2026 groundfish and calamari pre-season surveys in Falkland Islands waters, relative to the first year of the time series (2017), the previous year (2025), and the mean of the three preceding years (2023–2025). The spatial change in density is expressed as the ratio of density (kg/km^2) in 2026 relative to the density in the baseline year (2017, 2025, 2023–2025 mean). Isobaths at 100 m, 200 m, and 500 m are shown. The colour scale is $\log_{10}$-transformed to aid visualisation, with increases in density indicated above the horizontal white line towards dark red, and decreases in density indicated below the horizontal white line towards dark blue.

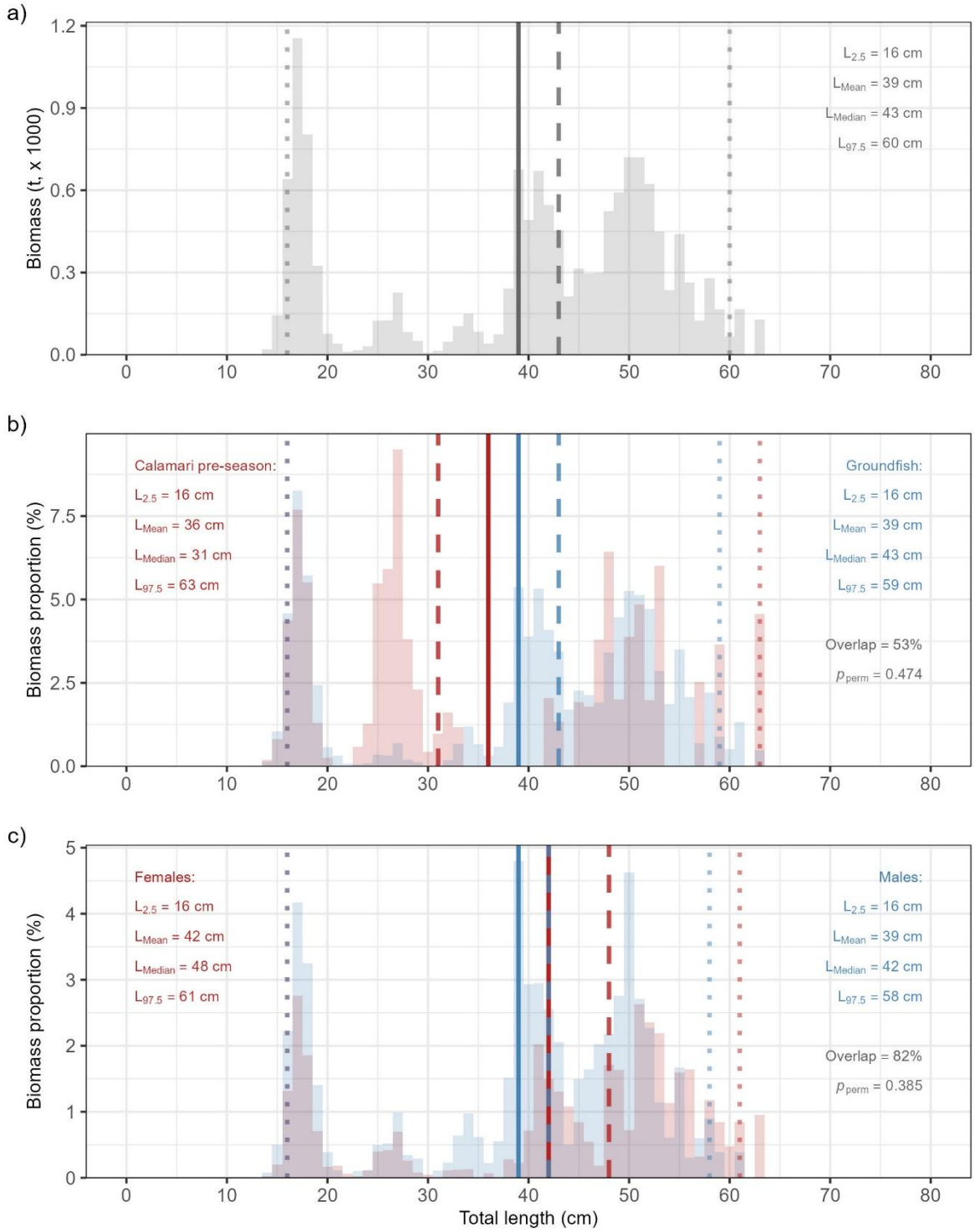

Fig. 78. Biomass-at-length class composition of southern blue whiting (*Micromesistius australis*) across all years combined, based on July groundfish and calamari pre-season surveys conducted in Falkland Islands waters in 2017, 2020, and 2022–2026. a) Overall biomass-at-length frequency distribution. b) Overlap in biomass-at-length distributions between calamari pre-season (red) and groundfish (blue) surveys. c) Overlap in biomass-at-length distributions between females (red) and males (blue). Solid vertical lines indicate the mean length (L_{Mean}), dashed lines the median length (L_{Median}), and dotted lines the 2.5th and 97.5th length percentiles ($L_{2.5}$ and $L_{97.5}$, respectively). p_{perm} is the significance of the weighted permutation test to assess differences between groups.

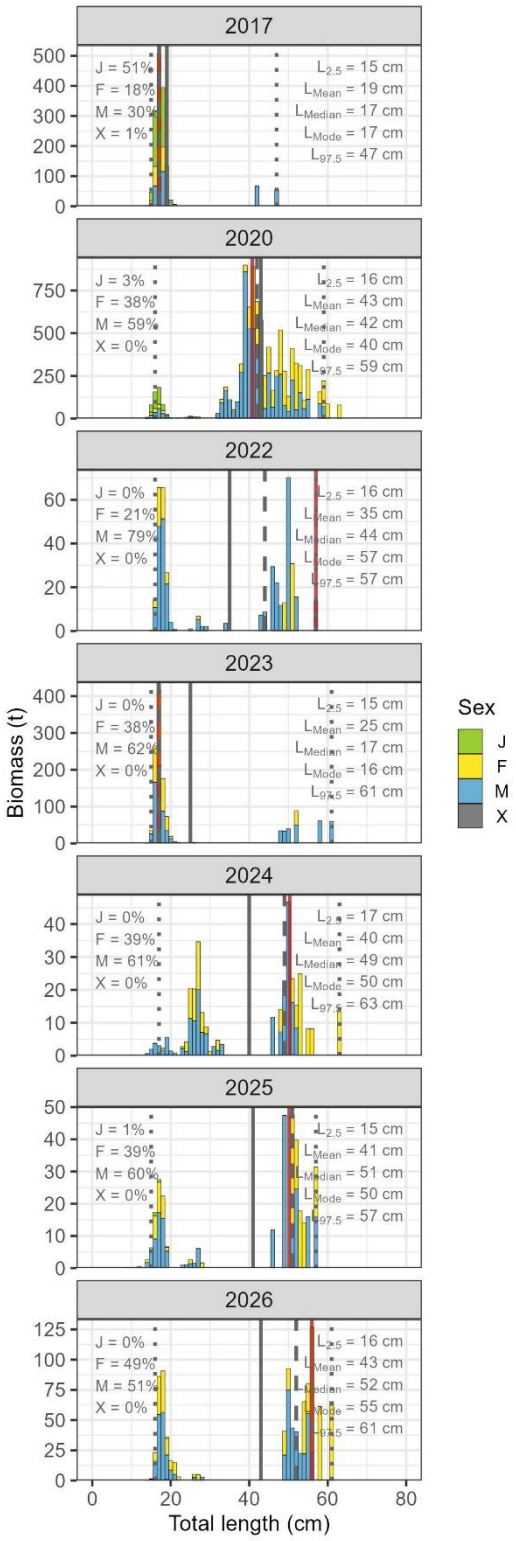

Fig. 79. Annual biomass-at-length class composition of southern blue whiting (*Micromesistius australis*) during July groundfish and calamari pre-season surveys conducted in Falkland Islands waters in 2017, 2020, and 2022–2026. Stacked bars represent biomass (t) per 1.0 cm length class, partitioned by sex (J = juvenile; F = female; M = male; X = undetermined), with the proportion of total annual biomass for each sex indicated in the upper left of each panel. Vertical lines indicate the mean length (L_{Mean}, grey solid), median length (L_{Median}, grey dashed), modal length (L_{Mode}, red solid), and 2.5th and 97.5th percentiles ($L_{2.5}$ and $L_{97.5}$, grey dotted) of the biomass-weighted length distribution. Note the different y-axis scales among years.

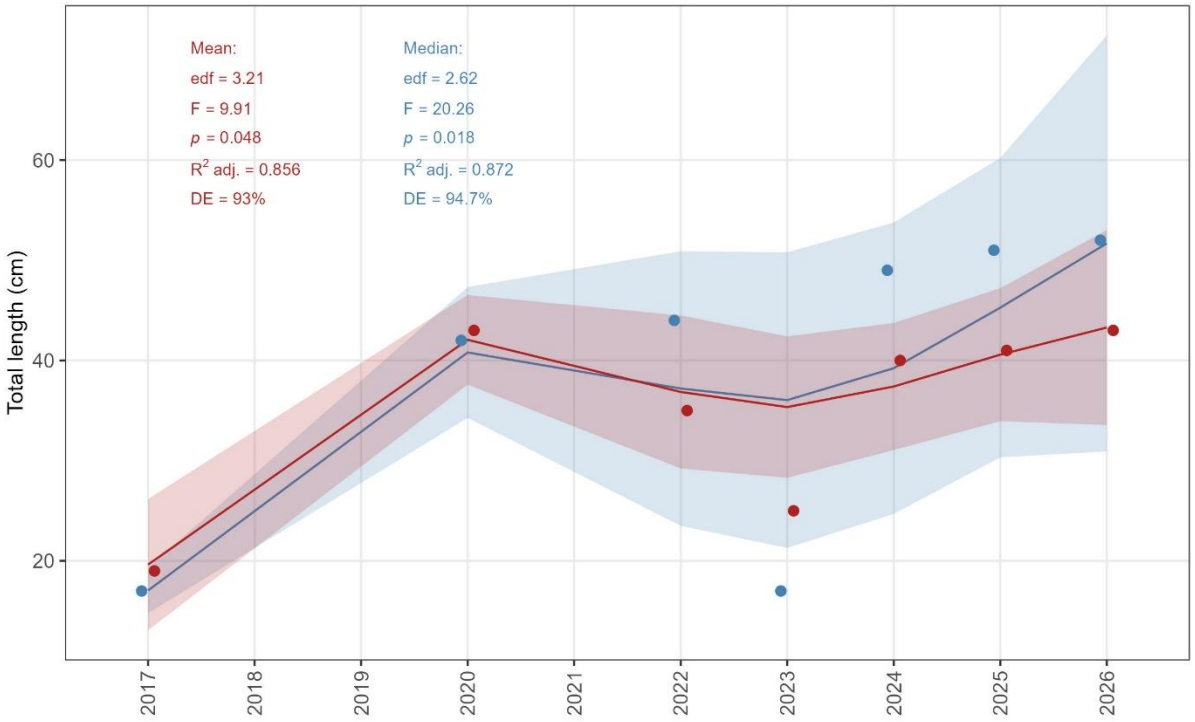

Fig. 80. Median (blue) and mean (red) total length of southern blue whiting (*Micromesistius australis*) during July groundfish and calamari pre-season surveys conducted in Falkland Islands waters in 2017, 2020, and 2022–2026. The line and shaded region represent the fitted Generalised Additive Model (GAM) smooth and its 95% pointwise confidence interval.

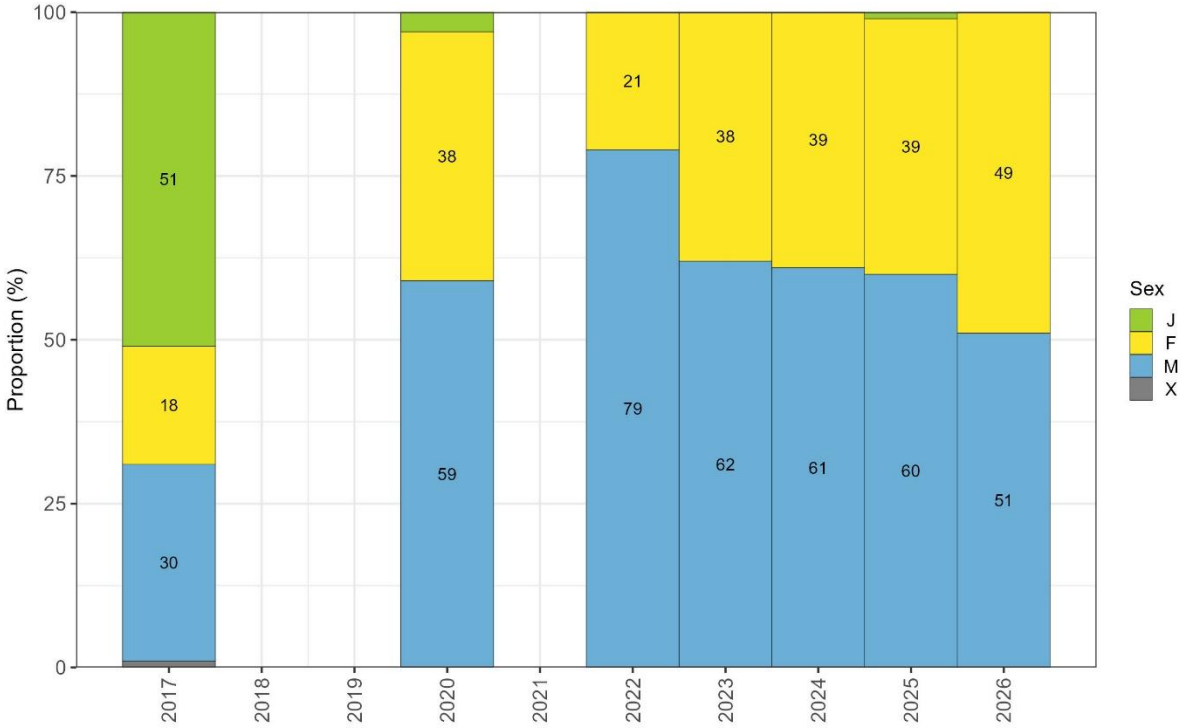

Fig. 81. Proportion by sex (J = juvenile; F = female; M = male; X = undetermined) of southern blue whiting (*Micromesistius australis*) during July groundfish and calamari pre-season surveys conducted in Falkland Islands waters in 2017, 2020, and 2022–2026. Labels for proportions < 3% are omitted.

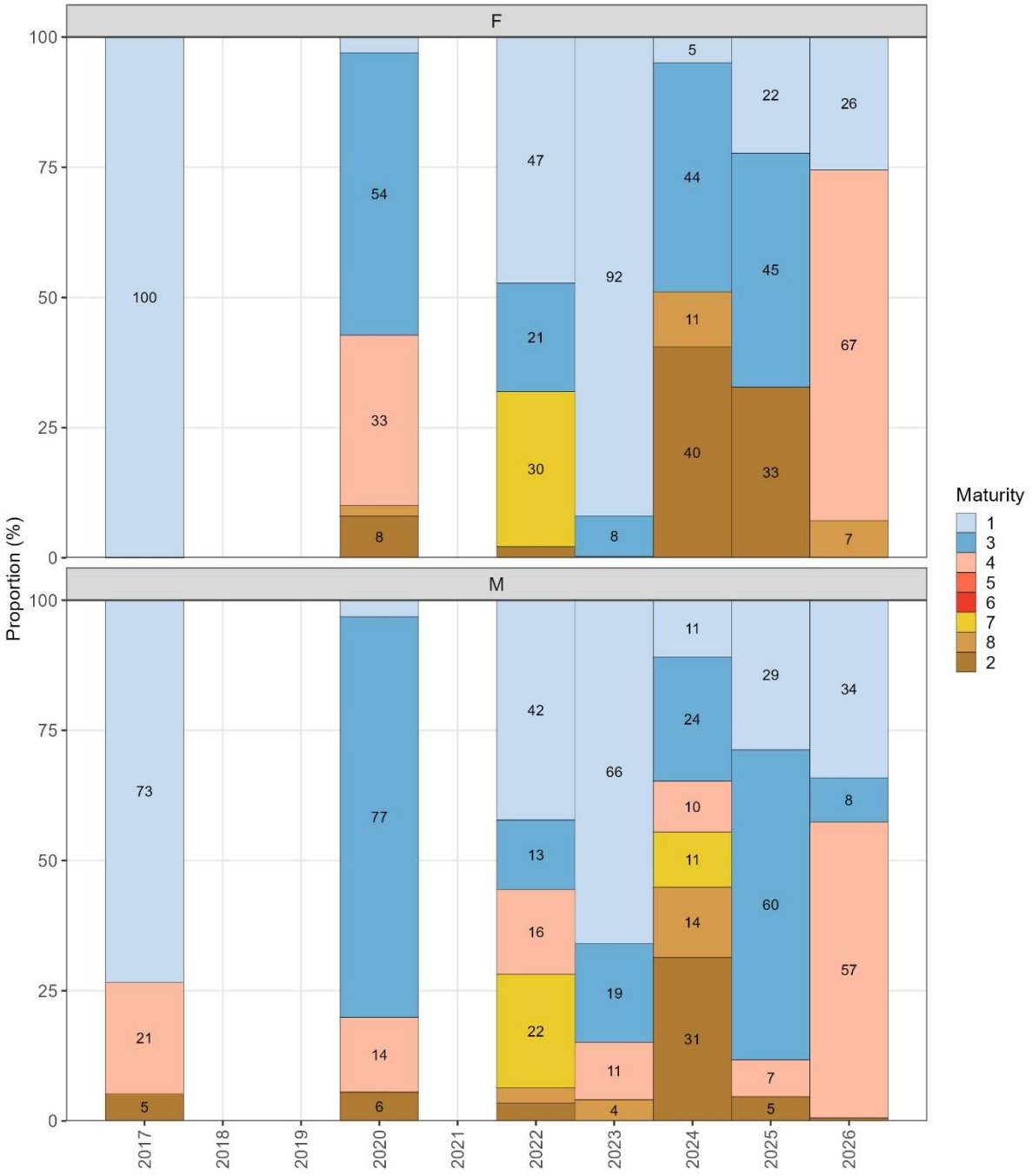

Fig. 82. Proportion by sexual maturity (1, immature; 3, early developing; 4, late developing; 5, ripe; 6, running; 7, spent; 8, recovering spent; 2, resting) of southern blue whiting (*Micromesistius australis*) during July groundfish and calamari pre-season surveys conducted in Falkland Islands waters in 2017, 2020, and 2022–2026. Maturity stages ordered by developmental sequence. Labels for proportions < 3% are omitted.

4.3.11. Southern hake (*Merluccius australis*)

4.3.11.1. Temporal patterns of abundance

Southern hake are caught in low numbers in Falkland Islands waters. On average, 73% of the total southern hake catches in the time series were from groundfish surveys and 27% from calamari pre-season surveys. Catch in 2026 (0.058 t) represented a 5% decrease relative to the 2017 catch (0.061 t), a 70% decrease relative to the 2025 catch (0.191 t; the highest in the time series), and a 36% decrease relative to the 2023–2025 mean catch (0.090 t; Fig. 83a; Appendix II). This species is often misidentified as large common hake (*M. hubbsi*). The extent of the effect of misidentification on catch recording, and on density and biomass calculations is unknown. Ongoing research is focused on enhancing the ability to distinguish southern hake from common hake with greater confidence, based on morphological characteristics (Soeth 2024).

Densities in 2026 (mean ± SE: 1.39 ± 0.59 kg/km²) corresponded to a 19% decrease relative to the 2017 densities (1.70 ± 0.68 kg/km²), a 69% decrease relative to the 2025 densities (4.53 ± 1.72 kg/km²; the highest in the time series), and a 37% decrease relative to the 2023–2025 mean densities (2.21 ± 0.66 kg/km²; Fig. 83b).

Southern hake biomass was highest in 2026 (3,730.83 t; CI = 2,180.52–5,755.89 t), and represented a significant seven-fold increase relative to 2017 levels (511.89 t; CI = 213.85–716.95 t; $p < 0.001$), a significant three-fold increase relative to 2025 (1,146.05 t; CI = 549.18–1,639.73 t; $p = 0.001$), and a significant seven-fold increase relative to the 2023–2025 mean biomass (511.73 t; $p < 0.001$; Fig. 83c; Table IV–V; Appendix III–IV). Analysis of the full time series revealed a significant increasing trend in biomass (GAM: edf = 3.76, F = 25.19, $p = 0.037$), with the model explaining 97.9% of the deviance (R^2 adj. = 0.945), indicating a strong and consistent pattern of increase over the time series (Fig. 83c; Appendix V).

4.3.11.2. Spatial patterns of abundance

In 2026, the highest densities of southern hake (71 kg/km²) were observed at approximately 52.5°S and 61.7°W at depths > 200 m, consistent with previous years. The highest density in the time series was recorded in 2025 (146 kg/km²; Fig. 84).

Densities in 2026 increased relative to 2017 but decreased in the south-west relative to 2025 and the 2023–2025 mean, which was largely driven by the higher densities in 2025 (Fig. 85). The increase in posterior densities noted to the north may be an artifact of the axial loop that resulted in the projection of densities in areas where this species was not caught, and should be interpreted with caution (Fig. 85).

4.3.11.3. Length composition

Southern hake (*M. australis*) is caught in small quantities in Falkland Islands waters and presents identification challenges within bulk catches of the comparatively more abundant common hake (*M. hubbsi*). Consequently, the number of southern hake individuals sampled per survey was insufficient for a robust analysis of size structure, and the results presented here should be interpreted with caution.

Across all survey years combined, total lengths of southern hake were in the range of 36 to 108 cm; however, 95% of the estimated biomass was comprised of individuals between 51 and 108 cm, with median and mean lengths (± SE) of 69 ± 2.01 cm and 71 ± 2.22 cm, respectively (Fig. 86a).

The distribution of biomass proportions by size class exhibited a 44% overlap between the groundfish and calamari pre-season surveys, with no significant differences between the groundfish survey (mean ± SE: 70 ± 2.35 cm) and the calamari pre-season survey (mean ± SE: 73 ± 3.07 cm; $p > 0.05$). In the groundfish survey, 95% of the biomass of southern hake was comprised of individuals between 51 and 108 cm (median ± SE: 69 ± 1.79 cm). In the calamari pre-season survey, 95% of the biomass was comprised of individuals between 54 and 95 cm (median ± SE: 74 ± 4.15 cm; Fig. 86b).

The distribution of biomass proportions by size class exhibited a 57% overlap between females and males, with no significant differences between females (mean ± SE: 71 ± 2.26 cm) and males (mean ± SE: 66 ± 2.85 cm; $p > 0.05$). For females, 95% of the biomass was comprised of individuals between 51 and 108 cm (median ± SE: 70 ± 1.99 cm). For males, 95% of the individuals were between 55 and 78 cm (median ± SE: 65 ± 4.02 cm; Fig. 86c).

Through the time series, the size structure of southern hake was broad and multimodal, with several length-groups not clearly distinguished because of size overlap. More than one length-group was dominant in the time series (Fig. 87). In 2026, lengths were in the range of 50 to 86 cm; however, 95% of the biomass was comprised of individuals between 52 and 86 cm, with median and mean lengths (± SE) of 69 ± 3.43 cm and 71 ± 2.45 cm, respectively. For females, 95% of the biomass was comprised of individuals between 52 and 86 cm, with median and mean lengths (± SE) of 70 ± 4.00 cm and 72 ± 2.64 cm, respectively. For males, 95% of the biomass was comprised of individuals between 56 and 66 cm, with median and mean lengths (± SE) of 64 ± 3.88 cm and 63 ± 2.81 cm, respectively (Fig. 87).

Analysis of the full time series revealed non-significant temporal trends in either mean (GAM: edf = 2.24, $F = 1.90$, $p = 0.296$, R^2 adj. = 0.405, DE = 61.8%) or median (GAM: edf = 1.55, $F = 0.27$, $p = 0.760$, R^2 adj. = -0.017, DE = 23.8%) total length. Fitted smooths for mean and median lengths remained at approximately 65–75 cm, with no directional change throughout the time series. Observed values revealed considerable interannual variability, likely in part due to the limited number of individuals caught or detected (Fig. 88).

4.3.11.4. Sex and maturity composition

The sex composition of southern hake was dominated by females (mean ± SE: 90.6 ± 3.4%), followed by males (9.4 ± 3.4%) throughout the time series. In 2026, sex composition consisted of 91% females and 9% males (Fig. 89).

Maturity composition comprised a mixture of post-spawning and developing individuals in both sexes throughout the time series, with no clear pattern. Females were mostly represented by recovering spent and resting stages (50–100%), except for 2023 when early developing individuals accounted for 81%. For males, post-spawning (spent, recovering spent, and resting) individuals were predominant (51–100%) in 2020, 2022, and 2026. Males in running stage were predominant in 2017 (86%); males in late developing stage were predominant in 2024 (100%), and males in early developing stage were predominant in 2025 (100%; Fig. 90).

4.3.11.5. Discussion

The significant non-linear increase in southern hake biomass in Falkland Islands waters observed in July surveys is consistent with the trend in February surveys in recent years (Ramos 2026). Difficulty distinguishing southern hake from common hake in bulk catches introduces additional uncertainty into these estimates, and results should be interpreted with caution. Falkland Islands fisheries contribute a minor share of the total southern hake catch in the Southwest Atlantic (≤ 12%), with most of the exploitation occurring in Argentine waters (Ramos & Winter 2022e). This suggests that the biomass trends observed in Falkland Islands surveys primarily reflect broader regional population dynamics and the species' availability to the survey area, rather than fishing pressure. Limited data from Falkland Islands fisheries further constrain independent assessment of the status of this stock.

The absence of temporal trends in both mean and median total length, combined with moderate interannual variability in annual length estimates, is consistent between July and February surveys (Ramos 2026), suggesting that the size composition of southern hake accessible to the surveys has remained relatively stable despite the fluctuating biomass.

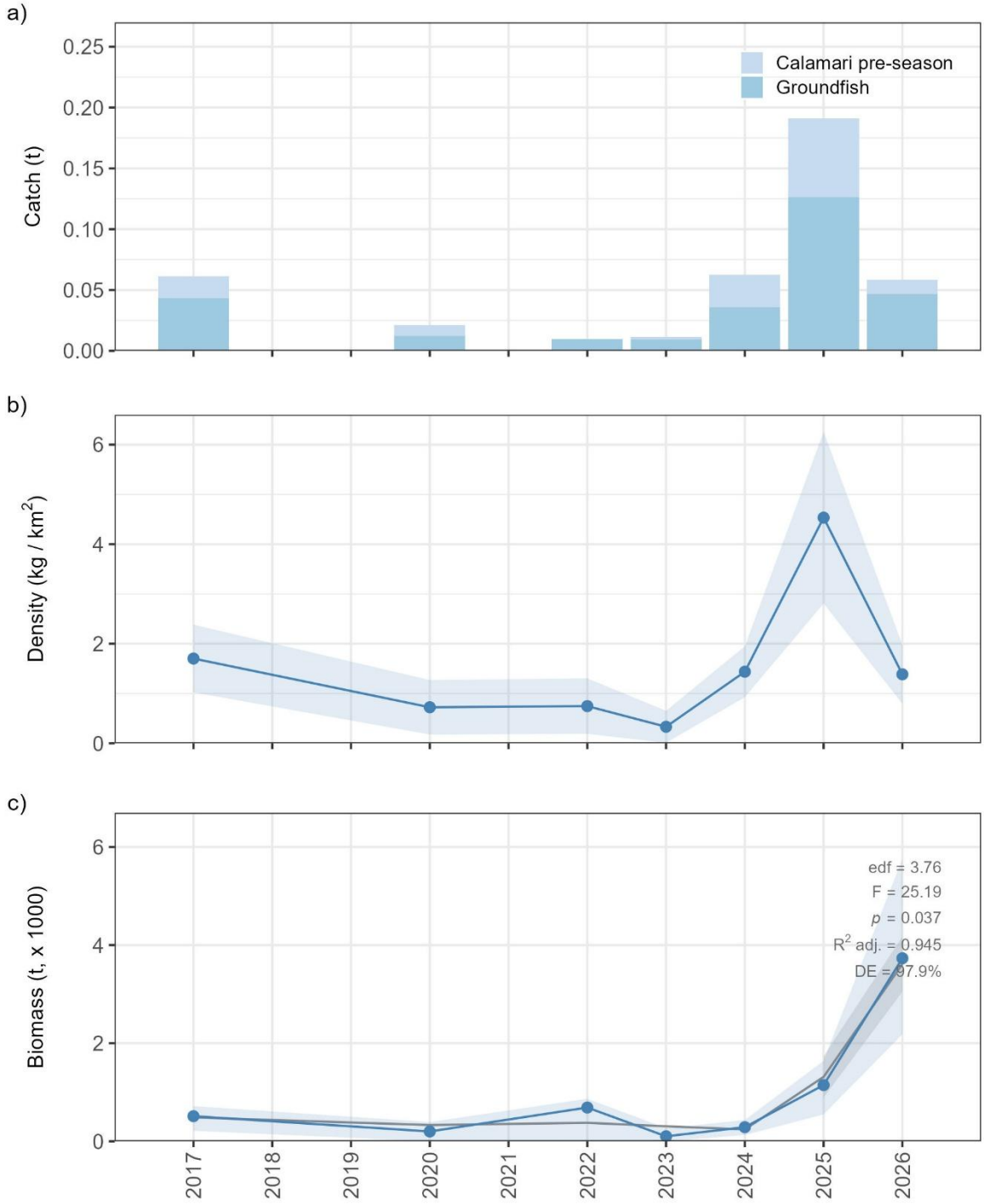

Fig. 83. Abundance of southern hake (*Merluccius australis*) during July groundfish and calamari pre-season surveys conducted in Falkland Islands waters in 2017, 2020, and 2022–2026. (a) Catch per survey, (b) annual mean density ± SE represented by the blue line and shaded region, respectively, and (c) estimated biomass, where the blue line and shaded region represent the median and 95% pointwise confidence interval derived from 10,000 bootstrap biomass estimates, and the grey line and shaded region represent the fitted Generalised Additive Model (GAM) smooth and its 95% pointwise confidence interval.

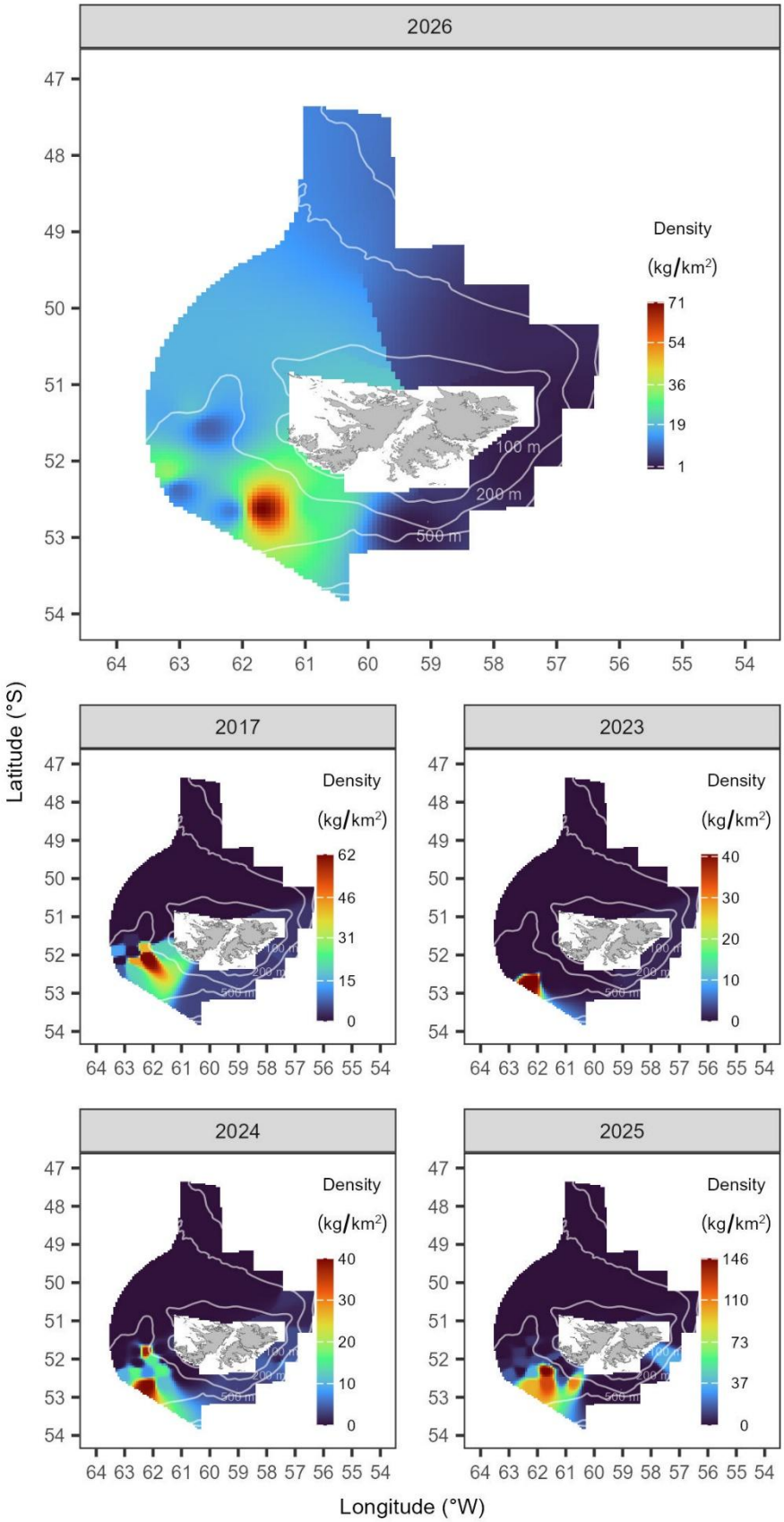

Fig. 84. Distribution and abundance of southern hake (*Merluccius australis*) derived from the July 2026 groundfish and calamari pre-season surveys in Falkland Islands waters, compared with the first year of the time series (2017) and the three preceding years (2023–2025). Colour scales are specific to each year. Isobaths at 100 m, 200 m, and 500 m are shown.

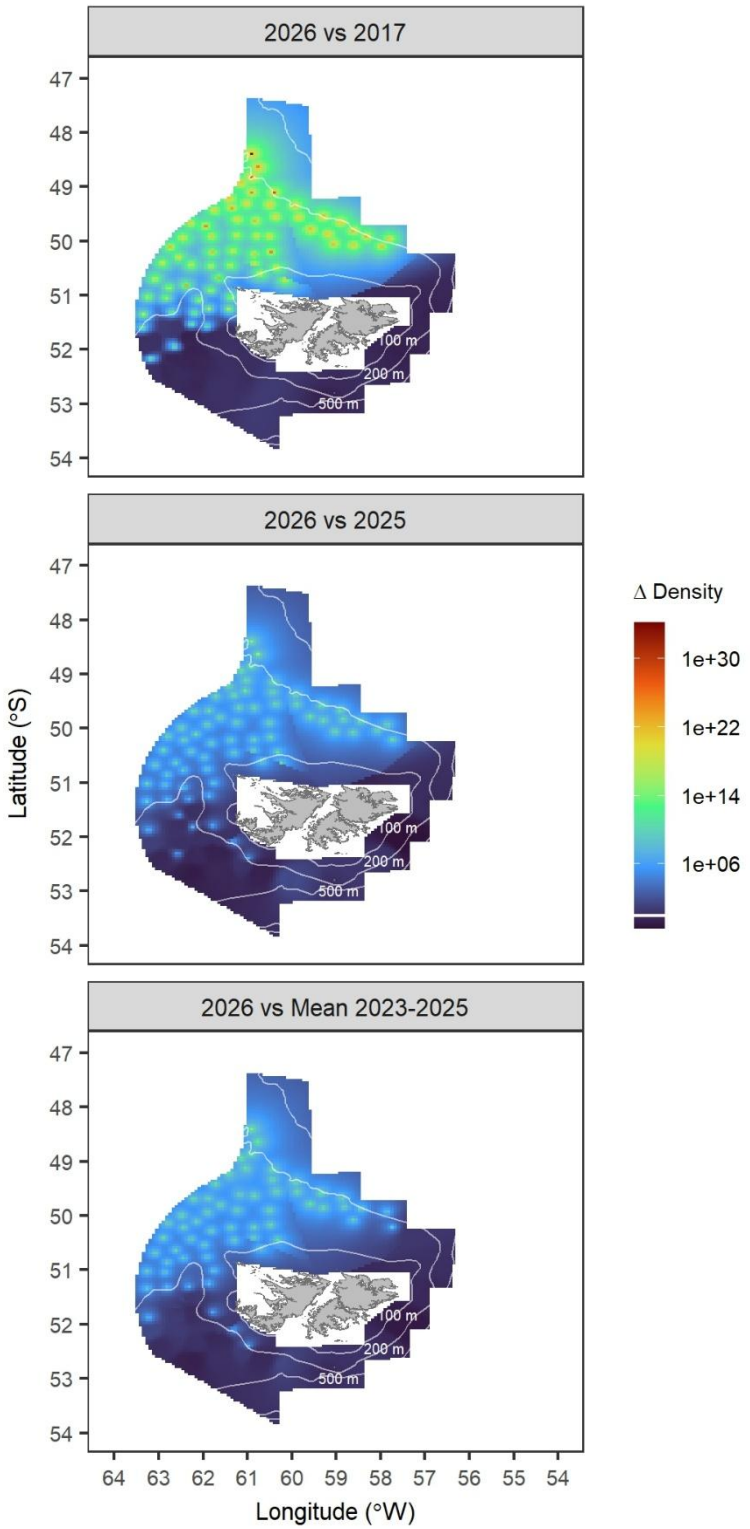

Fig. 85. Spatial change in density of southern hake (*Merluccius australis*) derived from the July 2026 groundfish and calamari pre-season surveys in Falkland Islands waters, relative to the first year of the time series (2017), the previous year (2025), and the mean of the three preceding years (2023–2025). The spatial change in density is expressed as the ratio of density (kg/km^2) in 2026 relative to the density in the baseline year (2017, 2025, 2023–2025 mean). Isobaths at 100 m, 200 m, and 500 m are shown. The colour scale is $\log_{10}$-transformed to aid visualisation, with increases in density indicated above the horizontal white line towards dark red, and decreases in density indicated below the horizontal white line towards dark blue.

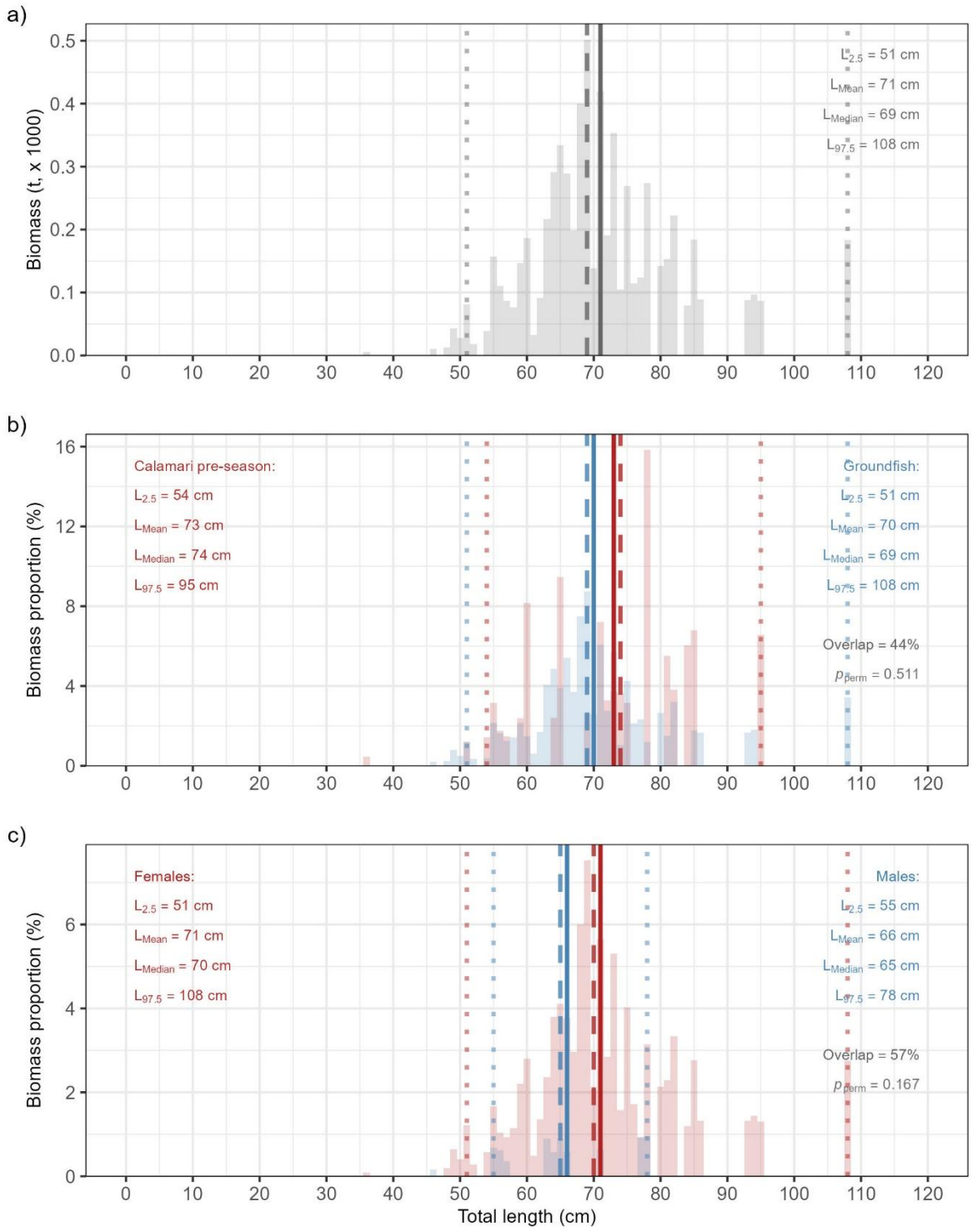

Fig. 86. Biomass-at-length class composition of southern hake (*Merluccius australis*) across all years combined, based on July groundfish and calamari pre-season surveys conducted in Falkland Islands waters in 2017, 2020, and 2022–2026. a) Overall biomass-at-length frequency distribution. b) Overlap in biomass-at-length distributions between calamari pre-season (red) and groundfish (blue) surveys. c) Overlap in biomass-at-length distributions between females (red) and males (blue). Solid vertical lines indicate the mean length (L_{Mean}), dashed lines the median length (L_{Median}), and dotted lines the 2.5th and 97.5th length percentiles ($L_{2.5}$ and $L_{97.5}$, respectively). p_{perm} is the significance of the weighted permutation test to assess differences between groups.

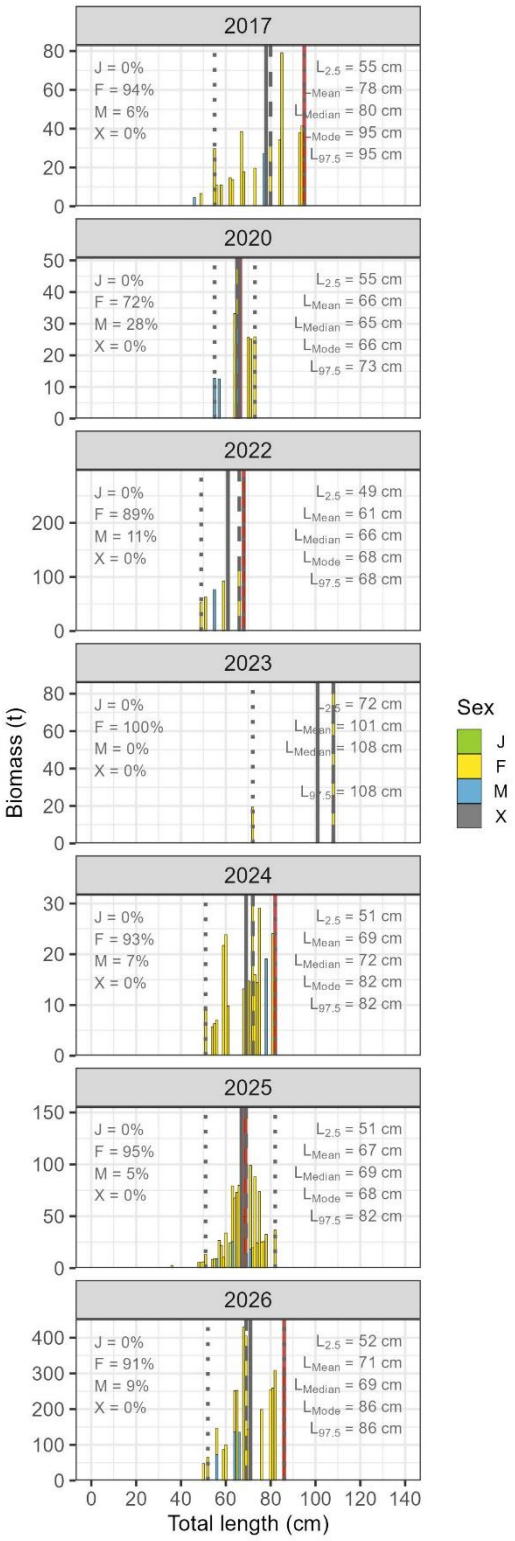

Fig. 87. Annual biomass-at-length class composition of southern hake (*Merluccius australis*) during July groundfish and calamari pre-season surveys conducted in Falkland Islands waters in 2017, 2020, and 2022–2026. Stacked bars represent biomass (t) per 1.0 cm length class, partitioned by sex (J = juvenile; F = female; M = male; X = undetermined), with the proportion of total annual biomass for each sex indicated in the upper left of each panel. Vertical lines indicate the mean length (L_{Mean}, grey solid), median length (L_{Median}, grey dashed), modal length (L_{Mode}, red solid), and 2.5th and 97.5th percentiles ($L_{2.5}$ and $L_{97.5}$, grey dotted) of the biomass-weighted length distribution. Note the different y-axis scales among years.

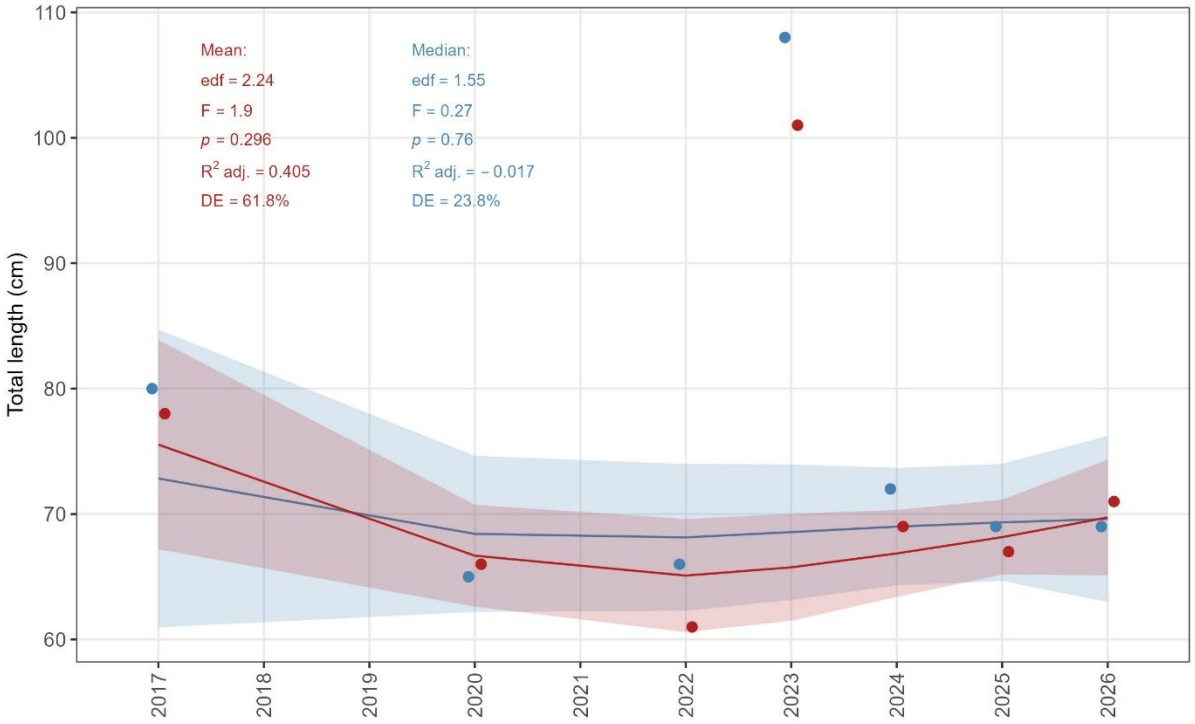

Fig. 88. Median (blue) and mean (red) total length of southern hake (*Merluccius australis*) during July groundfish and calamari pre-season surveys conducted in Falkland Islands waters in 2017, 2020, and 2022–2026. The line and shaded region represent the fitted Generalised Additive Model (GAM) smooth and its 95% pointwise confidence interval.

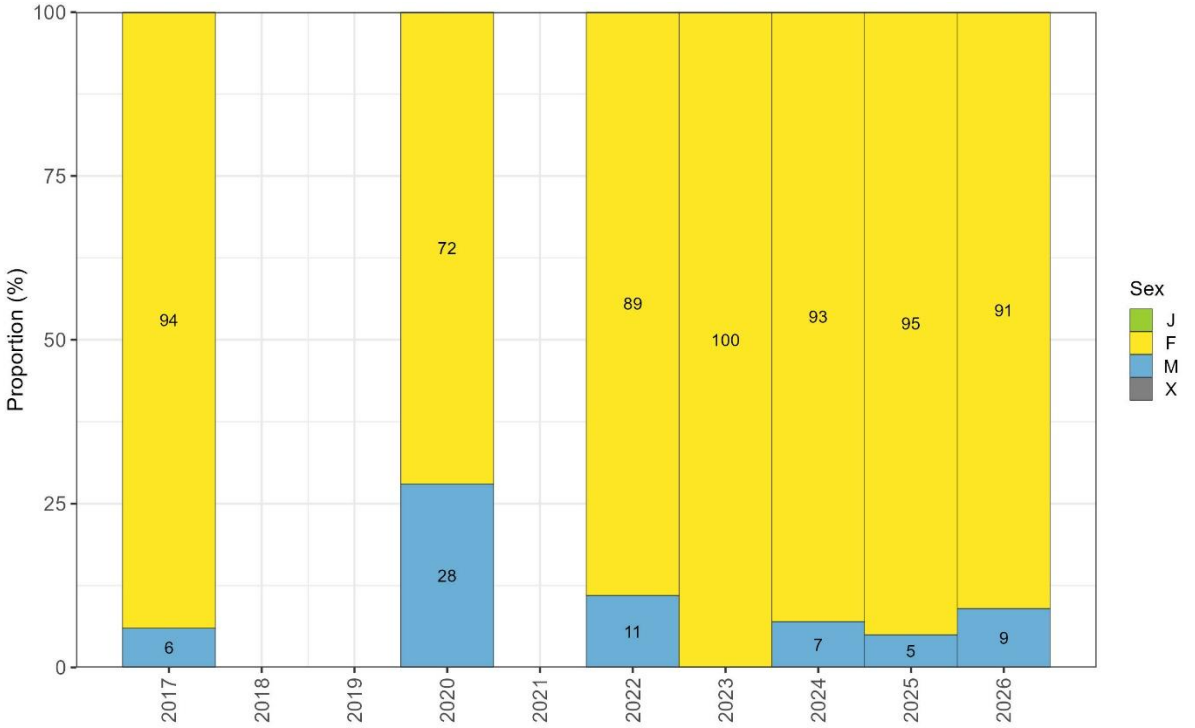

Fig. 89. Proportion by sex (J = juvenile; F = female; M = male; X = undetermined) of southern hake (*Merluccius australis*) during July groundfish and calamari pre-season surveys conducted in Falkland Islands waters in 2017, 2020, and 2022–2026. Labels for proportions < 3% are omitted.

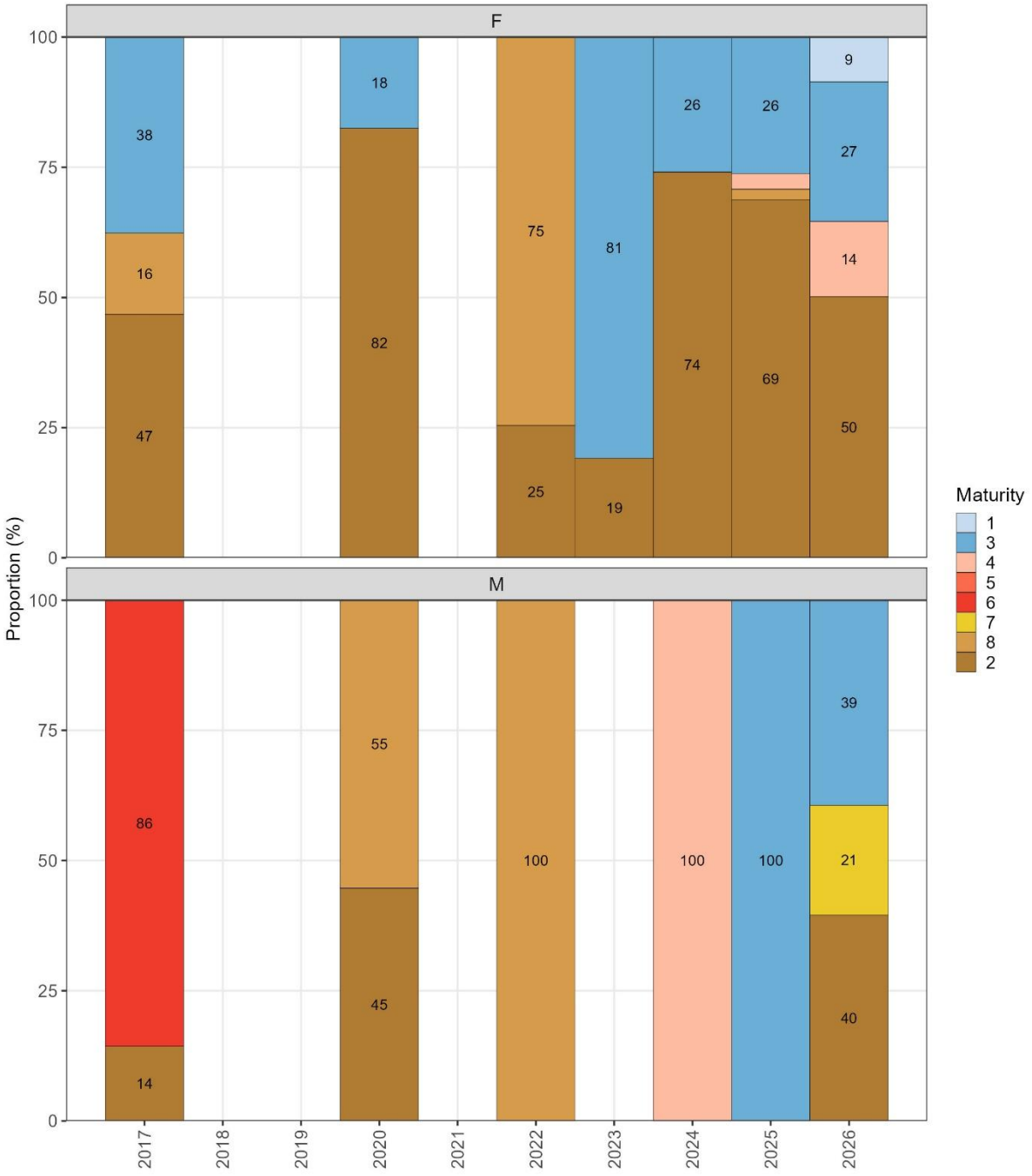

Fig. 90. Proportion by sexual maturity (1, immature; 3, early developing; 4, late developing; 5, ripe; 6, running; 7, spent; 8, recovering spent; 2, resting) of southern hake (*Merluccius australis*) during July groundfish and calamari pre-season surveys conducted in Falkland Islands waters in 2017, 2020, and 2022–2026. Maturity stages ordered by developmental sequence. Labels for proportions < 3% are omitted.

5. Conclusions

1. Argentine shortfin squid biomass increased significantly, while length showed no significant change throughout the time series. Females comprised the higher proportion of biomass, mainly at young or immature stages.

2. Banded whiptail grenadier showed no significant change in biomass nor length throughout the time series. Females comprised most of the biomass, mainly at post-spawning maturity stages. Information on this species in Falkland Islands waters is limited.
3. Common hake biomass showed a significant increasing trend, with densities increasing predominantly in the west of the FICZ and to the south, including within the 'Loligo Box'. Females contributed most of the biomass, mainly at post-spawning maturity stages, while length declined throughout the time series.
4. Hoki biomass showed a significant declining trend. Females contributed a higher proportion of biomass than males, mainly at resting maturity stage. Length showed a non-significant increasing trend.
5. Kingclip biomass remains at low levels with no clear trend. Females, mainly at resting maturity stage, contributed most of the biomass. Length increased significantly over the time series; the presence of large individuals in recent years suggests potential for recovery if size-selective management measures are implemented in the commercial bottom trawl fishery.
6. Patagonian squid biomass declined significantly, together with a declining trend in length, a lower proportion of females in July 2026, and a shift from preparatory to immature individuals since 2020, suggesting a shift towards smaller, less mature individuals in the spring-spawning cohort.
7. Patagonian toothfish biomass peaked in 2026, representing a significant increase, in part driven by growth in body size of the 2022–2023 recruit cohorts. Biomass was dominated by females, all at immature stage. It must be noted that bottom trawl demersal surveys are not representative of the adult component of the stock, which is caught by longlines.
8. Red cod biomass declined significantly in recent years. Most biomass was comprised of females at resting maturity, together with an increase in size. Persistent low biomass and historical declines beyond the FICZ may indicate region-wide vulnerability.
9. Rock cod biomass remains at low levels, although with signs of stabilisation and minor increase in recent years. Females contributed a slightly higher proportion of biomass than males, with no significant change in length, and in a variety of maturity stages. Currently, this species is of little commercial interest due to its small size, as evidenced by extremely high discard rates in commercial bottom trawl fisheries since 2016. Incidental capture of predominantly small and immature rock cod with low post-release survival, represents a source of fishing mortality that is poorly quantified due to inaccurate discard reporting. This unaccounted mortality, combined with the removal of individuals that have not yet reproduced, limits the capacity of stock assessments to reflect the true state of the stock and may consequently compromise the resource’s sustainability.
10. Southern blue whiting showed no temporal biomass trend, and biomass remains at low levels. Biomass consisted of a higher proportion of males than females, both mostly at immature and early developing stages. Length increased throughout the time series.

11. Southern hake biomass increased significantly in recent years, with females predominating, mostly at recovering spent or resting maturity, and no temporal trend in length. These results should be interpreted with caution, as estimates carry additional uncertainty arising from the difficulty of distinguishing this species from common hake (*M. hubbsi*) in bulk catches. Falkland Islands fisheries account for ≤ 12% of total southern hake catch across the Southwest Atlantic, and the limited local data further constrain comprehensive assessment of the status of this stock.

6. Recommendations

1. Long-term continuity of the February and July parallel demersal surveys should be maintained to ensure comparability between seasons and years, and a consistent station array across years is essential for robust trend detection. Additional surveys should be arranged without compromising these core surveys, which are often the only source of abundance indices for several finfish species, most of which are taken as bycatch in the commercial fishery. For example, TAC for common hake, red cod and rock cod are currently set under the ICES Category 3 framework using biomass estimates from the parallel demersal surveys; any discontinuity in the parallel demersal surveys could therefore affect TAC calculations for these species.
2. Station, catch, and biological data should continue to be recorded and quality-checked to the highest standard, with recording and correction protocols formally defined at a scientific meeting. Net geometry parameters, particularly horizontal net opening, directly influence density and biomass estimates and should be recorded using net sensors to maximise accuracy. Net sensors have been used in groundfish surveys since 2016 (Gras et al. 2016), except for July 2026 when these were tested in the calamari pre-season survey. An additional set of sensors will be purchased for the calamari pre-season surveys, aiming to be implemented from February 2027, to ensure consistent sensor-based records across both survey programmes.
3. The spatial coverage of the groundfish survey should be reassessed. Initial discussions and a follow-up plan are underway to evaluate and improve survey coverage, aiming to improve the reliability of biomass estimates for species likely under-represented in the current survey area.
4. Given the current high abundance of common hake and its potential ecosystem impacts, research into the species' population structure, dynamics and trophic ecology should continue, and would benefit from regional collaboration.
5. A precautionary approach should be maintained for the Patagonian squid spring-spawning cohort throughout both fishing seasons, given the declining biomass and low abundance that prompted cancellation or early closure of the second fishing season in recent years. The first fishing season, targeting mainly the autumn-spawning cohort, has remained relatively stable, although a portion of the spring-spawning cohort is suspected to be taken towards the end; however, this is currently not well understood and is under investigation. Adaptive management options are being discussed to help sustain a higher abundance of the spring-spawning cohort during the second fishing season, when it is primarily exploited. Improved understanding of environmental drivers would also strengthen predictions of recruitment variability.

6. Conservation measures should be implemented for finfish stocks in poor condition such as hoki, kingclip, Patagonian squid, red cod, rock cod, and southern blue whiting. Options that may help reducing fishing pressure include adjusting daily by-catch limits, reducing juvenile catch rates, spatial and temporal closures of high-catch grid squares including spawning ground protection, increasing observer coverage, improving catch reporting, or modifying fishing gear.
7. Biomass calculations should be included in stock assessments wherever commercial catch, effort, and biological data are available and appropriate. Their absence for several species since 2019 limits comparability with fisheries-independent trends and understanding of current stock status.
8. Change of biomass estimation approach. The inverse distance weighting method currently used for biomass estimation was originally implemented at FIFD for rock cod (Winter 2019), a species with a wide spatial distribution in the FICZ. This method appears adequate for species distributed widely across the survey area. However, it has limitations for species with restricted habitat preferences, as it may attribute biomass to areas where the species does not occur. It is intended to discontinue this approach in favour of sdmTMB (Anderson et al. 2025), a widely used method that allows oceanographic and topographic variables to be incorporated into the model. Models should be tailored to each species, incorporating depth and environmental effects, to improve estimate accuracy and understanding of the drivers of seasonal and inter-annual biomass fluctuations. Where a species is assessed by different groups for different purposes, the same estimation approach and assumptions should ideally be applied to ensure comparability across assessments conducted at FIFD.

7. References

Agnew DJ (2002) Critical aspects of the Falkland Islands pelagic ecosystem: distribution, spawning and migration of pelagic animals in relation to oil exploration. Aquatic Conservation 12: 39–50.

Akaike H (1974) A new look at the statistical model identification. IEEE Transactions on Automatic Control 19: 716–723. https://doi.org/10.1109/TAC.1974.1100705

Alglave, B, Rivot E, Etienne MP, Woillez M, Thorson JT, Vermard Y (2022) Combining scientific survey and commercial catch data to map fish distribution. ICES Journal of Marine Science 79: 1133–1149. https://doi.org/10.1093/icesjms/fsac032

Anderson SC, Ward EJ, English PA, Barnett LAK, Thorson JT (2025) sdmTMB: An R Package for Fast, Flexible, and User-Friendly Generalized Linear Mixed Effects Models with Spatial and Spatiotemporal Random Fields. Journal of Statistical Software 115: 1–46. https://doi.org/10.18637/jss.v115.i02

Arkhipkin AI, Schuchert PC, Danyushevsky L (2009) Otolith chemistry reveals fine population structure and close affinity to the Pacific and Atlantic oceanic spawning grounds in the migratory southern blue whiting (*Micromesistius australis australis*). Fisheries Research 96: 188–194. doi: 10.1016/j.fishres.2008.11.002

Arkhipkin AI, Laptikhovsky VV (2010) Convergence in life-history traits in migratory deep-water squid and fish. ICES Journal of Marine Science 67: 1444–1451.

Arkhipkin A, Brickle P, Laptikhovsky V, Winter A (2012) Dining hall at sea: feeding migrations of nektonic predators to the eastern Patagonian Shelf. Journal of Fish Biology 81: 882–902. https://doi.org/10.1111/j.1095-8649.2012.03359.x

Arkhipkin AI, Laptikhovsky VV, Barton AJ (2015) Biology and fishery of common hake (*Merluccius hubbsi*) and southern hake (*Merluccius australis*) around the Falkland/Malvinas Islands on the Patagonian shelf of the Southwest Atlantic Ocean. In H. Arancibia (Ed.), Hakes, Biology and Exploitation (pp. 154–184). Oxford: Wiley.

Arkhipkin AI, Winter AG, Nigmatullin CM (2022a) Heavy fishery exploitation does not affect sizes at recruitment and maturity of squid *Illex argentinus* and *Doryteuthis gahi*, in the Southwest Atlantic. ICES Journal of Marine Science 79: 182–192. https://doi.org/10.1093/icesjms/fsab253

Arkhipkin A, Evans D, Raczynski M, Winter A (2022b) Southern blue whiting and red cod spawning survey. Cruise Report ZDLV-09-2022. Fisheries Department, Directorate of Natural Resources, Falkland Islands Government, Stanley, Falkland Islands. 28 p.

Bianchi A, Massonneau M, Olevera RM (1982) Análisis estadístico de las características T–S del sector austral de la Plataforma Continental Argentina. Acta Oceanológica Argentina 3: 93–118. *In:* Arkhipkin A, Brickle P, Laptikhovsky V, Winter A (2012) Dining hall at sea: feeding migrations of nektonic predators to the eastern Patagonian Shelf. Journal of Fish Biology 81: 882–902. https://doi.org/10.1111/j.1095-8649.2012.03359.x

Boltovskoy D (Ed.) (1999) South Atlantic Zooplankton. *In:* Arkhipkin A, Brickle P, Laptikhovsky V, Winter A (2012) Dining hall at sea: feeding migrations of nektonic predators to the eastern Patagonian Shelf. Journal of Fish Biology 81: 882–902. https://doi.org/10.1111/j.1095-8649.2012.03359.x

Brickle P, Laptikhovsky V, Arkhipkin A (2005) Reproductive strategy of a primitive temperate notothenioid *Eleginops maclovinus*. Journal of Fish Biology 66: 1044–1059. https://doi.org/10.1111/j.1095-8649.2005.00663.x

Brickle P, Laptikhovsky V, Arkhipkin A, Portela J (2006) Reproductive biology of *Patagonotothen ramsayi* (Regan, 1913) (Pisces: Nototheniidae) around the Falkland Islands. Polar Biology 29: 570–580. https://doi.org/10.1007/s00300-005-0090-5

Chemshirova I, Hoyer P, Nicholls R, Winter A (2023) 2023 2nd Pre-Season Assessment Survey, Falkland calamari (*Doryteuthis gahi)*. ZDLC4-S2-2023. Fisheries Department, Directorate of Natural Resources, Falkland Islands Government, Stanley, Falkland Islands. 20 p.

Chemshirova I, Hoyer P, Amukwaya A, Shcherbich Z (2024) 2024 2nd Pre-Season Assessment Survey, Falkland calamari (*Doryteuthis gahi)*. ZDLZ1-S2-2024. Fisheries Department, Directorate of Natural Resources, Falkland Islands Government, Stanley, Falkland Islands. 19 p.

Chemshirova I, et al. (*in prep.*) 2026 2nd Pre-Season Assessment Survey, Falkland calamari (*Doryteuthis gahi)*. ZDLR1-S2-2026. Fisheries Department, Directorate of Natural Resources, Falkland Islands Government, Stanley, Falkland Islands.

Di Marco E (2022) Evaluación del efectivo de abadejo (*Genypterus blacodes*) en el Atlántico Sudoccidental (período 1980–2021). Captura biológicamente aceptable para el año 2022 y provisoria para el año 2023. Inf. Tec. Oficial INIDEP Nº 035/22. 39 p.

Efron B, Tibshirani RJ (1993) *An Introduction to the Bootstrap*. Chapman & Hall, New York.

Falkland Islands Government (1989) Fisheries Report 1987–88, FIG Stanley, Fisheries Department. 45 p.

Falkland Islands Government (2025) Fisheries Department Fisheries Statistics, Vol. 29 (2015–2024), FIG Stanley, Fisheries Department. 84 p.

Falkland Islands Government (2026) Fisheries Department Fisheries Statistics, Vol. 30 (2016–2025), FIG Stanley, Fisheries Department. 85 p.

Froese R (2006) Cube law, condition factor and weight–length relationships: history, meta-analysis and recommendations. Journal of Applied Ichthyology 22, 241–253. https://doi.org/10.1111/j.1439-0426.2006.00805.x

Gallo ND, Bowlin NM, Thompson AR, Satterthwaite EV, Brady B, Semmens BX (2022) Fisheries surveys are essential ocean observing programs in a time of global change: A synthesis of oceanographic and ecological data from U.S. west coast fisheries surveys. Frontiers in Marine Science 9: 1–18. https://doi.org/10.3389/fmars.2022.757124

García D (2024) Stock assessment of kingclip (*Genypterus blacodes*) in the Falkland Islands using JABBA. SA–2024–KIN. Fisheries Department, Directorate of Natural Resources, Falkland Islands Government. Stanley, Falkland Islands. 69 p.

García D (2025) Stock Assessment of kingclip (*Genypterus blacodes*) in the Falkland Islands using length-based methods and yield per recruit approach. SA–2025–KIN. Fisheries Department, Directorate of Natural Resources, Falkland Islands Government. Stanley, Falkland Islands. 45 p.

Guillen J, Holmes SJ, Carvalho N, Casey J, Dorner H, Gibin M, Mannini A, Vasilakopoulos P, Zanzi A (2018) A Review of the European Union Landing Obligation Focusing on Its Implications for Fisheries and the Environment. Sustainability 10: 900. https://doi.org/10.3390/su10040900

Gras M, Pompert J, Blake A, Boag T, Grimmer A, Iriarte V, Sánchez B (2016) Finfish and Rock cod Biomass Survey. Report number ZDLT1-02-2016. Fisheries Department, Directorate of Natural Resources, Falkland Islands Government, Stanley, Falkland Islands. 72 p.

Gras M, Pompert J, Blake A, Busbridge T, Boag T, Huillier JT, Concha F (2017) Report of the 2017 ground fish survey ZDLT1–07–2017. Fisheries Department, Directorate of Natural Resources, Falkland Islands Government. Stanley, Falkland Islands. 68 p.

Harrell FE (2024) *Hmisc: Harrell Miscellaneous*. R package version 5.2.4.

Hilborn R, Walters CJ (1992) Quantitative fisheries stock assessment: Choice, dynamics and uncertainty. New York, USA: Chapman & Hall.

Holm S (1979) A simple sequentially rejective multiple test procedure. Scandinavian Journal of Statistics 6: 65–70.

Kish L (1965) *Survey Sampling*. John Wiley & Sons, New York.

Komsta L & Novomestky F (2022) moments: Moments, Cumulants, Skewness, Kurtosis and Related Tests. R package version 0.14.1. https://CRAN.R-project.org/package=moments

Laptikhovsky VV, Arkhipkin AI, Brickle P (2008) Life history, fishery and stock conservation of the Patagonian toothfish around the Falkland Islands. American Fisheries Society

Symposium 49: 1357–1363. *In:* Arkhipkin A, Brickle P, Laptikhovsky V, Winter A (2012) Dining hall at sea: feeding migrations of nektonic predators to the eastern Patagonian Shelf. Journal of Fish Biology 81: 882–902. https://doi.org/10.1111/j.1095-8649.2012.03359.x

Laptikhovsky V, Arkhipkin A, Brickle P (2013) From small bycatch to main commercial species: Explosion of stocks of rock cod *Patagonotothen ramsayi* (Regan) in the Southwest Atlantic. Fisheries Research 147: 399–403. http://dx.doi.org/10.1016/j.fishres.2013.05.006

Le Cren ED (1951) The length-weight relationship and seasonal cycle in gonad weight and condition in the perch (*Perca fluviatilis*). Journal of Animal Ecology 20: 201–219.

Lee B, Trevizan T, Evans D, Sadd D, Kairua T, Nicholls R, Raczynski M (2022) Cruise Report ZDLT1-07-2022. Demersal Hake Survey. Fisheries Department, Directorate of Natural Resources, Falkland Islands Government. Stanley, Falkland Islands. 50 p.

Lipinski M (1979) Universal maturity scale for the commercially-important squids (Cephalopoda: teuthoidea). The results of maturity classification of the *Illex illecebrosus* (LeSueur. 1821) populations for the years 1973–1977. ICNAF Fish. Res. Doc. 79/. II/38.

Macchi GJ, Pájaro M, Wöhler OC, Acevedo MJ, Centurión RL, Urteaga DG (2005) Batch fecundity and spawning frequency of southern blue whiting (*Micromesistius australis*) in the southwest Atlantic Ocean. New Zealand Journal of Marine and Freshwater Research 39: 993–1000. https://doi.org/10.1080/00288330.2005.9517370

Macchi GJ, Martos P, Reta R, Dato C (2010) Offshore spawning of the Argentine hake (*Merluccius hubbsi*) Patagonian stock. Pan-American Journal of Aquatic Sciences 5: 22-35

Macchi GJ, Domínguez-Petit R, Militelli MI (2021) Dinámica reproductiva en el dominio demersal. Ecología Reproductiva y Pesquerías en el Contexto Iberoamericano. Red Iberoamericana de Investigación para el Uso Sostenible de los Recursos Pesqueros (RED INVIPESCA). 31 Diciembre de 2021. 61–94.

Manly BFJ (2007) *Randomization, Bootstrap and Monte Carlo Methods in Biology* (3rd ed.). Chapman & Hall/CRC.

MEP (2020) Annex 3: Review of Finfish Stock Assessments. Report for Falkland Islands Government. MacAlister Elliot & Partners Ltd. 47 p.

Navarro G, Rozycki V, Monsalvo M (2014) Estadísticas de la pesca marina en la Argentina. Evolución de los desembarques 2008-2013. Ministerio de Agricultura, Ganadería y Pesca de la Nación. Buenos Aires, 144 p.

Nikolsky GV (1963) The Ecology of Fishes. New York: Academic Press.

Pájaro M, Macchi GJ (2001) Spawning pattern, length at maturity, and fecundity of the southern blue whiting (*Micromesistius australis*) in the south-west Atlantic Ocean. New Zealand Journal of Marine and Freshwater Research 35: 375–385. https://doi.org/10.1080/00288330.2001.9517008

Padgham M, Sumner M (2025) geodist: Fast, Dependency-Free Geodesic Distance Calculations. https://doi.org/10.32614/CRAN.package.geodist

Payá I, Brickle P, Laptikhovsky V, Winter A (2010) Vessel Units, Allowable Effort, and Allowable Catch 2011. Fisheries Department, Directorate of Natural Resources, Falkland Islands Government, Stanley, Falkland Islands. 53 p.

Pedersen TL (2024) patchwork: The Composer of Plots. R package version 1.3.0. https://CRAN.R-project.org/package=patchwork

Peterson RG, Whitworth III T (1989) The Subantarctic and Polar fronts in relation to deep water masses through the Southwestern Atlantic. Journal of Geophysical Research 94: 10817–10838. *In:* Arkhipkin A, Brickle P, Laptikhovsky V, Winter A (2012) Dining hall at sea: feeding migrations of nektonic predators to the eastern Patagonian Shelf. Journal of Fish Biology 81: 882–902. https://doi.org/10.1111/j.1095-8649.2012.03359.x

R Core Team (2025). R: A Language and Environment for Statistical Computing. R Foundation for Statistical Computing, Vienna, Austria. https://www.R-project.org/.

Ramos JE, Winter A (2019) Stock assessment of hoki (*Macruronus magellanicus*) in the Falkland Islands. SA–2019–WHI. Fisheries Department, Directorate of Natural Resources, Falkland Islands Government. Stanley, Falkland Islands. 47 p.

Ramos JE, Winter A (2022a) Stock assessment of common hake (*Merluccius hubbsi*) in the Falkland Islands. SA–2022–HAK. Fisheries Department, Directorate of Natural Resources, Falkland Islands Government, Stanley, Falkland Islands. 36 p.

Ramos JE, Winter A (2022b) February bottom trawl survey biomasses of fishery species in Falkland Islands waters, 2010–2022. SA–2022–05. Fisheries Department, Directorate of Natural Resources, Falkland Islands Government, Stanley, Falkland Islands. 86 p.

Ramos JE, Winter A (2022c) Stock assessment of hoki (*Macruronus magellanicus*) in the Falkland Islands. SA–2022–WHI. Fisheries Department, Directorate of Natural Resources, Falkland Islands Government, Stanley, Falkland Islands. 39 p.

Ramos JE, Winter A (2022d) Stock assessment of red cod (*Salilota australis*) in the Falkland Islands. SA–2022–BAC. Fisheries Department, Directorate of Natural Resources, Falkland Islands Government, Stanley, Falkland Islands. 39 p.

Ramos JE, Winter A (2022e) Stock assessment of Southern hake (*Merluccius australis*) in the Falkland Islands. SA–2022–PAT. Fisheries Department, Directorate of Natural Resources, Falkland Islands Government, Stanley, Falkland Islands. 37 p.

Ramos JE, Winter A (2023a) Stock assessment of rock cod (*Patagonotothen ramsayi*) in the Falkland Islands. SA–2023–PAR. Fisheries Department, Directorate of Natural Resources, Falkland Islands Government, Stanley, Falkland Islands. 49 p.

Ramos JE, Le Luherne E, Shcherbich Z, Amukwaya A, Ongoro F, Peruzzo M, Piontek R (2023b) Cruise Report ZDLT1-2023-07. Groundfish survey. Fisheries Department, Directorate of Natural Resources, Falkland Islands Government. Stanley, Falkland Islands. 40 p.

Ramos JE, Winter A (2023c) Stock assessment of southern blue whiting (*Micromesistius australis*) in the Falkland Islands. SA–2022–BLU. Fisheries Department, Directorate of Natural Resources, Falkland Islands Government, Stanley, Falkland Islands. 36 p.

Ramos JE, Peruzzo M, Desmet L, Harris P, Ongoro F, Villarroel M, Vukasin V, Blake A (2024a) Cruise Report 2024-07-ZDLT1. Groundfish survey. Fisheries Department, Directorate of Natural Resources, Falkland Islands Government. Stanley, Falkland Islands. 48 p.

Ramos JE, Soeth M, García D (2024b) Analysis of net geometry across February groundfish surveys, 2010–2024. 2024-12-GSNG. Fisheries Department, Directorate of Natural Resources, Falkland Islands Government, Stanley, Falkland Islands. 25 p.

Ramos JE (2026) February bottom trawl survey biomasses of fishery species in Falkland Islands waters, 2010–2026. SA-2026-02. Fisheries Department, Directorate of Natural Resources, Falkland Islands Government, Stanley, Falkland Islands. 157 p.

Randhawa HS, Goyot L, Blake A, Ramos JE, Roberts G, Brewin J, Evans D (2020) Cruise Report ZDLT1-02-2020: 2020 Demersal Biomass Survey. Fisheries Department, Directorate of Natural Resources, Falkland Islands Government, Stanley, Falkland Islands. 97 p.

Santos BA, Villarino MF, Pedernera MF, Suby A (2024) Evaluación del estado de explotación del efectivo sur de 41°S de merluza (*Merluccius hubbsi*) y estimación de la captura biológicamente aceptable para 2025. Inf. Tec. Oficial INIDEP Nº 032/24. 34 p.

Seafish (2010) Bridle angle and wing end spread calculations. Research and development catching sector fact sheet. Available at: www.seafish.org

Shubnikov DA, Permitin YE, Voznyak SP (1969) Biology of the pelagic gadoid fish *Micromesistius australis* Norman. Trudy VNIRO 66: 299–306. *In:* Arkhipkin AI, Schuchert PC, Danyushevsky L (2009) Otolith chemistry reveals fine population structure and close affinity to the Pacific and Atlantic oceanic spawning grounds in the migratory southern blue whiting (*Micromesistius australis australis*). Fisheries Research 96: 188–194. https://doi.org/10.1016/j.fishres.2008.11.002

Skeljo F, Winter A (2025) Stock assessment of Falkland calamari (*Doryteuthis gahi*) in the 2nd season 2025. Technical Document, Falkland Islands Fisheries Department. 35 p.

Soeth M (2024) *Merluccius hubbsi* and *Merluccius australis* species identification: notes from February 2024 groundfish survey. Fisheries Department, Directorate of Natural Resources, Falkland Islands Government. Stanley, Falkland Islands. 6 p.

Soeth M, Ramos JE, Minichino R, Amukwaya A, Ongoro F, Elebrash O, Pedrero R, Blake A, Trevizan T (2025) Cruise Report 2025-07-ZDLU1. Groundfish survey. Fisheries Department, Directorate of Natural Resources, Falkland Islands Government. Stanley, Falkland Islands. 134 p.

Soeth M (2026) *Merluccius hubbsi* maturity scale. Fisheries Department, Directorate of Natural Resources, Falkland Islands Government. Stanley, Falkland Islands. 13 p.

Swanson GA, Krapu GL, Bartonek JC, Serie JR, Johnson DH (1974) Advantages in mathematically weighting waterfowl food habits data. *Journal of Wildlife Management* 38, 302–307.

Troccoli GH, Di Marco EJ, Cortés F (2024) Estimación de la biomasa del bacalao austral en el Atlántico Sudoccidental durante el periodo 1980–2023: una comparación entre el Modelo de Ensamble y el Modelo Bayesiano JABBA. Inf. Invest. INIDEP Nº 071/24. 23 p.

Ver Hoef JM, Boveng PL (2007) Quasi-Poisson vs. negative binomial regression: How should we model overdispersed count data? Ecology 88: 2766–2772. https://doi.org/10.1890/07-0043.1

Wickham H (2016) ggplot2: Elegant Graphics for Data Analysis. Springer-Verlag, New York. https://ggplot2.tidyverse.org

Winter A, Laptikhovsky V, Brickle P, Arkhipkin A (2010) Rock cod (*Patagonotothen ramsayi* (Regan, 1913)) stock assessment in the Falkland Islands. Fisheries Department, Directorate of Natural Resources, Falkland Islands Government, Stanley, Falkland Islands. 12 p.

Winter A (2015) Loligo Stock Assessment, First Season 2015. Fisheries Department, Directorate of Natural Resources, Falkland Islands Government, Stanley, Falkland Islands. 28 p.

Winter A, Shcherbich Z, Iriarte V, Derbyshire C (2017) *Doryteuthis gahi* Stock Assessment Survey, 2nd Season 2017. Fisheries Department, Directorate of Natural Resources, Falkland Islands Government, Stanley, Falkland Islands. 25 p.

Winter A, Lee B (2018) Stock assessment of grenadier (*Macrourus carinatus* and *Coelorinchus fasciatus*). Fisheries Department, Directorate of Natural Resources, Falkland Islands Government, Stanley, Falkland Islands. 13 p.

Winter A (2019) Rock cod stock assessment (*Patagonotothen ramsayi*). Fisheries Department, Directorate of Natural Resources, Falkland Islands Government, Stanley, Falkland Islands. 23 p.

Winter A (2020) Rock cod stock assessment (*Patagonotothen ramsayi*). Fisheries Department, Directorate of Natural Resources, Falkland Islands Government, Stanley, Falkland Islands. 33 p.

Winter A, Ramos J, Shcherbich Z, Tutjavi V, Matošević N (2020) 2020 2nd Season Assessment Survey Falkland calamari (*Doryteuthis gahi*). ZDLZ-S2-2020. Fisheries Department, Directorate of Natural Resources, Falkland Islands Government, Stanley, Falkland Islands. 16 p.

Winter A (2021) Rock cod (*Patagonotothen ramsayi*) stock assessment. SA–2021–PAR. Fisheries Department, Directorate of Natural Resources, Falkland Islands Government, Stanley, Falkland Islands. 29 p.

Winter A, Arkhipkin A, Matosevic N, Copping L (2022) 2022 2nd Pre-Season Assessment Survey, Falkland calamari (*Doryteuthis gahi)*. ZDLO1-S2-2022. Fisheries Department, Directorate of Natural Resources, Falkland Islands Government, Stanley, Falkland Islands. 17 p.

Winter A, Ander-Estevez J, Desmet L, Villarroel M (2025) 2025 2nd Pre-Season Assessment Survey, Falkland calamari (*Doryteuthis gahi)*. ZDLS4-S2-2025. Fisheries Department, Directorate of Natural Resources, Falkland Islands Government, Stanley, Falkland Islands. 16 p.

Wood SN (2003) Thin-plate regression splines. *Journal of the Royal Statistical Society: Series B* 65: 95–114. https://doi.org/10.1111/1467-9868.00374

Wood SN (2011) Fast stable restricted maximum likelihood and marginal likelihood estimation of semiparametric generalised linear models. *Journal of the Royal Statistical Society: Series B* 73: 3–36. https://doi.org/10.1111/j.1467-9986.2010.01122.x

Wood SN (2017) *Generalized Additive Models: An Introduction with R* (2nd ed.). Chapman and Hall/CRC. https://doi.org/10.1201/9781315370279

Zavatteri A, Giussi A (2022) Evaluación de la abundancia de merluza de cola (*Macruronus magellanicus*) del Atlántico Sudoccidental. Periodo 1985–2021. Inf. Tec. Oficial INIDEP Nº 057/22. 28 p.

Appendix I. Length-weight relationship

Length-weight relationship for main commercial species in Falkland Islands waters. Dorsal mantle length was measured for Argentine shortfin squid and Patagonian squid. Total length was measured for common hake, kingclip, red cod, rock cod, southern blue whiting, southern hake, and Patagonian toothfish. Pre-anal length was measured for banded whiptail grenadier and hoki.

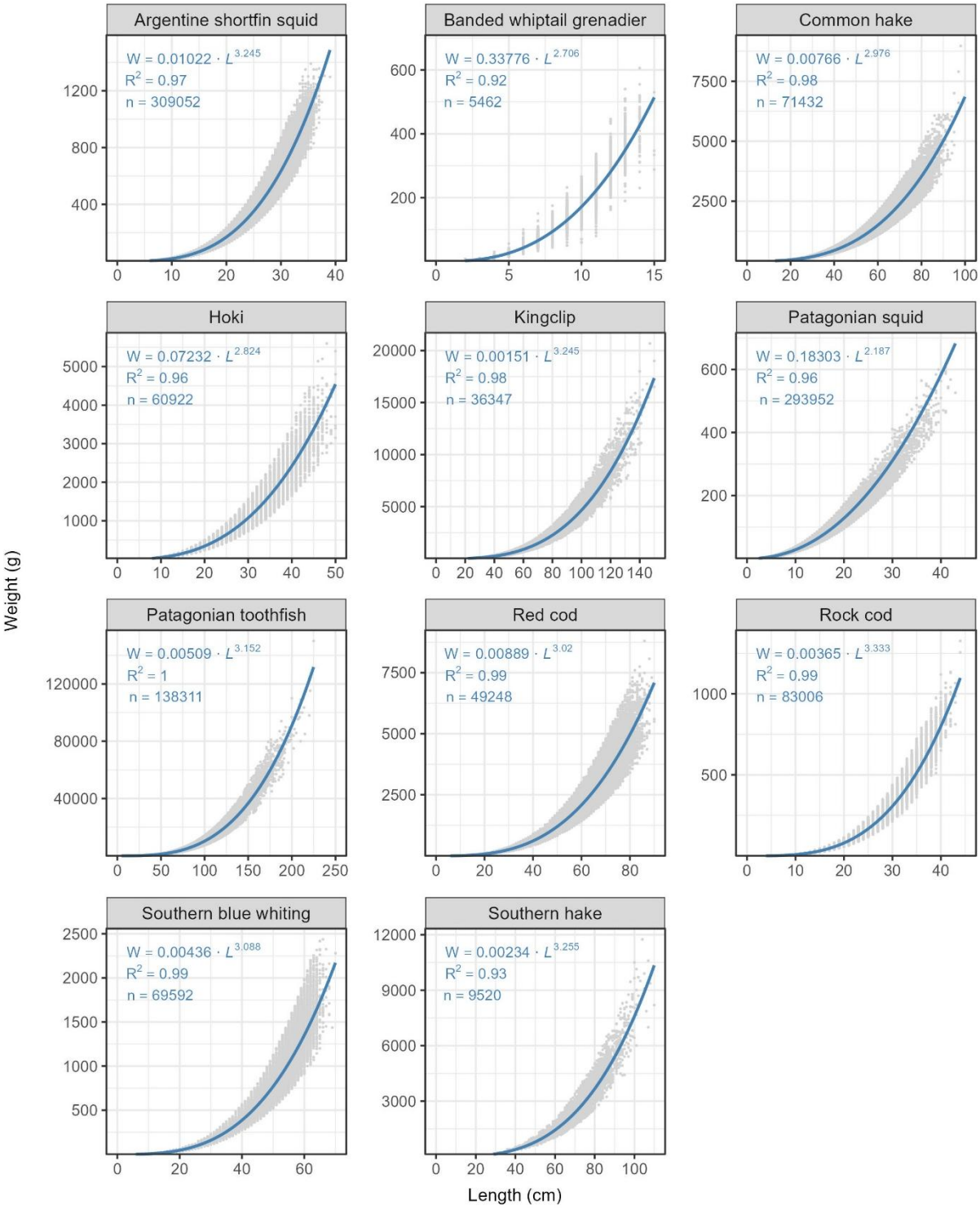

Appendix II. July surveys catches

Catch (t) of main commercial species during the July 2017, 2020, and 2022–2026 groundfish and calamari pre-season surveys in Falkland Islands waters.

Year	Argentine shortfin squid	Banded whiptail grenadier	Common hake	Hoki	Kingclip	Patagonian squid	Patagonian toothfish
2017	0.022	0.017	26.653	114.718	4.158	315.804	0.65
2020	0.014	0.728	85.652	1.954	2.546	580.078	0.606
2022	0.016	0.93	92.214	0.237	1.905	446.925	0.287
2023	0.016	0.034	102.292	0.2	4.738	301.047	0.297
2024	0.044	0.341	161.374	0.919	6.101	54.809	1.012
2025	0.198	1.098	250.807	0.49	12.418	205.812	3.834
2026	0.212	0.714	243.802	0.051	3.093	210.349	2.263
Mean	0.075	0.552	137.542	16.938	4.994	302.118	1.278

Appendix II. *continued*

Year	Red cod	Rock cod	Southern blue whiting	Southern hake
2017	2.563	32.91	0.7	0.061
2020	2.586	1.507	0.662	0.021
2022	4.498	20.091	0.354	0.01
2023	8.905	10.716	1.846	0.011
2024	5.439	25.802	0.198	0.063
2025	6.904	31.795	0.044	0.191
2026	4.324	22.536	0.044	0.058
Mean	5.031	20.765	0.550	0.059

Appendix III. Year-to-baseline biomass differences

L95) Lower 95% confidence interval; U95) Upper 95% confidence interval; p positive) p value of biomass increase at 95% significance; p negative) p value of biomass decrease at 95% significance. Argentine shortfin squid (ILL); Banded whiptail grenadier (GRF); Common hake (HAK); Hoki (WHI); Kingclip (KIN); Patagonian squid (LOL); Patagonian toothfish (TOO); Red cod (BAC); Rock cod (PAR); Southern blue whiting (BLU); Southern hake (PAT). Bold font indicates significant changes (p adjusted threshold = 0.017).

Species	Comparison	Mean difference	L95	U95	p positive	p negative	Change
ILL	2017 vs 2026	1177.85	794.13	1533.69	0.000	1.000	Increase
ILL	2025 vs 2026	608.46	140.11	1085.70	0.031	1.000	Increase
ILL	Mean vs 2026	-933.03	-1308.74	-550.80	1.000	0.000	Decrease
GRF	2017 vs 2026	30519.02	3311.77	44267.21	0.000	1.000	Increase
GRF	2025 vs 2026	19989.34	-8005.54	36224.58	0.420	1.000	None
GRF	Mean vs 2026	-26397.48	-40345.90	785.03	1.000	0.211	None
HAK	2017 vs 2026	547421.89	462836.05	645484.13	0.000	1.000	Increase
HAK	2025 vs 2026	-44384.93	-257506.72	173939.44	1.000	1.000	None
HAK	Mean vs 2026	-102531.33	-223562.24	13434.57	1.000	0.250	None
WHI	2017 vs 2026	-85062.94	-158681.92	-25211.66	1.000	0.000	Decrease
WHI	2025 vs 2026	-2726.46	-6848.91	340.31	1.000	0.260	None
WHI	Mean vs 2026	1465.49	-5.99	3046.84	0.179	1.000	None
KIN	2017 vs 2026	11790.43	-17121.96	52559.91	0.269	0.732	None
KIN	2025 vs 2026	-30323.85	-116135.37	42826.32	1.000	1.000	None
KIN	Mean vs 2026	11355.06	-35991.55	54095.87	1.000	1.000	None
LOL	2017 vs 2026	-245901.38	-340236.02	-148090.97	1.000	0.000	Decrease
LOL	2025 vs 2026	-28027.89	-62491.71	4505.88	1.000	0.234	None
LOL	Mean vs 2026	14824.75	-10414.07	42479.79	0.791	1.000	None
TOO	2017 vs 2026	8836.54	4331.38	12791.80	0.000	1.000	Increase
TOO	2025 vs 2026	387.38	-4449.92	4771.53	1.000	1.000	None
TOO	Mean vs 2026	-6048.36	-10102.42	-1505.34	1.000	0.007	Decrease
BAC	2017 vs 2026	2129.77	-8138.99	13044.93	0.358	0.642	None
BAC	2025 vs 2026	-6662.09	-19239.14	6226.95	1.000	1.000	None
BAC	Mean vs 2026	12284.25	-4691.79	29938.52	0.606	1.000	None
PAR	2017 vs 2026	34117.47	-10200.53	79083.79	0.073	0.927	None
PAR	2025 vs 2026	-3675.94	-68640.91	58779.64	1.000	1.000	None
PAR	Mean vs 2026	-29531.74	-73866.32	15693.95	1.000	0.668	None
BLU	2017 vs 2026	-491.22	-1910.28	743.25	0.687	0.313	None
BLU	2025 vs 2026	565.55	-44.57	1041.08	0.229	1.000	None
BLU	Mean vs 2026	-219.88	-733.70	417.19	1.000	1.000	None
PAT	2017 vs 2026	3264.26	1661.67	5244.98	0.000	1.000	Increase
PAT	2025 vs 2026	2628.07	931.55	4679.57	0.001	1.000	Increase
PAT	Mean vs 2026	-3254.89	-5246.24	-1653.29	1.000	0.000	Decrease

Appendix IV. Year-to-baseline biomass differences histograms

Biomass differences calculated from the year-to-baseline paired 10,000 bootstrap iterations. Zero represents equality and is indicated by the dashed red line.

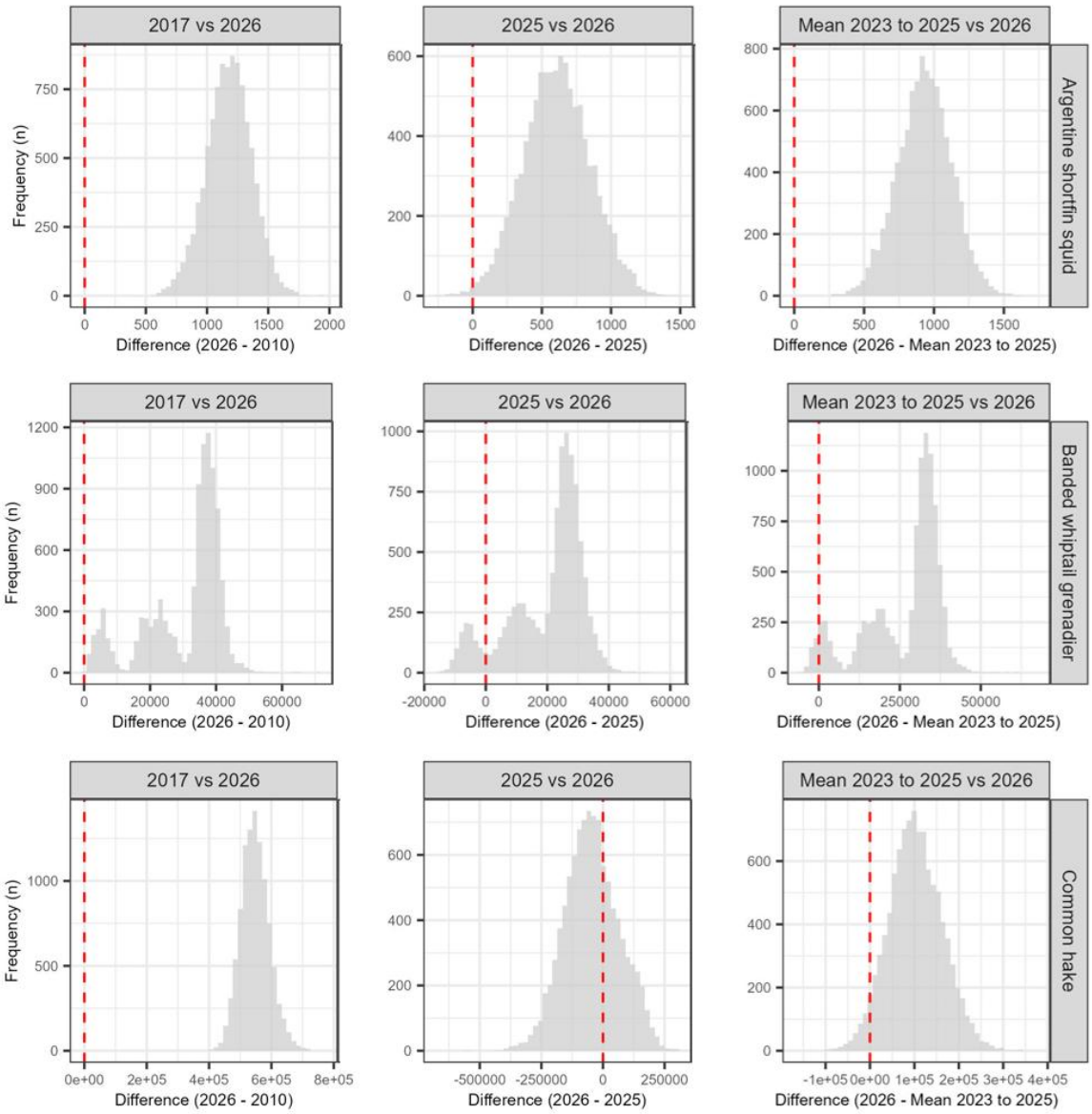

Appendix IV. *continued*

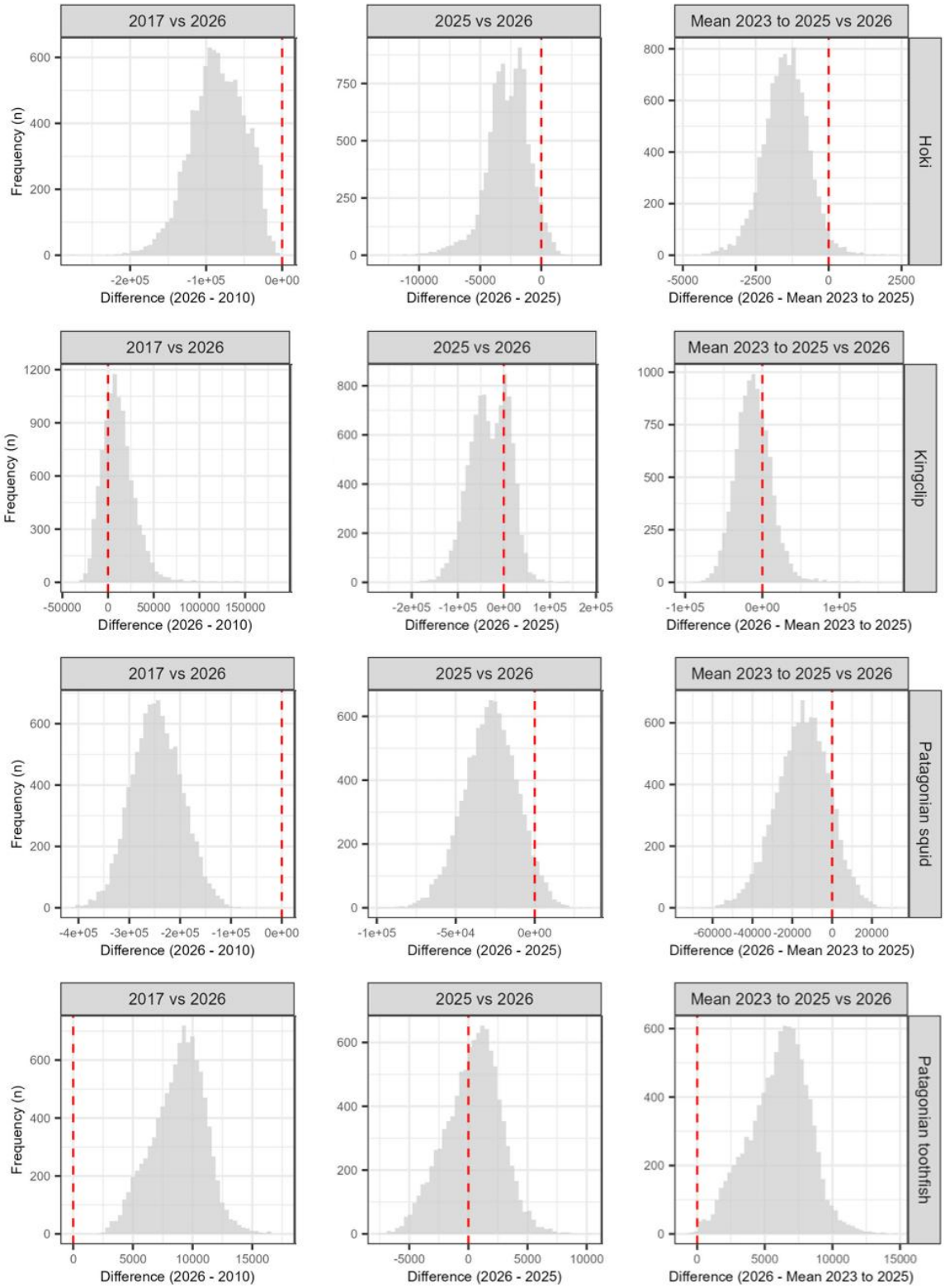

Appendix IV. *continued*

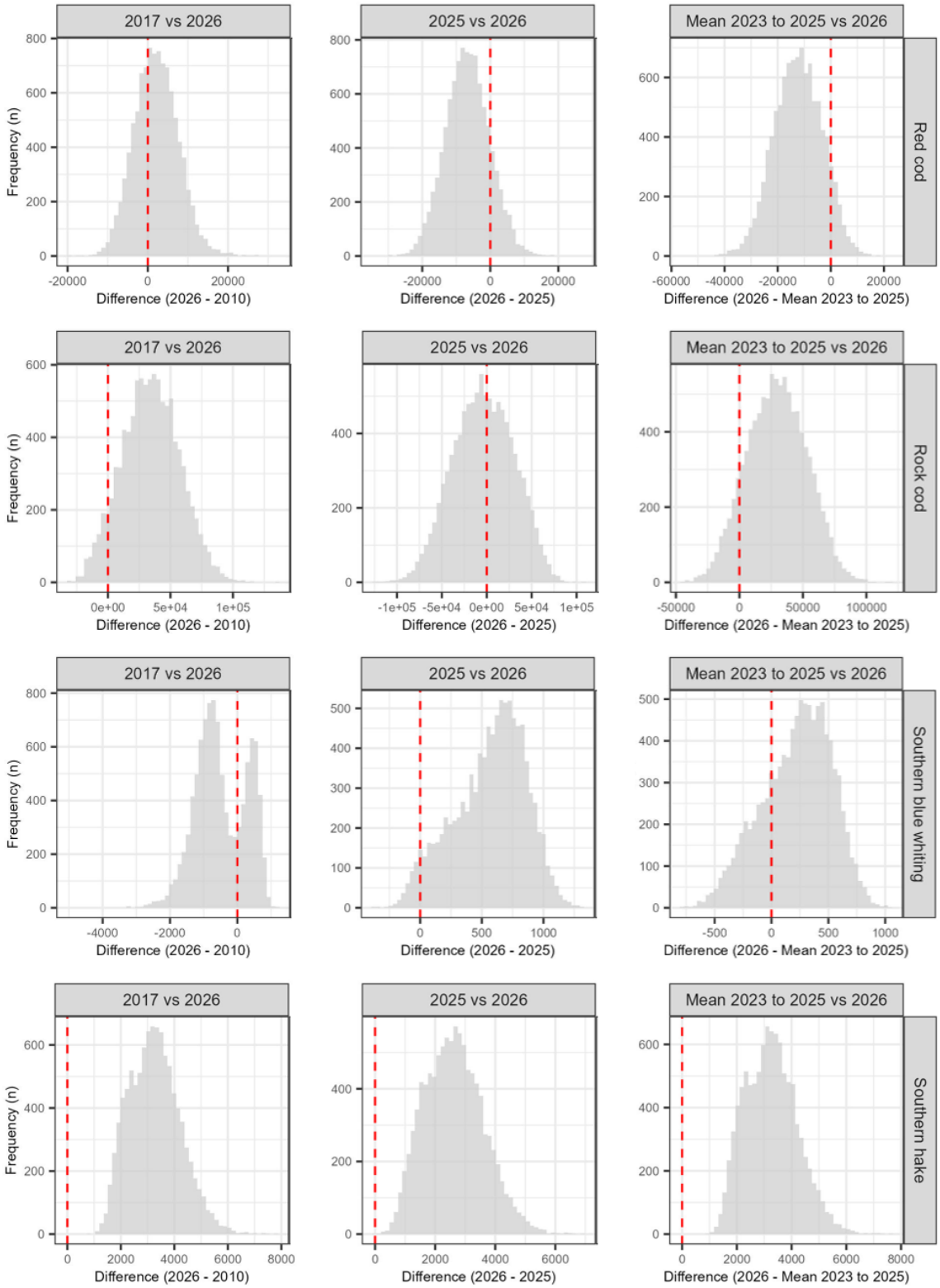

Appendix V. Generalised Additive Models for biomass trends

Inv. CV: normalised inverse coefficient of variation; Sqrt. Inv. Var.: square-root normalised inverse variance; edf: estimated degrees of freedom; Ref. df: reference degrees of freedom; F: F-statistic for the year smooth term; p value: Significance for the year smooth term; R^2 adj.: adjusted R^2; Dev. exp.: percentage deviance explained; AIC: Akaike Information Criterion; ΔAIC: difference in AIC relative to the best-fitting model for each species; *k*-index: basis dimension adequacy index; *k* p value: Significance for the *k*-index diagnostic.

Common name	Scientific name	Model	edf	Ref. df	F	p value	R2 adj.	Dev. Exp.	AIC	*k* index	*k* p value	ΔAIC
Argentine shortfin squid	***Illex argentinus***	**M3: Gaussian, unweighted**	**3.94**	**4.00**	**640.37**	**0.002**	**0.998**	**99.9**	**-29.5**	**2.169**	**1.00**	**0.0**
		M1: Gamma, unweighted	3.88	3.99	228.83	0.004	0.992	99.8	-27.6	1.902	0.983	1.9
		M4: Gaussian, Inv.var.sqrt	3.89	3.99	169.14	0.006	0.990	99.7	-27.6	2.106	1.00	1.9
		M2: Gamma, Inv.cv	3.89	3.99	262.26	0.004	0.993	99.8	-16.9	1.904	0.985	12.6
Banded whiptail grenadier	***Coelorinchus fasciatus***	**M2: Gamma, Inv.cv**	**1.00**	**1.00**	**1.23**	**0.318**	**0.126**	**9.5**	**38.4**	**0.870**	**0.425**	**0.0**
		M3: Gaussian, unweighted	3.78	3.97	23.82	0.039	0.942	97.8	39.3	2.011	0.988	0.9
		M1: Gamma, unweighted	1.58	1.92	1.69	0.266	0.188	22.5	49.7	0.936	0.392	11.3
		M4: Gaussian, Inv.var.sqrt	1.47	1.77	0.45	0.640	-0.099	22.3	50.5	0.528	0.33	12.1
Common hake	***Merluccius hubbsi***	**M2: Gamma, Inv.cv**	**2.05**	**2.46**	**14.14**	**0.015**	**0.624**	**86.4**	**56.7**	**1.584**	**0.863**	**0.0**
		M4: Gaussian, Inv.var.sqrt	1.00	1.00	37.07	0.002	0.847	88.1	89.7	1.544	0.88	33.0
		M3: Gaussian, unweighted	1.00	1.00	10.04	0.025	0.601	66.8	93.3	1.590	0.870	36.6
		M1: Gamma, unweighted	2.05	2.47	11.34	0.022	0.553	84.2	93.4	1.597	0.848	36.7
Hoki	***Macruronus magellanicus***	**M2: Gamma, Inv.cv**	**1.00**	**1.00**	**25.85**	**0.004**	**0.875**	**80.8**	**41.6**	**1.027**	**0.415**	**0.0**
		M4: Gaussian, Inv.var.sqrt	3.37	3.78	12.95	0.031	0.862	95.1	42.0	1.758	0.960	0.4
		M1: Gamma, unweighted	1.00	1.00	23.75	0.005	0.900	80.0	45.1	1.024	0.422	3.5
		M3: Gaussian, unweighted	3.27	3.67	83.91	0.002	0.981	99.1	45.7	1.691	0.905	4.1

Appendix V. *continued*

Common name	Scientific name	Model	edf	Ref. df	F	p value	R2 adj.	Dev. Exp.	AIC	*k* index	*k* p value	ΔAIC
Kingclip	***Genypterus blacodes***	**M2: Gamma, lnv.cv**	**1.00**	**1.00**	**1.43**	**0.286**	**0.018**	**22.3**	**33.0**	**1.606**	**0.900**	**0.0**
		M1: Gamma, unweighted	1.00	1.00	2.27	0.193	0.089	31.2	58.1	1.566	0.858	25.1
		M4: Gaussian, lnv.var.sqrt	1.00	1.00	0.98	0.367	-0.024	16.4	58.1	1.577	0.868	25.1
		M3: Gaussian, unweighted	1.00	1.00	1.58	0.264	0.088	24.0	60.4	1.539	0.82	27.4
Patagonian squid	***Doryteuthis gahi***	**M2: Gamma, lnv.cv**	**1.00**	**1.00**	**18.09**	**0.008**	**0.806**	**76.4**	**56.2**	**1.267**	**0.652**	**0.0**
		M3: Gaussian, unweighted	1.00	1.00	43.51	0.001	0.876	89.7	73.4	0.972	0.298	17.2
		M1: Gamma, unweighted	1.00	1.00	24.88	0.004	0.842	81.3	76.2	1.217	0.565	20.0
		M4: Gaussian, lnv.var.sqrt	1.51	1.84	8.17	0.037	0.690	78.2	77.8	1.171	0.657	21.6
Patagonian toothfish	***Dissostichus eleginoides***	**M2: Gamma, lnv.cv**	**3.94**	**4.00**	**43.11**	**0.023**	**0.921**	**98.7**	**15.6**	**1.680**	**0.922**	**0.0**
		M1: Gamma, unweighted	3.94	4.00	41.67	0.024	0.916	98.6	20.3	1.701	0.907	4.7
		M4: Gaussian, lnv.var.sqrt	3.20	3.63	5.21	0.102	0.706	88.4	31.7	1.680	0.948	16.1
		M3: Gaussian, unweighted	3.45	3.81	7.78	0.073	0.813	92.1	33.4	1.854	0.99	17.8
Red cod	***Salilota australis***	**M2: Gamma, lnv.cv**	**2.81**	**3.27**	**10.29**	**0.043**	**0.649**	**91.2**	**31.3**	**2.071**	**0.99**	**0.0**
		M4: Gaussian, lnv.var.sqrt	2.59	3.04	7.24	0.069	0.762	87.4	46.1	2.005	0.998	14.8
		M1: Gamma, unweighted	2.72	3.18	7.71	0.064	0.581	87.5	48.6	2.066	0.993	17.3
		M3: Gaussian, unweighted	2.47	2.93	4.38	0.100	0.654	79.6	50.5	2.088	0.995	19.2

Appendix V. *continued*

Common name	Scientific name	Model	edf	Ref. df	F	p value	R2 adj.	Dev. Exp.	AIC	*k* index	*k* p value	ΔAIC
Rock cod	***Patagonotothen ramsayi***	**M2: Gamma, lnv.cv**	**2.31**	**2.75**	**3.20**	**0.185**	**0.630**	**60.2**	**45.7**	**1.902**	**0.980**	**0.0**
		M4: Gaussian, lnv.var.sqrt	2.65	3.05	9.64	0.047	0.754	90.3	63.4	1.655	0.965	17.7
		M3: Gaussian, unweighted	2.07	2.49	3.77	0.126	0.570	71.8	66.2	1.862	0.978	20.5
		M1: Gamma, unweighted	1.65	2.01	1.87	0.271	0.517	36.9	72.5	1.722	0.99	26.8
Southern blue whiting	***Micromesistius australis***	**M2: Gamma, lnv.cv**	**1.51**	**1.85**	**2.52**	**0.193**	**-0.371**	**52.3**	**18.0**	**1.533**	**0.895**	**0.0**
		M1: Gamma, unweighted	1.00	1.00	3.86	0.107	-0.435	38.5	25.9	1.549	0.910	7.9
		M4: Gaussian, lnv.var.sqrt	1.00	1.00	0.64	0.460	-0.115	11.3	27.3	1.481	0.945	9.3
		M3: Gaussian, unweighted	1.00	1.00	1.12	0.338	0.020	18.3	39.7	1.691	0.938	21.7
Southern hake	***Merluccius australis***	**M3: Gaussian, unweighted**	**3.76**	**3.96**	**25.19**	**0.037**	**0.945**	**97.9**	**6.9**	**1.965**	**0.993**	**0.0**
		M2: Gamma, lnv.cv	2.32	2.76	3.50	0.123	0.820	77.6	13.3	1.249	0.618	6.4
		M1: Gamma, unweighted	2.07	2.49	2.32	0.193	0.680	66.4	14.5	1.287	0.640	7.6
		M4: Gaussian, lnv.var.sqrt	2.42	2.88	1.62	0.298	0.404	64.5	16.2	0.806	0.232	9.3

Appendix VI. Spatial distribution of Patagonian squid (*Doryteuthis gahi)* length

Spatial distribution of median dorsal mantle length of Patagonian squid (*Doryteuthis gahi*) during July groundfish and calamari pre-season surveys conducted in Falkland Islands waters in 2017, 2020, and 2022–2026. Isobaths at 100 m, 200 m, and 500 m are shown.

